TRANSPORT OF SIZE-GRADED AND UNIFORM SEDIMENTS UNDER OSCILLATORY SHEET-FLOW CONDITIONS

Promotion Committee:

Prof. dr. ir. H. J. Grootenboer,	University of Twente, chairman/secretary
Prof. dr. ir. H. J. de Vriend,	University of Twente, promotor
Dr. ir. J. S. Ribberink,	University of Twente, assistant-promotor
Prof. dr. ir. S. R. McLean,	University of California, Santa Barbara
Prof. dr. ir. M. J. F. Stive,	Delft University of Technology
Prof. dr. D. Lohse,	University of Twente
Prof. dr. J. Mellema,	University of Twente
Dr. ir. C. M. Dohmen-Janssen,	University of Twente

This study has been supported by different European research projects:

- The commission of the European Union, Directorate General for Science, Research and Development, in the SEDMOC project under contract No. Mas3-CT97-0115;
- Access to Large-Scale Facilities Action of the Training and Mobility of Researchers programme (TMR), contract ERBFMGE-CT-95-0045;
- Access to Research Infrastructures Action of the Improving Human Potential Programme (MRI), contract HPRI-CT-1999-0103;
- Delft Cluster project DC 03.01.01. 'Sediment transport: processes and modelling'.

Printed by: PINKSTERPRINT, Enschede, The Netherlands.

ISBN: 90-365-1889-x

TRANSPORT OF SIZE-GRADED AND UNIFORM SEDIMENTS UNDER OSCILLATORY SHEET-FLOW CONDITIONS

DISSERTATION

to obtain

the doctor's degree at the University of Twente,

on the authority of the rector magnificus,

prof. dr. F.A. van Vught,

on account of the decision of the graduation committee,

to be publicly defended

on Wednesday 07 May at 15.00 hr

by

Wael Neiazy Mohamed Hassan

born on 10 January 1967

in Shebin El-Kom, Egypt

This dissertation is approved by:

Prof. dr. ir. H. J. de Vriend	Promotor
Dr. ir. J. S. Ribberink	Assistant-promotor

Abstract

Sediment transport models form an essential link in the chain of mathematical models for predicting coastal and seabed morphology (erosion/sedimentation). Sand transport and morphological studies are of great importance for the analysis of coastal systems, coastal erosion problems, coastal defence, impact studies of coastal structures, seabed stability studies, offshore sand extraction studies etc. An increased understanding of the physics controlling sediment transport processes in the coastal zone is important in relation to the application of appropriate sand transport models in the real world problems.

There are several reasons to pay more attention to the influence of sediment characteristics (size, gradation, density) on the sediment transport processes. Beach or shoreface nourishments are generally carried out with different (dredged) materials than the sand as currently present. However, not much is known about the possibilities of using different bed materials (deviating from the present coastal profile) for the design of effective beach nourishments schemes.

Moreover, in the existing sediment transport and morphological models it is generally assumed that seabed sediments can be characterized by one representative grain. It is known however, that seabed and beach materials show large spatial differences in sediment size and gradation, which can be attributed to former marine (or river) deposits and/or to horizontal segregation of sizes related to presently existing sediment transport patterns (see Terwindt, 1962, Houwman and Hoekstra, 1994 and Guillen, 1995). Coastal cross-shore profiles generally show strong correlations between morphology (bars) and sediment composition of the seabed. It also known from beach profile observations that grain size is an important parameter for the shape of the beach profile (Dean, 1991).

Contrary to river morphological models the existing coastal morphological models are not able to account for spatial and temporal variations in grain size and gradation. Coastal long-shore transport models as well as the coastal profile models and the more general 2D/3D area models lack a size-fraction approach for the sediment transport. This is mainly caused by the fact that there is a lack of basic knowledge about sediment transport processes of graded sediments in wave-dominated conditions. As a result no sediment transport models are available which are able to compute magnitudes as well as size-composition of transported sediments.

Recently, Van Rijn (1997b) studied cross-shore sorting of sediment mixtures using a process-based model (CROSMOR) provided with a single and a multi-fraction

approach. Van Rijn found that the bed-load transport rates of sediments between 0.2 and 0.8 mm based on a multi-fraction method are slightly to significantly larger than those based on a single-fraction method. Besides, the suspended-load transport rates of the multi-fraction method are significantly smaller than those of the single-fraction method at small current velocities.

Basic sediment transport research as carried out during recent years in the Netherlands and abroad (e.g. Dohmen-Janssen, 1999; Dibajnia & Watanabe, 1996) has concentrated on the influence of the grain size on sediment transport in wave-dominated conditions. These studies and others (e.g. Hamm et al, 1998, Dibajnia & Watanabe, 2000 and Wright, 2002) all indicate that the grain-size and gradation of sediment are important parameters, which should be considered in cross-shore transport calculations.

The present study concentrates mainly on the influence of sediment gradation on the wave-induced sediment transport and can be considered as a logical next step in an ongoing line of cross-shore sand transport research. The study focuses at improving our basic understanding of size-graded and uniform sand transport mechanisms in cross-shore direction under oscillatory sheet-flow conditions. Sheet-flow is the dominant transport mode during storm conditions, when coastal and seabed erosion and deposition processes are generally very strong. Also, this study aims at improving the performance of model concepts for the description of both the rate and size-composition of the transported sand. Improved modelling tools will be developed through a strong interaction between experimental laboratory research, on the one hand, and different types of mathematical transport modelling on the other hand.

Experimental studies

In order to fill the present gap in our knowledge, full-scale laboratory models can be used to get more insight into the important sediment transport processes and to support modellers with reliable data to verify their models. The large oscillating water tunnel (LOWT) of WL | Delft Hydraulics is one of these laboratory models, which can simulate the near bed orbital velocities at full scale (1:1).

In total five series of laboratory experiments were carried out in the LOWT. Three series were performed using fairly uniform sand sizes and two series with non-uniform sands, under variable hydraulic conditions. The experiments aimed mainly at measuring net total transport rates and transport per size fraction, under 2^{nd}-order Stokes waves. One of these experimental series (D = 0.13 mm) aimed at measuring (and improving a measuring technique) of detailed time-dependent transport processes inside the sheet-flow layer, i.e. time-dependent concentrations, velocities and sediment-flux profiles.

The measured net transport rates under 2^{nd}-order Stokes waves showed that grain-size has almost no effect on net transport rates and transport rates are proportional to

the third power velocity moment ($<q_s> \sim <U^3>$), for sand sizes between $0.21 < D < 0.97$ mm. Meanwhile, finer grains ($D = 0.13$ mm) show a different behaviour in the high velocity range, i.e. for $<U^3> > 0.2$ m^3/s^3 as net sand transport rates change from the 'onshore' direction into the 'offshore' direction due to the presence of unsteady effects. Therefore, the assumption of quasi-steadiness of Al-Salem (1993) does no longer hold.

During the experiments a new measuring technique was improved (cross correlation between two CCM, Conductivity Concentration Meter, sensors) for the measurement of sediment dynamics in the lowest regions near the bed (inside the sheet-flow layer) where the most important transport processes take place (see McLean et al., 2001). This was achieved by reducing the distance between two CCM sensors to 11 mm, instead of 20 mm as used by McLean et al. (2001). Particle velocities could now be measured during the complete wave-cycle.

For relatively long waves ($T = 12.0$ s) time-dependent concentrations inside the sheet-flow layer are approximately in phase with the time-dependent flow velocity variations. Meanwhile, for shorter wave-periods (7.2 and 4.0 s) increasing phase-lags are observed. As the wave-period decreases, the sediment entrainment from the bed as well as the deposition process back to the bed lags behind the wave motion more and more. Moreover, the strength of the flow reversal peaks in the upper sheet-flow layer increases with decreasing wave-period. Reducing the wave-period from 12.0 to 4.0 s leads to gradual changes in the net wave-related fluxes in the sheet-flow layer from the 'onshore' to the 'offshore' direction.

Graded sand experiments showed that, size-gradation has almost no effect on the net total transport rates, provided that the grain sizes of the sand mixture are in the range of $0.21 < D < 0.97$ mm. If very fine grains ($D = 0.13$ mm) are present in the mixture net transport rates of graded sand may be different from those of uniform sand (with the same D_{50}) depending on the flow velocity regime.

Comparing the net transport rate of a size-fraction in a mixture with the transport rate of uniform sand with the same median diameter (D_{50}) shows that the transport of each size-fraction is strongly influenced by the presence of other fractions. Fine particles in sand mixtures are relatively less transported than in a uniform sand bed (hiding effect), while the opposite occurs for coarse fractions in a mixture (increased exposure effect). The experiments showed that, the relative contribution of the coarse grains to the transport is also generally larger than would be expected on the basis of their volume proportion in the original sand mixture.

Differences in entrainment and mixing characteristics of grain sizes, generally leads to vertical segregation of sizes in the water column (e.g. fines in suspension and coarse sizes in the bed-load layer). The suspended transport of the fines in a mixture is therefore influenced by time-history effects during a wave-cycle, while coarser sizes transported in the bed-load layer show a more quasi-steady transport behaviour. This selective behaviour of sizes might invoke e.g. a net 'onshore' motion of coarse

sizes, and at the same time a net ‘offshore’ motion of finer sizes in the general case of asymmetric waves.

Generally, the sand transported as bed-load in the ‘onshore’ direction is coarser than that in the ‘offshore’ direction. For both directions, the percentage of coarse material is larger than in the original sand bed mixture. This sorting process was observed for all flow conditions. The contribution of the coarse fraction in the bed-load transported material increases with increasing flow velocity. Vertical grain-size sorting is also taking place in the upper active bed-layers, which are disturbed by the wave action. The upper layer of the bed (thickness of a few millimeters) has roughly the same composition as the original sand bed or is even coarser. Beneath this upper layer there is a layer that mainly consists of fine sand. At larger depths below the sand-surface, the size-composition of the bed is again similar to the original sand bed mixture.

Oscillatory sand transport modelling

An important assumption in most of the existing sediment transport models is the uniformity of the sand mixture, which means that the sediment mixture is charactarised by a single sand size (D_{50}). This simplification is necessary because of a lack of knowledge about the influence of size-gradation and about the selective transport behaviour of different sediment sizes in a mixture, especially under waves. In the present study sand transport modelling focused mainly on i) studying the performance of different types of transport models for oscillatory sheet-flow conditions and different ways of modelling phase-lag effects in case of relatively uniform sands, ii) providing existing single size-fraction transport models with a multi-fraction approach for modelling graded sand transport, and iii) improving these multi-fraction techniques for predicting the net total transport rate and the size-composition of the transported sand.

Five different sediment transport models (quasi-steady, intermediate and fully unsteady models) were investigated, in combination with a large dataset of oscillatory sediment transport measurements (flat-bed/sheet-flow conditions) as collected in the LOWT and in the TUWT (Tokyo University Water Tunnel). The complete dataset consists of 118 different experiments with uniform sand and 37 experiments with size-graded sand.

Uniform sand transport modelling
The verification of transport models with uniform sand data reveals that, quasi-steady models are not always able to predict transport rates and transport directions correctly (‘offshore’ instead of ‘onshore’). ‘Offshore’ transport occurs especially for short wave-periods and small sand particles, indicating that the assumption of quasi-steadiness does not hold and phase-lag effects play a role in the transport process. Meanwhile, the inclusion of phase-lag effects in the transport models leads to a strong improvement of the model performance. For both intermediate model concepts (Dohmen-Janssen, 1999 and Dibajnia & Watanabe, 1996) the agreement

between measurements and computations is considerably better than for the quasi-steady transport models.

For the uniform sand data the fully unsteady POINT-SAND model (PSM model) is able to give good predictions of transport directions and net transport rates. This 1D-vertical model resolves the time-dependent turbulent water flow and suspended sediment fluxes in the water column, taking into account hindered settling of sand grains and flow stratification effects. So apparently the PSM model inherently gives a good representation of phase-lag effects. Moreover, adding the bed-load formula of Engelund & Fredsøe (1976) to the original PSM suspension model improves the model performance for uniform sand cases.

Non-uniform sand transport modelling
In general, for all (quasi-steady, intermediate and fully unsteady) transport models the use of a multi-fraction approach and assuming that there is no interaction between grain sizes is not sufficient for predicting correctly the magnitude and the size-composition of graded sand transport. Mutual interaction between grain-sizes should be accounted for when modelling graded sand transport under oscillatory sheet-flow conditions.

Applying an exposure correction to the critical Shields parameter in the model of Ribberink (1998) does not show much influence on the predicted net transport rates. On the other hand, correcting the effective shear stress (Day, 1980) has a clear improving effect on the transport rates per size-fraction. This is to be attributed to the fact that the effective shear stress under oscillatory sheet flows is much larger than the critical shear stress. The correction factor of Day, originally developed for steady (river) flow, increases the effective shear stress on the coarse grains and at the same time reduces the effective shear stress on the fine grains. Also the intermediate model of Ribberink/Dohmen-Janssen (1999) shows an improved performance using the exposure correction method of Day (1980). Further improvement of this intermediate model may be realized by accounting for the influence of dynamic armouring on the phase-lag behaviour of size fractions.

The performance of the model of Dibajnia & Watanabe (1996) is considerably improved for predicting fractional transport rates of sand mixtures, by including an exposure correction in the model. Reducing the entrainment height of fine grains and increasing the entrainment height of coarse grains can achieve this improvement. The proposed correction in the model of D&W (1996) is modelled as a general function of D_i/D_m and can be applied for any number of size-fractions.

The total-load PSM model does not perform well for predicting transport rate of sand mixtures, but is improved significantly by using the size-fraction approach of Zyserman & Fredsøe (1996) in combination with an exposure correction factor for the coarse grains in the mixture.

Finally, the modified graded transport models (D&W, Ribberink/D-J and the PSM model) are verified with a separated dataset consisting of all experiments of the LOWT with graded sediments. All models show a reasonably good performance for predicting net total transport rates as well as transport rates per size-fraction. The modified model of Ribberink/D-J performs slightly better than the other two models. The modified multi-fraction models of Ribberink/D-J and D&W predict the measured transport rates much better for the large-scale LOWT data than for the small-scale TUWT data. The LOWT data are more relevant for field conditions

Wael Neiazy Mohamed Hassan

Contents

Chapter 1

INTRODUCTION

1.1 Background

Cross-shore sediment transport is often an essential sediment transport component in the near-shore coastal system. In general, it has a complex three-dimensional and time-dependent character, as it is driven by the wave orbital motion and net currents near the seabed on time-scales smaller than the wave-period. Consequently, sediment transport in the marine environment generally varies in magnitude and direction during the wave-cycle. The complexity of the underlying process hampers accurate modelling of cross-shore transport rates. Moreover, the difficulty of performing accurate transport measurements in the field creates an additional hindrance in improving our understanding of the basic transport processes, especially under severe wave conditions. Under these conditions, ripples are washed out and the seabed becomes plane. Sand is transported in a thin layer (thickness < 20 mm) with very high concentrations above the sand bed in the so-called sheet-flow regime. In this transport regime sand is transported in big quantities near the bed. The storm/sheet-flow conditions can result in big morphological changes in the cross-shore profile in a relatively short time (one storm duration) and sheet-flow is therefore generally considered as an important transport regime.

In order to bridge the existing gap in our knowledge, full-scale laboratory facilities were developed and used during the last decades in different places (e.g. Tokyo University, the University of Aberdeen and WL | Delft Hydraulics) in the world. These water tunnels are useful tools in order to obtain more insight into the detailed cross-shore sediment transport processes and to support modelers with reliable data, especially under sheet-flow conditions. Most of the developed sand transport models are based on flat-bed data as a first step before including the rippled-beds.

The Large Oscillating Water Tunnel (LOWT) of WL | Delft Hydraulics is one of the large facilities, which can simulate the near bed velocities at full scale (1:1), see

Ribberink (1989). Based on experiments in the LOWT, Al-Salem (1993) showed that quasi-steady models give reasonable results for transport rate prediction in oscillatory sheet-flow conditions, as long as the grain diameter D is larger than 0.2 mm (see also Ribberink and Al-Salem, 1994). However, Ribberink and Chen (1993) showed that this is not necessarily the case for finer sand (D = 0.13 mm). They showed that a grain-size change could even be responsible for a change from onshore-directed to offshore-directed transport under the same wave condition. More recently, Dohmen-Janssen (1999) showed that grain-size has a significant effect on the sediment transport processes under oscillatory sheet-flow conditions. She studied three different sands with D = 0.13, 0.21 and 0.32 mm and sine waves superimposed on a net current. It is important to state that until now almost all experimental studies in the LOWT were done with uniform sands, ignoring effects of grain-size non-uniformity or size-gradation. The present study will focus mainly on size-gradation effects as well as on grain-size effects on the sand transport processes in the sheet-flow regime as a follow up of the previous work of Al-Salem (1993), Ribberink and Chen (1993), Cloin (1998), Dohmen-Janssen (1999), Dohmen-Janssen et al. (2001) and Dibajnia & Watanabe (1992, 1996 and 2000).

Field observations show that seabed sediments are hardly ever uniform, but are generally composed of a mixture of different grain sizes (Katoh and Yanagishima, 1995, Guillen, 1995 and Houwman and Hoekstra, 1994). For example, the Dutch coast consists mainly of sand with median grain-size in the range of 125-600 μm. Moreover, field observations generally show the existence of sorting of sediment grains along the cross-shore profile with coarse material generally present near the shore-line and fine material in deeper water. Until now, little attention is paid to grain-size sorting and its underlying selective transport mechanisms. Moreover, the effect of sediment size-gradation on the transport processes under wave conditions is still not investigated.

Recently, Hamm et al. (1998) performed a first series of experiments in the LOWT (series K) to study sediment transport processes with size-graded sediment. Their experiments showed a clear effect of size-gradation on the measured concentrations and transport rates in oscillatory sheet-flows (see also Cloin, 1998). They concluded that size-gradation is an important factor that should be taken into account in sediment transport models. Moreover, Dibajnia & Watanabe (1996 and 2000) showed that the transport rates of fine grains in a mixture are strongly affected by the presence of coarse grains in a mixture. De Meijer et al. (2002) showed that the transport rates of coarse grains in a mixture are increased with respect to uniform coarse material under similar plane-bed/sheet-flow conditions.

Meanwhile, Sistermans (2002) studied experimentally size-gradation effects on the time-averaged transport processes in the rippled-bed regime with non-breaking irregular waves and a following current. He concluded that suspended sediment concentrations of graded sand are higher than for uniform sand cases over the entire depth, except close to the bed. Furthermore, Sistermans (2002) found that a relatively

large amount of fine sediment is transported, compared to the coarser fractions transport rates in a mixture.

In fact, all these observations and results indicates our need for a profound understanding of size-gradation effects on net total transport rates as well as on transport rates of individual size-fractions.

1.2 Practical importance and relevance of the study

Economical values of coastal regions are increasing rapidly all over the world, due to the presence of cities and human activities, such as harbours, waterways and oil industry. It is important to ensure the safety and to protect these economical activities against any coastal changes (especially erosion). These changes can happen due to natural forces as well as due to human interference itself; both can change the shape of the coastline and the coastal profile.

Cross-shore as well as long-shore sediment transport processes affect the coastal morphological system. For closed almost uniform coastal systems the development of the coastal profile (shape) is strongly determined by cross-shore transport mechanisms. However, accurate prediction of cross-shore sediment transport rates is one of the most complicated problems in marine environments. Cross-shore transport occurs by the interaction of various hydrodynamic forces, waves and currents, and may involve different types of coastal materials.

Models of cross-shore sediment transport and coastal profile development have not yet reached the required degree of accuracy. Van Rijn et al. (1995) showed that predictions of yearly-averaged cross-shore sediment transport rates at the 8 m water depth contour along the Dutch coast varied between – 10 and + 10 m^3/m/year. Apparently, even the direction of the net sediment transport rate is uncertain. More research is required in this field to improve our present physical understanding of the transport processes and to improve existing models.

One of the uncertain aspects of cross-shore transport modelling is the fact that the available transport models generally assume uniformity of sand, which means that sand is characterised by a single sand size and that the size-distribution is fully neglected. This assumption is acceptable in case of relatively uniform sand. However, when the sand has a wide range in sizes it is generally not realistic to simulate sand transport with one size only. Following a multi-fraction approach as developed for uni-directional flows and rivers (see Ribberink, 1987) Van Rijn (1998a) incorporated size-gradation of sand in a cross-shore sediment transport and morphology model and carried out model simulations for some field cases. He concluded that in principle this kind of models can give valuable information and predictions on the distribution of sediments in the marine environment. Improved knowledge to understand the transport processes that cause sorting of sediments is still required (also see Van Rijn, 1997a, b).

In connection with practical applications the understanding of cross-shore sediment transport can be considered specifically important for designing beach nourishments, being one of the most common methods for protecting sand beaches. It is very important to know which nourishment location and characteristics of supplied sand would be most effective. Estimation of transport patterns and transport rates and the use of multi-fraction techniques can be of importance in the case of different grain-size characteristics of the natural (original) sand and the nourished sand. Figure 1.1 gives an indication about the increased amount of sand, which has been used for beach nourishment on the Dutch coast during the last 30 years.

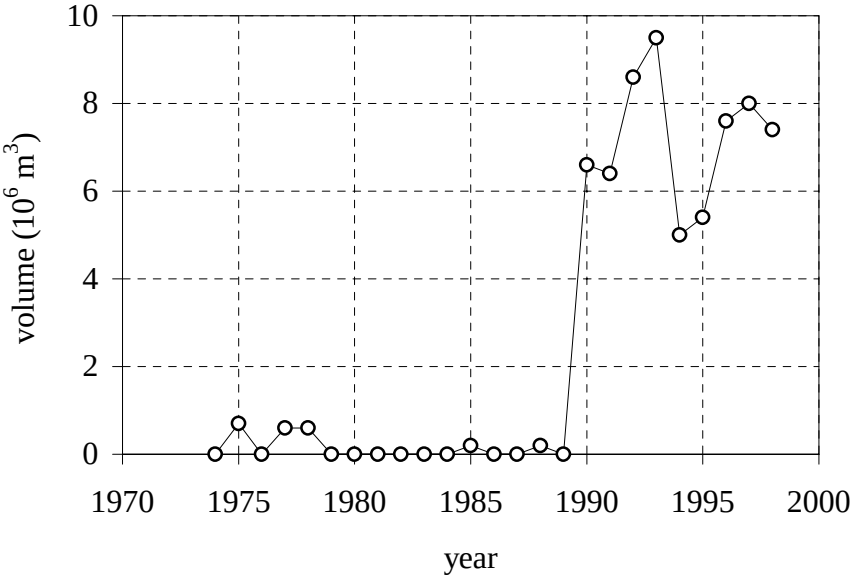

Figure 1.1: Time-history of sand extracted from the North Sea and used for beach nourishment on the Dutch coast (Stolk and Seeger, 2000).

In the Netherlands, coastal erosion and sedimentation is an important issue, related to its low lying lands and the pressure of the large-scale threat of sea-level rise. Also large-scale coastal zone development schemes, such as land reclamation in the North Sea like de Maasvlakte (Rotterdam harbour) and for example, a possible island in the North Sea (airport) require adequate understanding of erosion/sedimentation processes.

1.3 Scope of the study and research questions

The general goal of the present study is to improve our understanding of sand transport mechanisms in the marine coastal environment and to develop reliable, well-validated models for quantitative cross-shore transport predictions. Considering the gaps in our present knowledge the study focuses on the underlying processes and

the modelling of transport of size-graded sediments in wave-dominated sheet-flow conditions and ***aims***:

i) To obtain an improved understanding of the transport mechanisms of size-graded and uniform sediments in oscillatory sheet-flow conditions;
ii) To identify the most important transport processes in order to improve the existing sediment transport models;
iii) To evaluate and to improve the performance of model concepts for the description of the rate and size-composition of sand transport due to short waves in the marine/coastal environment.

The following ***research questions*** are related to the basic processes of sand transport in strong near-shore wave (sheet-flow) conditions:

i) How does size-gradation of bed sediments affect the magnitude, direction and size-composition of wave-induced sediment transport in the sheet-flow regime?
ii) How do individual size-fractions of a mixture of sizes interact with each other and how do these interactions affect the transport processes?
iii) What are the effects of grain-size and wave-period on the sediment transport processes and on net transport rates in oscillatory sheet-flows?

Models as presently used for the computation of cross-shore sediment transport still lack a validated size-fraction approach in which individual sizes are described separately. Therefore, existing models cannot predict the size-composition of the transported sand and it is questionable whether they are able to provide correct predictions of the net total transport rate (see Hassan, 2001a). The total transport rate as well as the size-composition of the transported sediment should be known for simultaneous simulations of sea-bed changes (morphology) as well as changes of grain-size distributions of the sea bed sediments (sediment sorting). See for example, Ribberink (1987).

The following ***research questions*** are related to the modelling of sand transport:

iv) Can size-fraction techniques as commonly used in river applications (uni-directional steady flow) also be used in the marine coastal environment (unsteady oscillatory flows)?
v) What are the effects of using a size-fraction transport modelling technique on the prediction of the net total transport rate with different model types?
vi) What is the performance of these multi-fraction models as far as the prediction of the size-distribution of the transported sand is concerned?
vii) What is the performance of the different transport models, varying from quasi-steady, intermediate, to fully unsteady boundary layer models, in the description of the transport rate of graded and uniform sediments?
viii) How can we improve these transport models for predicting both net transport rates and size-composition of the transported sand?

1.4 Research structure/methodology

The research started with an inventory and collection of existing knowledge and theories about sediment gradation effects on transport mechanisms, especially under oscillatory sheet-flow conditions.

In order to achieve the objectives of the present study and to answer the research questions both laboratory experiments and theoretical research were carried out.

Five different series of experiments were performed in the Large Oscillating Water Tunnel (LOWT) of WL | Delft Hydraulics in order to get more insight into different aspects of the transport processes in the case of graded and uniform sands. The LOWT is a full-scale facility offering the possibility to study sediment transport processes under oscillatory flow conditions with and without a net current. Two different series of experiments were carried out with mixed sand and 2^{nd}-order Stokes waves. Net total transport rates and transport rates of each individual size-fraction were measured in order to study size-gradation effects on transport rates as well as size-selective behaviour of sediment mixtures. These mixed sand experiments aimed also to study sorting processes in the upper sand bed layer, the bed-load layer and in the suspension layer.

The other 3 series of experiments were performed using relatively uniform sands (D = 0.13, 0.34 and 0.97 mm). The coarsest and the medium sand size (D = 0.34 and 0.97 mm) experiments aimed to study mainly the grain-size effects on net transport rates under 2^{nd}-order Stokes waves. The experiments with the fine sand (D = 0.13 mm) were focused on the spatial and temporal details of the transport processes very close to the bed (inside the sheet-flow layer) under sine waves superimposed on net current. Moreover, the last set of experiments was focused on the influence of the wave-period on the transport processes.

The new obtained laboratory data were analysed with previous data from the LOWT and from the water tunnel of Tokyo University. The (complementary) datasets involving uniform as well as size-graded sands were then used to verify and improve various sediment transport model concepts. These transport models are based on different assumptions/backgrounds and include different processes.

The used models vary from the simple quasi-steady, to intermediate and fully unsteady models. The quasi-steady models assume a simple direct relation between the flow velocity and the sand transport rates (Bailard, 1981 and Ribberink, 1998). Intermediate models take into account the observed unsteady effects under sheet-flow conditions (phase-lag between flow velocity and sand concentrations) without any detailed description of the velocity and concentrations during the wave-cycle (Dibajnia & Watanabe, 1996 and Dohmen-Janssen, 1999). The last model is the fully unsteady POINT-SAND model of Uittenbogaard et al. (2000). A size-fraction approach is implemented in all these models in order to predict size-graded sand transport and composition of the transported sand.

Model verifications were carried out with uniform and size-graded sand and revealed the importance of several processes in the transport descriptions. Finally, improved model concepts for graded sand situation were proposed and verified using separate sets of experimental data.

1.5 Thesis layout

In the following *chapter 2* some basic knowledge is presented about cross-shore morphology, important hydrodynamic forces and transport modes in cross-shore direction and observations of grain-size sorting along the cross-shore profile.
Chapter 3 presents existing knowledge about sediment transport processes especially in case of graded sediments. Topics that are discussed are initiation of motion of sand grains, the various transport modes and specific sheet-flow processes. Moreover, knowledge from previous experimental studies on graded sand under sheet-flow conditions are discussed.
In *chapter 4*, the modelling of oscillatory sediment transport is discussed. Different classes of transport models are presented in detail. These models include quasi-steady models, intermediate models and the time-dependent POINT-SAND model. Moreover, an intercomparison between these transport models is presented.
Chapter 5 considers modelling of graded sand transport under oscillatory flows. A size-fraction approach is implemented in different transport models and the behaviour of the models is studied.
The experimental set-up of the five experimental programmes in the LOWT is presented in *chapter 6*. A description is given of the measuring programme, the LOWT, the measuring instruments, and the methods used for data analysis.
The main results of the laboratory experiments are presented in *chapter 7* also in comparison with existing datasets.
In *chapter 8* selected sediment transport models are verified with a large selected set of existing data with graded sand, focusing on the validity of the size-fraction approach.
In *chapter 9* a number of model improvements are proposed for the graded sand transport models based on the model verification results. Finally, the new improved models are verified with the remaining part of the existing data and the new dataset with graded sand, as obtained in the present research.
Finally, *chapter 10* presents overall conclusions of the present study and a number of recommendations for further research.

Chapter 2

CROSS-SHORE MORPHOLOGY AND SEDIMENT SORTING

2.1 Introduction

Coastal zone morphology is part of a dynamic system, taking place on different time-scales, with various interactions between hydrodynamic forces, beach materials and bed topography.

For reasons of simplicity the coastal zone can be divided into various cells or subzones each with it is own spatial and temporal scale. Water and sediment motions drive the morphology of each subzone. Gradients in sediment transport result in morphological change, which in its turn influences the water and sediment motion and leads to a continuous cycle of dynamic processes in each zone. This feedback system makes understanding of the marine sediment transport and coastal morphology a complicated matter.

This chapter introduces some basic knowledge about important cross-shore processes and cross-shore morphology (see also Hassan and Ribberink, 2000). Important hydrodynamic forces are described in section 2.2. An overview of the cross-shore profile shape as well as description of the transport modes are presented in section 2.3. Some field examples that show observed cross-shore sediment sorting on the Dutch coast are introduced in section 2.4. Section 2.5 gives a short description of available cross-shore morphology models. Finally, a short summary is presented in section 2.6.

2.2 Important hydrodynamic forces

Cross-shore morphological behaviour is a result of sequence of erosional and depositional events due to variations of hydrodynamic and sediment transport processes along the cross-shore profile. The most basic hydrodynamic forces in the near shore coastal zone are:

- Breaking waves and wave-induced currents in the surf zone and varying over the seasons under calm and storm conditions;
- Non-breaking irregular waves combined with tide-, density-gradient- and wind-induced currents in the shoreface zone seaward of the surf zone.

Waves moving in the near-shore zone play a dominant role. Waves processes are responsible for large oscillatory fluid motions, which drive currents, sediment transport and bed level changes. During its propagation to the shore, the relatively well-organized motion of offshore waves is transformed into several motions of different types, directions and scales, including small-scale turbulence, large-scale coherent vortex motions and oscillatory low frequency wave motions.

Waves entering shallow water are subject to shoaling, refraction, diffraction, bottom friction and breaking. Shoaling and breaking waves become asymmetric (peaked crests and shallow troughs) resulting in large onshore-directed velocities under the wave crest and small offshore-directed velocities under the wave trough.

Wave asymmetry increases with increasing relative wave height (H/h = wave height/water depth), which is of fundamental importance to the occurrence of net onshore-directed transport rates causing accretion of beaches. Moreover, wave asymmetry plays an important role in the grain-size composition of the transported material in both onshore and offshore directions. Figure 2.1 shows the transport process due to an asymmetric wave motion over a plane bed. Onshore velocity (u_{crest}) is higher than the offshore velocity (u_{trough}) resulting in a net onshore movement of the sand particles.

Non-breaking progressive waves generate an onshore drift very close to the seabed ($u_{b,on}$) and an onshore flux of water above the trough level of the waves ($u_{s,on}$). Because there is no net-flux of water in cross-shore direction, the average velocity at the intermediate elevations must be directed offshore to balance the two onshore fluxes. This *'undertow'* is directed offshore and will therefore generate an offshore-directed transport of sediment. Figure 2.2 shows the velocity profile outside the surf zone with $u_{m,off}$ representing the undertow velocity. This vertical variation in mean velocity directions and magnitudes plays an important role in the selective behaviour of different sediment sizes and the composition of the transported materials. Fine grains are picked up into the suspension layer away from the bed and are transported into the offshore direction with the undertow velocity. While, coarse grains are more likely to be transported close to the sand bed and are transported by the onshore drift into the onshore direction.

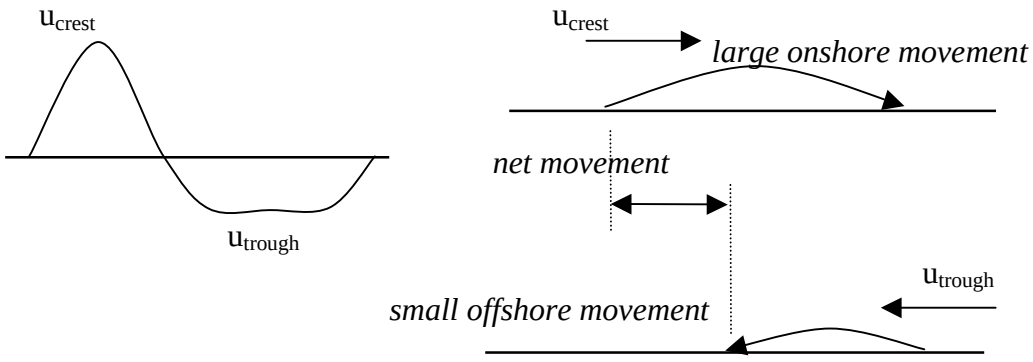

(asymmetric wave velocity) (net-transport in wave direction)

Figure 2.1: Sand transport process in asymmetric wave motion over plane bed.

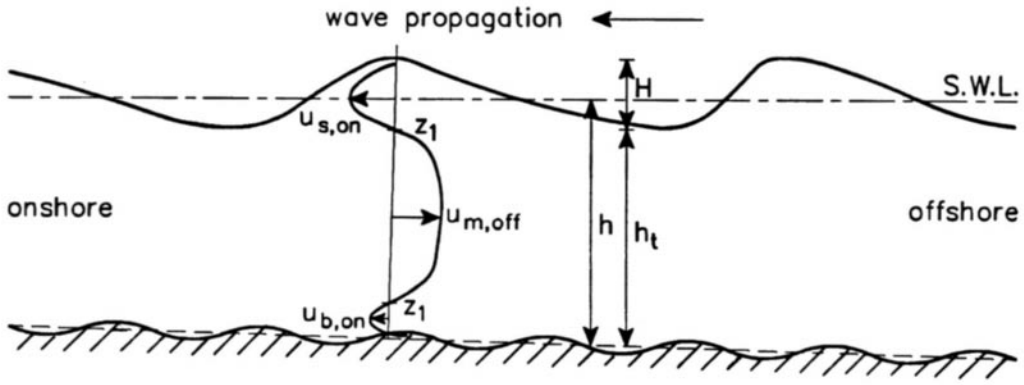

Figure 2.2: Velocity profile in cross-shore direction, $u_{b,on}$ is the drift velocity and $u_{m,off}$ is the undertow velocity (according to Longuet-Higgins, 1953).

Cross-shore bed slopes in combination with the earth's gravity generally generates an extra offshore-directed force on the sediment grains. In case of an equilibrium cross-shore profile the mechanisms described above should balance each other.

2.3 Cross-shore profile and transport modes

Generally, the cross-shore beach profile can be divided into dunes, beach, surf zone, shoreface and shelf. The shoreface is a morphological zone that lies between the shoreline and the inner continental shelf. This zone marks an important transition

between the morphology and associated processes of the shelf and those of the surf zone and beach. Many unsteady dynamic processes determine the shoreface morphology. Measuring these process in the field is difficult, because the shoreface zone is often too close to the shore for most research vessels, and too far from the beach to be studied using techniques normally applied in the surf zone.

A typical cross-shore profile for sand conditions is shown in figure 2.3. In cross-shore direction the coastal system between the shoreline and the shelf may be divided in the following subzones: upper shoreface (surf zone), middle shoreface and lower shoreface.

In the lower and middle shoreface zones the sand transport rates are relatively small and hence the response of the morphology is generally slow. In the upper shoreface where the waves are breaking the sand transport rates are relatively large and the response of the morphology is relatively fast, almost on the scale of the events (e.g. storms). Ripples usually are the dominant type of small-scale bed forms on the seabed in the upper, middle and lower shoreface zones. Both symmetrical wave-induced ripples and asymmetrical current-induced ripples may be generated, depending on the relative strength of the wave and current motions. Generally, the ripples in the upper and middle shoreface are washed out during storm events and sand is transported in big quantities in a thin layer close to the (flat) sand bed. This transport regime is called sheet-flow.

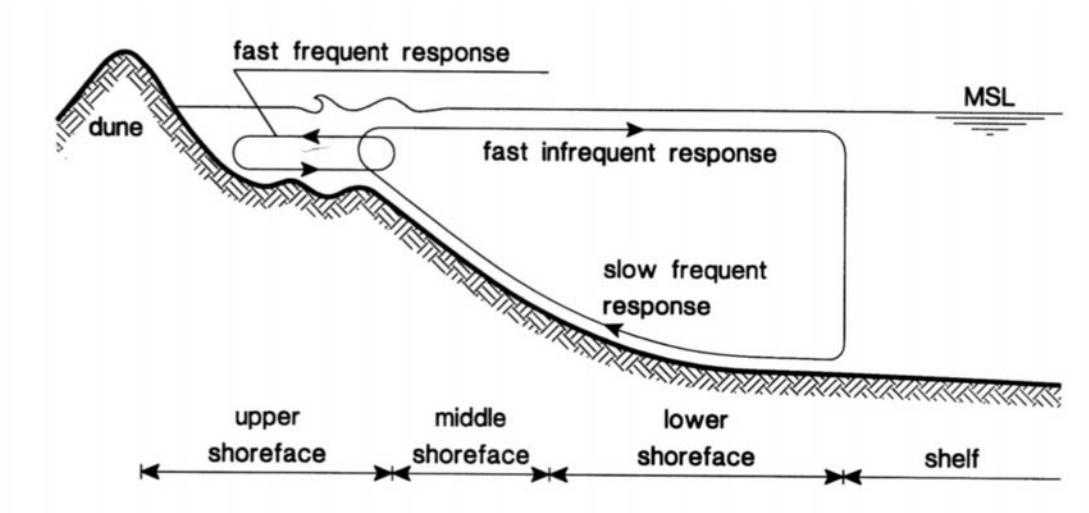

Figure 2.3: Cross-shore profile (after Short et al., 1991).

In deep water outside the breaker zone the sediment transport is generally concentrated in a layer close to the seabed in close interaction with small bed forms (ripples) and large bed structures (dunes and bars). Suspended load transport will become increasingly important with decreasing depth, increasing waves and

increasing strength of the tide- and wind-driven mean currents due to the turbulence-related mixing capacity.

In shallow water zones (swash zone and over the sand bars) the near-bed wave orbital velocities are relatively large and sand is commonly stirred and transported in a very thin layer above the bed in the sheet-flow regime. Figure 2.4 shows a schematic outline of the different transport modes, which may occur along a cross-shore profile during normal wave conditions. It is clear that sediment can be transported in different modes along the cross-shore profile, which can affect the magnitudes and the directions of the net sediment transport rates.

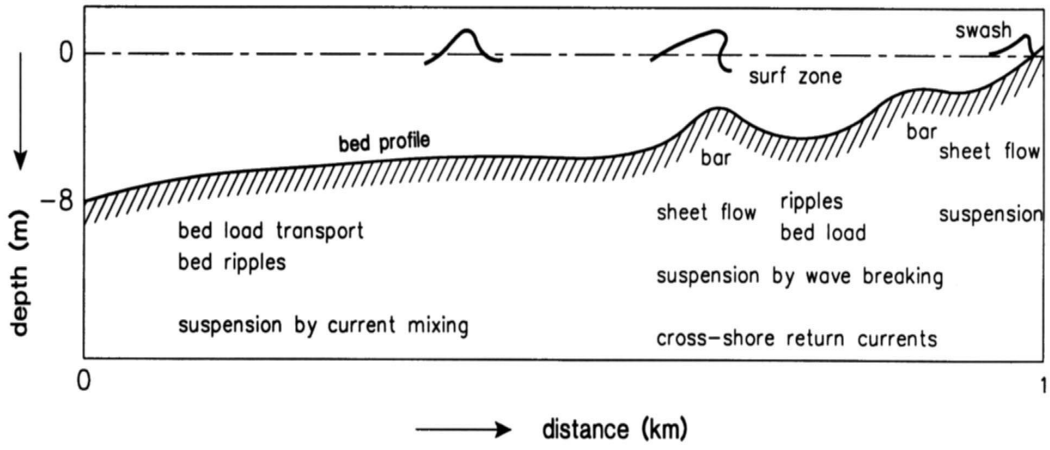

Figure 2.4: Sand transport mechanisms along a cross-shore profile (Van Rijn, 1998b).

In order to emphasize the relation between the sediment transport mode and the net transport rate (magnitude and direction), Van Rijn (1993) analysed laboratory data of Sato and Horikawa (1986) and Ribberink and Al-Salem (1991, 1994).

The measurements of Sato and Horikawa were carried out in the rippled-bed regime for regular asymmetric waves over a bed of 180 μm sand. The measurements of Ribberink and Al-Salem were mainly carried out in the plane bed/sheet-flow regime for irregular and regular asymmetric wave motion over a sand bed with almost the same grain-size (210 μm). Figure 2.5 shows the measured net cross-shore transport rate as a function of increasing wave orbital velocity.

The main conclusions from these results in figure 2.5 can be summarised as follows:

- The data of Sato and Horikawa show an increasing negative net transport rate (i.e. directed opposite to the direction of wave propagation) up to orbital velocities $\hat{u}_{crest} \approx 0.6$ m/s, when steep ripples are present;

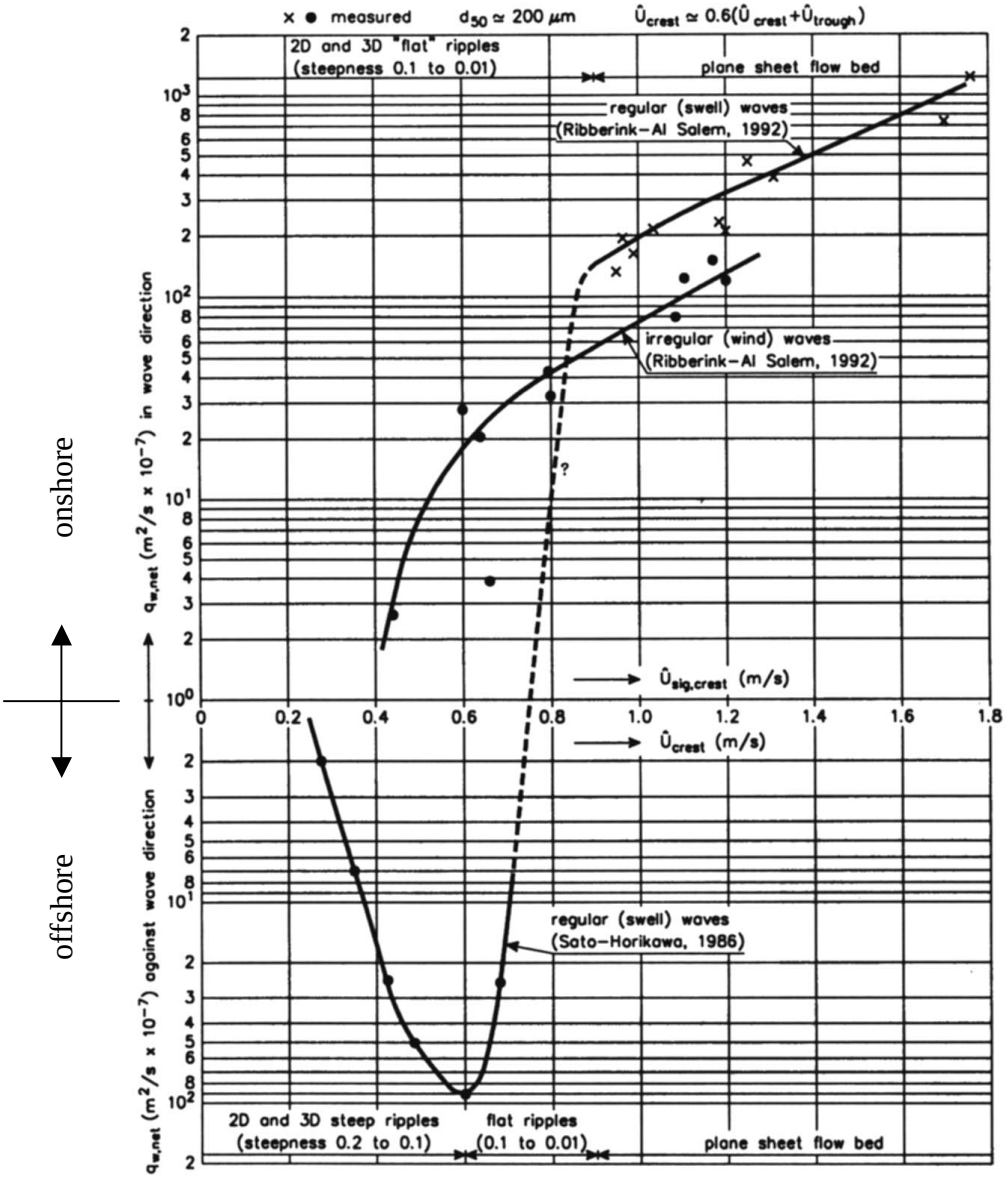

Figure 2.5: Measured net sediment transport rates in regular and irregular asymmetric wave motion (sand bed of 0.18 to 0.21 mm), Van Rijn (1993).

- The same data show that the net transport rates decrease considerably when the ripples are gradually washed out for $\hat{u}_{crest} > 0.6$ m/s;
- The results of Ribberink and Al-Salem show that for irregular asymmetric waves mainly plane beds and sheet-flow occur. Now positive net transport rate is found (in the direction of the wave propagation), which increases for increasing wave velocity;
- It seems that net transport direction is reversed from offshore to onshore in the velocity range $\hat{u}_{crest} \approx 0.7$ to 0.8 m/s, when the ripples are fully washed out;

- The absolute magnitude of the net transport rates under sheet-flow conditions are generally higher than under rippled-bed conditions.

This analysis shows that the net sediment transport rates and directions are highly dependent on the type of waves, bed form regime and associated transport modes. The limited understanding of these dependencies forms the main basis for the present research.

2.4 Cross-shore sediment sorting

Many researchers have observed and studied sorting of sediment grains along the cross-shore profile, for example Pruszak (1993), Liu and Zarillo (1987), Katoh and Yanagishima (1995), Guillen (1995) and Houwman and Hoekstra (1994).

Generally, cross-shore grain-size sorting studies show that the mean grain-size is greatest (coarsest) near the wave plunge point at the base of the beach face (slopes between 1 to 10 and 1 to 30). The mean grain-size decreases up the foreshore beach as well as down the offshore bottom. A slight coarsening of the sediments has been observed over the bar crests in the surf zone where the waves break.

Terwindt (1962) studied the grain-size variation and the effect of a storm event for location Katwijk along the Dutch coast, see figure 2.6. The data of Terwindt are based on samples collected in a summer period under different hydraulic conditions.

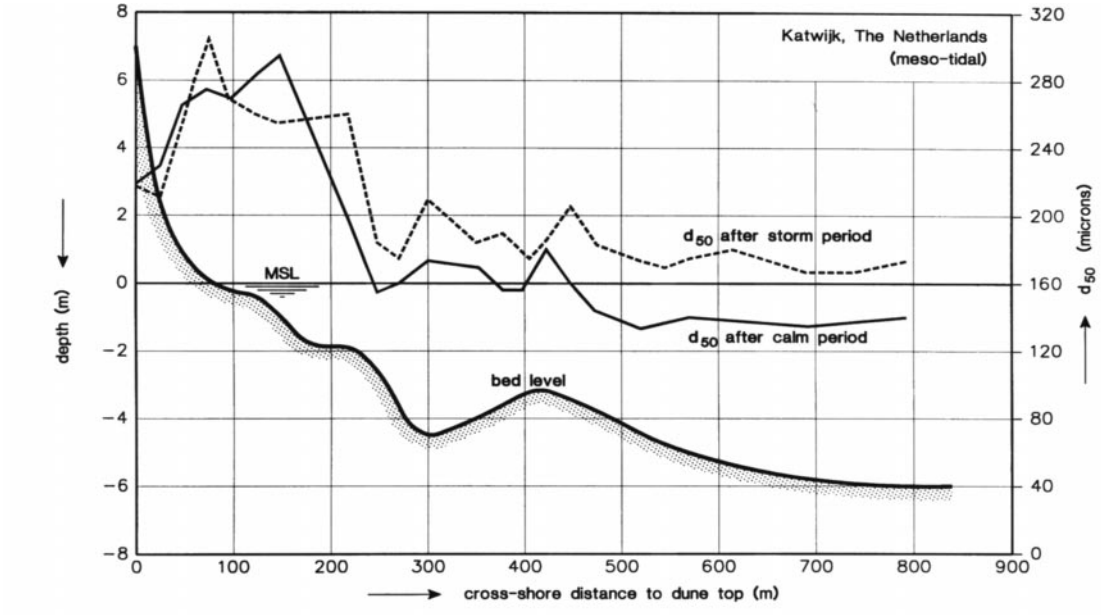

Figure 2.6: Sediment size variations along the cross-shore profile (location Katwijk, The Netherlands) during storm and calm conditions (Terwindt, 1962).

The cross-shore grain-size variations show the following:

- Coarse material (D_{50} of about 300 μm) is present in the shallow swash zone near the shore-line;
- Fining of sand from the swash zone (300 μm) to the dune top (220 μm);
- Fining of sand from the shallow water (300 μm) to the deep water (140 μm);
- The sand in the outer surf zone is found to be somewhat coarser (10% to 20 %) after a storm period.

Guillen (1995) analysed in detail grain-size data on the cross-shore profile of the barrier-island Terschelling on the Dutch coast. The results are presented in figure 2.7. Spring tidal range is 2.1 m. Offshore wave heights can be as large as 7 m during storm events. The surf zone consisting of fine sand (150 to 200 μm) shows the presence of multiple bar system (maximum heights of 3 to 4 m).

The grain-size data at the location of Terschelling show the following:

- Relatively coarse sand (230 μm) in the swash zone near the shoreline;
- Systematic fining of sand in seaward direction from 230 μm at the shoreline to about 150 μm at the outer edge of the surf zone;
- Systematic fining of sand in landward direction from 230 μm at the shoreline to about 190 μm at the dune foot;
- Alternating pattern of relatively fine sand in the trough zones and relatively coarse sand in the crest zones of the multiple bar system (grain-size difference of 5 % to 10 %);
- The grain-size fractions (see the lower panel in figure 2.7) show a seaward increasing percentage for the finer fractions (100 to 150 and 150 to 200 μm) and a seaward decreasing percentage of the coarser fractions; the coarsest fractions show peaks at the crests of the inner bars.

A qualitative explanation for sorting of particle sizes in cross-shore direction is that each grain-size-fraction responds differently to the same hydrodynamic condition (selective behaviour). Finer grains can be eroded from the bed in the most energetic areas by turbulent processes and are carried away to less energetic areas, resulting in coarsening of the bed in the more energetic areas.

In general terms, sorting of sediment particles in cross-shore direction is related to selective movement of sediment grains in a natural sand mixture. Bed sediment particles in the shoreface zone are fining in seaward direction due to offshore-directed bottom currents (rip- and storm-induced currents). Sometimes, relatively coarse grains are found on the shoreface.

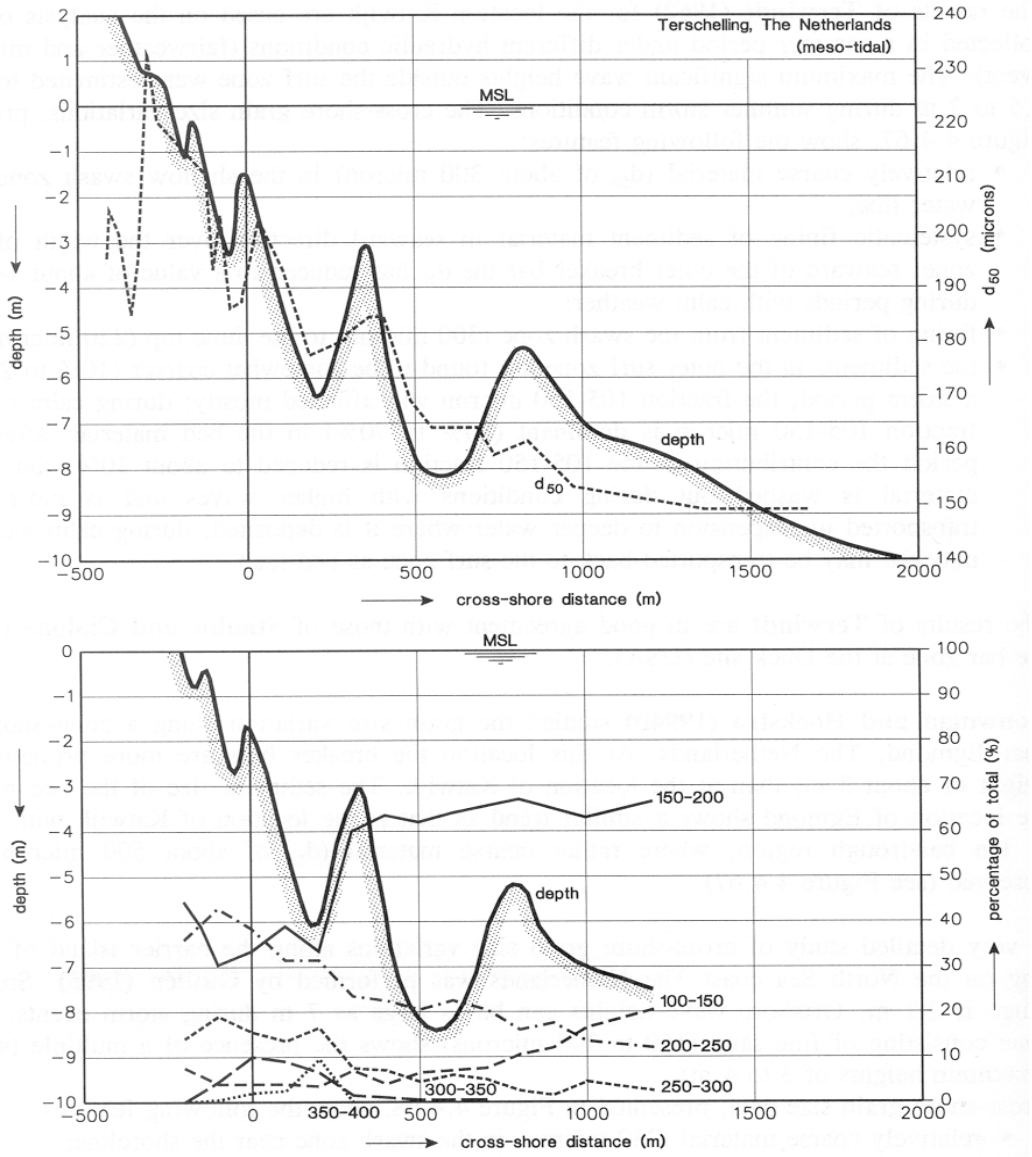

Figure 2.7: Sediment-size variation along the cross-shore profile (location Terschelling, The Netherlands); top panel: median-size (D_{50}) distribution; lower panel: size-fraction percentages (Guillen, 1995).

2.5 Modelling of cross-shore morphology

Field observations show that the sediment bed of the coastal zone usually exhibits a large variation of sediment sizes (see, section 2.4). Although cross-shore sorting due to selective transport processes is a process observed in nature, most of the available cross-shore morphology models do not take into account these sorting processes. In fact, these effects can only be represented by taking the full size composition of the seabed material, which may vary across the profile, into account.

Recently a range of useful mathematical model concepts has been developed (Van Rijn, 1998b), which can be classified into two broad categories: behaviour-related models and process-related models. The ultimate objective of morphological modelling is to describe the long-term behaviour of morphological features of water systems in relation to human interference and climate changes.

Behaviour-related models describe the behaviour of morphological features using relatively simple expressions formulated to represent the phenomena at the large scales of interest (time-scale of centuries up to geological time-scales). In this type of models all process-related information and additional empirical information is represented by coefficients or parameterised functional relationships. Long-term datasets are indispensable for calibration of the model coefficients and of these functional relationships. A review has been given by de Vriend et al. (1993).

On the other hand the process-related models are based on a detailed description of all relevant processes. By implementation of a series of submodels representing wave propagation, tide, wind, wave, density-driven currents, sediment transport and bed level changes in a loop system, the dynamic interaction of the processes are included (spatial scale up to 10 km, time scale up to 10 years). Process-related cross-shore models of various degrees of sophistication have been developed by Dally and Dean (1984), Stive (1986), Roelvink (1993), Roelvink et al. (1993) and Van Rijn (1997a, b).

Van Rijn (1997b) studied cross-shore sorting of sediment mixtures using a process related model (CROSMOR) in order to compute the hydrodynamics, the sand transport rates, the bed composition and bed evolution based on a multi-wave and a multi-sediment fraction approach in cross-shore direction. Sensitivity computations using a single-fraction and multi-fraction method were made for various conditions with a constant water depth and with a barred cross-shore profile (Duck-site, USA; Katwijk-site, The Netherlands).

Van Rijn concluded from this study that sorting processes occur when the cross-shore profile consists of graded sediments. Each grain-size fraction within a mixture will respond differently to the same hydrodynamic regime. The bed-load transport rates of sediments between 0.2 and 0.8 mm based on a multi-fraction method are slightly to significantly larger than those based on a single-fraction method. The suspended-load transport rates of the multi fraction method are significantly smaller than those of the single fraction method at small current velocities. The migration rates of breaker bars is significantly affected by the number of size-fractions and the modelling of selective transport processes.

This study shows that including the size composition of the bed material in sediment transport and morphological models may be of great importance for the simulation of cross-shore morphology.

2.6 Summary

Chapter 2 gave a general qualitative overview of some of the important processes, which control cross-shore morphology. A description is given of the most important hydrodynamic forces, and the main sediment transport processes including grain-size sorting along the cross-shore profile. Finally, the last section presented some experiences of existing cross-shore morphology models. The main outcome of this inventory can be summarised as follows:

- On the shoreface waves are responsible for the dominant hydrodynamic forces in the cross-shore direction. Wave processes generate large oscillatory fluid motions, drive net currents and sediment transport during their propagation to the shore;
- Wave asymmetry is of fundamental importance for cross-shore transport and often leads to a net onshore-directed sediment transport causing accretion of beaches. Moreover, wave asymmetry plays an important role in the composition of the transported material in both ‘onshore’ and ‘offshore’ direction;
- Also wave-generated mean velocities such as onshore drift near the seabed and offshore directed undertow (see figure 2.2) probably play an important role in the selective behaviour of different sediment sizes and the composition of the transported materials. Coarse grains are likely to be transported close to the bed in onshore direction while fine grains can be transported in the offshore direction in the suspension layer;
- Based on the magnitude and character of the near-bed wave induced oscillatory flows sediment can be transported in different modes (ripples and sheet-flow) along the cross-shore profile. The net sediment transport rates and directions are highly dependent on these bed form modes;
- Field observations show that there is a variation in bed material sizes along the coastal profile. It is very likely that these variations, called grain-size sorting, can be explained by selective transport processes. At present there is little known about net cross-shore sediment transport and its relation with grain-size selective transport mechanisms during storm conditions (sheet-flow conditions);
- Although including the grain-size composition is probably important for cross-shore morphology models, most of these available models assume uniformity of sediment and do not account for size-composition changes of bed material due to selective transport. This can be explained by the present existing lack in our knowledge about transport mechanisms of size-graded sand.

For the development of grain-size selective cross-shore morphology models (e.g. multi-fraction models) reliable models for the prediction of total net transport rate as well as of grain-size composition of the transported sediment are needed. The next chapter will give a general overview of sediment transport processes with a special focus on transport of graded sand under the influence of waves. More details about oscillatory sediment transport models will be given in chapter 4.

Chapter 3

SAND TRANSPORT PROCESSES AND SIZE GRADATION

3.1 Introduction

It was shown in chapter 2 that a variation in bed material sizes along the cross-shore profile is generally observed. Considering the dynamic character of the coastal profile it is likely that these variations, called sorting, are due to selective transport processes. Selective transport occurs when sediment particles in a mixture react differently to the water flow. For understanding the transportation of the graded sediment clearly a profound understanding of the different sorting processes is needed. Slingerland (1984) distinguished the following four different types of sorting processes:

- Entrainment sorting: difference in the threshold velocity to initiate motion of different grain-sizes;
- Shear sorting: vertical sorting resulting in a layered structure of the bed by interactions between sediment grains;
- Suspension sorting: separation of suspended sizes in the water column by different settling velocities;
- Transport sorting: separation of sediment particles due to differences in transport velocity, entrainment and suspension sorting.

These transport processes in case of graded sediment and other important transport processes will be described briefly in the following sections (see also Hassan and Ribberink, 2000). Section 3.2 introduces basic information about initiation of motion of sediment particles in a mixture. Short descriptions of the different transport modes

and the sheet-flow transport regime are presented in section 3.3. Phase-lag effects and its importance under oscillatory sheet-flow conditions are presented in section 3.4. Section 3.5 gives a description of the vertical structure of the active bed layers. The distribution of suspended particles and grain-size sorting in the water column are presented in section 3.6. Section 3.7 introduces some measured experiences with effects of the size-gradation on the transport modes. Finally, section 3.8 presents a short summary and the main conclusions of chapter 3.

3.2 Initiation of motion

3.2.1 Uniform sediment

Sediment grains start to move on the bed when the combined lift and drag forces produced by the fluid become large enough to counteract the gravity and frictional forces that hold the grain in place. In nature (graded sediment), it is very complicated to define the balance of forces acting on grains. Some grains lie in positions from which they are moved more easily than others do. It is equally impossible to define a single fluid force that applies to all grains: some grains are more exposed to the flow and subjected to larger fluid forces than other grains. The hydraulic conditions near the bed (nearly uniform flows) can be expressed by the grain Reynolds number ($R_e = u_* D/\nu$, in which u_* = shear velocity, D = grain diameter and ν = kinematic viscosity).

The bed shear stress (τ_b) exerted by the fluid on the bottom is particularly easy to measure with steady flow. In case of turbulent steady uniform flows the following empirical relation between bottom friction and flow velocity can be used:

$$\theta_b = \frac{1}{2}\rho\, f_c\, \bar{u}^2 \qquad (3.1)$$

where: θ = the depth-averaged velocity; ρ = fluid density and f_c = friction coefficient.

This empirical coefficient (f_c) is related to the bottom roughness expressed in terms of roughness height k_s (the Nikuradse roughness height). There are various expressions in the literature to calculate k_s depending on the nature of the bed morphology. When bed forms, like ripples, are present, k_s is directly related to the height and length of such structures. However, in a flat bed situation the roughness is determined by the sediment grain size. Used values for k_s in such cases vary from D_{50} to $3D_{90}$ in case of a moving bed.

For waves an equation for the bed shear stress and its peak value is used that is similar to the one for steady uniform flow:

$$\theta_b = \frac{1}{2}\rho\, f_w\, u_b|u_b| \qquad \text{hence} \qquad \theta_{b,max} = \frac{1}{2}\rho\, f_w\, \hat{u}_b^2 \qquad (3.2)$$

where: f_w = the wave friction factor, u_b = time-dependent horizontal near-bed orbital velocity and $\hat{u}_b$ = amplitude of the horizontal near-bed orbital velocity.

The wave friction factor depends on the relative bottom roughness, expressed as the ratio between the Nikuradse roughness height k_s and the semi-excursion length of the water particles $\hat{A}_b = \hat{u}_b T / 2\pi$ (T is the wave-period). Based on the data of Jonsson (1966) the following expression was found:

$$f_w = \exp[-6 + 5.2\,(\hat{A}_b/k_s)]^{-0.19} \qquad \text{with} \qquad f_w \leq 0.3 \tag{3.3}$$

The classical approach of describing the ability to move sediment grains is the one by Shields (1936); in a study of incipient sediment motion in steady flow Shields used the ratio of shear stress to normal stress to determine the ability to move sediment grains. This ratio is known as the Shields parameter and reads:

$$\theta(t) = \frac{\theta_b(t)}{(\rho_s - \rho_w)gD} \tag{3.4}$$

where: θ = Shields parameter; τ_b = bed shear stress; ρ_s = density of sediment; ρ_w = density of water; g = gravity acceleration and D = grain-size.

In connection with wave motion a maximum Shields parameter (corresponding to total stress) is generally used in terms of the peak bed shear stress $\hat{\tau}_b$:

$$\hat{\theta} = \frac{\theta_b}{(\rho_s - \rho_w)gD} \tag{3.5}$$

Many experiments have been performed with uniform sediments to determine the relation between critical Shields parameter and Reynolds number, $\theta_{cr} = f(R_e)$, see Shields (1936), Bonnefille (1963), Yalin (1972) and Madsen & Grant (1976). This relation can also be represented as a function of a dimensionless particle diameter D_* that incorporates the density and diameter of the sediment grain (see figure 3.1). The definition of D_* can be found in equation 4.8. It is clear that the Shields parameter is proportional to D^{-1}, which for a constant critical (threshold) value θ_{cr} indicates the relatively smaller mobility of larger particles and larger mobility of small particles. The gray dashed zones in figure 3.1 show the ranges of the Shields parameter representing initiation of motion (according to Shields) and initiation of suspension (according to Van Rijn).

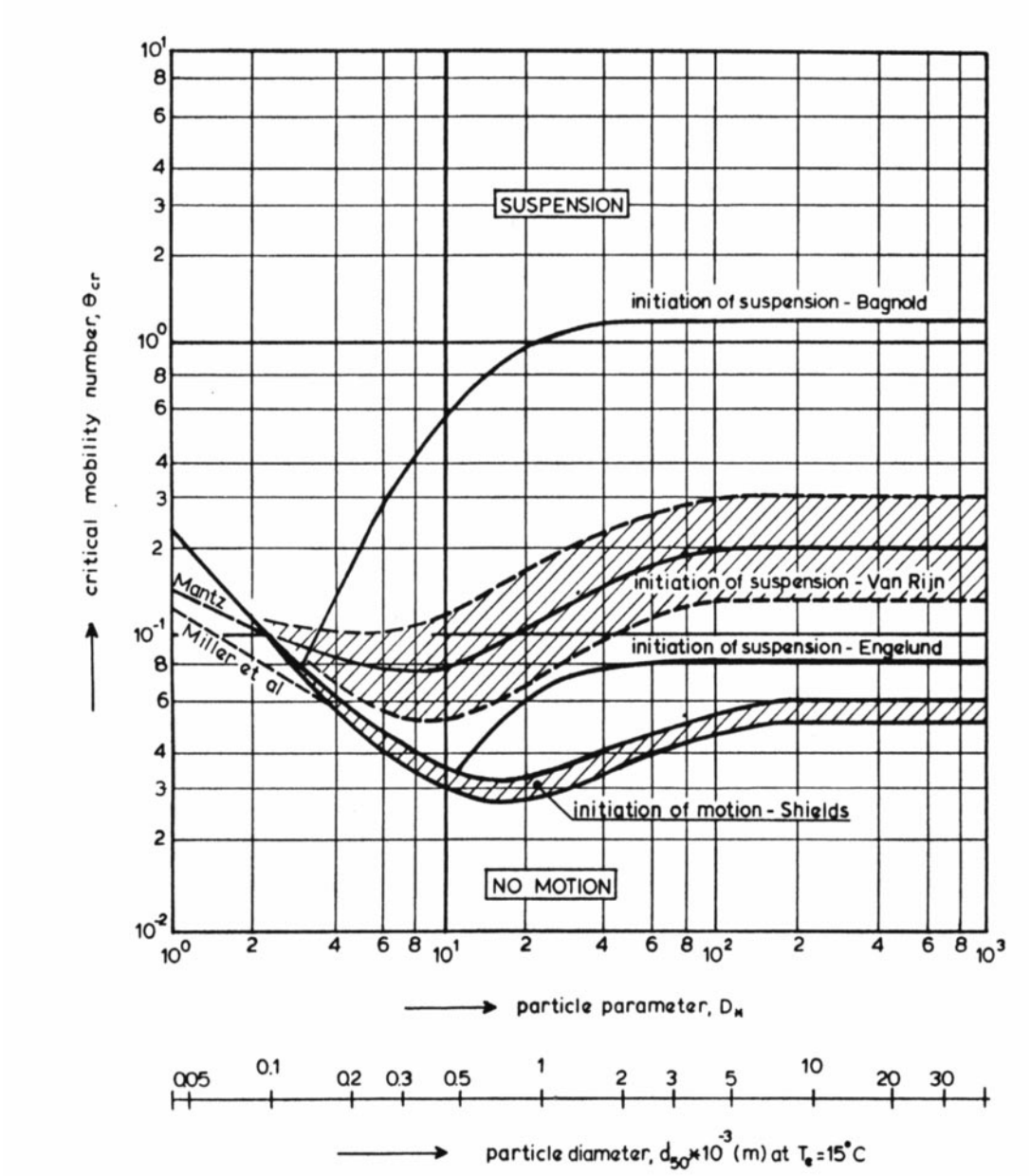

Figure 3.1: Initiation of motion and suspension for a current over plane bed, θ_{cr} = f (D_*), Van Rijn (1989).

In oscillatory flow there is no generally accepted relationship for initiation of motion on plane bed. Many equations have been proposed. Van Rijn (1989) analysed different data to describe a critical velocity amplitude $\hat{U}_{\delta,cr}$ as a function of the particle size D_{50} and the wave period T. Figure 3.2 shows the results of experiments with sand particles (ρ_s = 2650 kg/m^3) and wave periods in the range of 4 to 15 seconds. This represents a particle size range from 90 to 3300 μm. The data show a clear increase of $\hat{U}_{\delta,cr}$ with increasing wave period T.

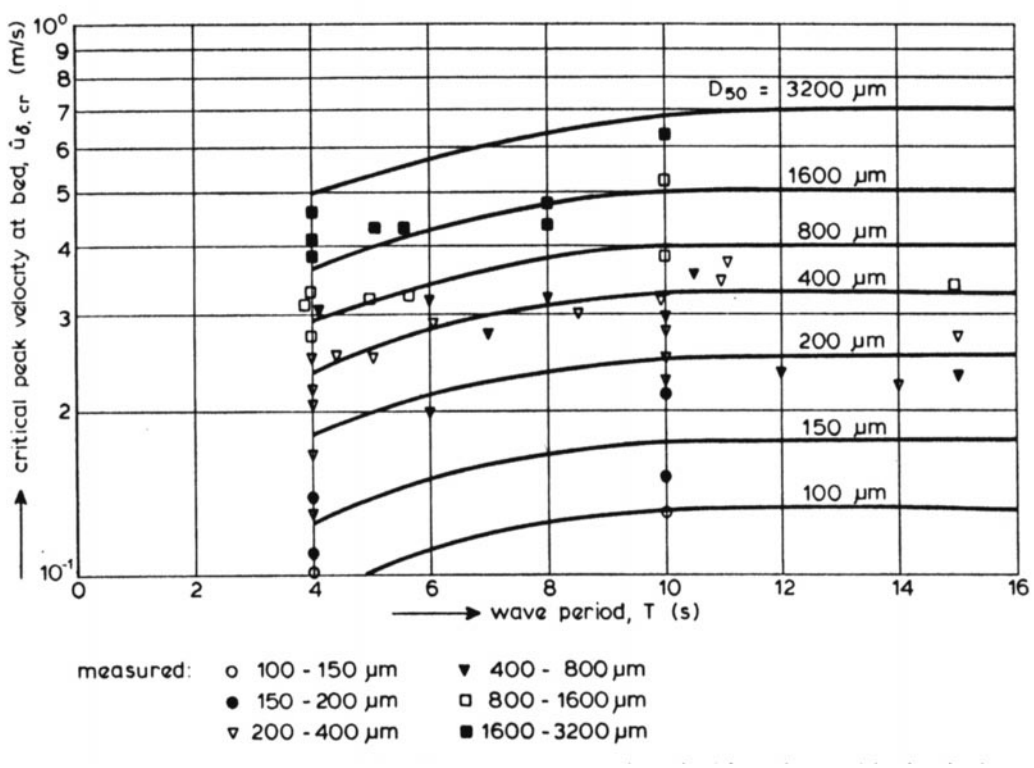

Figure 3.2: Initiation of motion for waves over a plane bed based on critical velocity (Van Rijn, 1989).

3.2.2 Graded sediment

A basic question appears when the sediment is not uniform (natural sediment): does the initiation of motion of a particular size-fraction in a mixture occur at the same critical velocity $\hat{U}_{\delta,cr}$ as found for uniform material of the same size? Coarse particles can be more exposed to the flow and fine particles can be sheltered by the coarse particles in the sand mixture, resulting in different critical Shields parameters for each fraction (exposure effects). Very little is known about the size-gradation effect on the initiation of motion under waves.

Normally, the bed material contains grains of a range of sizes. Particles with different sizes influence each other. Large grains are often more exposed to the flow. In combination with a larger surface area this leads to a higher drag force. On the other hand these large particles have a larger weight. The large grains often shelter the fine particles, which is called hiding effect. Figure 3.3 illustrates the hiding/exposure of the different grain-sizes.

There is no information about hiding and exposure of sediment particles under waves. All the available information is related to steady flows only. Modelling of hiding/exposure effects will be described in detail in chapter 9.

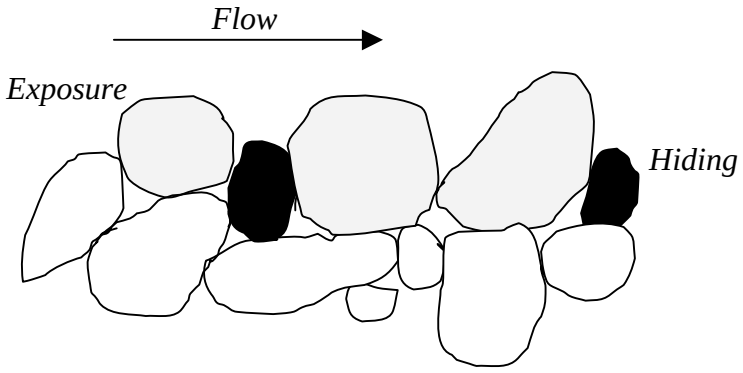

Figure 3.3: Hiding/exposure of sediment particles in a mixture.

The degree of exposure of a grain with respect to surrounding grains obviously is the most important parameter for determining the bed-shear stress for initiation of motion, as shown by Fenton and Abbott (1977). They studied the effect of relative protrusion (p/D = protrusion of a particle above others/grain diameter) on the initial movement of grains in the transitional and fully turbulent regime. They used two types of grains: 2.5 mm angular polystyrene grains and 5 to 10 mm well-rounded pea gravel. The critical bed shear stress for incipient motion was found to decrease for increasing positive relative protrusion and to increase for negative relative protrusion. The protrusion p of a grain is measured relative to the top of adjacent sediment grains.

Figure 3.4 shows the critical bed-shear stress as a function of particle diameter based on uni-directional flow measurements of Wilcock (1993), Wilcock et al. (1988) and Petit (1994) for unimodal sediment mixtures. The Shields curve for uniform sand is also shown. From these results we can notice the following:

- Most of the data refer to relatively coarse sediment materials (D > 1 mm);
- The curves intersect with the Shields curve (uniform sediment) at approximately the median diameter (D_{50}). As regards the data intersecting with the Shields curve, the larger sizes are set into motion at bed shear stresses that are smaller than the required for uniform sizes, while the smaller size fractions require higher bed shear stresses the uniform material. This can be explained by changes in flow exposure of sizes in a mixture;
- A slightly larger critical bed-shear stress is observed for the coarser fractions within a mixture;
- More experimental data are needed to determine the critical bed shear stress of mixtures in the fine sand range (0.1 mm < D < 0.6 mm).

The available data of figure 3.4 can be used to derive the exposure or hiding correction factor for particles in a sand mixture.

In case of graded sediment and a bed shear stress that is not large enough to move the largest particles of the bed material, partial transport may lead to armouring. When there is no upstream supply of smaller particles, most of the smaller particles will eventually be eroded, and the coarser particles will form an armor layer, preventing any further erosion.

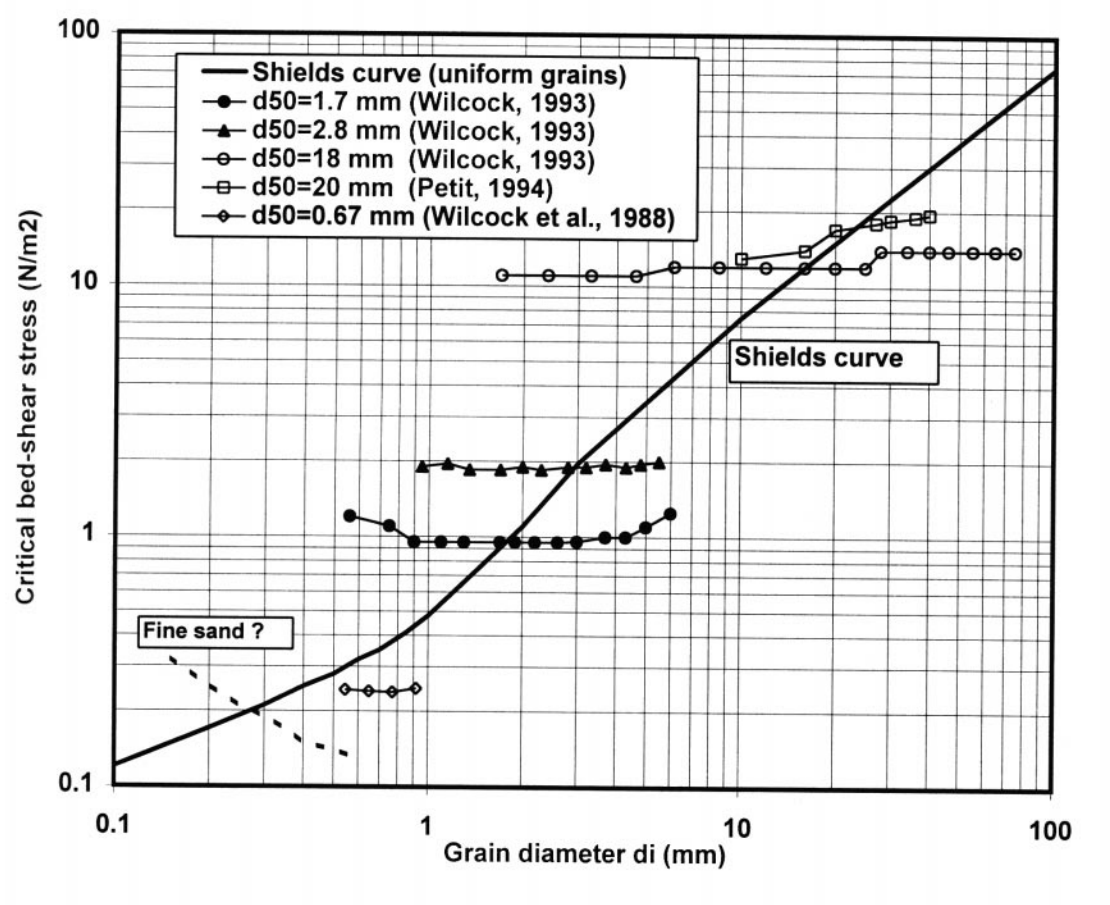

Figure 3.4: Critical bed-shear stress of individual size fractions in a sand mixture as a function of grain diameter (modified after Wilcock, 1993).

3.3 Transport modes and sheet-flow under waves

In offshore waters outside the surfzone with breaking waves sediment transport processes are generally concentrated in a layer close to the seabed. Sediment is being stirred by the wave orbital motion and transported by wave asymmetry and/or mean currents.

When waves exert a small force on a movable bed, i.e. very small values of the Shields parameter, there is no sediment motion. The critical Shields parameter for the

initiation of sediment motion depends on the sediment size and the sediment density; see section 3.2. For natural conditions the critical Shields parameter varies between 0.03 and 0.06. For increasing Shields parameter, the sediment particles start to roll, slide and jump over each other, but the bed remains flat. Because the sediment particles are in almost in continuous contact with the bed and with each other, intergranular forces are important. This is called the bed load regime. The bed load layer is usually assumed to be only a few grain diameters thick.

If the Shields parameter increases further bed forms are developed, ranging from small vortex ripples to large mega ripples and dunes. The transport over vortex ripples can be either bed-load transport or suspended-load transport. Fine sediment particles are generally carried into suspension by vortices generated behind ripple crests (flow separation), which results in very different transport mechanisms compared to the mechanisms in the bed-load regime. According to Grant and Madsen (1982) ripples can go through two distinct stages. The first stage is known as the equilibrium stage, in which the flow is relatively slow (u_{max} < 0.3 m/s) and sediment transport is low. Both ripple height and ripple length tend to increase until ripple steepness and ripple roughness reach their maximum. As flow strength is further increased, ripples enter the second stage defined as break-off range. When this break-off range is reached, the ripple height will decrease while the ripple length stays roughly constant or decreases slightly. This will lead to a decrease in ripple steepness and ripple roughness. Figure 3.5 shows a classification diagram given by Allen (1982), which is based on 648 data sets. Ripples occur where the near-bed orbital velocity is about 1.2 times the critical velocity for initiation of motion.

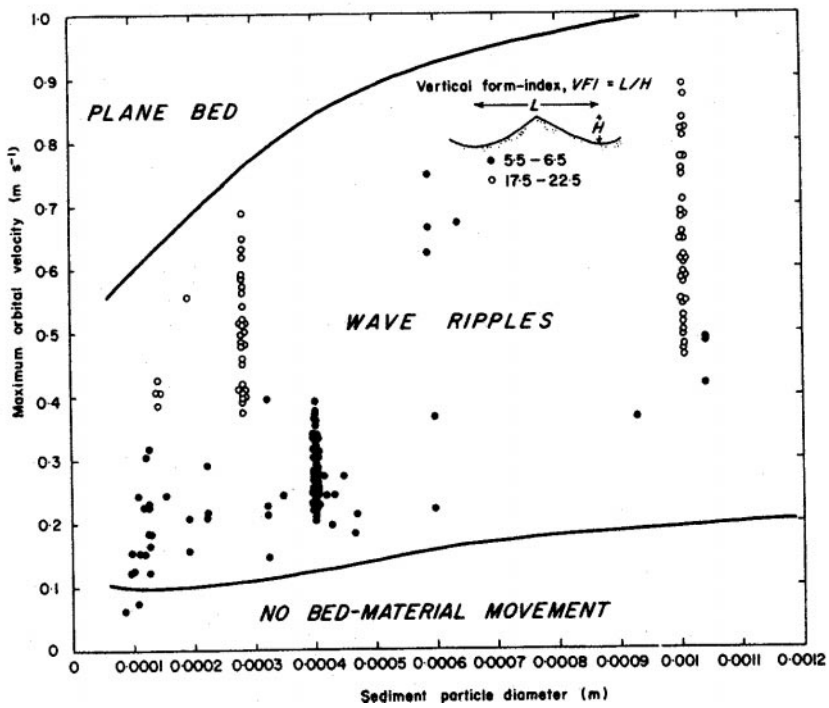

Figure 3.5: Bed form classification diagram for waves, Allen (1982).

As flow strength and Shields parameter are further increased ripples are washed out and the bed becomes plane again. A thin layer with high sand concentrations is moving in a sheet along the bed. This is called sheet-flow. The thickness of the sheet-flow layer is generally much larger than a few grain diameters (10-100 grain layers) and grains are not just rolling, sliding and jumping over each other. Nevertheless, the concentrations are so high, that intergranular forces and grain-water interactions are important. According to Wilson (1987), the sheet-flow regime occurs when $\theta > 0.8$.

As an illustration of oscillatory sheet-flow figure 3.6 shows the time-dependent concentration behaviour in the sheet-flow layer as observed in the LOWT of WL | Delft Hydraulics, Katopodi et al. (1994). The experiments were performed using uniform sand with D_{50} = 0.21 mm under combined wave-current flow. The flow velocity above the wave boundary layer is shown in the upper panel (measured at 100 mm above the bed) and the sand concentrations at different levels are shown in the lower panel. Note that the initial bed level is used as a reference (z = 0).

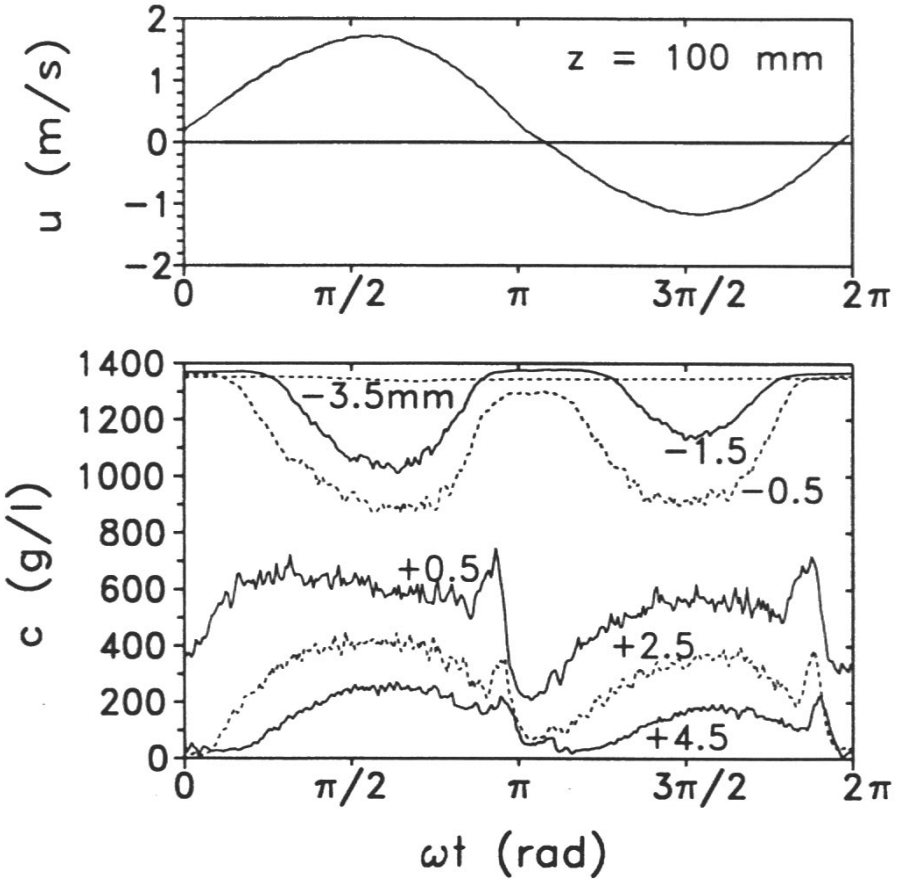

Figure 3.6: Time-dependent sediment concentrations inside the sheet-flow layer, for combined wave-current flow and uniform sand D_{50} = 0.21 mm (data of Katopodi et al., 1994).

From figure 3.6 we can observe the following concentration behaviour:

- Below a certain level ($z \leq -3.5$ mm) the concentration remains constant throughout the wave-cycle, indicating that no sediment is moving below this level;
- For $-1.5 < z < -0.5$ the concentration is maximum at zero velocity and minimum under the maximum velocity (positive or negative). At these levels the concentration is decreasing for increasing velocities, because sediment is being picked up from the bed. When the velocity decreases the sediment particles settle back on the bed and the concentration increases again. Therefore, this layer is called the pick-up layer. It is located below the initial bed level;
- At higher levels, $z \geq +0.5$ mm, the concentration is minimum at zero velocity and maximum under the maximum velocity (positive or negative). The increase in concentration for increasing velocity is caused by the fact that sediment is entrained into the flow. When the velocity decreases the sediment settles down to the bed and the concentration decreases again. This layer, called the upper sheet-flow layer, is located above the initial bed level;
- The change in the sediment concentration behaviour in the pick-up layer and the upper sheet-flow layer reflect the exchange of sediment particles between these two layers (see also Al-Salem, 1993 and Dohmen-Janssen, 1999);
- Sharp peaks in concentration are observed just before flow reversal. These peaks are present in the upper sheet-flow layer and not in the pick-up layer.

The present study focuses on sand transport in the sheet-flow regime. Transport mechanisms due to the presence of bed forms are not considered in the present study.

3.4 Sheet-flow and phase-lag effects

It is known that in steady flow sand transport rate is proportional to a power of the velocity, larger than one. If the sand transport reacts instantaneously to changes in velocity the same would hold for sand transport in oscillatory flows. The reaction can be considered instantaneous if the sediment concentration reacts instantaneously to changes in the velocity or more general if the phase-lag between the sediment concentration and the velocity is small compared to the time scale at which the velocity varies, i.e. the oscillation period T. In that case the sand transport rate in oscillatory flows behaves quasi-steady and is again proportional to the power of the instantaneous velocity. Moreover, under this assumption net transport rates will be generally in the direction of the largest velocity in oscillatory flow conditions. Many existing sand transport models in oscillatory sheet-flows are based on the assumption of instantaneous sediment response. These types of models are called quasi-steady models and are presented in chapter 4.

However, Ribberink and Chen (1993) found that for fine sand and large asymmetric oscillatory velocities the net transport rate could be against the direction of the

largest velocity, even under sheet-flow conditions. Figure 3.7 shows measured net transport rates of Ribberink and Chen (1993) versus flow velocity (root-mean-square value U_{rms}), of fine sand experiments (D_{50} = 0.13 mm) with asymmetric 2nd-order Stokes oscillatory flows.

It is also shown in figure 3.7 that under the same flow conditions the net transport rates of somewhat coarser sand (D_{50} = 0.21 mm) are still positive, i.e. in the ('onshore') direction of the largest velocity. Ribberink and Al-Salem (1994) show that for this sand the transport is proportional to the third power velocity moment (Ribberink and Al-Salem 1994). For the 0.13 mm sand the response time of the sediment particles is not small any more compared to the oscillatory period and the concentration significantly lags behind the flow velocity. This is caused by the fact that both sediment entrainment into the flow and settling of the particles back to the bed are time-dependent processes. They depend on the settling time of a particle and on the height to which the particle is entrained into the flow. It is clear that the results of Ribberink and Chen (1993) violate the assumption of quasi-steadiness of sediment transport in oscillatory flows.

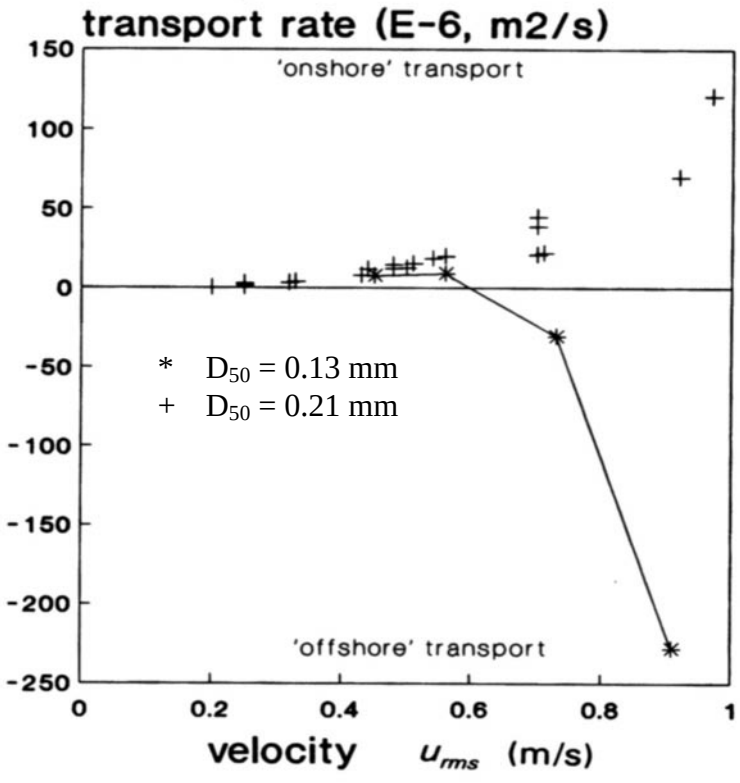

Figure 3.7: Measured net transport rates versus U_{rms}, (*) data of Ribberink and Chen (1993) D_{50} = 0.13 mm, (+) data of Ribberink and Al-Salem (1991) and (1992) D_{50} = 0.21 mm.

The negative net transport rates are explained as follows.
Under asymmetric oscillatory velocity (with a crest and a trough half wave-cycle) the flow velocity in the crest direction is higher than in the trough direction. The sediment particles can be stirred up during the crest part to such a high level that they can not settle to the bed within the same crest part of the wave-cycle. A part of the sediment particles will remain in suspension and will be transported in the opposite direction during the successive trough part of the wave-cycle. If the settling time of a sediment particle is larger than the part of the wave period in which it is stirred up, it is very likely that these so-called unsteady or phase-lag effects will occur.

Phase-lag effects are expected to be important for large flow velocities, fine sand and small wave periods. This can be explained as follows:

- The larger the flow velocity and the smaller the grain-size, the higher the sand will be entrained into the flow;
- The finer the sand (and the smaller the settling velocity) the more time is required for sand particles to settle back to the bed;
- The smaller the wave period, the faster the variation in velocity and thus the smaller the available settling time for a particle before the flow reverses and starts to accelerate again in opposite direction.

The importance of phase-lag effects can therefore be characterised by the ratio of the required settle time (t_{settle}) of a particle to the available settle time, determined by the wave period T. The required settling time is equal to the height δ to which a particle is entrained into the flow, divided by its settling velocity. Dohmen-Janssen (1999) found that the maximum flow velocity and the grain-size mainly determine the height δ (see equation 4.23). The phase-lag effects can be characterised by the following parameter:

$$\frac{t_{settle}}{T} = \frac{\delta / w_s}{T} = \frac{\delta}{w_s T} \tag{3.6}$$

Some transport models take into account the phase-lag effects on the net transport rates without detailed simulation of flow velocities and concentrations over the water column. These models are called intermediate or semi-unsteady transport models. These models will be described in detail in chapter 4.

3.5 Dynamics of upper bed layers

During sediment transport due to currents (like in rivers) vertical sorting takes place in the upper layers of the sand bed (active layer). The sediment grains that take part in the transportation process are present in this layer. Finer particles are generally dominating in the upper layers and coarser particles are dominating in the lower

layers (figure 3.8). For example, coarse particles are generally present at the trough level of bed forms (see Ribberink, 1987, Blom et al., 2003 and Kleinhans 2002).

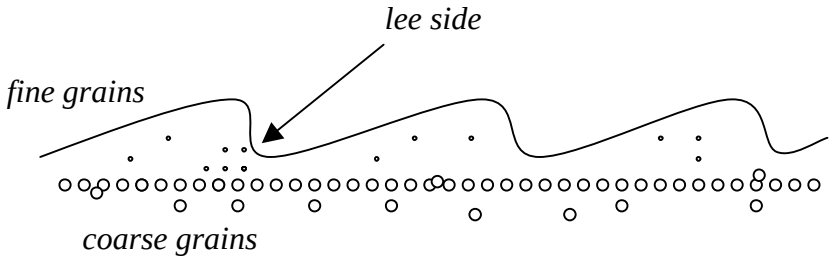

Figure 3.8: Vertical-sorting of grain-sizes in case of bed forms (propagating dunes).

There is hardly any knowledge about vertical bed sorting under wave conditions. Present knowledge is based on sediment transport due to currents only. The principle of vertical sorting is that the combined fluid/sediment motion creates a reorganization of grain-sizes in the upper bed layers leading to a kind of stratified bed. Due to this change the sizes become differently exposed to the flow (i.e. sizes which are mainly present deep in the bed are most of the time covered by other sizes and therefore less exposed). In the case of propagating dunes in rivers the following vertical sorting mechanisms are known (see Blom et al., 2003):

- Avalanching due to gravity at lee side of dunes, coarse grains fall deeper than fine grains;
- Selective entrainment of finer sizes that move as bed forms on top of coarser sizes, which are not transported.

Whether vertical sorting occurs and how it occurs in the flat bed/sheet-flow regime is not known.

In fact, due to this lack of understanding of basic processes mathematical modelling of the near bed sediment dynamics of graded sand in the sheet-flow regime is still problematic. Generally, the available models are based on dividing the bed material into an active or transport layer, which is exposed to the flow, and a non-moving bed, e.g. the model of Ribberink (1987). The thickness of the active layer (transport layer) depends on the bed configuration, e.g. flat bed or bed forms, and is usually calculated with an empirical formula for the bed form height. Blom (2003) propose a new depth-continuous model concept for the description of the active bed layer.

The transportation processes can contribute to the bed stratification/vertical sorting when coarser particles have critical stresses larger than the mean bed-shear stress,

while the finer particles have critical stresses smaller than the mean bed-shear stress. In these partial transport conditions, bed erosion will only be associated with the erosion of the fine particles and the coarser particles remain stable. Consequently, the composition of the active bed layer (upper bed layers) will change: the bed surface will become coarser.

3.6 Distribution of suspended particles and vertical sorting

Observations in flume and field conditions with graded sediment have shown that suspended sediment particles are not uniformly distributed over the depth in case of graded bed material (see Cloin, 1998 and Sistermans, 2002). The bed material and the suspended sediment material have different particle size distributions. Usually, the suspended sediment particles are considerably smaller than the bed material particles.

Near-bed concentrations and pick-up rates of suspended sediment are generally computed by contributions from the different grain-sizes, which are present in the bed. There is little information available about the selective entrainment of different sand sizes under waves. Nielsen suggested that the relative pick-up of a sand fraction with size D be proportional to D_{50}/D. Based on wave data over rippled beds of Nielsen (1983) and McFetridge and Nielsen (1985) Nielsen suggested the following simple formula as a first estimate (see figure 3.9):

$$\frac{\text{fraction in bed}}{\text{fraction in near-bed suspension}} = \frac{D}{D_{50}} \tag{3.7}$$

Additionally, Hamm et al. (1998) and Cloin (1998) observed the vertical sorting in suspension during their experiments in the water tunnel of WL | Delft Hydraulics under sheet-flow/flat bed conditions. Although the original sand bed in their experiments has a D_{50} of 0.20 mm, the largest median diameter in the lowest measured points of the suspension layer ($z < 10$ mm) was only about 0.13 mm for different flow conditions, see figure 3.10. In addition, the median sediment diameter showed a slow reduction from 0.13 to 0.11 mm for $0 < z <$ 50-70 mm (see also Chatelus et al., 1998 and Katopodi et al., 1999).

In fact, the presence of different sediment sizes (sand gradation) does not affect only the vertical grain-size distribution in suspension, but also the shape of the concentration profiles. Figure 3.11 shows the time-averaged concentration profiles of two different sediment fractions in the same flow.

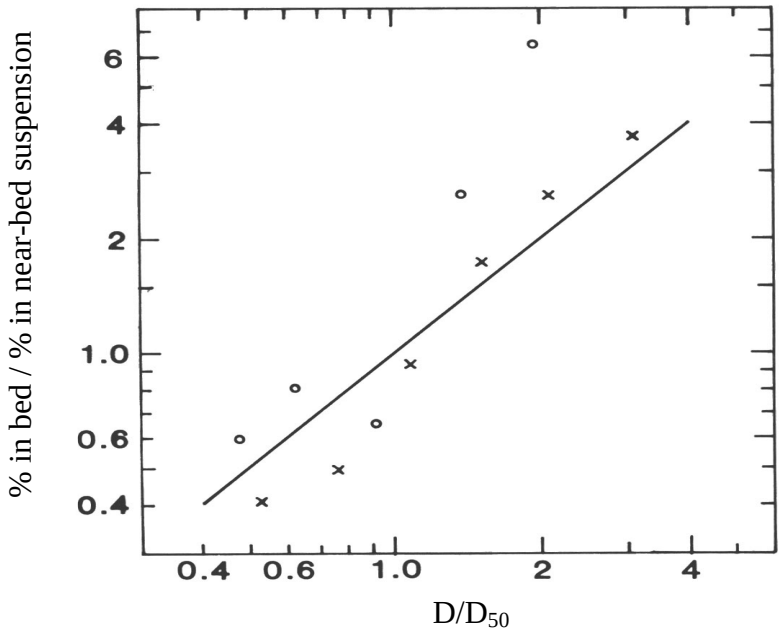

Figure 3.9: Relative abundance of sediment fractions in the bed and in near-bed suspension (data of Nielsen (1983) (x) and McFetridge and Nielsen (1985) (o), rippled beds under waves.

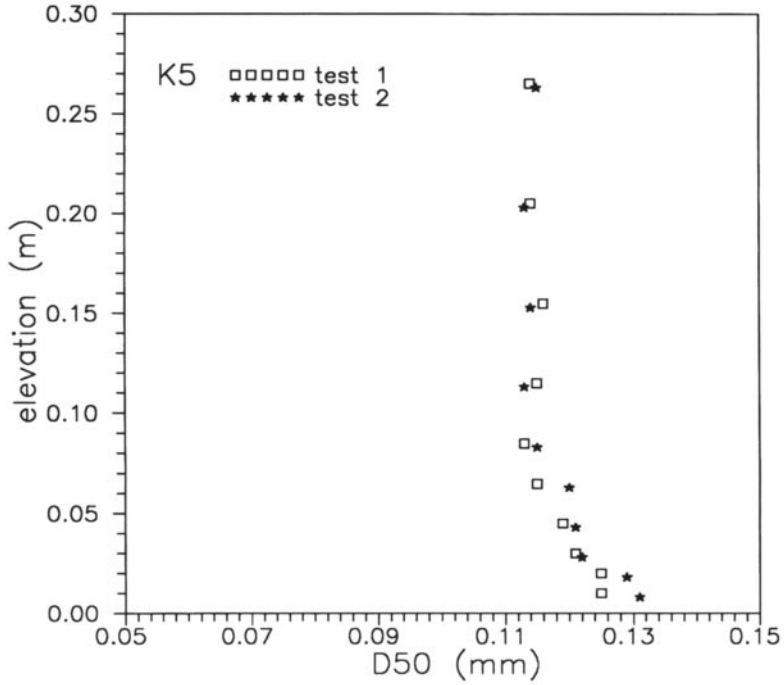

Figure 3.10: Vertical distribution of D_{50} of suspended sediment (measurement of Hamm et al., 1998, test K5). The original sand bed has D_{50} = 0.2 mm.

Figure 3.11 includes the field data of Nielsen (1983) and laboratory data of McFetridge and Nielsen (1985). Both are measured over rippled beds under non-breaking waves. Despite the scatter, it is quite clear that the two sieve fractions display different trends. For the fine material (D = 0.06 - 0.11 mm) the trend is convex upward for the coarse material (D = 0.42 - 0.60 mm) it is concave upward. According to Nielsen (1992) it shows that the entrainment process can neither be described as purely diffusive nor as purely convective.

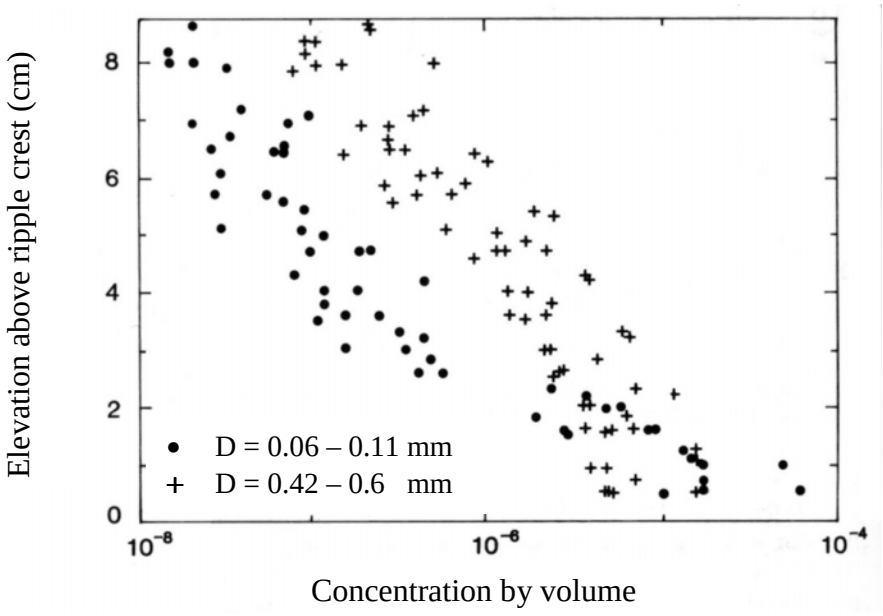

Figure 3.11: Concentration profiles for two sieve fractions of sand suspended in the same flow (waves over natural ripples), measurements of Nielsen (1983) and McFetridge and Nielsen (1985).

Nielsen (1992) distinguishes convective and diffusive processes, which can be described in terms of mixing length l_m as follows: if the mixing length is large compared to the overall scale of the sediment distribution, the process is convective. Conversely, if the mixing length is small compared to the overall scale, the process may be described as diffusive, see figure 3.12.

Travelling vortices, which can carry sediment particles directly from the bed to higher elevations, can generate convective sediment entrainment. The travelling vortices that carry suspended sand in a fairly organised manner over rippled beds under waves are generally large and of the same spatial scale as the suspended sediment layer. At the same time small-scale turbulence is present.

The hand-drawn trends of the data of McFetridge and Nielsen (1985) for all six-sieve fractions are shown in figure 3.13. The curves show a continuous transition from the upward convex for the fine sand fractions to the upward concave for the coarse

fractions. This transition can be explained in terms of the distribution mechanism being partly diffusive and partly convective. The fine fractions are more affected by the diffusive characteristics, while the coarse fractions are more influenced by the convective processes.

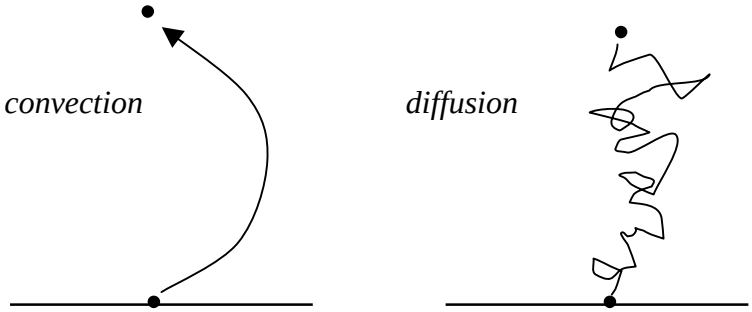

Figure 3.12: Convection and diffusion processes of suspended sand.

The consequence of vertical sorting in the suspension concentration profile is that different sizes can be transported in different magnitudes and different directions due to different net current directions under waves, see figure 2.2 in section 2.2. Wave oscillatory motion is dominant very close to the bed in the wave boundary layer. The present knowledge on the vertical sorting of suspension in the case of flat and ripple beds in wave conditions is very limited.

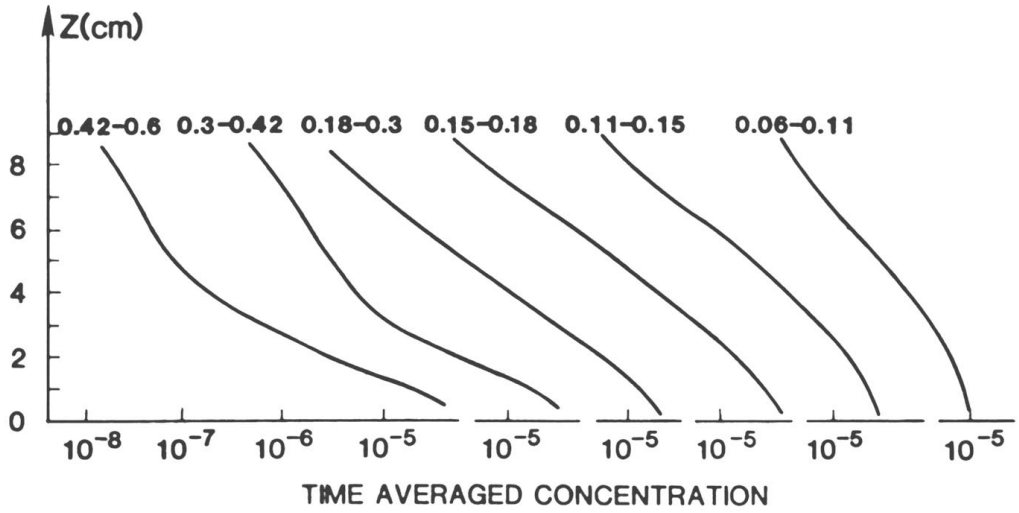

Figure 3.13: Hand-drawing of concentration profiles for the data from McFetridge and Nielsen (1985).

Recently, Sistermans (2002) successfully used a pure diffusion model for describing time-averaged suspended sediment concentration profiles and vertical sorting in the water column for wave-current conditions. He performed laboratory flume experiments in the rippled-bed regime for different size-graded sediments (D_{50} = 168-255 μm). Sistermans related D_{50} and D_{90}/D_{10} ratio of suspended sediment (just above ripple crest level) to D_{50} and D_{90}/D_{10} of the sand bed.

3.7 Size-gradation and transport modes

Dibajnia and Watanabe (1996) conducted experiments on the transport of mixed grain-size sand under non-linear waves, over both rippled and flat beds in a small water tunnel at the University of Tokyo. The sand mixture was composed of fine sand with median diameter of 0.2 mm and coarse sand with median diameter of 0.87 mm. In their experiments they used three types of mixed sands with percentage of fine sand, $P_{0.2}$ equal to 25 %, 50 % and 75 %.

Dibajnia and Watanabe measured the net sand transport rates of each size fraction over rippled beds as well as under sheet–flow conditions. Additionally, they investigated also the conditions for initiation of sheet-flow with different sand mixtures. In some tests they started the test with a flat bed, in others they started with a rippled bed. The main conclusions from the study of Dibajnia and Watanabe (1996) can be summarised as follows:

- Due to armouring and hiding effects, the transport rate of fine sand is significantly reduced by the presence of the coarse sand, whereas the coarse sand behaves almost as if there is no finer sand present;
- For graded sand sheet-flow occurs under lower velocities than those required for uniform sand, at least when the bed was initially flat. Figure 3.14 shows the different transport modes for the different sand mixtures (wave period = 3 s). Note that this contains only the cases in which the bed was initially flat;
- Graded sand makes a firm bed structure and thus the bed may not deform as easily as in the case of uniform sands with the same D_{50}. It was found that a higher velocity than that in the case of uniform sand is required to wash out the ripples from the mixed sand bed. Figure 3.15 shows the initiation of sheet-flow for different initial bedforms.

More details about the experiments of Dibajnia and Watanabe can be found in Suzuki et al. (1994) and Inui et al. (1995).

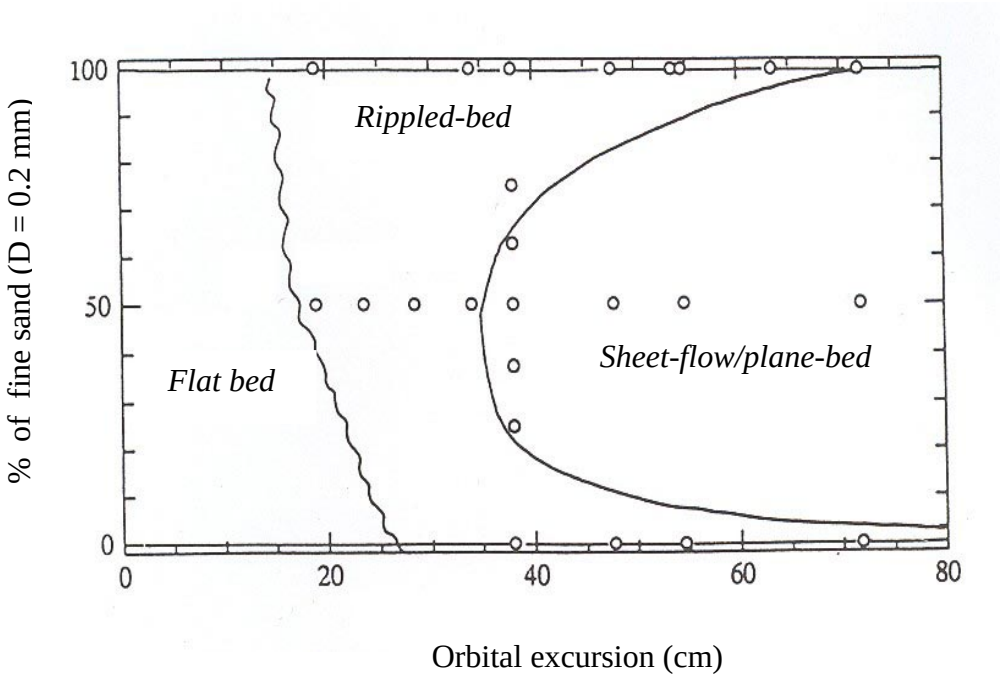

Figure 3.14: Sand gradation effects on the occurrence of different transport modes, data of Dibajnia and Watanabe (1996); the bed was initially flat.

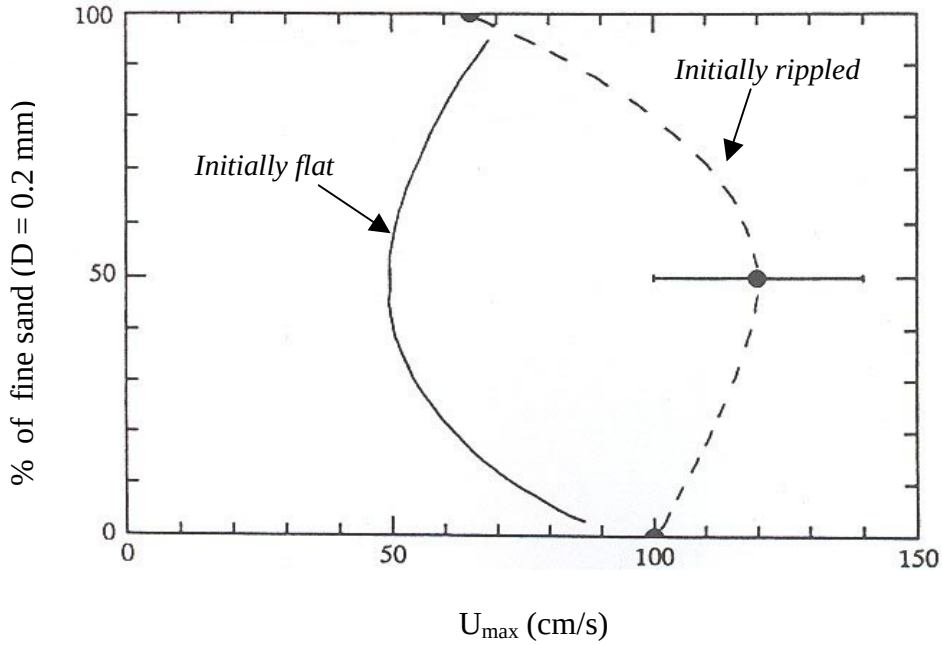

Figure 3.15: Sand gradation effects on the initiation of sheet-flow, data of Dibajnia and Watanabe (1996).

3.8 Summary and conclusions

In chapter 3 an overview was given of existing knowledge of graded sediment transport processes in wave-current flows. A literature study was concentrated on the effects of size-gradation and on issues like selective transport and sheet-flow, which are the main topics of the present study. The results of this chapter can be summarised as follows:

- Four different types of sorting (selective) processes can take place during sand transport: Entrainment sorting (difference in the threshold velocity to initiate motion of different grain-sizes); Sand bed vertical sorting (resulting in a layered structure of the bed); Suspension sorting (separation of suspended sizes in the water column) and transport sorting (separation of sediment particles due to differences in transport velocity);
- The Shields parameter is proportional to D^{-1}, which indicates the relatively smaller mobility of larger particles and larger mobility of small particles. This forms the origin for selective transport processes of size-fractions in a mixture. For oscillatory flows there is no generally accepted relationship for initiation of motion on plane bed;
- Very little is known about the size-gradation effect on the initiation of motion under waves. All available information is related to steady flows only where hiding/exposure effects are taken into account. The information about hiding /exposure effects under wave conditions is very limited;
- When the Shields parameter becomes larger than 0.8, small bed ripples are washed out and the bed becomes plane. A thin layer with high sand concentrations is moving in a sheet along the bed, which is called the sheet-flow layer. The thickness of the sheet-flow layer is generally much larger than a few grain diameters (10-100 grain layers). Inside the sheet-flow layer concentrations are so high that intergranular forces and grain-water interactions are important;
- Although under oscillatory sheet-flow conditions sand grains are transported very close to the bed laboratory observations show that for asymmetric waves unsteady effects can play a very important role on the magnitude and direction of net transport rates. Ribberink and Chen showed that the direction of net transport rates can change from the onshore to the offshore direction by reducing the sand size from 0.21 to 0.13 mm;
- It is known that during sediment transport due to currents (like in rivers) vertical sorting takes place in the upper layers of the sand bed (active layer). The sediment grains that take part in the transportation process are present in this layer. However, there is hardly any knowledge about vertical bed sorting under wave conditions. Whether vertical sorting occurs and how it occurs in the flat bed/sheet-flow regime is not known;
- Laboratory observations with graded sand under rippled-bed as well as under sheet-flow/flat-bed conditions show that suspended sand sizes are smaller than the original sand bed. This fining of suspended sand increases with the height above the bed;

- The presence of different sediment sizes in a mixture does not only affect the vertical grain-size distribution in suspension, but also the shape of the concentration profiles. Nielsen (1992) distinguishes convective and diffusive mechanisms, which can suspend the sediment particles. The fine fractions behave as if they are dominated by a diffusion process, while the course fractions behave more as if their motion was controlled by a convection process resulting in different shapes of the concentration profile for different sand-sizes;
- The present knowledge on the vertical sorting of suspension in the case of flat bed and ripple beds in wave conditions is very limited;
- Dibajnia & Watanabe (1996) carried out a limited series of experiments with graded sand and oscillatory flows. The following results were obtained:
    - The transport rate of fine sand in a mixture is significantly reduced by the presence of the coarse sand, whereas the coarse sand behaves almost as if there were no finer sand present. This indicates that hiding effects are taking place under oscillatory sheet-flow conditions;
    - For sand mixtures sheet-flow occurs under lower oscillatory velocities than those required for uniform sand;
    - A higher velocity is required to wash out ripples that were formed from a mixed sand bed than from a uniform sand bed.

The results of Dibajnia & Watanabe are only limited to one oscillatory period. More experiments are required with higher velocities and larger wave periods.

It is concluded from the literature survey that, although some laboratory work focused on graded sediment transport under waves, there is still a considerable lack in knowledge about transport processes of graded sediment in rippled-bed and in flat-bed/sheet-flow conditions. Therefore, in the present study new laboratory experiments are carried out in order to improve our understanding of oscillatory sheet-flow transport processes with graded and uniform sands, see chapters 6 and 7.

Chapter 4

OSCILLATORY SAND TRANSPORT MODELS

4.1 Introduction

In order to simulate and predict large-scale and long-term morphological changes in coastal zones, the use of accurate sediment transport models is essential. In fact, these mathematical transport models are representing the basic hydrodynamic and sediment transport processes. The available transport models are the reflection of our quantitative knowledge of the sediment transport processes.

An important assumption in most of the existing models is the uniformity of the sand, which means that the sediment mixture is characterised by a single sand size. Additionally, the existing models assume that sediment density and shape are constant in space and in time. These simplifications are mainly caused by the lack of knowledge of the physical behavior of sediment particle mixtures. Especially for oscillatory flows, such as under waves not much is known about their transport dynamics.

In this chapter a general classification of sediment transport models is given in section 4.2. Sections 4.3 to 4.5 introduce detailed descriptions of transport models, which have been used in the present study. In section 4.6 the general behaviour of these sediment transport models is studied and an intercomparison is made. Finally, section 4.7 presents a short summary.

4.2 Classification of sediment-transport models

In the most basic form the sediment transport rate can be described as the product of the sediment particles velocity and the sediment concentration integrated over the water depth. This results in the following equation:

$$q_s(t) = \int_0^h \varphi(z,t)\ dz = \int_0^h u(z,t)\cdot c(z,t)\ dz \tag{4.1}$$

where: q_s (t) = time-dependent sediment transport rate per unit width; h = water depth; φ = sediment flux; z = height above the sand bed; t = time; u = sediment particle velocity (assumed to be equal to the flow velocity) and c = sediment concentration.

Neglecting turbulent components (Nielsen, 1985) and on the short time scale of the waves the velocity and the sand concentration in equation 4.1 can be split up in a steady component, related to current (e.g. due to the tidal motion), and a periodic component, related to the oscillating wave motion:

$$\begin{aligned} u(z,t) &= \langle u(z)\rangle + \tilde{u}(z,t) \\ c(z,t) &= \langle c(z)\rangle + \tilde{c}(z,t) \end{aligned} \tag{4.2}$$

where: < > = steady component and ~ = periodic component.

Substituting equation 4.2 in equation 4.1 yields:

$$q_s(t) = \int_0^h \left[\langle u(z)\rangle.\langle c(z)\rangle + \langle u(z)\rangle.\tilde{c}(z,t) + \tilde{u}(z,t).\langle c(z)\rangle + \tilde{u}(z,t).\tilde{c}(z,t)\right]dz \tag{4.3}$$

The wave-averaged transport rate is given by:

$$\langle q_s\rangle = \underbrace{\int_0^h \langle u(z)\rangle\cdot\langle c(z)\rangle\ dz}_{(1)} + \underbrace{\frac{1}{T}\int_0^T\int_0^h \tilde{u}(z,t)\cdot\tilde{c}(z,t)\ dz\ dt}_{(2)} \tag{4.4}$$

The first term on the right-hand side is the current-related transport rate, while the second term is the wave-related transport rate.

In the last decades many models have been developed to predict the sediment transport rate. These models can be divided into the following four different classes:

1. Time-averaged models
2. Quasi-steady models
3. Intermediate models
4. Unsteady models

These different model classes can be described briefly as follows:

1. Time-averaged transport models

Time-averaged models were the first type of models to predict the net sediment transport rate under waves and currents, by applying a similar approach as was used in uni-directional currents (rivers). In these models the transport is considered on a time scale that is much larger than the wave period, but smaller than the tidal period. Wave-averaged values of the velocity and the concentration are used (part 1 of equation 4.4), while the wave periodic components (part 2 of equation 4.4) are neglected (e.g. Bijker, 1971). Consequently, the wave-related sediment transport is not included in this kind of models. Since this transport component is crucial for predicting cross-shore sediment transport, these models are left out of consideration in this study (for a description of time-averaged models see Van Rijn, 1993).

2. Quasi-steady transport models

In this type of models the sediment transport is considered on an intra-wave time scale, i.e. a time-scale is much shorter than the wave period. It is assumed that sediment transport reacts immediately to the time-dependent horizontal flow velocity throughout the wave-cycle, without any phase difference between the flow velocity and the concentration, as if the flow is steady at each phase during the wave-cycle (quasi-steadiness). In this way the wave-related sediment flux is implicitly included in the models.

According to the assumption of quasi-steadiness this type of model is only valid for conditions in which the response time of the sediment particles is relatively short. In other words, the pick-up and settling process of the sediment grains from/to the bed during the wave motion must take place in a much shorter time than the wave period. This means that the settling time of a sediment particle suspended at elevation z above the bed (z/w_s, w_s = particle settling velocity) must be much smaller than the wave period (see also section 3.4). For this type of model the time-dependent velocity is the only main input parameter, which makes this kind of model easy to use.

Most of these models are empirical and based on experimental data. These data were generally obtained from small-scale and full-scale laboratory experiments. Examples are the models of Madsen and Grant (1976), Sleath (1978), Watanabe et al. (1980), Sawamoto and Yamashita (1986), Ribberink and Al-Salem (1994) and Ribberink (1998).

Another group of quasi-steady models is based on a theoretical analysis of the sediment transport process, but with a number of empirical coefficients. Examples

are the models of Bagnold (1963), Bailard and Inman (1981) and Bailard (1981). The models of Bailard (1981) and Ribberink (1998) will be described in more detail in section 4.3.

3. Intermediate transport models

Intermediate sediment transport models are positioned between the quasi-steady and the unsteady models. This kind of models tries to include the effect of the observed time-lag between the flow velocity and the sediment concentration under waves in a parameterized way, but without the detailed simulation of velocity and concentration profiles that underlies the unsteady models. Intermediate sediment transport models were developed by Dibajnia & Watanabe (1996) and Dohmen-Janssen (1999). These two models are described in more detail in section 4.4.

4. Unsteady models

Unsteady sediment transport models are the most advanced type of transport models. They are based on a full time-dependent simulation of both velocities and concentrations during the wave-cycle at different elevations above the bed. In case of a combined wave-current motion both the flow velocity and the sediment concentration consist of a steady component and a periodic component (see also equation 4.3). The net sediment transport rate is then calculated by averaging the time-dependent horizontal sediment-fluxes over the wave-cycle and over the depth.

In many unsteady models, the unsteady flow velocity is derived from the basic Navier-Stokes equation, while the sediment concentration is derived from an advection-diffusion equation. Some unsteady models ignore the sediment-flow interaction, i.e. the flow velocities are not affected by the presence of sediment concentrations (Fredsøe et al. (1985), Armanini and Ruol (1988) and Ribberink and Al-Salem (1995)). Other unsteady transport models include sediment-flow interaction processes, for example Smith (1977), Xu (1993), Li and Davies (1995), Dong & Zhang (1999) and the POINT-SAND model (PSM) of Uittenbogaard et al. (2000) as developed at WL | Delft Hydraulics. The PSM model provides a sophisticated description of wave-current interaction as it includes the vertical orbital motion and wave-induced net currents in the water column, such as boundary layer streaming. The latter processes are not considered in the present work since only horizontal oscillatory flows are studied.

Existing unsteady models mainly differ in the applied boundary conditions and turbulent closure schemes. The unsteady transport models are relatively difficult to use compared to the other model types (quasi-steady and intermediate models). The detailed calculations require much insight of the various physical transport processes and demand much computing time.

4.3 Quasi-steady transport models

4.3.1 Bailard's model (1981)

The quasi-steady model of Bailard (1981) is based on Bagnold's energetic approach (1963). This approach implies that the available fluid power for sediment transport is a constant fraction of the local rate of energy dissipation. The model of Bailard is a *total load model* of time-dependent sediment transport over a plane sloping bed, applied to coastal areas. A distinction is made between bed load and suspended load transport. This model was developed for computing sediment transport under wave conditions only. The bed-load transport for a horizontal bed is given by:

$$q_{s,b}(t) = \frac{\varepsilon_b u \varepsilon_b}{(\varepsilon_s - \varepsilon) g \tan\phi} = \frac{\frac{1}{2} f_w \varepsilon_b}{\Delta g \tan\phi} u^3(t) \qquad (4.5)$$

The suspended-load transport is given by:

$$q_{s,s}(t) = \frac{\frac{1}{2} f_w \varepsilon_s}{\Delta g w_s} \left| u^3(t) \right| u(t) \qquad (4.6)$$

where: $q_{s,b}$ = bed-load transport (= transported volume per unit width and time); $q_{s,s}$ = suspended-load transport; Δ = relative density = $(\rho_s - \rho)/\rho$; τ_b = bed shear stress; f_w = wave friction factor; g = gravity acceleration; ϕ = angle of internal friction of the sediment; u = horizontal near-bed flow velocity and w_s = settling velocity of sediment particles.

In this model Bailard used two efficiency factors ε_b and ε_s for bed-load and suspended-load transport, respectively. These two factors account for the fraction of the energy expenditure spent to the transport process. Both are obtained by calibration of the net transport rates against field data. Bailard (1982) found that ε_b = 0.1 and ε_s = 0.02.

Bailard does not specify an expression for the wave friction factor f_w. In the case of purely oscillatory flows the formula of Jonsson (1966), or the slightly modified formulation by Swart (1974) can be applied. For combined wave-current flow a wave-current friction factor f_{cw} rather than the wave friction factor can be used. The method for computing the friction factors is described in the following section. Finally, the time-dependent total transport rate is determined by adding the two components, the bed-load transport and the suspended-load transport: $q_s(t) = q_{s,b}(t) + q_{s,s}(t)$.

4.3.2 Ribberink's model (1998)

One of the goals of this *bed-load model* was to create a formula that is valid under waves as well as under steady flow conditions. In this model the Shields parameter θ is the parameter determining sediment transport motion. Therefore, it uses a type of formula that was empirically obtained by Meyer-Peter and Muller (1948) for steady flows, but which also shows good agreement with observed transport rates under wave conditions and combined wave-current flows.

Ribberink (1998) assumed that the shear stress is the driving force for sediment transport. The sediment transport is assumed to be a function of the effective shear stress, the difference between the actual time-dependent effective bed shear stress and the critical bed shear stress θ_{cr}. Under waves the sediment transport direction is determined by $\theta/|\theta|$. The bed shear stress is expressed in terms of the (non-dimensional) Shields parameter. Normalising the sediment transport rate by the parameter $\sqrt{\Delta g D_{50}^3}$ leads to the following basic time-dependent formula for computing sediment transport rate:

$$\varepsilon(t) = \frac{q_s(t)}{\sqrt{g\Delta D_{50}^3}} = m\left[|\varepsilon(t)| - \varepsilon_{cr}\right]^n \frac{\theta(t)}{|\varepsilon(t)|} \qquad (4.7)$$

where: φ = non-dimensional sediment transport rate; m = empirical coefficient; n = empirical coefficient; $\theta(t)$ = time-dependent Shields parameter and θ_{cr} = critical Shields parameter.

The two coefficients (m and n) in equation 4.7 were determined by curve fitting of experimental data. Ribberink (1998) found for a large data set of steady and unsteady laboratory experiments m=11 and n=1.65. The critical value of the Shields parameter ε_{cr} depends on the non-dimensional grain-size D_*. See Van Rijn (1993) for this relationship D_* is defined as:

$$D_* = D_{50}\left(\frac{g\Delta}{\varepsilon^2}\right)^{1/3} \qquad (4.8)$$

where: D_* = non-dimensional grain-size and ν = kinematic viscosity of water.

In order to calculate the Shields parameter the model of Ribberink uses the theory of Jonsson (1966) to calculate the bed shear stress for waves. The time-dependent shear stress is written as a function of the density of the sediment, the imposed velocity and a certain friction factor:

$$\varepsilon_b(t) = \tfrac{1}{2}\varepsilon_s f_w |u(t)|\, u(t) \qquad (4.9)$$

where: τ_b = bed shear stress; f_w = wave friction factor and u(t) = horizontal oscillatory flow velocity directly above the wave boundary layer.

For combined wave-current flow the bed shear stress is derived from:

$$\varepsilon_b(t) = \tfrac{1}{2}\varepsilon_s \, f_{cw} \, |u(t)| \, u(t) \qquad (4.10)$$

In the above formula f_{cw} is a friction factor, induced by a combination of waves and a steady current. Ribberink used the expression of Madsen and Grant (1976) for the combined friction factor (see also Van Rijn, 1990):

$$f_{cw} = \varepsilon f_c + (1-\varepsilon) f_w \qquad (4.11)$$

where: f_{cw} = friction factor in case of waves and a steady current; f_c = friction factor in case of currents only and f_w = friction factor in case of waves only.
The parameter α gives the relation between the net current and the oscillating flow velocity, and is given by:

$$\varepsilon = \frac{|\langle u \rangle|}{|\langle u \rangle| + \hat{u}} \qquad (4.12)$$

where: <u> = time-averaged velocity and $\hat{u}$ = velocity amplitude of the oscillatory flow.

To estimate the wave friction factor f_w the formula of Swart (1974) is used. In case of turbulent flow the wave friction factor is a function of the relative roughness (i.e. the ratio of the amplitude of the horizontal oscillatory flow near the bed ($\hat{a}$) and the roughness height (k_s)):

$$\begin{aligned} f_w &= \exp\left(-6 + 5.2\left(\frac{\hat{a}}{k_s}\right)^{-0.19}\right) && \text{for} \quad k_s/\hat{a} < 0.63 \\ f_{w,max} &= 0.3 && \text{for} \quad k_s/\hat{a} \geq 0.63 \end{aligned} \qquad (4.13)$$

where: $\hat{a}$ = amplitude of horizontal excursion of water particles near the bed and k_s = bed roughness height.
To estimate the friction factor for currents only, the following formula is used, which is based on the logarithmic velocity distribution:

$$f_c = \left(\frac{\varepsilon}{\ln z / z_0} \right)^2 \qquad (4.14)$$

where: κ = Von Karman coefficient (= 0.4); z = height above the sand bed where the velocity is prescribed; $z_0 = k_s/30$ is zero velocity level.

Both friction factors depend on bed roughness height k_s. Ribberink found that the formula showed the best results for waves and for steady currents when two different values of k_s were used: $k_{s,c}$ for the net current flow and $k_{s,w}$ for the oscillatory flow. He suggests that this may be caused by the different structure of the boundary layer of a steady current flow and the wave boundary layer.

Generally it is assumed that the bed roughness height is related to the diameter of the bed material. For k_s values like for example D_{50}, $2.5*D_{50}$ or D_{90} are used. In sheet-flow conditions k_s may also depend on the Shields parameter. The Shields parameter varies during the wave-cycle. In order to simplify the calculation the time-averaged value of the Shields parameter is used. This implies that the bed roughness height must be calculated by use of an iterative process. In order to compute the net transport rates the calculated instantaneous transport rates are time-averaged over the wave-cycle.

4.4 Intermediate transport models

4.4.1 Model of Dohmen-Janssen (1999)

Based on new experiments in the oscillating water tunnel of WL ⎜ Delft Hydraulics and on earlier experiments in the same water tunnel Dohmen-Janssen (D-J) developed a new intermediate transport model, which is closely linked to the existing quasi-steady model of Ribberink (1998). Phase-lag effects are taken into account by this model (i.e. delayed settling of the sediment particles and delayed entrainment into the flow).

Phase-lag effects become important and reduce the net transport rates when the response time of sediment particles is not small compared to the oscillation period. The concentration may lag behind the flow velocity caused by the fact that both sediment entrainment into the flow and settling of the particles back to the bed takes time. The latter depends on the settling time of sand particles and on the height to which the sand particles are entrained. Phase-lag effects are expected to be important for large flow velocities, fine sand and small wave periods, as discussed before in section 3.4.
D-J used the analytical diffusion model of Nielsen (1979) for modelling the phase-lag effects due to delayed entrainment and delayed settling of sediment particles. The analytical model is used to calculate a ratio (r) of the net sand transport rate with

phase-lag effects (<$q_{s,r}$>, real transport rate) and without phase-lag effects (<$q_{s,eq}$>, equilibrium transport rate).

This ratio r is used as a phase-lag correction factor for the transport rates predicted by the quasi-steady bed-load model of Ribberink. If phase-lag effects are not important, then r = 1 and the new model returns to the quasi-steady model of Ribberink (1998).

For sine waves with an imposed net current (described with $u(t) = u_0+u_1\sin(\omega t)$), the basic formulae are:

$$< q_{s,r} > = r < q_{s,eq} >_{\text{Ribberink}} \tag{4.15}$$

$$r = \frac{< q_{s,r} >}{< q_{s,eq} >} = \frac{u_0^2 + \frac{1}{2}u_1^2 + u_1^2 G_1}{u_0^2 + \frac{3}{2}u_1^2} \tag{4.16}$$

$$G_1(p) = \frac{P_1\cos\varphi_1 + Q_1\sin\varphi_1}{\left(P_1^{\,2} + Q_1^{\,2}\right)^{3/2}} \tag{4.17}$$

$$\varphi_1 = \arctan\left(-\frac{Q_1}{P_1}\right) \tag{4.18}$$

$$P_1 = \frac{1}{2} + \left(\frac{1}{16} + p^2\right)^{\frac{1}{4}} \cos\left(\tfrac{1}{2}\varepsilon_1\right) \tag{4.19}$$

$$Q_1 = \left(\frac{1}{16} + p^2\right)^{\frac{1}{4}} \sin\left(\tfrac{1}{2}\varepsilon_1\right) \tag{4.20}$$

$$\varepsilon_1 = \arctan(4p) \tag{4.21}$$

$$p = \frac{\varepsilon_s \varepsilon}{w_s^{\,2}} = \frac{\varepsilon_s \varepsilon}{w_s} = \frac{\mu\,\varepsilon_w D_{50}\varepsilon}{w_s} = \frac{\mu\, f_w \hat{u}^2 \varepsilon}{2\Delta g w_s} \quad (\text{“}\textit{phase-lag parameter p}\text{”}) \tag{4.22}$$

where: u_0 = net current velocity; u_1 = oscillatory velocity; ω = angular frequency of the wave ($=2\pi/T$); ε_s = sediment mixing coefficient; μ = constant; w_s = settling velocity; δ_s = thickness of the sheet-flow layer; f_w = wave friction factor and $\hat{u}$ = amplitude of horizontal oscillatory velocity. The wave friction factor f_w is calculated from Swart’s formula, using a roughness height k_s equal to D_{50} of the sediment.

Equations 4.15 to 4.22 show that the phase-lag reduction factor depends on the ratio u_0/u_1 (represent the importance of the net current velocity compared to the oscillatory velocity) and on the parameter $p = \varepsilon_s\omega/w_s^2$ (characterising the phase-lag effects). The ratio of sediment mixing coefficient to settling velocity can be considered as a characteristic height δ_s to which particles are entrained. The ratio δ_s/w_s is equal to the settling time of a particle that is entrained to a level δ_s. In order to calculate the phase-lag parameter p and the reduction factor r, either the value of the sediment-mixing coefficient ε_s or the characteristic height δ_s must be known. D-J assumed that δ_s is equal to the thickness of the sheet-flow layer.

First D-J calculated the sheet-flow layer thickness according to the sheet-flows expression of Wilson (1987), $\delta_s/D_{50} = 10\theta$ ($\mu = 10$ in equation 4.22). However, it was found by Dohmen-Janssen (1999) that the measured sheet-flow layer thickness δ_s is generally larger than predicted by the expression of Wilson (1987). Therefore, D-J proposed a grain-size dependent relation for the sheet-flow layer thickness based on wave tunnel experiments at WL | Delft Hydraulics (series E of Katopodi et al., 1994; series I of Janssen and Van der Hout, 1997; series H of Janssen et al., 1996):

$$p' = \frac{\varepsilon_s \varepsilon}{w_s} = \begin{cases} \dfrac{17.5 f_w \hat{u}^2 \varepsilon}{\Delta g w_s} & \text{for} \quad D_{50} = 0.13\,\text{mm} \\ \\ \dfrac{6.5 f_w \hat{u}^2 \varepsilon}{\Delta g w_s} & \text{for} \quad D_{50} \geq 0.20\,\text{mm} \end{cases} \tag{4.23}$$

This means that for fine sand (D_{50} = 0.13 mm) p' is a factor 3.5 larger than p (equation 4.23), and for coarser sand ($D_{50} \geq 0.2$ mm) p' is a factor 1.3 larger than p. In case of a steady current u_1 is equal to zero and the correction factor r equals 1, according to equation 4.15.

The relations between the phase-lag parameter p and the reduction factor r are shown in figure 4.1, which show this relation for different values of u_0/u_1. It is clear that for a small value of p (small phase-lag effects) the value of r is equal to 1. For increasing phase-lag effects (increasing value of p), the value of r decreases. Therefore, the net transport rates are reduced if the phase-lag effects become important. The minimum value of r is equal to 1/3 in case of pure sine waves. This value approaches zero in case of 2nd-order Stokes waves.

The basic formulae for the more general case with 2nd-order Stokes waves and an imposed net current (described with $u(t) = u_0 + u_1\cos(\omega t) + u_2\cos(2\omega t)$) are described in Appendix A.

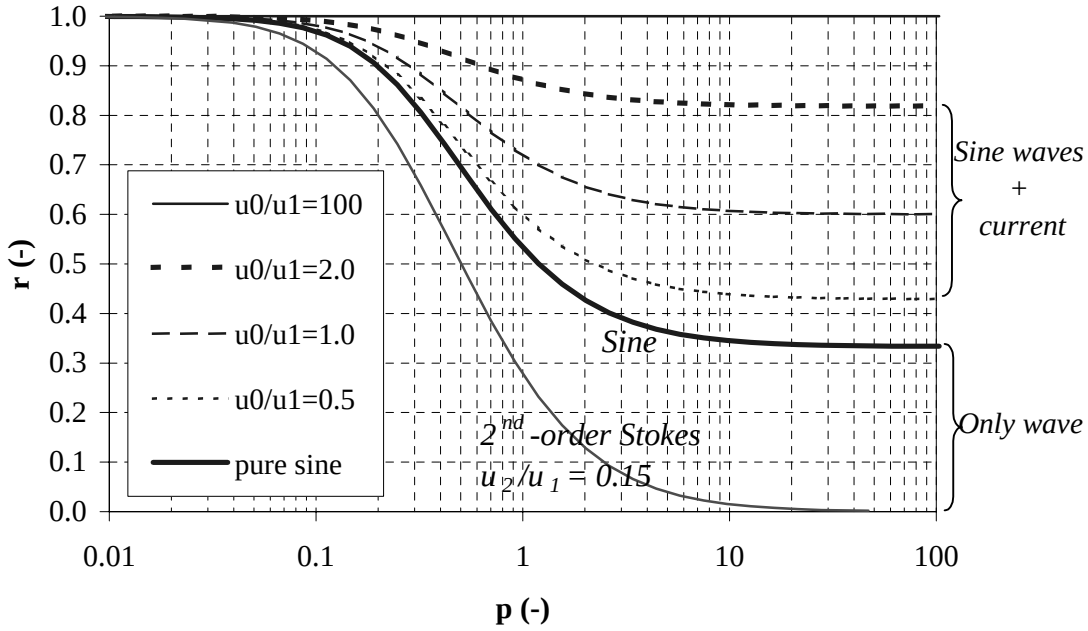

Figure 4.1: Phase-lag reduction factor (r) as a function of phase-lag parameter (p) for different values of u_0/u_1 and for 2^{nd}-order Stokes waves.

4.4.2 Model of Dibajnia & Watanabe (1996)

The model of Dibajnia & Watanabe (1996) is an intermediate model, as it does not contain the full unsteady equations, while it is able to take into account unsteady effects. The model is based on a consideration of the kinetic and potential energy of sediment particles. Dibajnia & Watanabe (D&W) assumed that the particles travel with the same velocity as the fluid and that the kinetic energy of the flow is transferred to potential energy of the sediment grains when the latter are raised.

If for example the flow velocity in the positive direction is high, the sediment particles can be stirred up to such a high level that they cannot settle to the bed within the same positive part of the wave-cycle. A part of the sediment particles will remain in suspension and will be transported in the negative direction during the next part of the wave-cycle. If the settling time of a sediment particle is larger than the part of the wave period in which it is stirred up, it is very likely that unsteady effects will occur.

The 'time-lag' effect is incorporated in the model by considering the settling velocity of the sand and the thickness of the sheet-flow layer δ_s under crest and trough of the wave. The sheet-flow layer thickness δ_s is calculated by an energy concept:

$$\varepsilon_s = \frac{E_k}{(\varepsilon_s - \varepsilon)Vg} = \frac{0.5\varepsilon V u_i^2}{(\varepsilon_s - \varepsilon)Vg} = \frac{u_i^2 \varepsilon}{2(\varepsilon_s - \varepsilon)g} \qquad (4.24)$$

where: E_k = the kinetic energy of a sand particle; V = sand volume; ρ_s = sand density; ρ = water density and u_i = the equivalent sinusoidal velocity amplitude under crest or trough.

The equivalent velocity amplitude under crest (u_c) and trough (u_t) can be described by:

$$u_c^2 = \frac{2}{T_c}\int_0^{T_c} u^2 dt \qquad u_t^2 = \frac{2}{T_t}\int_{T_c}^{T} u^2 dt \tag{4.25}$$

where: $T_t = T - T_c$ (see figure 4.2)

T_c and T_t are the duration of the positive and negative part of the wave velocity, respectively. The required time to settle back the sediment particle T_f is then equal to the thickness of the sheet-flow layer δ_s (equation 4.25) divided by the settling velocity w_s:

$$T_f = \frac{u_i^2}{2\Delta g w_s} \tag{4.26}$$

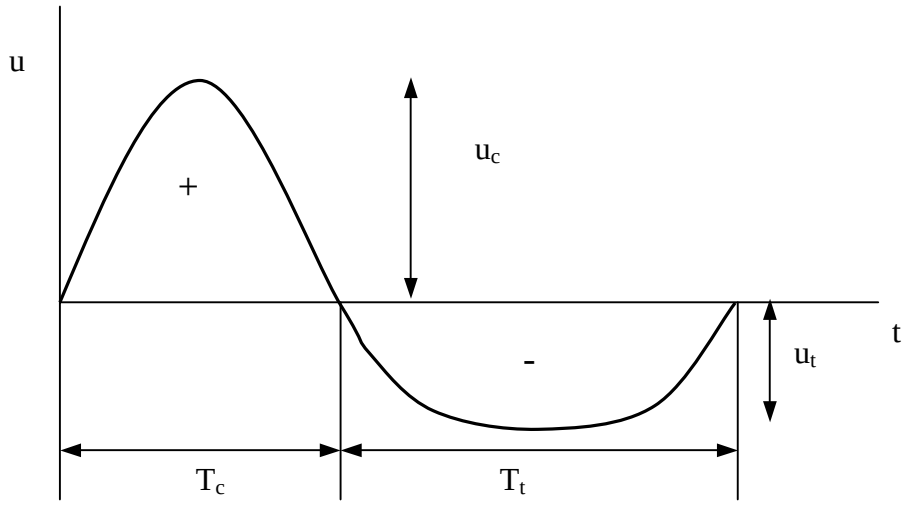

Figure 4.2: Definition sketch of Dibajnia & Watanabe model (T_c, T_t = periods of the positive and negative parts of the wave-cycle, respectively).

Dibajnia & Watanabe (1992) defined a non-dimensional parameter Γ to represent the net (non-dimensional) transport rate, giving the difference between the transport during the positive part and the negative part of the wave-cycle:

$$\varepsilon = \frac{u_c T_c \left(\varepsilon_c^3 + \varepsilon_t'^3\right) - u_t T_t \left(\varepsilon_t^3 + \varepsilon_c'^3\right)}{\left(u_c + u_t\right) T} \tag{4.27}$$

where: Ω_c represents the sand brought into suspension and transported during the positive half wave-cycle (see also equation 4.29); Ω'_c represents the sand remaining in suspension from the positive half wave-cycle and transported by the negative half wave-cycle; Ω_t represents the sand brought into suspension and transported during the negative half wave-cycle; Ω'_t represents the sand remaining in suspension from the negative half wave-cycle and transported by the positive half wave-cycle.

In the above formula unsteady effects become important only if the time required for a sediment particle to settle back to the bed after being brought into suspension (T_f) is larger than the period of the half wave-cycle. If the settling time T_f is larger than T_c or T_t a sediment particle remains in suspension and will be transported during the next half wave-cycle in the opposite direction (Ω'_c or $\Omega'_t > 0$). On the other hand if the settling time is smaller than T_c or T_t then all the sediment particles will settle down before flow reversal and no unsteady effects will take place ($\Omega'_c = \Omega'_t = 0$).

Dibajnia and Watanabe used the parameter ω_i to determine the importance of unsteady effects. The ratio of the settling time and the period of the positive and the negative half wave-cycle reads:

$$\varepsilon_c = \frac{T_f}{T_c} = \frac{1}{2}\frac{u_c^2}{\Delta g w_s T_c} \qquad \varepsilon_t = \frac{T_f}{T_t} = \frac{1}{2}\frac{u_t^2}{\Delta g w_s T_t} \tag{4.28}$$

Whether sediment particles remain in suspension after half a wave-cycle or not depends on the magnitude of ω_i. The relation between the parameters Ω_i, Ω'_i and ω_i is described by:

$$\begin{cases} \varepsilon_i \le \varepsilon_{cr} & \begin{cases} \varepsilon_i = \varepsilon_i T_i \sqrt{\dfrac{\Delta g}{D_{50}}} \\ \varepsilon'_i = 0 \end{cases} \\ \varepsilon_i > \varepsilon_{cr} & \begin{cases} \varepsilon_i = \varepsilon_{cr} T_i \sqrt{\dfrac{\Delta g}{D_{50}}} \\ \varepsilon'_i = \left(\varepsilon_i - \varepsilon_{cr}\right) T_i \sqrt{\dfrac{\Delta g}{D_{50}}} \end{cases} \end{cases} \tag{4.29}$$

Dibajnia & Watanabe (1996) proposed this new method to evaluate Ω (equation 4.29) as a follow-up of the method they used in their model of 1992. This new method is based on the results of Sawamoto and Yamashita (1986), that the half

cycle averaged sheet-flow transport rate is proportional to the third power of ratio of the friction velocity and the sediment settling velocity.

The value of ω_{cr} in equation 4.29 is equal to 1 for sheet-flow conditions. In the presence of ripples ω_{cr} is equal to 0.03 for 0.2 mm sand and equal to 0.05 for 0.87 mm sand.

Using the data of Sawamoto and Yamashita (1986) with uniform sand and the original data of Dibajnia and Watanabe (1992) (D = 0.2 mm) Takasawa et. al. (1996) found the following generalized transport formula:

$$\varepsilon_* = \frac{< q_s >}{w_s D_{50}} = 0.0015 |\varepsilon_*|^{0.5} \frac{\varepsilon_*}{|\varepsilon_*|} \tag{4.30}$$

According to Dibajnia and Watanabe (1996) this method is applicable to estimate the sediment transport with different grain sizes and densities.

4.5 Unsteady transport models

In unsteady sediment transport models the velocity and sediment concentration are determined at each level above the bed and at each instant during the wave-cycle. Various researchers have proposed different transport models to predict the suspended sediments under wave conditions. In these models the velocity is derived from the momentum balance for horizontal oscillatory flow. The sediment concentration is derived from the mass balance of sediment by assuming that sediment can be transported by advection and by turbulent diffusion. However, all these models are based on a 1DV and long wave approach (shallow water).

Many models are based on these two basic equations, for example Fredsøe et al. (1985), Ribberink and Al-Salem (1995), Huynh Thanh et al. (1994) and Li and Davies (1996). In order to solve these two equations four boundary conditions and expressions for the eddy viscosity and the sediment diffusivity (turbulence closure) are required. Also the horizontal pressure gradient must be known. Basically, the difference between the unsteady models results from differences in the applied boundary conditions, the used turbulent closure schemes and considering the sediment-flow interaction or not. The POINT-SAND model (Uittenbogaard et al., 2000) is an example of a sophisticated unsteady model. The POINT-SAND model is used in the present study and therefore, it will be described in more detail in the following section.

The POINT-SAND model (PSM)

The POINT-SAND model is a computer code solving the relevant equations for momentum, turbulence and sediment as a function of the vertical co-ordinate, as well

as in time, for wave-current-turbulence-sediment interactions in free-surface flows as well as in wave tunnels. The POINT-SAND model contains state-of-the-art formulations of sand transport processes and particularly a novel direct simulation of wave-current-turbulence interactions. The PSM model can be used for simulating, in time, the vertical distribution of suspended sand in horizontal and vertical orbital motion, possibly superimposed on a turbulent current, in tunnels, free-surface wave channels or in the field with different wave and current directions.

The user can select between two different versions of the PSM model:

1) For real waves including the vertical orbital velocities and net wave-induced currents (as in field conditions);
2) For horizontal oscillatory flows only (as in wave tunnels).

In order to study sediment transport phenomena under controlled simulated wave conditions often oscillating water tunnels are used. The generated oscillatory flow is purely horizontal. Therefore, a special version of the PSM model is prepared for oscillatory flows alone, which can be considered as the first-order representation of the sediment transport phenomena in the boundary layer under progressive waves. More detail about the PSM model can be found in Uittenbogaard et al. (2000), Uittenbogaard (2000) and Bosboom and Klopman (2000). The following part shows a detailed description of the wave-tunnel version of the PSM model.

Basic equations of the wave-tunnel version

In the POINT-SAND model the flow velocity is derived from the momentum balance of water in the flow direction. The sediment concentration over the whole depth is derived from the mass balance of sediment by assuming that sediment can be transported by advection and by turbulent diffusion (even inside the sheet-flow layer). Davies et al. (1997) showed that it is possible to predict quite well sand transport under sheet-flow conditions using the advection-diffusion model. The basic momentum equation describing the horizontal flow velocity inside the wave boundary layer reads:

$$\varepsilon \frac{\partial u}{\partial t} = - \frac{\partial p}{\partial x} + \varepsilon \frac{\partial}{\partial z}\left((\varepsilon + \varepsilon_t)\frac{\partial u}{\partial z}\right) \tag{4.31}$$

The mass balance of sediment results in the following advection-diffusion equation:

$$\frac{\partial c}{\partial t} = \frac{\partial}{\partial z}\left(w_s c + \varepsilon_s \frac{\partial c}{\partial z}\right) \tag{4.32}$$

where: t = time; p = pressure; c = sediment concentration; ν = kinematic viscosity; ν_t = eddy viscosity; ρ = fluid density and ε_s = sediment diffusivity.

The sediment diffusivity ε_s is assumed to be equal to ν_t/σ_ρ. Where σ_ρ is Prandtl/Schmidt number and assumed to be equal to 0.7.

The POINT-SAND model takes into account the sediment-flow interaction in the momentum equation by replacing the density of water (ρ) by the density of sand-water mixture. In order to solve these two equations (4.33, 4.34), four boundary conditions and expressions for the eddy viscosity and the sediment diffusivity (turbulence closure) are required. Also the horizontal pressure gradient must be known. The horizontal pressure gradient in equation 4.31 is prescribed by:

$$\frac{1}{\rho}\frac{\partial p}{\partial x} = -\frac{\tau_b}{h} + \frac{u(t) - u_o(t)}{2\Delta t} \tag{4.33}$$

where: τ_b = bed shear stress, h = total depth, u(t) = depth-averaged flow velocity computed in the previous time step, $u_o(t)$ = the desired depth-averaged velocity prescribed by the user either by time series or a harmonic series and $2\Delta t$ = relaxation time empirically equal to twice the time step Δt of the numerical solution procedure.

In the right hand side of equation 4.33 the first part is due to the depth-integrated momentum balance and the second part is a simple pressure correction.

Turbulence closure

The standard POINT-SAND model is equipped with a κ-ε turbulence model. The κ-ε model is a two-equation model with the following generic equations for turbulent kinetic energy (TKE) and for energy dissipation rate ε, respectively:

$$\frac{\partial k}{\partial t} = \frac{\partial}{\partial z}\left[(\nu + \nu_t/\sigma_k)\frac{\partial k}{\partial z}\right] + P_k - \varepsilon - B_k \tag{4.34}$$

$$\frac{\partial \varepsilon}{\partial t} = \frac{\partial}{\partial z}\left[(\nu + \nu_t/\sigma_\varepsilon)\frac{\partial \varepsilon}{\partial z}\right] + \frac{\varepsilon}{k}(c_{1\varepsilon} P_k - c_{2\varepsilon}\varepsilon - c_{3\varepsilon} B_k) \tag{4.35}$$

$$B_k = \frac{\nu_t}{\sigma_\rho N^2} \quad , \quad N^2 = -\frac{g}{\rho}\frac{\partial \rho_m}{\partial z} \tag{4.36}$$

where: B_k = the buoyancy flux; ν_t = eddy viscosity; P_k = turbulence production; ε = dissipation rate; N^2 = buoyancy frequency; ρ_m = density of sand water mixture; σ_ρ = Prandtl/Schmidt number, $c_{1\varepsilon}$, $c_{2\varepsilon}$, σ_ρ, σ_k, σ_ε are constants equal to 1.44, 1.92, 0.7, 1.0 and 1.3, respectively. $c_{3\varepsilon}$ is a constant equal to 0 when $N^2 > 0$ and equal to 1 when $N^2 < 0$.

The turbulent kinetic energy is derived from a separate transport equation of k (equation 4.36). This is an advanced way of modelling turbulence, because the memory of turbulence is taken into account. The equation of k includes a buoyancy term, which reduces the turbulent kinetic energy and therefore the eddy viscosity and sediment diffusivity if a negative vertical density or sediment concentration gradient is present (turbulence damping due to flow stratification).

The buoyancy flux B_k (= $\nu_t/(\sigma_\rho N^2)$) in equation 4.36 represents the conversion of turbulent kinetic energy to mean potential energy or vice versa. In equations 4.34 and 4.35 P_k is the turbulence production term that is extended in the model by wave-turbulence interaction. The eddy viscosity ν_t is equal to $0.09(k^2/\varepsilon)$. The exact formulation and all details can be found in Uittenbogaard et al. (2000).

Boundary conditions for momentum equation

In general two boundary conditions are required for solving the momentum equation. The first one at the upper point of the flow (z = h):

$$\frac{\partial u}{\partial z} = 0 \qquad \text{at} \qquad z = h \tag{4.37}$$

While the second boundary condition is to describe the velocity close to the bed and to define the zero velocity level. The PSM model uses a partial slip condition for the turbulent flow along a bed in the fully rough regime, close to the approach of Hinze (1975) and Jackson (1981). In this approach the flow velocity is assumed to be zero at a certain level below the reference level z_0 inside the sand bed. The reference level z_0 can be defined by the user or is usually assumed to be equal to $k_s/30$ with k_s is the roughness height, which in general is related to the grain diameter (for example $k_s = 2.5D_{50}$). However, different expressions can be also used. The near-bed velocity distribution is assumed to follow the log-law as follows:

$$\frac{u(z)}{u_*} = \frac{1}{\kappa}\ln\left(9+\frac{z}{z_0}\right) \qquad , \qquad u_*^2 = \left(\upsilon_t(z)\frac{\partial u}{\partial z}\right)_{z=0} \tag{4.38}$$

where: u_* = the shear velocity and κ = Von Karman coefficient (= 0.4).

According to equation 4.38 the velocity gradient at z = 0 can be described by:

$$\left.\frac{\partial u}{\partial z}\right|_{z=0} = \frac{u_*}{9\kappa z_0} \qquad \text{at} \qquad z = 0 \tag{4.39}$$

Boundary conditions for κ-ε model

The following boundary conditions are required for solving the κ-ε model:

1. At the bed and the water surface the vertical diffusion of turbulent kinetic energy is equal to zero;
2. On the bed a usual boundary condition for high-Reynolds turbulence models is imposed (equation 4.38) and a logarithmic boundary layer must hold.

$$\varepsilon = \upsilon_t \left(\frac{\partial u}{\partial z}\right)^2 = \frac{u_*^3}{\kappa(z+9z_0)} \tag{4.40}$$

More detail can be found in Uittenbogaard et al. (2000).

Boundary conditions for the advection-diffusion equation

The advection-diffusion equation is subjected to the boundary conditions of zero flux at the water surface and a specified time-dependent boundary condition at a reference level close to the bed ($z_a = 2D_{50}$).

1. Reference concentration c_a at a certain elevation z_a above the bed;
2. Level at the upper boundary, where the vertical sediment flux is equal to zero.

The user can choose between two different forms for the boundary condition based on reference concentration. The first one prescribes the sediment concentration at a certain reference level z_a:

$$c(z_a, t) = c_b(t) \tag{4.41}$$

or reformulated in terms of a pick-up function:

$$w_s c_b(t) + (\varepsilon_s)\left.\frac{\partial c}{\partial z}\right|_{z=z_a} = 0 \tag{4.42}$$

The formulation of Zyserman & Fredsøe (1994a) for the reference concentration $c_b(t)$ was implemented in the POINT-SAND model:

$$c_b(t) = \frac{0.331(\theta-\theta_{cr})^{1.75}}{1+\frac{0.331}{C_m}(\theta-\theta_{cr})^{1.75}} \qquad \text{at} \qquad z_a = 2D_{50} \tag{4.43}$$

where: θ is the Shields parameter and θ_{cr} is the critical Shields parameter and C_m = maximum concentration.

The Zyserman and Fredsøe (1994a) expression for c_b is an empirical relation, based on near-bed concentration measurements in steady flow. This expression contains a coefficient C_m, representing the bed concentration, which for steady flow is set at 0.48. However, Zyserman and Fredsøe (1994b) noticed that it might be smaller and

found for oscillatory flow better results, if the value of this coefficient was set at 0.32. Zyserman and Fredsøe (1994a) found that there is no significant influence of the critical value of the used Shields parameter on the values of the bed concentrations c_b. In the present study, the critical Shields parameter θ_{cr} is calculated according to the proposed method of Van Rijn (1993).

Hindered settling

In the POINT-SAND model the settling velocity of sediment particles is computed according to Van Rijn (1993) but reduced by hindered settling. The settling velocity $w_{s,0}$ of a single particle in infinite fluid, without wall effects, reads:

$$w_{s,0} = \frac{\Delta g D_s^2}{18\nu} \qquad 0.01\ mm < D_s \le 0.1\ mm$$

$$w_{s,0} = \frac{10\nu}{D_s}\left(\sqrt{1+\frac{0.01\Delta g D_s^3}{\nu^2}}-1\right) \qquad 0.1\ mm < D_s \le 1.0\ mm \qquad (4.44)$$

$$w_{s,0} = 1.1\left(\Delta g D_s\right)^{0.5} \qquad 1.0\ mm < D_s$$

where: D_s = diameter of the suspended sediment.

In high concentration mixtures, the settling velocity of a single particle is reduced by the flow as well as fluid stresses induced by other particles. Following Richardson & Zaki (1954) the POINT-SAND model takes into account the hindered settling effect on the particle settling velocities as follows:

$$w_s = \left(1-\frac{C}{C_s}\right)^5 w_{s,0} \qquad (4.45)$$

where $w_{s,0}$ defined by equation 4.44 and C = the volume fraction of the all suspended sediment. C_s = 0.65 is taken as the maximum volume fraction of solids in a non-cohesive porous bed.

Flow stratification

Due to the relatively small thickness of the sheet-flow layer, the vertical concentration gradient is extremely large. If the sand-water mixture is considered as a continuum, the density of the mixture ρ_m is determined by the density of the water ρ, the density of the sediment ρ_s and the sediment concentration c, i.e. $\rho_m = c\,\rho_s + (1-c)\,\rho$. The large vertical negative concentration gradient corresponds to a large vertical negative density gradient.

The upward mixing of suspended sediment involves the conversion of turbulent kinetic energy (TKE) of the fluid into an increasing potential energy of the sediment. The latter is subsequently destroyed by the viscous drag while the particles settle. The rate of conversion of TKE into the sediment's potential energy is called buoyancy flux. The latter is included in the implemented k-ε turbulence model by assuming the analogy between sediment-laden flows and flows with density stratification. Accordingly, the total fluid-sediment density then estimates the buoyancy flux for the sediment.

4.6 Behaviour of quasi-steady, intermediate and unsteady models

As described before, phase-lag effects of sediment become important when sediment particles are entrained from the bed to relatively high levels in the water column and much time is needed for the re-settling process of the particles back to the bed. The assumption of a quasi-steady process is only valid if this settling time T_f is an order of magnitude smaller than wave period T. In principle, this type of time-history effects become relatively more important for short wave periods and large sediment entrainment levels. The latter may be expected for relatively fine sands and high flow velocities.

Quasi-steady models totally ignore the phase-lag effect on sediment transport. While, intermediate models take into account the phase-lag effects on the total-transport rates. Although the two intermediate models of D&W and of D-J are of a different origin, they contain a similar 'phase-lag parameter' (ω and p), representing the ratio of T_f and the (full or half-cycle) wave period T.

Following D-J's approach, figure 4.3 shows the validity regime of the 'quasi-steady' model of Ribberink in terms of velocity amplitude and wave period of the oscillation for three-grain sizes (below the three lower lines). Above the lines phase-lag effects become important and the 'semi-unsteady' model approach of D-J is required. The upper bold line represents the maximum velocity constraint due to wave breaking (criterion of Miche). It is shown that phase-lag effects may easily occur for relatively large flow velocities and fine sand.

Although the concepts of D&W and D-J describe the same phase-lag phenomenon, considerable differences are present in model behaviour. Figure 4.4 shows a comparison between the three 'quasi-steady' formulae of Bailard, Ribberink and D&W-qua (= quasi-steady version of D&W with phase-lag effects switched off), the two 'intermediate' formulas of D-J, D&W and the POINT-SAND model (PSM). Computed net transport rates are shown for increasing (oscillatory) flow velocity (U_{rms}= root mean square velocity). The oscillatory flow is caused by an asymmetric (2^{nd}-order Stokes) wave with constant asymmetry (i.e constant ratio of second-order and first-order velocity amplitude $u_2/u_1 = 0.26$) and a constant wave period (T = 6.5 s). The sand used in the calculations has a median diameter D_{50} = 0.13 mm.

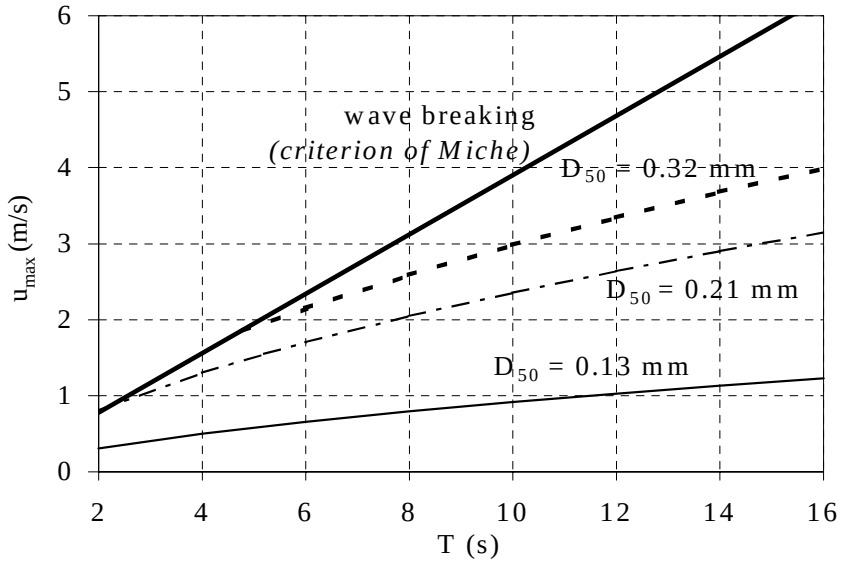

Figure 4.3: Velocity–period–grain size regime for the importance of phase-lag effects (above the curves; after Dohmen-Janssen et al., 2002).

In figure 4.4 the onshore direction means that the sediment is transported in the direction of the maximum flow velocity, i.e. the crest direction. The offshore direction means that the sediment is transported in the direction opposite to the maximum flow velocity, i.e. in the direction of the trough velocity.

The calculated transport rates in figure 4.4 show that the quasi-steady models of Bailard, Ribberink and D&W-qua always lead to positive (= onshore) net transport rates, which increase progressively for increasing flow velocity. As could be expected the two intermediate models of D&W and D-J lead to a reduction of the transport rate, which becomes stronger for increasing velocities. The phase-lag effect in model of D-J shows a clear effect on the results for the cases with $U_{rms} > 0.4$ m/s. While the phase-lag effect in the model of D&W changes the transport rates for the cases with $U_{rms} > 0.58$ m/s. However, both intermediate models show considerable differences in their behaviour and strength of the phase-lag correction. D&W's correction even leads to a reversal of the net transport direction (from 'onshore' to 'offshore').

The PSM model shows a similar behaviour as the model of D&W. The PSM model shows a clear reduction in transport rates in the velocity range $0.6 < U_{rms} < 0.75$ m/s and even negative transport rates for higher velocities. The PSM model is implicitly able to account for phase-lag effects through modelling of the time-dependent concentrations over the complete water column. Including hindered settling of sand particles and modelling the flow stratification effects leads to stronger phase-lag effects on the computed transport rates. Figure 4.5 shows a comparison between the

PSM model results in case of including and excluding the effects of hindered settling of sand particles and flow stratification.

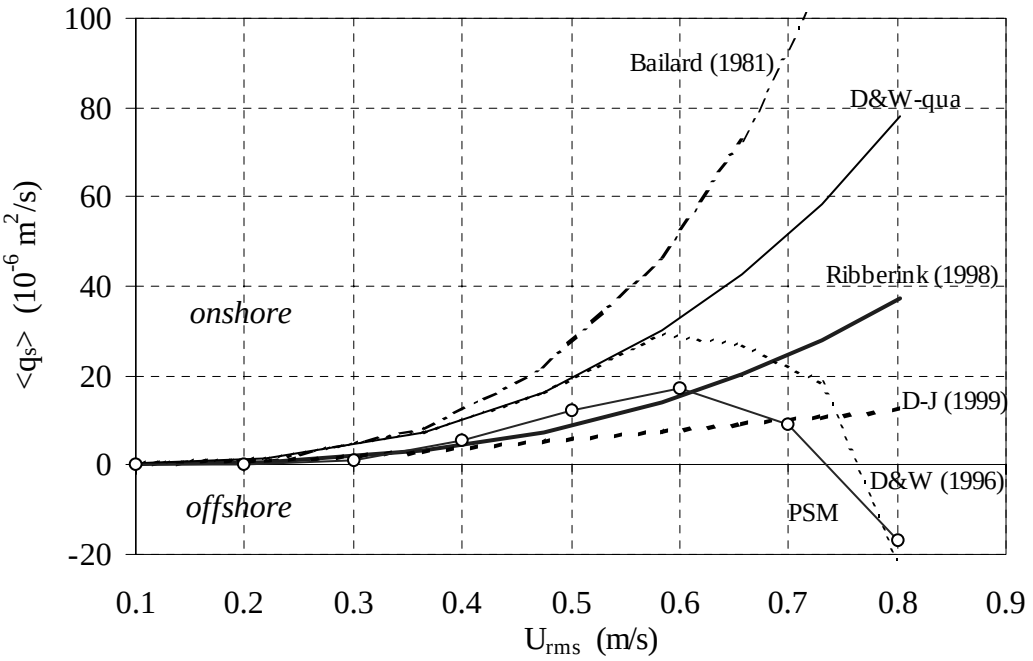

Figure 4.4: Comparison of quasi-steady, intermediate and unsteady transport models, computing net transport rates under 2nd-order Stokes waves (T= 6.5 s, u_2/u_1 = 0.26, D_{50}= 0.13 mm).

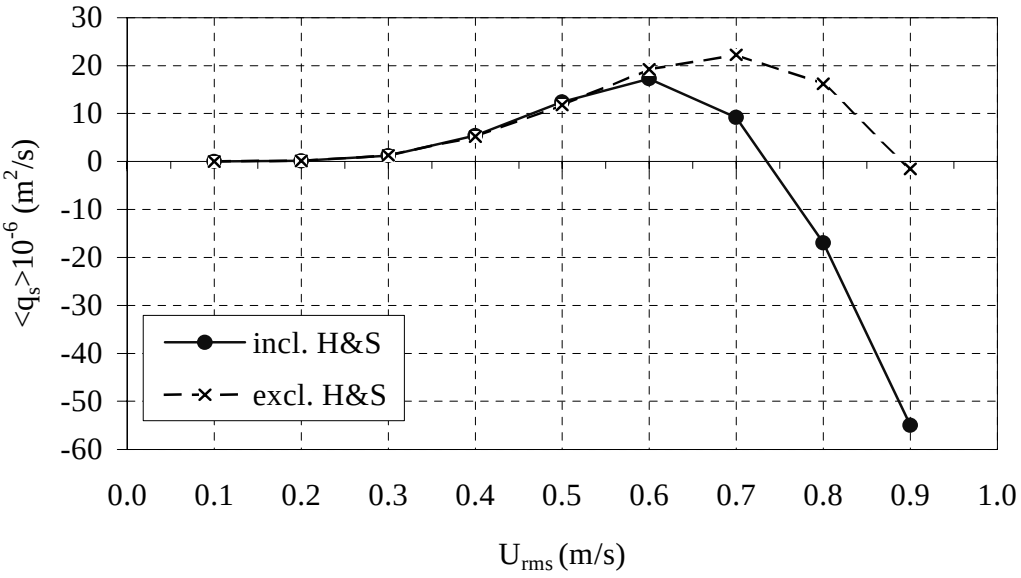

Figure 4.5: Comparison between the PSM model results in case of including and excluding hindered settling of sand particles & flow stratification (H&S), computed net transport rates under asymmetric waves (D_{50}= 0.13 mm, T= 6.5 s, u_2/u_1 = 0.26).

It is shown in figure 4.5 that including hindered settling and flow stratification effects leads to significant reduction in the net transport rates (U_{rms} > 0.6 m/s) and even leads to change in transport direction from onshore to offshore direction. The model results are identical in the low velocity range (U_{rms} < 0.6 m/s). Indicating that hindered settling and flow stratification effects are negligible in low velocity regime, U_{rms} = 0.5 m/s.

4.7 Summary

In the present chapter different classes of sediment transport models are discussed. These models are widely used in oscillatory flow conditions and can be classified into 3 main groups as follows:

- Quasi-steady models: In these models it is assumed that sediment transport reacts immediately to the time-dependent horizontal flow velocity throughout the wave-cycle, without any phase difference between the flow velocity and the concentration (quasi-steadiness). According to the assumption of quasi-steadiness this type of models is only valid for conditions in which the response time of the sediment particles is relatively short. Since the time-dependent velocity and parameters such as grain-size and bed roughness height are the main input parameters, this kind of models is relatively easy to use. Quasi-steady models were developed by Bailard (1981) and Ribberink (1998). They have a semi-empirical character and are strongly based on experimental data;
- Intermediate models: In this kind of models the effect of the observed time-lag between the flow velocity and the sediment concentration under waves is included in a parameterised way, without simulating the details of velocity and concentration profiles. Intermediate semi-empirical sediment transport models were developed by Dibajnia & Watanabe (D&W, 1996) and Dohmen-Janssen (D-J, 1999);
- Unsteady models: These models are based on a full time-dependent simulation of both velocity and concentration profiles during the wave-cycle. Many unsteady models derive the unsteady flow velocity from the basic Navier-Stokes equation, while the sediment concentration is derived from an advection-diffusion equation. Existing unsteady models mainly differ in the applied boundary conditions and turbulent closure schemes. Moreover, some unsteady models include sediment-flow interaction effects, i.e. the flow velocities are affected by the presence of sediment concentrations and vice versa. Unsteady transport models are relatively difficult to use compared to the other (quasi-steady and intermediate) model types. The detailed calculations require much insight of the various physical transport processes and demand much computing time. The POINT-SAND model (PSM) of Uittenbogaard et al. (2000) is a flexible unsteady transport model including i) wave-current interactions over the complete water column, ii) various turbulence closure schemes with and without sediment/flow interactions.

The quasi-steady and the intermediate transport models of Ribberink (1998) and D-J (1999) were calibrated using uniform sand data from the LOWT of WL | Delft Hydraulics. The model of Dibajnia & Watanabe (1996) was developed using data from the small water tunnel of Tokyo University. In general, the described transport models were only verified against limited ranges of conditions (velocities, grain-sizes). In chapter 8 a more extensive model verification will be carried out, using laboratory data from different experimental facilities covering a wide range of conditions.

A comparison between the described quasi-steady, the intermediate transport models and the POINT-SAND model for 2nd-order Stokes waves and 0.13 mm uniform sand showed the following:

- The transport rates calculated by the quasi-steady models are always in the onshore direction (wave crest velocity direction) and they have the same order of magnitude (± factor 2);
- The two intermediate models show similar onshore transport rates for low flow velocities. However, due to phase-lag effects much lower transport rates are predicted above a certain flow velocity (u_{rms} = 0.4-0.6 m/s). Both intermediate models show considerable differences in the large velocity regime. D&W's correction even leads to a reversal of the net transport direction (from 'onshore' to 'offshore') in this regime;
- The unsteady PSM model shows a similar behaviour as the intermediate model of D&W. The PSM model is implicitly able to account for phase-lag effects through modelling of the time-dependent concentrations over the complete water column. The PSM model shows reducing transport rates for increasing velocity, in the velocity range U_{rms} > 0.6 m/s and negative transport rates for U_{rms} > 0.75 m/s;
- Including hindered settling and flow stratification effects in the PSM model leads to a significant reduction in the net transport rates and even leads to a change in transport direction from 'onshore' to 'offshore' in the high velocity range. The model results are hardly affected in the low velocity range (U_{rms} < 0.6 m/s).

Considering the large differences in model behaviour a systematic further verification with data covering a wide range of conditions is needed in order to obtain more insight into the validity and limitations of the different model types (see chapter 8).

Finally, an important assumption in these five existing transport models is the uniformity of the sand, i.e. the assumption that the sediment mixture can be characterised by a single sand-size (D_{50}). This simplification is mainly caused by a lack of knowledge of the behaviour of different size fractions in a mixture, especially for oscillatory flows. One of the main goals of the present study is to develop a model for predicting transport rates of mixed sand and to predict also the size-composition of the transported sand (selective processes). In the next chapter 5 a

multi-fraction approach will be discussed for all transport models to study size-graded sand transport in more detail.

Chapter 5

MODELLING OF GRADED SAND TRANSPORT

5.1 Introduction

In the different types of transport models as described in chapter 4 the sediment is characterised by the median diameter only (D_{50}). In fact, this assumption is satisfactory in the case of uniform sediment. Applying this assumption on graded sediment may not always be sufficient to simulate the sediment behaviour correctly, see Dibajnia & Watanabe (1996) and Van Rijn (1997). The transport rate of the coarse size-fractions may be different from the transport rate of the fine size-fractions and consequently the total transport rates of all sand sizes can be different (see also Dohmen-Janssen, 1999).

For improved transport modelling the bed material can be divided into size-fractions (i = 1, ….. N) with diameter D_i and with a volume probability of occurrence in the bed P_i. In this chapter this size-fraction or multi-fraction approach is applied to the sediment transport models. This approach will be verified in chapter 8 using laboratory data with graded sand.

A general description of the multi-fraction approach is given in section 5.2. In section 5.3 the multi-fraction versions of quasi-steady models of Bailard and Ribberink are described. The multi-fraction intermediate models of D-J and D&W are described in section 5.4. Section 5.5 describes how the size-fraction approach is implemented in the POINT-SAND model. Section 5.6 shows an inter-comparison of the various graded sediment models for a wide range of flow velocities and the behaviour of the models is studied in more detail. Finally, section 5.7 presents a summary of chapter 5.

5.2 Size-fraction approach

In order to take into account the variation of grain-sizes in the bed material, the so-called size-fraction method can be used. In the size-fraction method, the bed material is divided into a number of size-fractions, each characterised by a certain diameter D_i and by a volume percentage of occurrence in the bed material (probability) P_i. The simplest hypothesis is that the transport rates for each size-fraction can be calculated as follows (see e.g. Ribberink, 1987):

$$q_i = P_i \; q_{u,i} \tag{5.1}$$

where: q_i = transport rate for fraction i and $q_{u,i}$ = transport rate for fraction i as if the sand bed was composed of a single sand size D_i alone.

The total transport rate in the case of N size-fractions q_N is equal to the sum of the transport rates of all size-fractions:

$$q_N = \sum_{i=1}^{N} q_i \tag{5.2}$$

For N = 1 there is only one size-fraction and the bed material is considered to be uniform. The parameter q_N/q_1 is the ratio of the transport rate of a mixture characterised by N fractions with different diameters and the transport rate for a mixture characterised by D_{50} only. This parameter gives an indication of the impact of the use of the size-fraction method on the predicted total transport rates.

The contribution of fraction i to the net total transport rate $P_{T,i}$ can be calculated using:

$$P_{T,i} = q_i / q_N \tag{5.3}$$

The ratio of the mean diameter of the transported material and the bed material, D_T/D_m is an indication for selective transport, i.e. the deviation in composition of the transported material and the bed material. If D_T/D_m is larger than 1, the transported material is coarser than the bed material. This means that the coarse fractions are more mobile than the fine fractions and the contribution of the coarse fractions to the transport is larger than their probability in the bed. If D_T/D_m is smaller than 1 the fine fractions are more mobile. The mean diameter D_m of the bed material is defined as:

$$D_m = \sum_{i=1}^{N} (D_i \cdot P_i) \tag{5.4}$$

The mean diameter of the transported material D_T is determined by:

$$D_T = \sum_{i=1}^{N} (D_i \cdot P_{T,i}) \qquad (5.5)$$

It must be emphasized that the size-fraction method as given in equation (5.1) does not include any interaction between the different sediment fractions.

In the present study the size-fraction method has been implemented in the transport models of Bailard, Ribberink, Dohmen-Janssen, Dibajnia & Watanabe and the POINT-SAND model, as described in sections 4.3 to 4.5. The new multi-fraction models are described in the following sections (see also Kroekenstoel et al., 2000 for the description of the multi-fraction quasi-steady and intermediate models).

5.3 Quasi-steady transport models

Bailard's model (1981)

Applying the size-fraction approach, equation (5.1), to the model of Bailard gives:

$$q_{b,i}(t) = P_i \frac{\frac{1}{2} f_w \rho_b}{\rho g \tan\varphi} u^3(t) \qquad \textit{(bed-load transport)} \qquad (5.6)$$

$$q_{s,i}(t) = P_i \frac{\frac{1}{2} f_w \rho_s}{\rho g w_{s,i}} \left| u(t)^3 \right| u(t) \qquad \textit{(suspended-load transport)} \qquad (5.7)$$

In the model of Bailard, the friction coefficient f_w is related to the bed roughness height. The bed roughness height is not determined by a single grain, but by the combination of all grains in the bed material. It is assumed to be the same for all size-fractions and is related to the D_{50} of the sand mixture ($k_s = D_{50}$ in the formula of Swart, 1974, see equation 4.13).

It is clear from equation (5.6) that the bed-load transport does not depend on the diameter of the fraction D_i. Therefore, the total bed-load transport for N fractions is equal to the total bed-load in case of one fraction. The total suspended-load transport depends on the diameter of the fraction D_i through the settling velocity $w_{s,i}$. Therefore, it can be expected that finer sizes in a mixture (with smaller D_i) contribute more to the total suspended transport than the coarser sizes.

Ribberink's model (1998)

Applying the size-fraction approach, equation (5.1), to the model of Ribberink gives:

$$\Phi_i(t) = \frac{q_{s,i}}{\sqrt{g\Delta D_i^3}} = P_i \cdot 11\left[\left|\theta_i(t)\right| - \theta_{cr,i}\right]^{1.65} \frac{\theta_i(t)}{\left|\theta_i(t)\right|} \tag{5.8}$$

In the model of Ribberink the transport rate is directly related to D_i, since the Shields parameter depends on the grain-size. For each size-fraction i the effective Shields parameter is defined as follows:

$$\theta_i = \frac{\tau_b}{(\rho_s - \rho_w) g D_i} \tag{5.9}$$

The bed shear stress (τ_b) is related to the combined friction factor, f_{cw} (see equation 4.11). The friction coefficient on its turn is related to the bed roughness height k_s (see equations 4.13 and 4.14) and is not determined by a single grain. For a sand-mixture the bed roughness height is selected the same for all size-fractions, i.e. $k_s = D_{50}$ of the mixture for each size fraction.

5.4 Intermediate transport models

Model of Dohmen-Janssen (1999)

The model of Dohmen-Janssen gives in combination with the size-fraction approach:

$$< q_{s,i} > = r_i < q_{s,i} >_{\text{Ribberink}} \tag{5.10}$$

This model uses the transport rates predicted by the model of Ribberink (1998). The phase-lag correction factor r depends on the phase-lag parameter p, which on its turn depends on the settling velocity $w_{s,i}$ (which is different for each size-fraction) and the wave friction factor f_w. If an empirical relation is chosen for p (see equation 4.23), then the expression for the phase-lag parameter p also directly depends on the grain diameter. Larger grain-sizes in a mixture will result in smaller values for the phase-lag parameter p and, as a result, the phase-lag correction factor r will be closer to 1.

Model of Dibajnia & Watanabe (1996)

Applying the size-fraction approach, equation (5.1), to the model of Dibajnia & Watanabe gives:

$$q_{s,i} = P_i \, w_{s,i} \, D_i \, 0.0015 \, |u|^{0.5} \frac{u}{|u|} \tag{5.11}$$

$$u_j = \frac{1}{2} \frac{u_j^2}{\nu g \, w_{s,i} T_j} \tag{5.12}$$

The model of D&W varies for the different sediment size-fractions through $w_{s,i}$ and D_i. The parameter Γ is also dependent on the settling velocity $w_{s,i}$ and the diameter D_i, see equations 4.27 and 4.28 in section 4.4.

Model of Dibajnia & Watanabe (1996 Adjusted)

Originally, the model of D&W was developed for uniform sands. In 1996 D&W found that the model results did not give a very good fit with experimental data of a mixture consisting of two sands (0.20 mm and 0.87 mm). During their water tunnel experiments at the university of Tokyo they noticed that the transport rate of the fine sand was reduced by the presence of the coarse sand in the mixture. Therefore, D&W suggested an adaptation for their model in case of sand mixtures. A limitation of this adaptation is that it can only be applied to mixtures consisting of two size-fractions. The modified model is as follows:

$$q_{s,i} = w_{s,i}\, D_i\, 0.0015\, |\blacksquare|^{0.5}\, \frac{\blacksquare}{|\blacksquare|} \qquad (5.13)$$

$$\blacksquare_j = \frac{1}{2} \frac{u_j^2}{\blacksquare g w_{s,i} T_j} \cdot (P_i)^{\frac{1}{\blacksquare_i}} \qquad (5.14)$$

where: α_i = empirical coefficient, depending on the ratio of the mean diameter of each size-fraction to that of the other size-fraction. For a mixture consisting of 0.2 mm sand and 0.87 mm sand Dibajnia & Watanabe proposed $\alpha_{0.2} = 1$ and $\alpha_{0.87} = 4$.

The modification of Dibajnia & Watanabe is based on correcting the parameter ω instead of correcting the net transport rate. The parameter ω represents the ratio of the time required of a suspended sand particle to reach the bed to the period of each half-wave-cycle ($T_{f,i}/T_j$). According to their correction in equation 5.14 D&W assumed that more flow energy is consumed to entrain coarse grains into the flow (increased exposure) and less flow energy is consumed to entrain fine grains into the flow (decreased exposure or hiding) compared to the uniform situation. This correction leads to increasing the transport rates of the coarser grains and reducing the transport rates of the finer grains in a mixture.

Dibajnia & Watanabe did not indicate how the empirical coefficient α_i should be determined for other mixtures than the one of two sizes they investigated experimentally.

5.5 Unsteady transport models

The size-fraction approach (equations 5.1 and 5.2) has been implemented in the POINT-SAND model in order to take into account the size-gradation of the sand

particles. Moreover, to give the POINT-SAND model the ability to predict the size-composition of the transported sand.

Basically, it is possible to compute the suspended-load for any known type of bed material and flow condition by dividing the bed material into a number of size-fractions. Applying this approach will result in using different settling velocities ($w_{s,i}$) and different reference concentration $c_i(a)$ for each size-fraction. The basic hypothesis to compute the reference concentration of any sand mixture is based on dividing the bed material in a number of size-fractions and to compute the reference concentration $c_i(a)$ of each size-fraction using an existing single-fraction method. The reference concentration of each size-fraction can be calculated as follows:

$$c_i(a) = P_i \; c_{a(D_i)} \tag{5.15}$$

where: $c_{a(Di)}$ = reference concentration of size-fraction i, based on uniform bed material, with median diameter $D_i = D_{50}$ of each size-fraction.

It is important to state that according to the size-fraction approach the PSM model does not account for any interaction between the different grain-sizes in predicting the bed reference concentrations. Meanwhile, the model takes into account the interaction between different sizes in computing both the flow stratification and hindered settling. In other words, these two parameters are computed for the whole sand mixture (all fractions together) before calculating the net total transport rates of all sizes.

5.6 Behaviour of graded-sand transport models

5.6.1 Number of size-fractions

In this section the behaviour of the graded transport models discussed in the previous sections is analysed in more detail. A series of computations are carried out with the models of Bailard (1981), Ribberink (1998), Dohmen-Janssen (1999), Dibajnia & Watanabe (1996) and the POINT-SAND model. The main goals of this analysis can be summarised as follows:

1. To study the effect of using the size-fraction approach on the predicted total net transport rates;
2. To study the sensitivity of the model results to the number of size-fractions N in the calculations (indicated by 'q_N/q_1');
3. To gain more insight into the selective transport behaviour of the different graded transport models and intercompare these models, through studying the difference between the mean diameter of the transported material and the mean diameter of the original bed material (indicated by D_T/D_m, see equation

5.4 and 5.5). Moreover, studying the influence of the total number of fractions N on this ratio D_T/D_m.

A basic research question associated with selective behaviour of size fraction is: Are mainly the fine or mainly the coarse fractions transported and to what extent is the composition of the transported material different from the composition of the bed material? See also the research questions in section 1.3.

In order to see if the selective transport behaviour depends on the imposed flow velocities, two different hydraulic conditions have been compared (each 2^{nd}-order Stokes waves). For practical reasons these conditions are equal to two of the imposed hydraulic conditions of the wave tunnel experiments as described in section 6.2.3 (series P). Also the same bed material has been used, a bi-modal mixture of 70% fine sand (D_{50} = 0.21 mm) and 30% coarse sand (D_{50} = 0.97 mm). Each sand fraction has a geometric standard deviation $\blacksquare_g$ equal to 1.3 (see section 6.2.2).

The sand mixture is divided into respectively, 1,2,4,6 and 8 fractions, which are each characterised by grain-size D_i and probability P_i. In case of a distinction in N (= 4,6,8) fractions both parts of the bi-modal sand are split up in N/2 sub-fractions.
The D&W-adjusted model is not included in this model intercomparison because this model was developed for the cases with two size-fractions only, while the present computations used more size-fractions.

Figures 5.1 to 5.5 show the sensitivity of the models for changing the number of size-fractions N for two different flow velocities (U_{rms} = 0.6 and 0.9 m/s). In all figures q_N represents the total transport rate of all fractions, when the sediment is split up in N fractions (N = 1,2,4,6,8) and q_1 is the total transport rate using only 1 fraction with $D_1 = D_{50}$ of the sand mixture. The number of size-fractions N is plotted on the x-axis and the two ratios of q_N/q_1 and D_T/D_m are on the y-axis. The main conclusions from the results of the models of Bailard, Ribberink, D-J, D&W and the POINT-SAND are discussed in the following subsections, respectively.

Model of Bailard

Figure 5.1 shows the results of the model of Bailard. It can be seen that the predicted total transport rate remains more or less constant if the number of fractions N is increased. Moreover, using the size-fraction method does not change the predicted total transport rates for the two hydraulic conditions. The ratio of q_N/q_1 seems to be independent of the number of fractions and of the imposed flow velocities ($q_N/q_1 \approx 1$).
Figure 5.1 also shows that in multi-fraction calculations (N > 1) the transported material has a much smaller mean diameter than the bed material ($D_T/D_m \approx 0.75$). Apparently, the finer fractions contribute more and the coarser fractions contribute less to the total transport rate than their contribution in the bed material would suggest. The grain-size composition of the transported material (D_T) seems not to be affected by increasing the total number of size-fractions N ($N \geq 2$) and changing the

hydraulic conditions. Increasing the number of fractions N only slightly reduces the ratio of D_T/D_m. The differences however are very small. For higher flow velocities (U_{rms} = 0.9 m/s) the ratio of D_T/D_m is a little smaller than for lower flow velocities (U_{rms} = 0.6 m/s), indicating that increasing the flow velocity leads to transporting relatively more fine particles than the coarse ones.

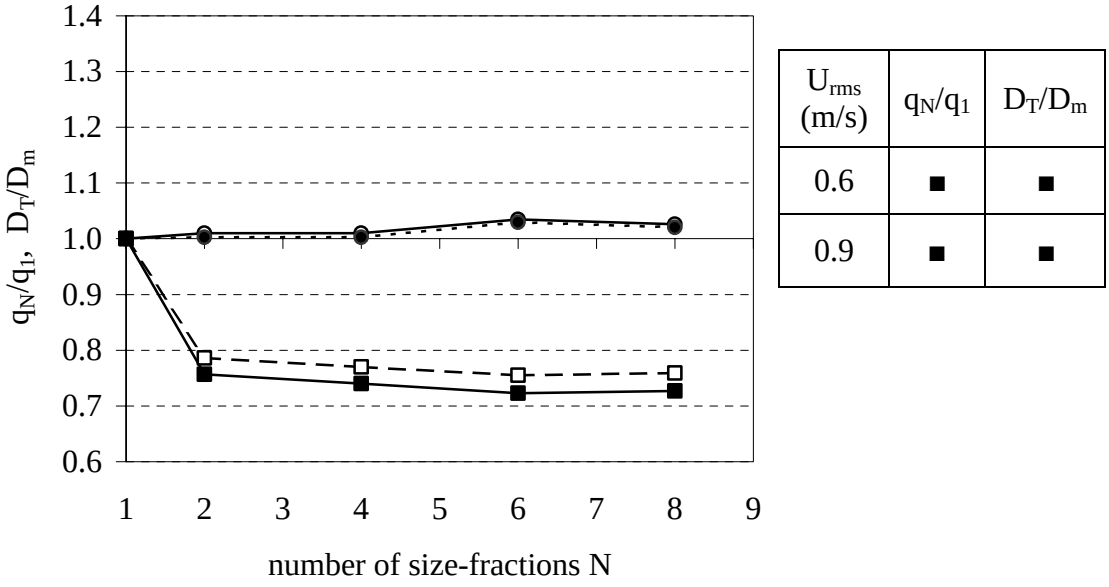

Figure 5.1: Sensitivity of the multi-fraction model of Bailard to changing the number of size-fractions N (U_{rms} = 0.9 and 0.6 m/s).

From the results of the model of Bailard it can be concluded that the multi-fraction method has a very limited effect on the calculated total transport rates. The composition of the transported material is generally finer than the bed material for the chosen sand mixture (selective transport).

For the selected conditions the optimum number of size-fractions for a minimum computation time (minimization of N) but still accurate transport rate and transport composition seems to be about N = 2.

Model of Ribberink

Figure 5.2 shows similar computation results of the model of Ribberink. From figure 5.2 it can be seen that the multi-fraction method leads to about 10% higher transport rates than the single-fraction method ($q_N/q_1 \approx 1.1$). For $N \geq 2$ the ratio of q_N/q_1 seems to be independent of the number of fractions N and of the imposed flow velocities ($q_N/q_1 \approx 1.1$ for both hydraulic conditions).

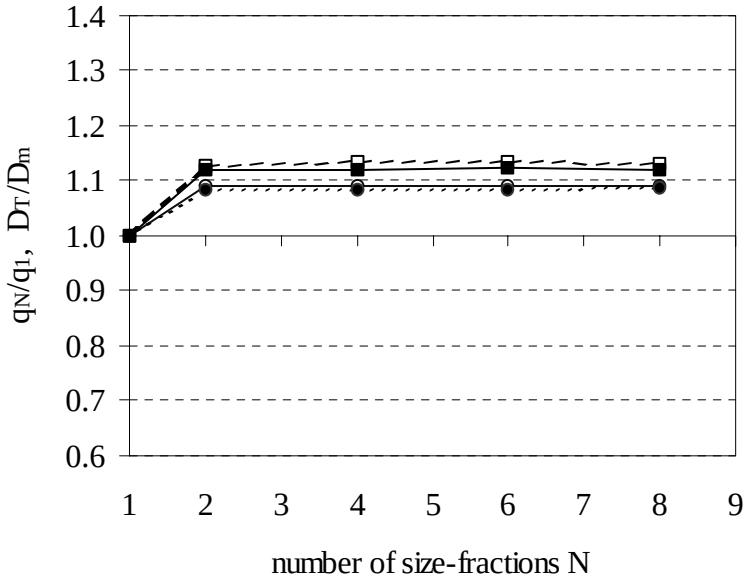

U_{rms} (m/s)	q_N/q_1	D_T/D_m
0.6	■	■
0.9	■	■

Figure 5.2: Sensitivity of the multi-fraction model of Ribberink to changing the number of size-fractions N (U_{rms} = 0.9 and 0.6 m/s).

A fundamental difference with the Bailard model is that the transported material has a larger mean diameter than the original bed material ($D_T/D_m \approx 1.13$). Apparently, now the coarse fractions contribute relatively more to the net total transport than the fine fractions. The composition of the transported sediment is more or less constant and seems not to be affected by the number of fractions N ($N \geq 2$), or by the imposed hydraulic condition.

It can be concluded that the multi-fraction Ribberink-model gives slightly larger transport rates than its uniform (single-fraction) version. Contrary to the Bailard model in the Ribberink model the coarse fractions (instead of the fine) contribute relatively more to the net transport. For the model of Ribberink, the optimum number of fractions is 2.

Model of Dohmen-Janssen

Figure 5.3 shows the results of the model of Dohmen-Janssen. It is clear that compared to the two previous quasi-steady models the predicted transport rates are more sensitive to the number of fractions N. The results become more or less stable when $N \geq 4$. The ratio of q_N/q_1 and D_T/D_m are only weakly dependent on the imposed flow velocities. The transported material has again a larger mean diameter than the original bed material ($D_T/D_m \approx 1.25$). For the model of D-J the optimum number of fractions is 4.

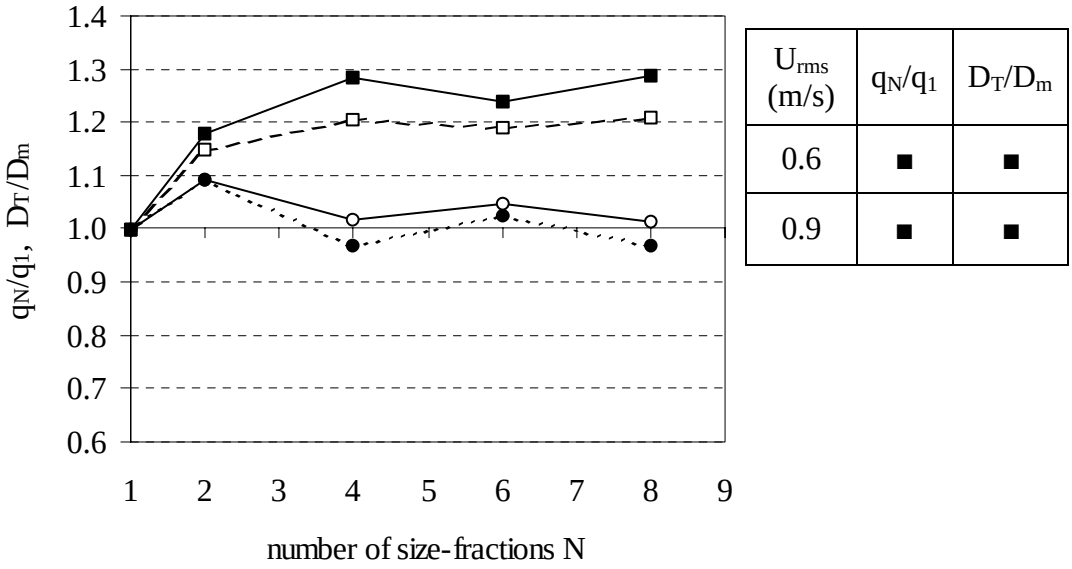

Figure 5.3: Sensitivity of the multi-fraction model of D-J to changing the number of size-fractions N (U_{rms} = 0.9 and 0.6 m/s).

A comparison between the results of the model of Ribberink and the model of D-J in figures 5.2 and 5.3 shows that including phase-lag effects in the model of D-J leads to a reduction in calculated transport rates and to a more coarse size composition of the transported sediment. In fact, this is caused by a reduction in transport of the finer sizes in the mixture due to phase-lag effects. This leads to an increase in the contribution of coarse sizes in the transported material. The ratio D_T/D_m has a value of about 1.25 according to the model of D-J, while it has a value of 1.13 according to the model of Ribberink.

Model of Dibajnia & Watanabe

Figure 5.4 shows the computational results of the multi-fraction model of Dibajnia & Watanabe (see equations 5.11 and 5.12). It is clear that the predicted transport rates are not sensitive for using the size-fraction approach in case of low velocity (for U_{rms} = 0.6 m/s $q_N/q_1 \approx 1$). The ratio of q_N/q_1 seems to be dependent on the imposed flow velocities. Increasing the velocity has a slight effect on the predicted transport rates.

In general, the transported material has a smaller mean diameter than the original bed material. Apparently, the fine fractions contribute relatively stronger to the transport than the coarse fractions. The size composition of the transported sediment seems not to be affected by the number of fractions N ($N \geq 2$) for the case with smaller flow velocity (U_{rms} = 0.6 m/s). On the other hand, increasing the number of fractions N does influence the ratio of D_T/D_m for the case with the high velocity (U_{rms} = 0.9 m/s).

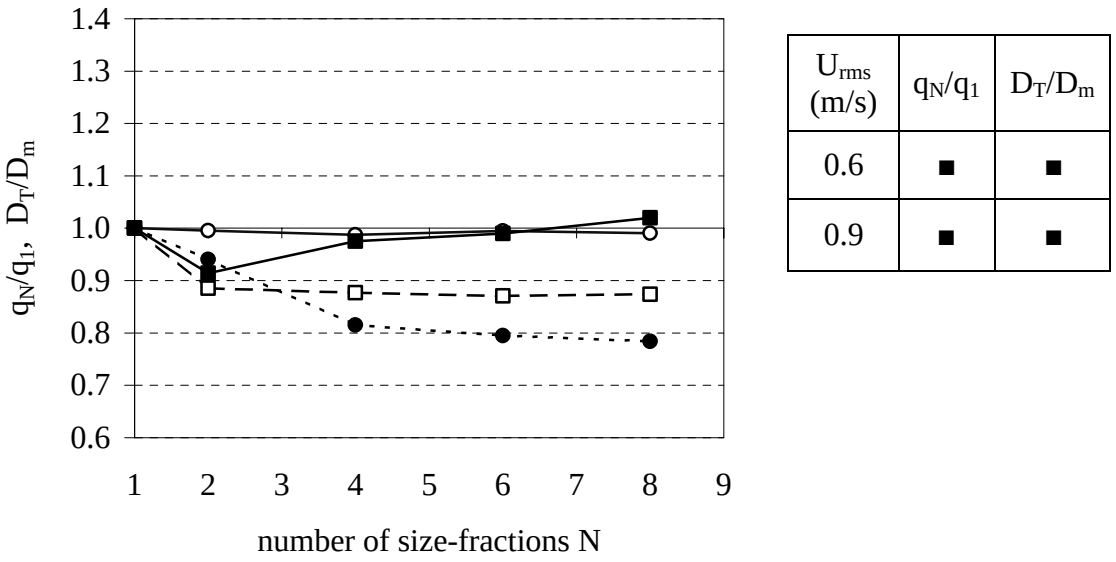

Figure 5.4: Sensitivity of the multi-fraction model of D&W to changing the number of size-fractions N (U_{rms} = 0.9 and 0.6 m/s).

From this it can be concluded that mean grain-size of the transported material according to the model of D&W is more sensitive to the number of fractions, with high velocities. Therefore, it is recommended to use a relatively large number of fractions ($N \geq 6$) to obtain stable results compare to the other models.

The POINT-SAND model

Figure 5.5 shows the results of the POINT-SAND model (PSM). It is clear that using the size-fraction approach in the PSM model leads to a reduction of the total transport rate and a relatively finer size composition of the transported material ($q_N/q_1 < 1$ and $D_T/D_m < 1$). The predicted transport rates are almost insensitive to the number of fractions for $N > 2$. The ratio of q_N/q_1 (≈ 0.8) seems to be more or less independent of the imposed flow velocities.

The transported material has a much smaller mean diameter than the original bed material ($D_T/D_m \approx 0.5$). Apparently, the fine fractions contribute much more to the net total transport than the coarse fractions. The ratio of D_T/D_m hardly changes anymore for $N > 2$ and slightly increases with increasing flow velocity, indicating that more coarse sizes are taking part in the suspension process.

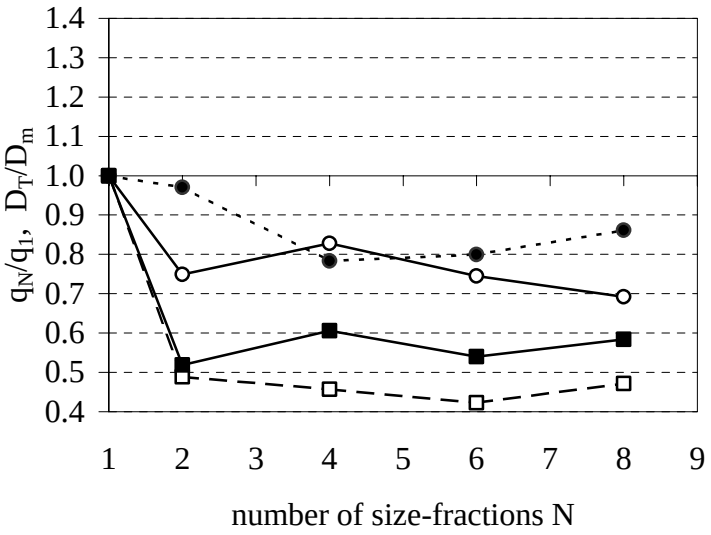

U_{rms} (m/s)	q_N/q_1	D_T/D_m
0.6	■	■
0.9	■	■

Figure 5.5: Sensitivity of the multi-fraction PSM model to changing the number of size-fractions N (U_{rms} = 0.9 and 0.6 m/s).

Intercomparison between graded-sand transport models

Figure 5.6 shows a comparison between the results of all graded transport models as a function of U_{rms} (for N = 4). The upper panel shows the ratio q_N/q_1 and the lower panel shows the ratio D_T/D_m.

It is clear from figure 5.6 that splitting up the sand mixture into several size-fractions has a distinct effect on the calculated transport rates ($q_N/q_1 \neq 1$). Besides, the transported sand has a different size composition compared to the original sand bed ($D_T/D_m \neq 1$). The models of Bailard, Ribberink and D-J show that the transport rates are increased compared to the uniform sand case, $q_N/q_1 > 1$. This increase in transport rates is slightly dependent on the flow velocity. On the other hand, the model of D&W and the PSM show a clear reduction in the computed transport rates, $q_N/q_1 < 1$. However, both models deviate strongly in their dependence on U_{rms}: D&W model shows a strong decrease of q_N/q_1 for large U_{rms} while the PSM model shows further increase. In fact, the non-linear relation between the calculated transport rates and the grain-size can explain these differences in behaviour between these 5 transport models (see also Dohmen-Janssen, 1999).

The lower panel of figure 5.6 shows that the models of Ribberink and D-J predict that the transported sand generally has a larger grain diameter than the original sand bed, $D_T/D_m > 1$. For these two models there are no significant effects for changing flow velocities on the composition of the transported sand. The models of Bailard, D&W and the PSM show that the transported sand generally has a smaller diameter than the original sand bed, $D_T/D_m < 1$.

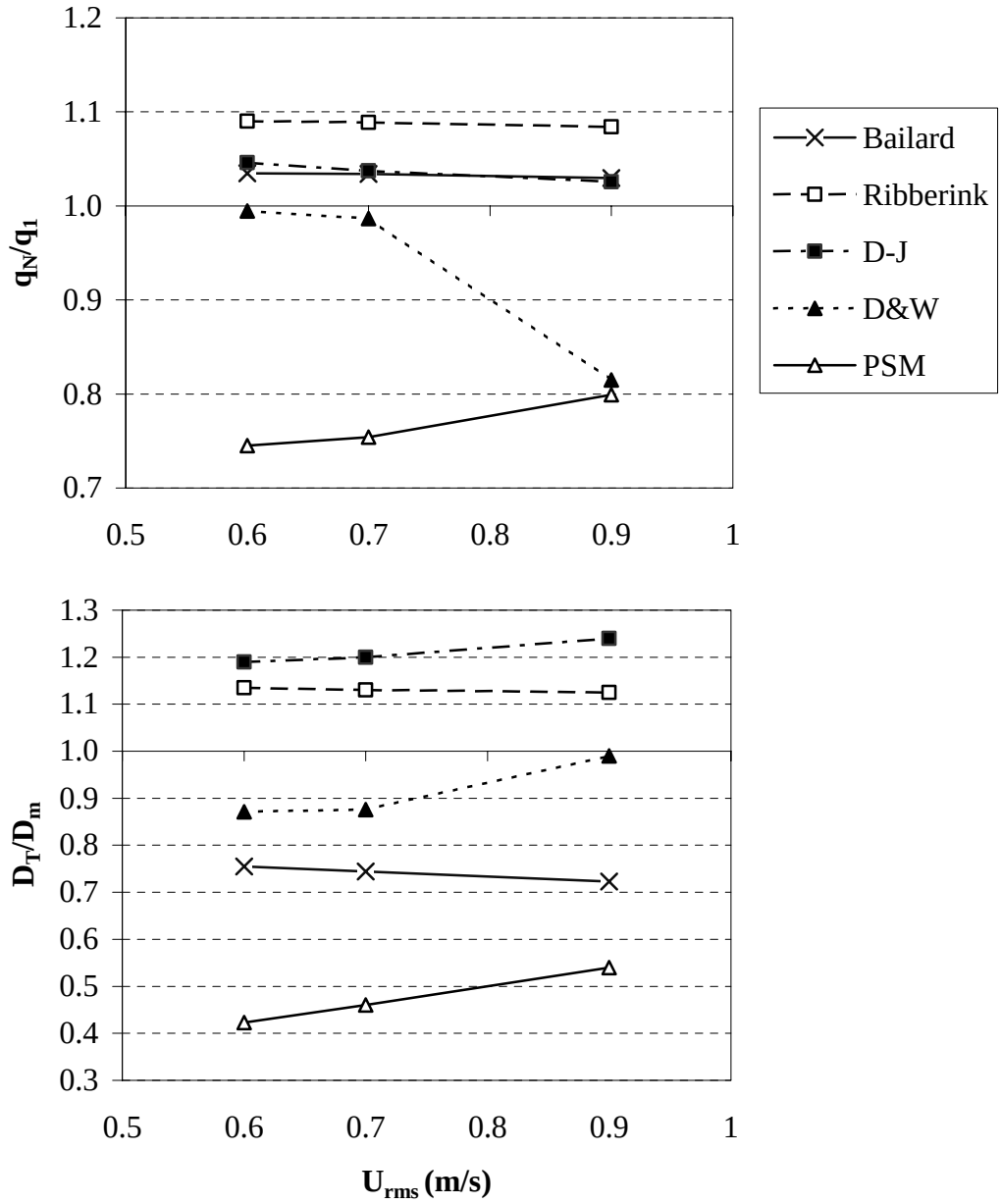

Figure 5.6: Graded sand transport models intercomparison with different flow velocities (U_{rms}), as a function of q_N/q_1 and D_T/D_m (N = 4).

The quasi-steady models (Bailard, Ribberink) show only a minor influence of U_{rms} on the transport size composition. However, the intermediate models (D-J, D&W) as well as the unsteady PSM model show that the transported material becomes increasingly coarser for increasing U_{rms}. This can be explained by the increasing influence of phase-lags of the finer sizes in the sand mixture.

5.6.2 Flow velocity influence on selective transport behaviour

In order to study the influence of the flow velocity on the selective transport behaviour of the transport models in more detail, additional calculations were performed. Nine velocities were selected U_{rms} = 0.1, 0.2, 0.26, 0.3, 0.4, 0.5, 0.8, 1.0 m/s and U_{rms} = 1.1 m/s using the same bed material as for the previous computations.

The results of this analysis are shown in figure 5.7. The contribution of the fine part of the bi-modal mixture to the total transport rate ($P_{T,fine}$. 100%) is plotted against the root mean square velocity (U_{rms}). Note that in figure 5.7 % $P_{T,fine}$. 100% = 70 means that the transported material has the same composition as the original sand bed.

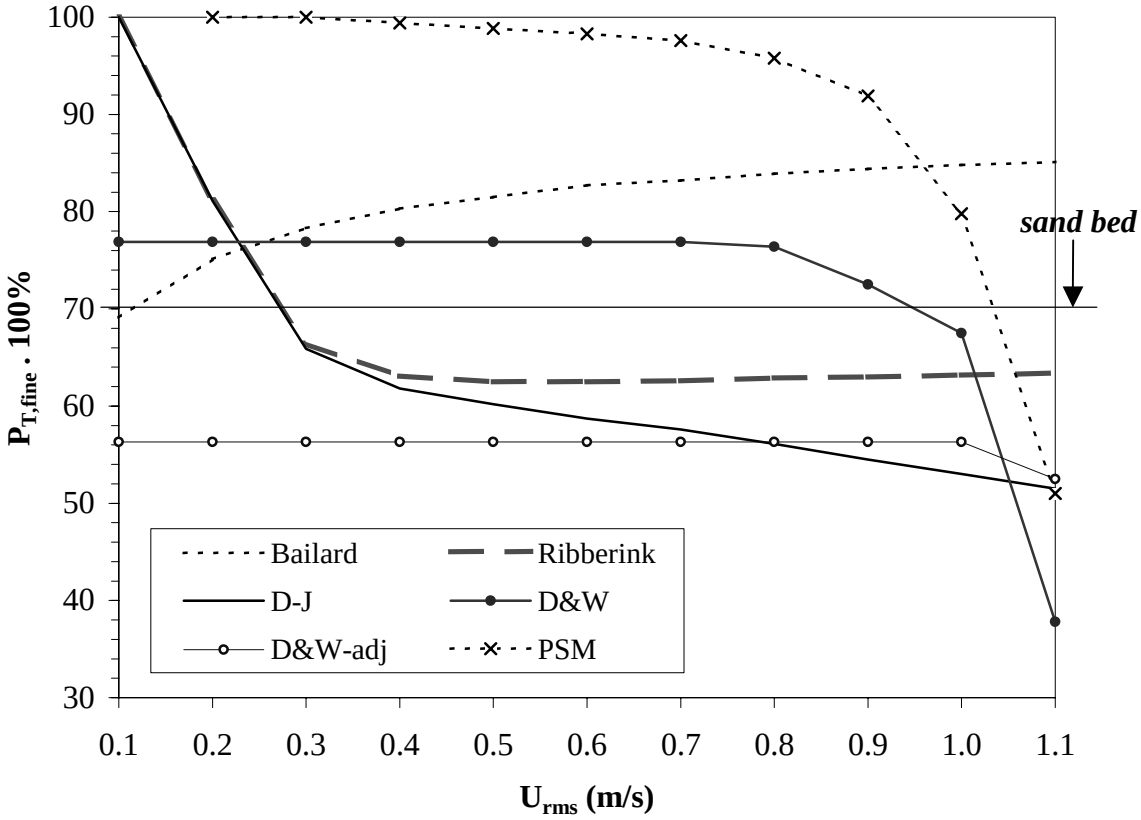

Figure 5.7: Graded sand transport model results, showing the contribution of fine fraction $P_{T,fine}$ to total transport rate as a function of U_{rms}.

In general figure 5.7 shows a strong disagreement between the selected transport models regarding their description of selective transport. A number of models generally show a finer transport than the bed (Bailard, D&W, PSM), while others generally a coarser transport than the bed (D&W-adj, Ribberink, D-J). Moreover, the influence of the flow velocity (U_{rms}) on the selective transport behaviour strongly differs between the models.

For the model of Bailard, the transported sand is generally finer than the original sand bed. The contribution of the fine fractions to the total transport rate slightly increases for increasing U_{rms}. In the model of Bailard the dependence for U_{rms} almost disappears for very large U_{rms}.

For the model of Ribberink, the contribution of the fine fractions to the total transport rate increases sharply as the flow velocity becomes smaller and smaller ($U_{rms} < 0.4$ m/s). For higher velocities ($U_{rms} > 0.4$ m/s) however, the contribution of the fine fractions to the total transport rate is almost constant and smaller than the original sand bed. So, the model of Ribberink can give coarser as well as finer transport compositions than the bed material, depending on the velocity regime.

Adding phase-lag effects in the model of Ribberink (model of D-J) has no effect on the results for small flow velocities ($U_{rms} < 0.3$ m/s). On the other hand a further increase of the flow velocities leads to an increasing contribution of the coarse particles in the transport. This is due to the phase-lag effects of the finer sizes in the mixture.

For the model of D&W the contribution of the fine fractions to the total transport rate is constant and larger than their contribution in the bed (70%) at low flow velocities ($U_{rms} < 0.7$ m/s). However, at higher flow velocities ($U_{rms} > 0.7$ m/s) this contribution decreases strongly even below 70%. As mentioned before this can be explained by the prediction of phase-lag effects for the finest fractions at high flow velocities.

The adjusted version of the model of D&W for graded sediment shows a strong overall reduction of the contribution of fine particles in the transport ($P_{T,fine} = 58\%$) in comparison with the original D&W model. The transported material is now always coarser than the bed material and the influence of phase-lag effects is shifted to a higher value of U_{rms}.

The multi-fraction PSM (suspension model) shows that only the fine particles are transported for low velocities ($U_{rms} < 0.4$ m/s). This contribution reduces strongly to values below 70% in the high velocity regime when phase-lag effects start to play a role in the transport processes.

5.7 Summary

In chapter 5 a size-fraction approach was applied in 5 different sediment transport models. This approach was proposed to improve these models regarding their prediction of net transport rates of mixed sands and to enable the prediction of the size composition of the transported material (selective transport processes). The size-fraction approach is based on dividing the bed material into a number of sizes, each with its diameter D_i and probability of occurrence P_i in the bed material. The net total transport rate in the case of N size-fractions is equal to the sum of the net transport rates of all individual size-fractions weighted by its probability of occurrence in the

bed P_i. According to this simple hypothesis there is no interaction between different grain-sizes taking place under sheet-flow conditions.

Originally, the model of D&W (1996) was developed for uniform sands. In 1996 D&W used their water tunnel experiments to adjust their model for mixed sand cases, see equations 5.13 and 5.14. A limitation of their adapted graded-sand-model is that it is calibrated with one dataset and can only be applied to mixtures consisting of two size-fractions only.

Detailed analysis was carried out in order to study the behaviour of all described graded transport models through studying: the effect of using the size-fraction approach on the predicted net total transport rates, (indicated by 'q_N/q_1', equation 5.3) and the selective transport behaviour of each model (indicated by 'D_T/D_m', equations 5.4 and 5.5). Two different wave conditions were used and one bi-modal sand mixture. The conclusions from this analysis are summarised in table 5.1. Table 5.1 includes the values of q_N/q_1 and D_T/D_m and their relation with the flow velocity and the minimum number of fractions, which must be used in order to get stable model results.

Table 5.1: General overview of the behaviour of all graded sand transport models

Model	**q_N/q_1**		**D_T/D_m**		**Minimum number of fractions (N)**
	value	Dependent on flow velocity	value	Dependent on flow velocity	
Bailard	1.0-1.1	no	0.7-0.8	no	≥ 2
Ribberink	1.1	no	1.1-1.15	no	≥ 2
D-J	1.0-1.1	no	1.1-1.3	slightly	≥ 4
D&W	0.8-1.0	yes for high velocities	0.85-1.0	yes for high velocity	≥ 6
PSM	0.7-1.0	yes for high velocities	0.4-0.6	yes	≥ 4

It is clear that the results of these graded transport models show large differences in behaviour. Part of these models gives an increase in transport rates when using a multi-fraction approach ($q_N/q_1 > 1$) (Bailard, Ribberink and D-J), while others give a reduction in net transport rates (D&W and the PSM). Moreover, the models show clear differences in predicting the composition of the transported sand (D_T/D_m). Both

the model of Ribberink and D-J generally predict that the transported material is coarser than the original sand bed ($D_T/D_m > 1$) While, the models of Bailard, D&W and the PSM showed the opposite behaviour, the transported material is finer than the original sand bed.

In order to develop and improve the performance of these graded transport models a large dataset of (fractional) transport measurements with graded sands is required. Therefore, new experiments with graded sand are carried out in this study, see chapters 6 and 7. The new experimental results are used in combination with existing laboratory data to verify the selected transport models (chapter 8) and later to improve graded sand transport modelling in chapter 9.

Chapter 6

EXPERIMENTAL SET-UP

6.1 Introduction

At present little is known about net cross-shore sediment transport quantities and selective transport processes during storm/sheet-flow conditions. Measurements in the field in and immediately above the wave boundary layer are very difficult. Sand transport can hardly be measured directly. Therefore, most of the measurements are carried out in laboratory experiments using different facilities, such as wave flumes or water tunnels. These measurements can be performed in either small-scale or full-scale experiments. A major advantage of large-scale laboratory facilities is that natural sands can be used and scaling of the sediment is not necessary.

Experimental data on sand transport in wave-induced sheet-flow conditions are scarce, especially with graded sand. Therefore, new experiments were carried out in the Large Oscillating Water Tunnel (LOWT) of WL | Delft Hydraulics. These experiments include 5 different series with uniform and size-graded sands. The new experiments are in the same research line of previous experiments of Al-Salem (1993), Ribberink and Chen (1993), Ramadan (1994), Hassan (1996), Janssen et al. (1996), Hamm et al. (1998) and Dohmen-Janssen (1999).

Objectives of present experiments

The overall objective of the new experiments is to obtain quantitative data for net transport rates and transport processes under sheet-flow/flat-bed conditions with different sand types, and to investigate size-gradation effects on sediment transport in oscillatory sheet-flow conditions. The measurements are carried out mainly under asymmetric waves (2^{nd}-order Stokes).

Advanced measuring techniques are applied in order to increase the physical insight into the time-dependent transport processes inside and directly above the wave

boundary layer. More traditional techniques are used for reference and calibration purposes. The main objectives of the new experiments are:

- To investigate grain-size effects on the net transport rate;
- To study the dynamics of sheet-flow processes with uniform and size-graded sand;
- To gain more insight into selective transport processes in sheet-flow/flat bed conditions under regular asymmetric waves (2^{nd}-order Stokes);
- To extend the existing database of net full-cycle and half-cycle sediment transport rates, transport rates per size-fraction (selective transport), suspended sediment concentrations and size composition of the bed material (vertical stratification) for oscillatory flows over sand beds consisting of a mixture of grain-sizes.

These new data will be used to increase physical insight into the sand transport processes (chapter 7) and to answer the research questions formulated in chapter 1. Moreover, these new data will be used to verify existing and improved sediment transport models, and to identify which transport processes are important and what their effects are on sand transport under oscillatory sheet-flow conditions (see chapters 8 and 9).

This chapter introduces the experimental set-up of the LOWT experiments. Section 6.2 gives a detailed description of the LOWT, the measuring programme, the bed sand materials, the hydraulic conditions and an overview of the experiments. The measuring set-up, which includes the measuring instruments and the measuring procedures, is presented in section 6.3. Finally, in section 6.4 a short description is given of the methods used for data analysis.

6.2 The LOWT and the measuring programme

6.2.1 The Large Oscillating Water Tunnel

The experiments are carried out in the Large Oscillating Water Tunnel (LOWT) of WL | Delft Hydraulics (see Ribberink, 1989). The general outline of the wave tunnel is shown in figure 6.1. The tunnel has the shape of a vertical U-tube, with a long horizontal rectangular test section. At each end there is a vertical cylindrical tube. One of them has an open connection to the air; in the other riser a piston is constructed. This piston is in direct contact with the water and is driven by a hydraulic servo-cylinder mounted on the top of the riser. An electric/hydraulic valve controls the piston motion based on the measured difference between the (measured) actual piston position and the desired piston position (feedback system).

In the horizontal test section the piston motion induces the desired horizontal orbital wave motion close to the bed. It is possible to generate purely sinusoidal, regular asymmetric and irregular oscillatory motions within the test section of the wave

tunnel, although there are some constraints for piston velocity and piston acceleration. The maximum piston amplitude is 0.75 m, which results in a maximum semi-excursion length of the water particles in the test section of 2.45 m. The range of the velocity amplitudes is 0.2-1.8 m/s and the range of oscillating periods is 4-15 seconds. Figure 6.2 shows the working range of the LOWT in terms of oscillation periods T and oscillatory velocity amplitudes U_a.

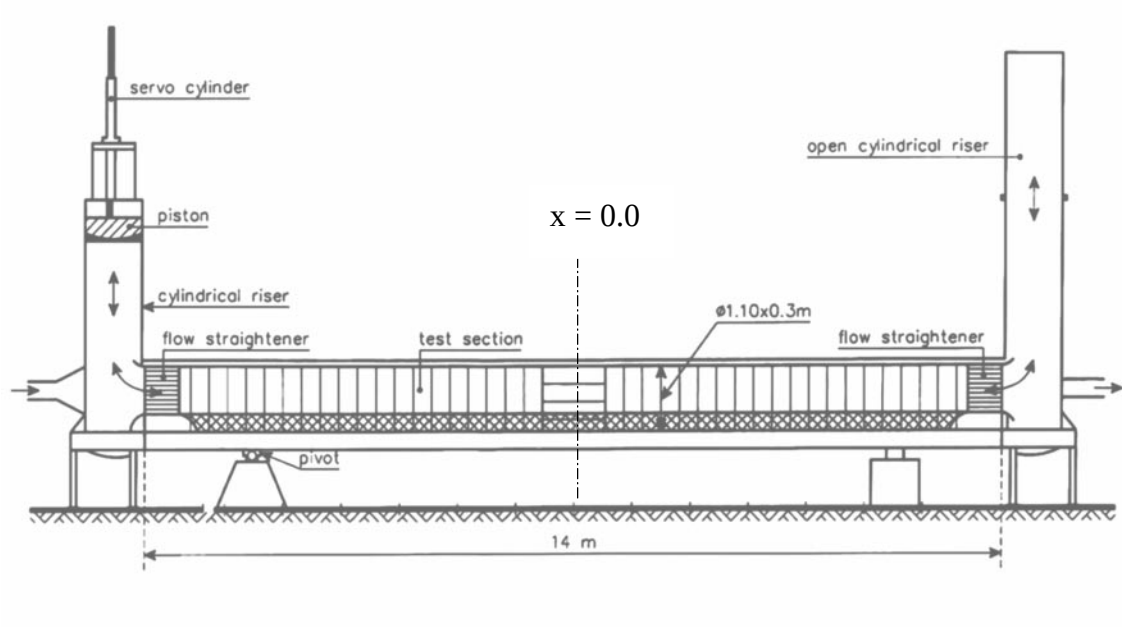

Figure 6.1: General outline of the Large Oscillating Water Tunnel (LOWT) of WL | Delft Hydraulics.

The test section has a length of 14 m, a height of 1.1 m, a width of 0.3 m and is provided with flow straighteners at each end. The sidewalls of the test section consist of thick glass windows in a steel frame (I-beams). Usually a 0.3 m thick layer of sand is brought into the test section, so 0.8 m height is left for the oscillating water flow. The roof of the test section is formed by 13 steel plates, which can be removed separately. By removal of some steel plates it is possible to install instruments inside the test section, to put the sand in or to remove it.

At the bottom of both vertical tubes sand traps are constructed in order to collect the sand that leaves the test section during a test. This sand can be removed after a test. In 1992 the wave tunnel was extended with a recirculating flow system, in order to superimpose a net current on the oscillating motion. The recirculating flow system is provided with a third sand trap consisting of a 12 m long pipe with a diameter of 1.2 m. Downstream of the trap two pumps are installed for generating a net current.

Due to the large dimensions of the wave tunnel, the velocities and wave-period in the tunnel are comparable to those occurring in nature. Therefore, it is possible to

perform full-scale experiments. But still there are some differences between the orbital flow field in nature and the simulated flow field in the tunnel. In nature waves (surface waves) propagate in a certain direction and phase shifts are present in the direction of wave propagation. However, in the LOWT there is no free surface, the oscillatory flow is enclosed by the conduit. This means, that in contrast to the situation with progressive surface waves, the flow is uniform along the tunnel without vertical orbital velocities. Apart from the tunnel, all mathematical models considered in this study are based on the same 1DV-approximation

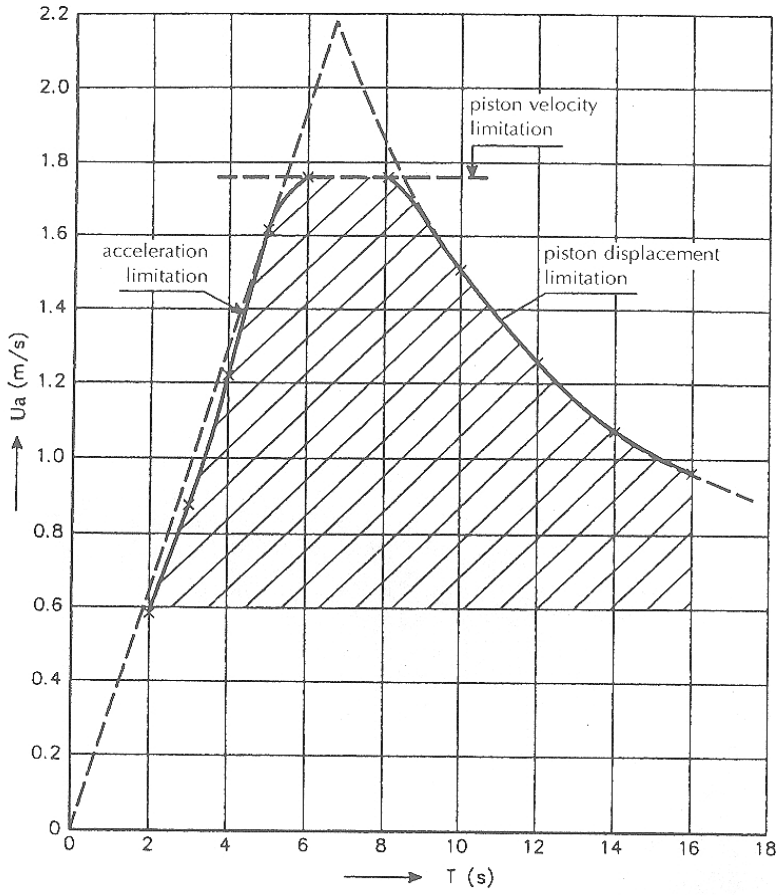

Figure 6.2: Working range of the LOWT of WL | Delft Hydraulics.

This 1DV-approximation is acceptable for the near-bed flow under surface waves if both the horizontal flow velocity is small compared to the wave celerity and the water depth is small compared to the wave length. In shallow coastal zones this is generally the case. This means that an oscillatory water tunnel can be used to simulate the near-bed orbital motion under surface waves and the 1DV-approach adopted in the models is an acceptable first-order approximation (see Dohmen-Janssen, 1999).

6.2.2 Sand bed

During the present study five different series of experiments are carried out in the Large Oscillating Water Tunnel (LOWT) of WL | Delft Hydraulics using different types of sand (uniform and graded). Table 6.1 shows the characteristics of sands used in each series of experiments. In total 119 tunnel runs were carried out during 30 weeks in the period between 1999 and 2001. More details about the experiments can be found in Hassan et al. (1999), Hassan (2001), Trouw et al. (2001) and Hassan et al. (2002).

Table 6.1: Characteristics of sand used in the new laboratory experiments.

Series	**number of weeks / year**	**Sand type**	**D_{10} (mm)**	**D_{50} (mm)**	**D_{90} (mm)**	**σ_g**	**w_s (mm/s)**
O	5 / 2000	uniform	0.10	0.13	0.18	1.30	11.4
R	3 / 2001	uniform	0.23	0.34	0.39	1.28	43.8
Q	4 / 2001	uniform	0.85	0.97	1.20	1.32	110.0
P	10 / 1999	graded	0.16	0.24	0.99	2.67	33.0
S	8 / 2001	graded	0.11	0.15	1.08	4.21	12.5

In table 6.1 D_i denotes the diameter at which i% by weight is finer; w_s is the settling velocity of a grain with diameter D_{50} in still-water and σ_g is the geometric standard deviation, defined by.

$$\sigma_g = 0.5\left[\frac{D_{50}}{D_{16}} + \frac{D_{84}}{D_{50}}\right] \qquad (6.1)$$

The main focus of the research programme is on the test series P and S, in which sand mixtures were used. Series Q and series R were carried out to collect adequate reference data of 'half wave-cycle mean' transport rates of 'uniform' sand (see wave conditions in section 6.2.3). Moreover, series O is used to investigate the detailed transport process (time-dependent concentrations and grain velocities) inside the sheet-flow layer.

Grain-size distributions of the 'uniform' sands O, R and Q and sand mixtures of series P and S are shown in figure 6.3. Moreover, this figure includes also the grain-

size distribution of the uniform sand with D_{50} = 0.21 mm, which has been used in the sand mixture P. Note that the sand mixture P consists of 30% of sand Q (D_{50} = 0.97 mm) and 70% of the medium sand with D_{50} = 0.21 mm. Sand mixture S consists of 20% of the coarse sand Q, 20% of the medium sand R (D_{50} = 0.34 mm) and 60% of the fine sand O (D_{50} = 0.13 mm). The sand mixtures were prepared by mixing the dry base materials in a mechanical mixer with a volume of about 100 liters.

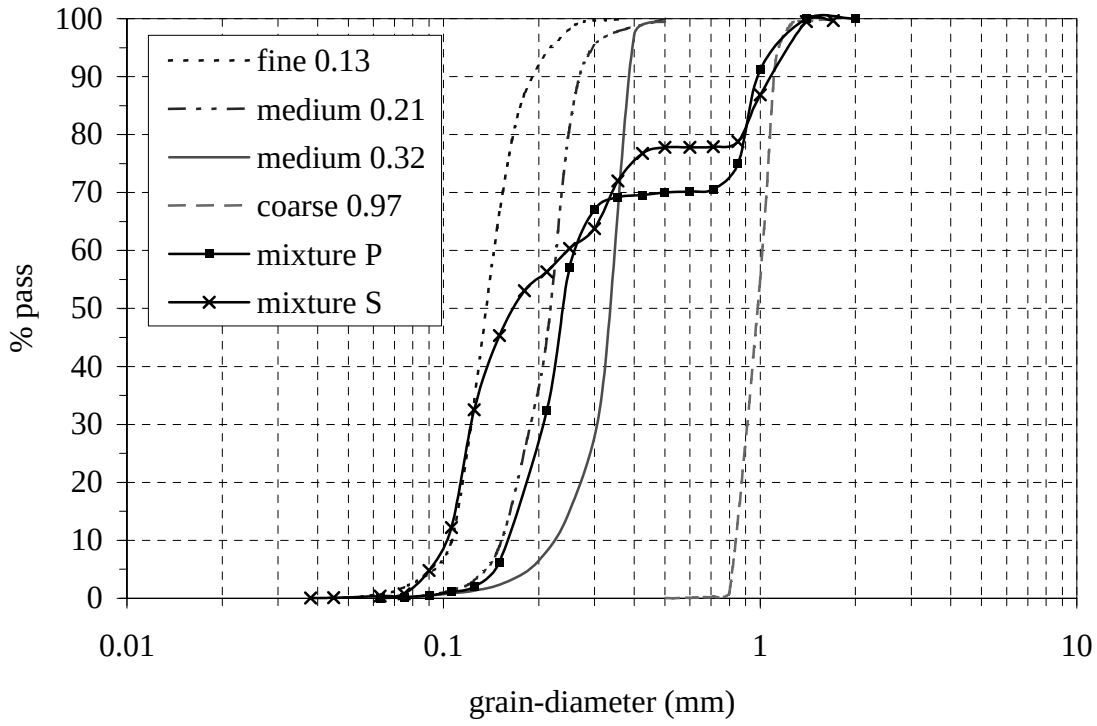

Figure 6.3: Grain-size distributions of the 'uniform' and 'graded' sands used in the new LOWT experiments.

The sand characteristics were selected in order to study the effect of grain-size and size-gradation on the transport processes. The experiments with uniform sand are in line with previous LOWT series (D_{50} = 0.13 and 0.21 mm) reported by Ribberink and Chen (1993) and Al-Salem (1993). Therefore, uniform sands with D_{50} = 0.34 and 0.97 mm were selected, in order to extend the existing data in the 'coarse' direction. The compositions of the two sand mixtures P and S were mixtures of existing uniform sands, in order to be able to study the net total transport rates in direct comparison with the transport of uniform sands, and to compare the transport processes of a certain grain-size in a mixture with those in the uniform case.

6.2.3 Hydraulic conditions

One of the main goals of the present experiments is to gain more insight into the selective transport processes under sheet-flow conditions for regular asymmetric waves without a current. In the past some experimental series were carried out with regular asymmetric waves (2^{nd}-order Stokes waves) and uniform sand (Al-Salem, 1993, D_{50} = 0.21 mm and Ribberink and Chen, 1993, D_{50} = 0.13 mm). For reasons of comparability, it was therefore decided to choose the same flow conditions as in those previous experiments and to obtain a set of comparable data with uniform as well as graded sands.

The new experimental program mainly concentrated on asymmetric wave conditions (2^{nd}-order Stokes waves without superimposed current). The time-dependent velocity of 2^{nd}-order Stokes wave can be described with: $u(t) = u_1 \cos(\omega t) + u_2 \cos(2\omega t)$.
where: u_1 and u_2 = the velocity amplitude of the first and 2^{nd}-order components of the horizontal velocity and ω = the angular frequency of the wave (which is equal to $2\pi/T$). Table 6.2 shows a general overview of the hydraulic conditions used in all series of experiments. In this table, U_{rms} is approximated by $[\frac{1}{2}(u_1^2 + u_2^2)]^{0.5}$, the crest velocity $u_c = u_1 + u_2$, the trough velocity $u_t = u_1 - u_2$. The degree of asymmetry R, defined as $u_c/(u_c+u_t) = (u_1 + u_2)/2u_1$, was kept at around 0.65. The wave-period T was varied in a limited number of tests, in order to study the influence of time-dependency and flow acceleration effects.

Only for series O a sine wave (U_c = 1.1 m/s) superimposed on a net current (+ 0.25 m/s) was used, in order to be able to compare the new results with the previous study of McLean et al. (2001). Series O is aimed mainly at obtaining better insights into particle velocities and sediment concentrations inside the sheet-flow layer (see section 6.4.4). The test program is given in table 6.2.

During the series P experiments, Hassan et al. (1999) performed a few introductory tunnel runs with uniform coarse sand (0.97 mm). Large bed forms developed in the tunnel when 2^{nd}-order Stokes waves were imposed. These large bed forms would generate another transport regime with vortex-induced suspended sediment transport, which would be outside the scope of the present study (sheet-flow/flat bed regime).

In order to obtain a set of sheet-flow data with uniform coarse sand (0.97 mm), series Q was carried out. Instead of imposing a series of full asymmetric wave-cycles, series of half (crest and trough) cycles were imposed separately (see also King, 1991) during different runs in order to create large net transport rates in a short period (see Hassan et al., 2002). A large transported volume is needed for accuracy reasons of the net sediment transport measuring technique (see section 6.4.1) and the short period was supposed to be short enough to avoid substantial bed form growth.

A basic underlying assumption of these half-cycle tests is that unsteady transport phenomena associated with the time-development of oscillatory boundary layers and the time-dependent vertical sediment exchange with the bed (time-history effects) are

not important for the transport behaviour of the coarse sediment (0.97 mm). Based on net transport measurements with medium and fine sands and comparisons with 'quasi-steady' and 'unsteady' transport formulations, Dohmen-Janssen (1999) and Ribberink et al. (2001) conclude that this type of time-history effects only become important for sands finer than about 0.2 mm. Under this assumption, the net transport of a series of full asymmetric wave cycles can also be obtained by subtracting the net transported sediment volumes of a series of 'crest' half-cycles and a series of 'trough' half-cycles (see equation 7.1).

Table 6.2: Hydraulic conditions of all series of experiments O, Q, R, P and S.

Series	Test	Hydraulic conditions					Sand Type
		Wave-cycle	U_{rms} (m/s)	U_c (m/s)	Period (s)	Wave type	
O	Oc4	Full		1.1	7.2	Sine + current (0.25 m/s)	O (uniform)
	Oc7				4.0		
	Oc12				12		
Q	Q6c	Crest		1.07	2.75	2^{nd}-order Stokes	Q (uniform)
	Q7c			1.20			
	Q9c			1.57			
	Q6t	Trough		0.58	3.75		
	Q7t			0.65			
	Q9t			0.85			
R	R6f	Full	0.6		6.5		R (uniform)
	R7f		0.7				
	R9f		0.9				
	R5f		0.7		5		
	R12f				12		
P	P6f	Full	0.6		6.5		P (mixture)
	P7f		0.7				
	P9f		0.9				
S	S45f	Full	0.45		6.5		S (mixture)
	S6f		0.6				
	S7f		0.7				
	S9f		0.9				
	S12f		0.7		12		

6.2.4 Overview of experimental series

For each sand type, various sediment transport and flow parameters were measured, using different types of instruments. The main objectives of each series of experiments and the measured parameters are summarised in table 6.3. The measuring techniques and instruments are described in detail in section 6.3.

Table 6.3: Main objectives and the measured parameters of all series of experiments.

Series	Main objectives	Measured parameters
O	⌜ Measuring grain-velocities/transport processes inside the sheet-flow layers; ⌜ Wave-period effects on transport processes; ⌜ Importance of phase-lag within the sheet-flow layer.	⌜ Time-dependent velocity; ⌜ Time-dependent concentrations.
R	⌜ Grain-size effect on net transport rates; ⌜ Onshore and offshore bed-load concentrations.	⌜ Net transport rates; ⌜ Time-averaged bed-load concentrations.
Q	⌜ Grain-size effect on net transport rates	⌜ Net transport rates (half- and full-wave-cycle averaged).
P	⌜ Size-gradation effects on net total transport rates; ⌜ Size-gradation effects on net transport rates of individual size-fractions; ⌜ Onshore and offshore bed-load concentrations; ⌜ Size-gradation effects on suspended sand; ⌜ Vertical sorting of grain-sizes.	⌜ Net total transport rates; ⌜ Transport rates per size-fraction; ⌜ Time-averaged suspended concentrations; ⌜ Time-averaged bed-load concentrations; ⌜ Grain-size distribution in the bed, the bed-load and in the suspended sand.
S		

6.3 Measuring set-up

6.3.1 Measuring instruments

The different instruments/measuring techniques that have been used during the present series of experiments are presented in table 6.4. All measuring instruments will be described briefly hereafter.

Table 6.4: Measured parameters and measuring techniques/instruments.

Measured parameter	Measuring technique/ instrument	Used in series
Net (half or full-cycle averaged) sediment transport rates	Mass Conservation Technique (MCT) with sand traps and bed-level profiling (PROVO)	P, Q, R and S
Oscillatory flow velocity above the boundary layer	2DV Laser-doppler system (LDA) at 10-20 cm above the sand bed	O, R, Q, P and S
Time-averaged suspended sediment concentration profiles	Transverse Suction System (TSS)	P and S
Half-cycle mean sediment concentrations in the sheet-flow / bed-load layer	Pumping Bed-load Trap sampler (PBLT)	R, P and S
Time-dependent concentration profiles in the sheet-flow layer	Conductivity Concentration Meter (CCM)	O
Bed sampling/cores	Bed Sampler (BS)	P and S
Grain-size distributions of: bed samples, PBLT samples, sand trap samples and TSS samples	Settling velocity analysis with (VAT)	R, P and S

More details about the measuring instruments can be found in appendix B.

6.3.2 Measuring procedure

For all series of experiments tests were generally repeated three or four times, in order to measure variations related to small differences in bed refilling/arrangement and achieve more accurate results by averaging.

In series P and S (mixture of sand) the upper layer of the sand bed was removed (about 5 cm) from the test section after each test and replaced by a new sand mixture, to eliminate the effect of the tunnel ends. Since the tunnel was not provided with 'upstream' sand feeding arrangement, a bed erosion wave migrated slowly into the tunnel and also the bed size composition of the upper sand layer changed during a tunnel run.

Generally, each tunnel run starts with preparing the sand bed (flattening/replacing the upper sand layer, filling the erosion holes at both ends of the tunnel) and profiling the bed surface using the PROVO system. The next step is filling the tunnel with water and adjusting the instruments at the right positions. Normally there is only one instrument inside the test section during one test, in order to minimize the disturbance inside the test section. The duration of each test (6 to 20 minutes) is determined based on the bed condition (i.e. the bed is still flat) and the development of the erosion holes at the two ends of the tunnels. After stopping the water motion the tunnel is drained, the PROVO system is used again to measure the bed levels and bed samples are collected (for experiments with sand mixtures). The bed level profiling before and after a tunnel test, in combination with the sand collected inside the two sand traps, are used to calculate the net sand transport rates along the tunnel, as described in section 6.4.1.

6.4 Methods of data analysis

6.4.1 Net total transport rates (Mass Conservation Technique)

A mass conservation technique (MCT) was used for calculating the net total sediment transport rates along the tunnel test section. After a tunnel run, the sand eroded from the test section was removed from the traps at the bottom of the two cylindrical risers and weighed under water. The total volume of the trapped sand should be equal to the overall volume change in the tunnel test section (as derived from the bed profiling).

Because the sand traps are located at either end of the test section, the sediment continuity equation can be integrated from the left hand-side (piston side) and also from the right hand-side (open-leg side), using the measured bed level changes along the test section. This results in two estimates of the net transport rate at the measuring location in the middle of the test section, under the assumption that the porosity of the sand bed in the test section is known. The porosity of the sand bed can be determined from the weights of the sand collected in the traps and the volume change (including pores) in the test section.

For the calculations of the net sediment transport rates using the MCT a computer program was available. The following input information is needed for the computation:

- Bed level profiles of the sand bed before and after a test;
- Underwater weights of the sand collected in the sand traps;
- Duration of the experiment;
- Imposed porosity.

The computer programme calculates the following:

- Calculated porosity;
- Sand volume change across the tunnel, in the left and right half of the test section;
- Two estimates of the sediment transport rates (from the left as well as the right side).

The following equations are used in the analysis:

measured porosity:

$$1-\varepsilon_0 = \frac{G}{\rho_s}\frac{1}{\Delta V_{ip}} \tag{6.2}$$

transport rate at the measuring location. *left trap estimate:*

$$q_{s,l} = \frac{\Delta V_{l,ip}(1-\varepsilon_0)}{\Delta t W} - \frac{G_l}{\rho_s}\frac{1}{\Delta t W} \tag{6.3}$$

transport rate at the measuring location. *right trap estimate:*

$$q_{s,r} = \frac{-\Delta V_{r,ip}(1-\varepsilon_0)}{\Delta t W} + \frac{G_r}{\rho_s}\frac{1}{\Delta t W} \tag{6.4}$$

where:

ΔV_{ip} = $\Delta V_{l,ip} + \Delta V_{r,ip}$ = total eroded volume, including pores, from the tunnel test section during one test;

$\Delta V_{l,ip}$ = total eroded volume, including pores, from the part of the tunnel test section to the left of the measurement location during one test;

$\Delta V_{r,ip}$ = total eroded volume, including pores, from the part of the tunnel test section to the right of the measurement location during one test;

G = $G_l + G_r$ = total (dry) weight of the sand collected in both traps;

G_l = total (dry) weight of the sand collected in the left trap (underneath the piston);

G_r = total (dry) weight of the sand collected in the right traps (underneath the open cylindrical riser);

ρ_s = density of sand;

ε_0 = porosity of sand bed;
W = width of tunnel test section;
q_s = net transport rate without pores per unit width and time for one test at a certain location;
Δt = test duration.

Ideally, both equations (6.3 and 6.4) should give the same answer for the measured transport rate for any test. However, porosity changes/variations and small errors in the measured bed profiles sometimes lead to unrealistic values for the calculated porosity (between 0.25 and 0.78). It is known from earlier tunnel experiments and from direct porosity measurements that the porosity of the loosely packed sand has a value of about 0.4. A porosity of 0.4 was therefore used in all computations.

The following mechanisms are held responsible of the unrealistic measured porosities:

- Refilling and flattening of the sand surface in the tunnel section before each test may increase the porosity;
- Compaction processes may reduce the porosity of the refilled/flattened sand;
- Fluidisation of the upper sand layer (the active sand layer), due to the oscillatory motion during a test, can increase the porosity of the upper layer;
- Errors in the bed level measurements (before and after a test) can increase or reduce the calculated porosity. Because bed-level measurements are taken with a high accuracy, the relative errors of the eroded volumes (left, right) are small. For short tunnel runs and therefore relatively small eroded volumes, these errors become relatively more important. In the case of an erosion in the left part of the test section and a deposition of approximately the same magnitude in the right part (which often occurs), two large quantities are subtracted in order to compute the total eroded volume, which may lead to a large relative error.

Also the eroded volumes are corrected for porosity changes in order to avoid artificial erosion/deposition, that has nothing to do with transport gradients along the test section. The bed level measurements along the test section (after the test) are therefore also corrected by increasing or decreasing all measured levels along the tunnel with a constant amount, such that the total eroded sand volume matches the collected sand in the traps. Here it is assumed that the porosity changes occur uniformly along the test section. In the present tests these bed-level corrections were between 0.5 and 3 mm.

6.4.2 Net sand transport rates per size-fraction

The Pump Bed-Load Trap sampler (PBLT), developed by Van Rijn (1997), was used to measure the ‘onshore’ and ‘offshore’ time-averaged bed-load concentrations (see figure B.5). These concentrations in combination with the measured flow velocity

above the wave boundary layer (measured by LDA) are used to determine the net transport rates as well as the transport rates of each size-fraction as follows:

Net transport rates using the PBLT

The dry weight of the sand samples collected with the PBLT is determined using calibrated tubes. Knowing the dry weight of the sand and the extracted volume it is possible to calculate the 'onshore' and 'offshore' bed-load (volume) concentrations. The measured time-averaged 'onshore' C_{on} and 'offshore' C_{off} bed-load concentrations can be used to determine the 'onshore' and 'offshore' bed-load transport rates (Van Rijn, 1997) as follows:

$$q_{b,on} = \alpha D C_{on} U_{\max,on} \tag{6.5}$$

$$q_{b,off} = \alpha D C_{off} U_{\max,off} \tag{6.6}$$

where: α = calibration factor; D = internal diameter of intake nozzle (= 0.008 m) and $U_{max,i}$ = onshore or offshore peak velocity in the free stream (ca. 0.1 m above the bed).

The net total bed-load transport for the full wave-cycle is:

$$q_{b,net} = \alpha D \left(C_{on}\, U_{\max,on}\, T_{crest} - C_{off}\, U_{\max,off}\, T_{trough} \right) / T \tag{6.7}$$

in which T_{crest} = period of the wave crest; T_{trough} = period of the wave trough and T = total wave-period (= T_{crest} + T_{trough}).

It is assumed that the thickness of the bed-load layer is smaller than 0.008 m. The calibration factor α accounts for:

- Scour effects;
- Variable thickness of the bed-load/sheet-flow layer;
- Variable velocity and concentration profiles in the sheet-flow layer.

The calibration of the PBLT was extended in the present study using new measurements in the LOWT. A new concentration-dependent calibration factor α was obtained (see appendix B). Note that the calibration factor α is not similar to the calibration factor of Van Rijn (1997) because he did not include the half-wave period effects (T_{crest} and T_{trough}) on the computations (see equation 6.7).

Net sand transport rates per size-fraction

The sand samples collected with the PBLT have been also used to determine the grain-size distribution of the 'onshore' and 'offshore' bed-load transport, using the Visual Accumulation Tube (VAT).

The net transport rate per size-fraction was calculated in a similar way as the net total bed-load transport rates. The following data are required to determine the transport rates per size-fraction:

- The measured time-averaged 'onshore' and 'offshore' bed-load concentrations using the PBLT;
- The percentages of coarse and fine fractions in the 'onshore' and 'offshore' directions (determined by the VAT analysis);
- The measured 'onshore' and 'offshore' peak flow velocities, measured by the LDA;
- The measured net total transport rates (using the MCT).

First, the PBLT calibration factor α is determined using equation 6.7, starting from the net total transport rates resulting from the MCT. The mean transport rates per size-fraction in the 'onshore' and 'offshore' directions can be computed, using the following equations:

$$q_{fine,\,on} = \alpha\, DC_{fine,on}\, U_{max,on} \quad , \quad q_{fine,\,off} = \alpha\, DC_{fine,off}\, U_{max,\,off} \tag{6.8}$$

$$q_{coarse,\,on} = \alpha\, DC_{coarse,on}\, U_{max,on} \quad , \quad q_{coarse,\,off} = \alpha\, DC_{coarse,off}\, U_{max,off} \tag{6.9}$$

The net transport rate per size-fraction is then equal to

$$q_{net,fine} = (q_{fine,on} T_{crest} - q_{fine,off} T_{trough}) / T \tag{6.10}$$

$$q_{net,coarse} = (q_{coarse,on} T_{crest} - q_{coarse,off} T_{trough}) / T \tag{6.11}$$

6.4.3 Orbital velocities outside wave boundary layer

The time-dependent orbital flow velocities outside the wave boundary layer were measured using a forward scatter Laser Doppler Flow Meter (LDA) with a sampling frequency of 40 Hz. The orbital velocities were determined along the following steps:

- Flow velocities were measured usually at 0.1 or 0.2 m above the bed, depending on the amount of suspended sand in the flow. Below these levels, it turned out to be impossible to measure velocities, because the suspended sediment concentrations inhibited the penetration of the laser beams;
- The measured two velocity components V_A and V_B (with slope 45^o, see figure 6.4) are transferred to horizontal (in flow direction) and vertical (perpendicular to the flow) directions. Ensemble-averaged time-dependent flow velocities during a wave-cycle are based on choosing a certain number of waves for each test. The first minute at the beginning of each tunnel run has been ignored so as to avoid initial effects;
- The downward zero-crossing of the piston velocity has been used as reference to determine the start and the end of each wave;
- The ensemble-averaged velocities in x direction have been used to calculate the mean flow velocity <u>, maximum crest and trough velocities u_c and u_t, the root-mean-square U_{rms} and the third order velocity moment $<U^3>$.

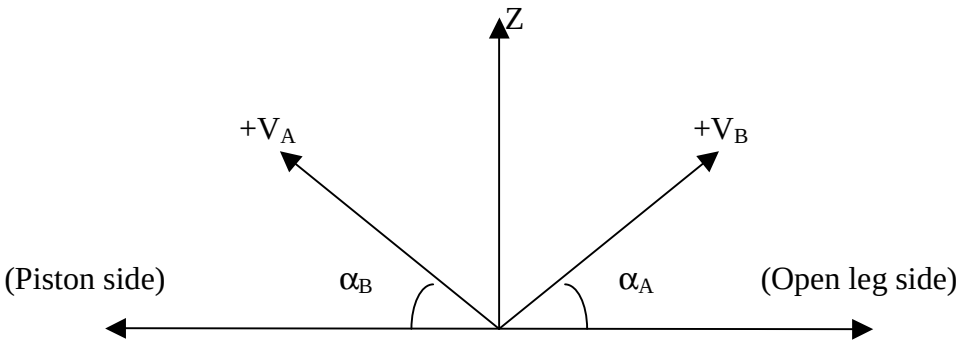

Figure 6.4: Configuration of measured flow velocity components by LDA in the LOWT.

6.4.4 Sand concentrations and particle velocities inside the sheet-flow layer (CCM results)

It is possible to transfer the measured signals of the two CCM sensors into concentrations, using equations B.2 and B.3 in appendix B. The ensemble-averaged (i.e. averaged at fixed phase) concentrations were computed for each CCM probe individually, using the calibration factors (K) as obtained during the present study and shown in figure B.8. The averaged values of the two probes are used to present the ensemble-averaged concentrations inside the sheet-flow layer, see chapter 7.

The measured data/time-series of the two CCM sensors were used to calculate the time-dependent grain velocities inside the sheet-flow layer using a cross-correlation technique (see, McLean et al., 2001 and Hassan, 2001). The following steps are important for the data processing:

- The initial processing step was to locate in time the zero crossing of the piston motion/velocity, to be used as a reference for determination of wave phases;
- The next step was to divide each wave-period into 36 phases/intervals. Using the center point of these phases/intervals, cross-correlations between the time series for the two conductivity probes (CCM) were calculated for different time-shifts about the center point of the time interval. Through this step it is possible to determine the correlation between 36 phases/intervals of the complete wave-cycle;
- Cross-correlations from each wave having period-averaged concentration within a given concentration range was averaged together phase by phase;
- Correlations from several waves (n > 20 waves) were averaged together, because the cross-correlations for a given phase from a single wave-period were extremely noisy.

Typical plots of ensemble-averaged cross-correlations versus time lag, at –0.5 mm below the initial sand bed, are shown in figure 6.5 for the condition Oc4 (see table 6.2). The upper panel (A) shows the crest part of the wave-cycle and the lower panel (B) the trough part. The numbers on the right hand side indicate wave phase number. Phase 1 occurs just after flow reversal from trough to crest direction and phase 36 just before the flow reversal.

For clarity, the trace for each phase has been displaced vertically from the previous one. Even through the correlation maximum is often quite small (sometimes less than 0.05), the pattern is unmistakable. The velocity of the sediment particles is given by $u = \Delta x/\Delta t$, where: Δt is the time-shift of the maximum correlation from the zero lag line. Rather than simply choosing the maximum value, the center of mass of all cross-correlation values between zero-crossings on either side of the maximum was calculated.

6.4.5 Sand-size composition from settling tube tests (VAT)

A Visual Accumulation Tube (VAT) or settling tube was used to analyse the grain-size distribution of each graded sand sample and to determine the percentages of the fine and coarse fractions. The grain-size distribution was calculated from the settling velocity distribution of sand grains, using Van Rijn's formula (equation 4.44) for non-spherical particles ('Van Rijn corrected' by multiplying the settling velocity with a factor = 0.87).

From sieve analysis, it is known that the base mixture of bed material (series P and S) hardly contains grains with a size of 0.5 mm. Thus, all grains smaller than 0.5 mm belong to the fine fraction and all grains larger than 0.5 mm belong to the coarse fraction. The settling time of 0.5 mm sand in the VAT is about 37 seconds. Therefore, the percentage of the coarse fraction of a sand sample is given by relative sand surface level after about 37 seconds.

A more easy way to determine the percentages of the fine and coarse fractions is by visual observation of the sand in the glass tube at the bottom. The coarse fraction has a much higher settling velocity than the fine fraction and it will reach the bottom of the tube first. The fine and coarse fractions are completely separated, whence it is very easy to read the surface level of the coarse fraction and the fine fraction. Using the total level, one can determine the individual percentages.

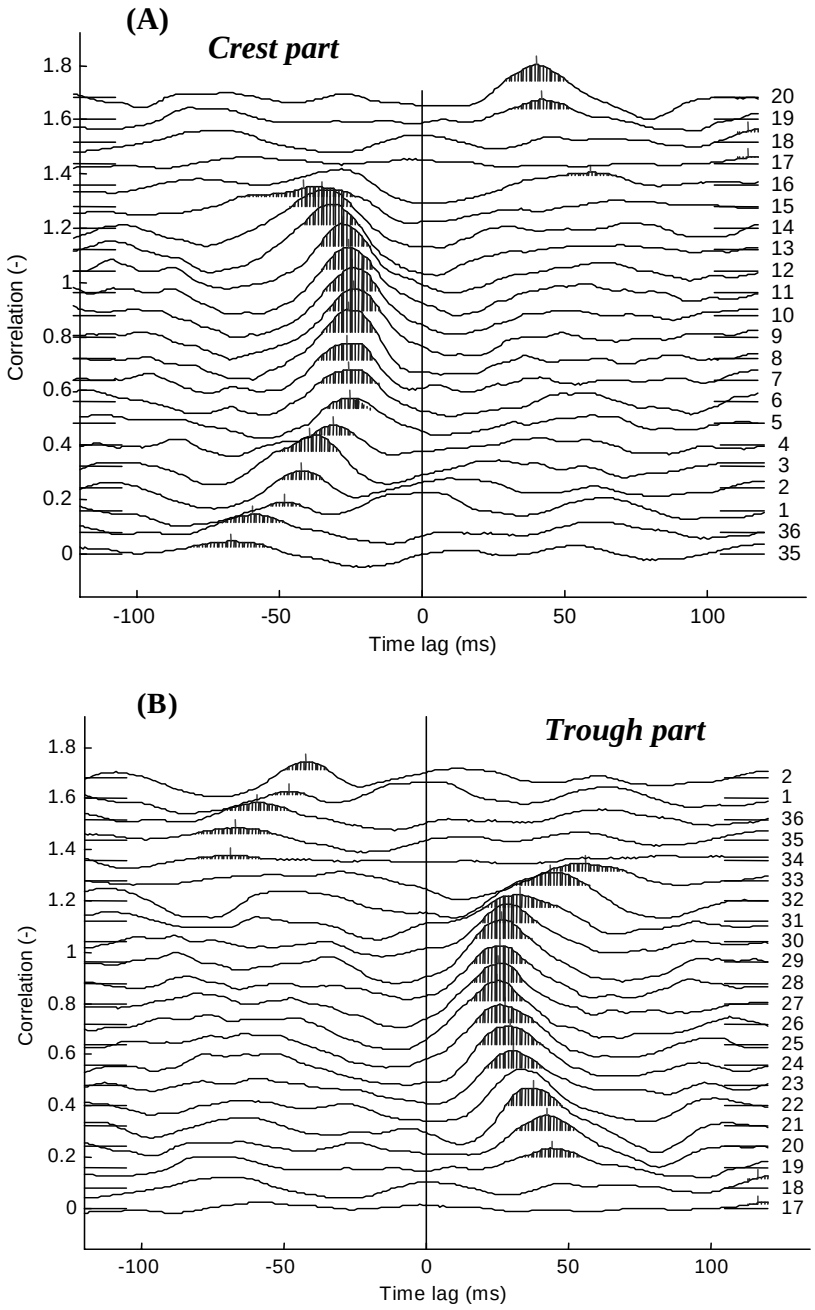

Figure 6.5: Ensemble-averaged cross-correlations of two CCM sensors versus time lag (z = -0.5 mm, condition Oc4). The numbers at the right indicate the wave phase, numbered from 1 to 36.

Chapter 7

EXPERIMENTAL RESULTS AND DATA ANALYSIS

7.1 Introduction

New experiments were carried out in the Large Oscillating Water Tunnel (LOWT) of WL | Delft Hydraulics. The experiments were aimed to increase our insights into selective transport processes under oscillatory sheet-flow conditions and to obtain data for the verification and the development of sediment transport models. The experiments were aimed also to study the grain-size effect on net transport rates under regular asymmetric (2^{nd}-order Stokes) wave conditions. Part of the experimental studies was focused exclusively on the important detailed transport processes inside a sheet-flow layer of uniform sand (Hassan, 2001).

In this chapter, a selection of the processed data and the main experimental results will be presented. Moreover, the new data are compared with previous experimental data, in order to improve our knowledge about grain-size effects as well as size-gradation effects on the sediment transport processes. New experiments with uniform sand are reported in Hassan (2001), Trouw et al. (2001) and Hassan et al. (2002), while the size-graded sand experiments are reported in Hassan (1999) and Hassan et al. (2002).

Section 7.2 presents measured net transport rates with uniform sand and focuses on the grain-size effect on the transport rates. The measured net transport rates of the graded-sand experiments are presented in section 7.3. This section also presents measured net transport rates per size-fraction, as well as evidence of grain-size interactions in a mixture. Section 7.4 includes the onshore and offshore bed-load concentrations and their size composition. The measured time-averaged sediment concentrations and the observed vertical size sorting in the suspension layer and in the upper-bed-layer/active-bed-layer are presented in section 7.5. In section 7.6 the

detailed transport processes inside the sheet-flow layer with uniform sand are presented. These detailed processes include time-dependent concentrations, grain velocities and sediment fluxes. Finally, section 7.7 presents a summary of the main results obtained from the experimental data and data comparisons.

7.2 Net transport rates of uniform sand

The bed level along the test section was measured twice before and twice after the experiment with the bed level profiling system (PROVO). The second measurement was a check on the first one. The underwater weight of the sand collected in the sand traps was also measured. The net sand transport rate was then computed by integrating the mass balance equation (using the Mass Conservation Technique, MCT) twice for each test starting either from the left (piston side) or from the right sand trap (open-leg side). See section 6.4.1 for a description of MCT.

7.2.1 Measured net transport rates

In the tables 7.1 and 7.2 the net sand transport rates with uniform sand are summarised for series Q (D_{50} = 0.97 mm) and series R (D_{50} = 0.32 mm), respectively. A mean value is determined by averaging the results of 3-5 tests. The measured net transport rates of the half-cycle tests of series Q are half-cycle averaged values. These tables include also data on the flow characteristics, measured by LDA at $z \geq 0.1$ m above the wave boundary layer (see Ramadan, 1994). Each table includes the following information:

- Name of test condition;
- Oscillation period T;
- Maximum velocity in crest direction U_c;
- Maximum velocity in trough direction U_t;
- Root-mean-square value of the flow velocity during the wave-cycle U_{rms};
- Time-averaged value of the third power of the velocity $<U^3>$;
- Average net transport rate per unit width $<q_s>$;
- Standard deviation of the averaged net transport rate σ.

The measured width-averaged values of net transport rates are corrected, such that they correspond to the velocities in the centreline of the tunnel test section. It was found earlier that net transport rates are closely proportional to the time-averaged third power velocity moment $<U^3>$ (Al-Salem, 1993). Therefore, the correction is based on the distribution of $<U^3>$ over the width of the tunnel; see Al-Salem (1993), Ramadan (1994) and Cloin (1998).

Figure 7.1 shows the measured net transport rates of series Q with coarse sand (D_{50} = 0.97 mm). The figure includes the half-cycle averaged transport rates of both the

crest part (Δ) and the trough part (□) of the wave-cycle. It is clear that the crest part of the wave-cycle has much higher velocities, hence higher $<U^3>$ and transport rates are found (about factor 10 higher).

Table 7.1: Measured net transport rates of series Q (D_{50} = 0.97 mm).

Test	**T (s)**	**U_{laser} (m/s)**			**$<U^3>$ (m^3/s^3)**	**q_s (10^{-6} m^2/s)**	**σ (10^{-6} m^2/s)**
		U_c	U_t	U_{rms}			
Q6c	2.75	1.14		0.72	0.490	52.6	1.5
Q6t	3.75		0.67	0.50	0.140	6.6	2.2
Q7c	2.75	1.34		0.85	0.807	79.1	20.1
Q7t	3.75		0.77	0.57	0.215	9.4	0.6
Q9c	2.75	1.64		1.08	1.645	162.8	31.1
Q9t	3.75		1.02	0.73	0.444	14.2	3.1

Table 7.2: Measured net transport rates of series R (D_{50} = 0.32 mm).

Test	**T (s)**	**U_{laser} (m/s)**			**$<U^3>$ (m^3/s^3)**	**q_s (10^{-6} m^2/s)**	**σ (10^{-6} m^2/s)**
		U_c	U_t	U_{rms}			
R6f	6.5	1.07	0.58	0.59	0.129	20.8	1.1
R7f	6.5	1.22	0.66	0.68	0.204	29.9	1.2
R9f	6.5	1.57	0.84	0.89	0.450	77.1	5.9
R5f	5.0	1.20	0.72	0.68	0.184	38.2	2.5
R12f	12.0	1.15	0.69	0.67	0.155	24.4	1.6

As mentioned in chapter 6, the main reason for performing half-cycle experiments with the coarse sand was to determine the net transport rates of coarse sand for the full wave-cycle. It was possible to compute the net transport rates of the full wave-cycle, using the measured transport rates of each half wave-cycle as follows:

$$< q_s > = \frac{1}{T} \left[\int_0^{T_c} q_{sc}\, dt + \int_{T_c}^{T} q_{st}\, dt \right] = \frac{1}{T} \{ T_c < q_{sc} > + T_t < q_{st} > \} \qquad (7.1)$$

where: $<q_s>$ = net total transport rate during the full wave-cycle, q_{sc} = net transport rate during the crest period (T_c) of the wave-cycle, q_{st} = net transport rate during the trough period (T_t) of the wave-cycle and T = wave period.

The integrated result of the two half-cycle results (net transport rates) can also be found in figure 7.1. It is clear that the measured net transport rates as well as the measured transport rates per half wave-cycle (crest 'onshore' or trough), are directly proportional to the third power velocity moment $<U^3>$. This is in agreement with the earlier results of Al-Salem (1993) and Dohmen-Janssen (1999).

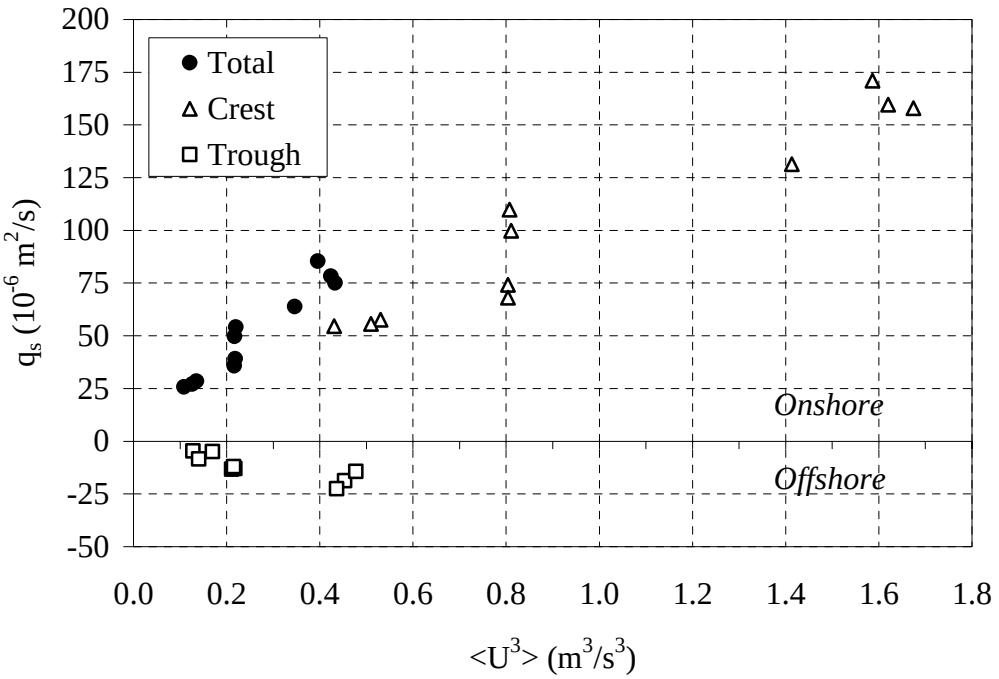

Figure 7.1: Measured net transport rates as a function of the third power velocity moment $<U^3>$ for series Q (uniform sand, D_{50} = 0.97 mm).

The measured net transport rates of series R (D_{50} = 0.32 mm) are shown in figure 7.2 as a function of the third power velocity moment. The measured transport rates are again directly proportional to $<U^3>$.

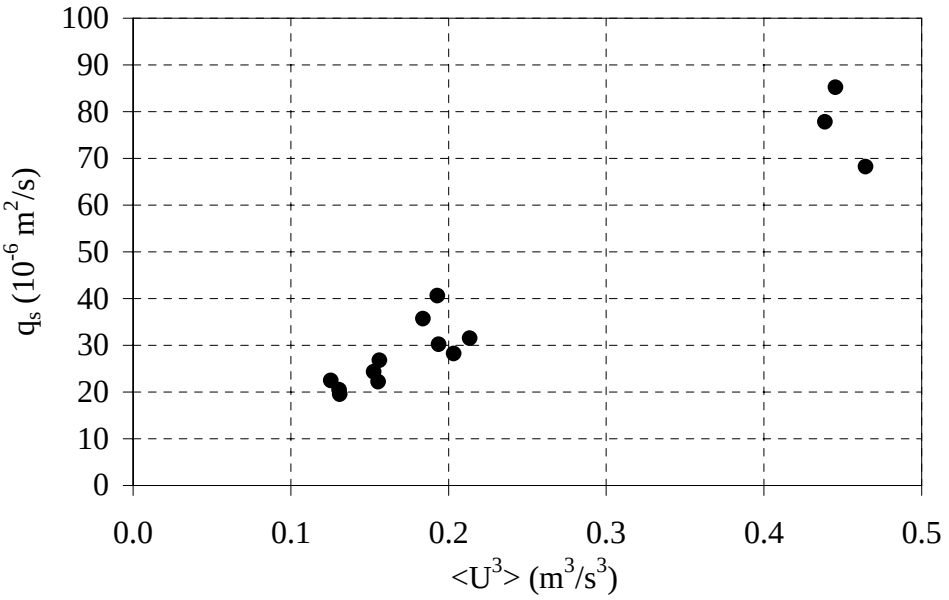

Figure 7.2: Measured net transport rates as a function of the third power velocity moment $<U^3>$ for series R (uniform sand, D_{50} = 0.32 mm).

7.2.2 Influence of grain-size on net transport rates

In order to study the influence of the grain-size on the net transport rates under asymmetric waves, the new data with uniform sand are compared with previous experimental data from the LOWT. They include the data of Ribberink and Chen (1993) (D_{50} = 0.13 mm), Ramadan (1994) (D_{50} = 0.21 mm) and Al-Salem (1993) (D_{50} = 0.21 mm). All of these data were collected under similar 2nd-order Stokes wave conditions as in the present experiments (series R and Q).

Figure 7.3 shows the measured net transport rates as a function of the third power velocity moment $<U^3>$ for uniform sand with different grain-sizes (D = 0.13, 0.21, 0.32 and 0.97 mm). The results show that for sand with grain-size ≥ 0.21 mm the net transport rates are always directed 'onshore', i.e. in the direction of the maximum crest velocity. The earlier finding of Al-Salem (1993) for D = 0.21 mm ($<q_s> \sim <U^3>$) is still valid for D ≥ 0.21. The results do not show a clear influence of grain-size on the net transport rates for 0.21 < D < 0.97 mm.

On the other hand, fine grains (D = 0.13 mm) show a strongly deviating behaviour. Measured net transport rates are 'onshore' directed in the lower velocity regime ($<U^3> < 0.1$ m^3/s^3) and 'offshore' directed in the higher velocity regime ($<U^3> > 0.2$ m^3/s^3). Apparently, the assumption of quasi-steadiness (Al-Salem, 1993) does not always hold for the fine sand (D < 0.21 mm). It can be concluded that grain-size plays a very important role in sediment transport processes under unsteady flow

conditions. This role is more pronounced in the higher velocity regime with fine sand. Earlier experimental results of Dohmen-Janssen (1999), with sine waves superimposed on net currents and different grain sizes also showed the importance of unsteady effects under sheet-flow conditions. They revealed that net transport rates are smaller for fine grains (D = 0.13 mm) when unsteady effects are more pronounced.

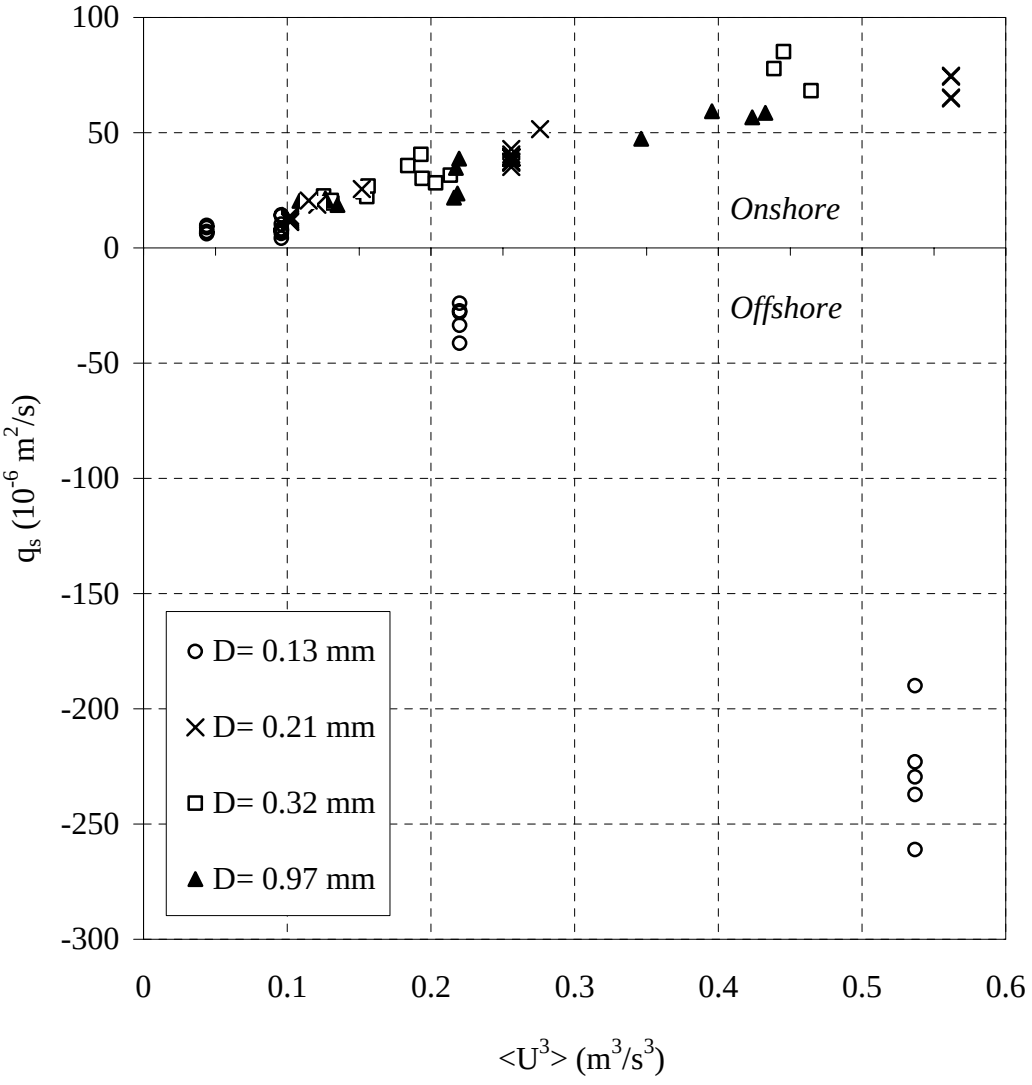

Figure 7.3: Measured net transport rates as a function of the third power velocity moment $<U^3>$ for uniform sand with different grain-sizes.

7.3 Net transport rates of graded sand

7.3.1 Net total transport rates

Tables 7.3 and 7.4 show the measured net total transport rates during series P (mixed sand with D_{50} = 0.15 mm) and S (mixed sand with D_{50} = 0.24 mm), respectively. These tables also include some information about measured flow velocities above the sand bed ($z \geq 0.1$ m) and the standard deviation σ of measured transport rates. In the graded sand results, the measured net total transport rate refers to the total of all size-fractions in a sand mixture. The net total transport rates were computed using the MCT (see section 6.4.1).

Table 7.3 Measured net total transport rates of series P (graded sand with D_{50} = 0.15 mm, 2nd-order Stokes waves).

Test	**T (s)**	**U_{laser} (m/s)**			**$\langle U^3 \rangle$ (m^3/s^3)**	**q_s (10^{-6} m^2/s))**	**σ (10^{-6} m^2/s)**
		U_c	U_t	U_{rms}			
P6f	6.5	1.08	0.57	0.59	0.147	19.5	2.4
P7f	6.5	1.23	0.64	0.64	0.221	30.5	4.4
P9f	6.5	1.59	0.85	0.85	0.473	64.3	6.9

Table 7.4 Measured net total transport rates of series S (graded sand with D_{50} = 0.24 mm, 2nd-order Stokes waves).

Test	**T (s)**	**U_{laser} (m/s)**			**$\langle U^3 \rangle$ (m^3/s^3)**	**q_s (10^{-6} m^2/s)**	**σ (10^{-6} m^2/s)**
		U_c	U_t	U_{rms}			
S45f	6.5	0.87	0.45	0.45	0.070	10.4	1.5
S6f	6.5	1.14	0.57	0.61	0.168	19.0	2.5
S7f	6.5	1.30	0.65	0.70	0.261	22.4	2.9
S9f	6.5	1.63	0.82	0.90	0.535	8.7	21.5
S12f	12.0	1.17	0.67	0.67	0.179	20.8	3.9

Figure 7.4 shows the measured net total transport rates as a function of the third power velocity moment $<U^3>$. The figure includes the results of the two graded sand series P and S.

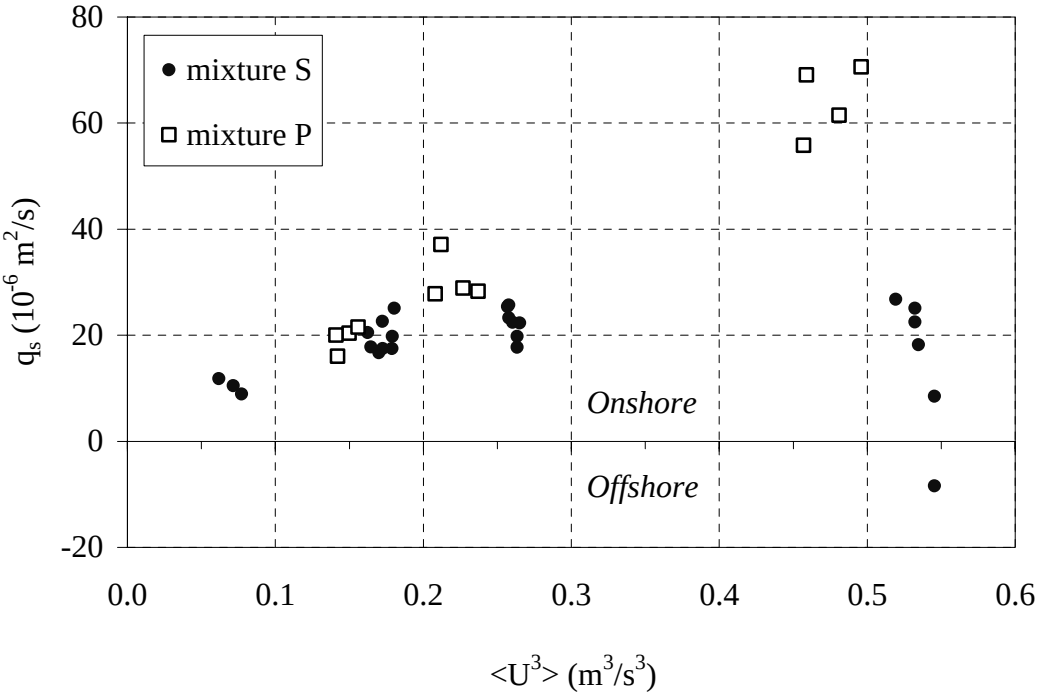

Figure 7.4: Measured net total transport rates as a function of the third power velocity moment $<U^3>$ for series P and S (graded sand).

The measured transport rates with mixed sands showed the following characteristics:

- The net sand transport rates for all conditions of series P are positive, i.e. in the direction of the flow during the wave crest half-cycle ('onshore'). The sand transport rate follows the power law $<q_s> \sim <U^3>$ over the used velocity range;
- Only in the low velocity regime $<U^3> < 0.2$ the net sand transport rates of series S also follows the power law $<q_s> \sim <U^3>$;
- This power law is not valid in the higher velocity range ($<U^3> > 0.2$ m^3/s^3) during series S. This can be explained by unsteady effects of the fine size-fraction (D = 0.13 mm), which included 60% in mixture S;

The net sand transport rates for each individual test have a small deviation around the mean value, except the condition S9f, where $<U^3> > 0.5$ m^3/s^3. This may be due to the fact that the velocity in this particular case is very high (U_{rms} = 0.9 m/s) and the net transport rates are small (very close to zero). In all these tests, the results are more sensitive to changes in the other parameters, such as the sand bed composition, the flow velocity or the test duration.

7.3.2 Size-gradation effect on net total transport rates

Figure 7.5 shows a comparison between measured net total transport rates of graded sand P with D_{50} = 0.24 mm and two different datasets with uniform sand. The first dataset has a D_{50} = 0.97, as measured in the present study (series Q), and the second has a D_{50} = 0.21 mm (data of Al-Salem (1993) and Ramadan (1994)). It is clear that the graded sand P, which is a mixture of the two other uniform sands (D_{50} = 0.24 mm), shows similar transport rates as the uniform sands and that the size-gradation has no clear effect on the measured net total transport rates. The net transport rate is closely proportional to the third power velocity moment $<U^3>$, also in the graded-sand case (see also Hassan et al., 2001a, b).

A similar comparison was performed for the measured net total transport rates of the graded sand of series S and individual uniform sand data. In figure 7.6 measured net transport rates of series S are compared with measured net transport rates of the uniform sands D = 0.13, 0.32 and 0.97 mm, as a function of $<U^3>$. The fine sand data (D = 0.13 mm) are of Ribberink and Chen (1993), while the other sand sizes (D = 0.32 and 0.97) are new data obtained in the present study (series R and Q). Note that the graded sand S is a mixture of the three uniform sands used for the comparison (D = 0.13 (60%); D = 0.32 (20%) and D = 0.97 (20%)). The solid line in figure 7.6 shows the general trend of the measured net transport rates of series S.

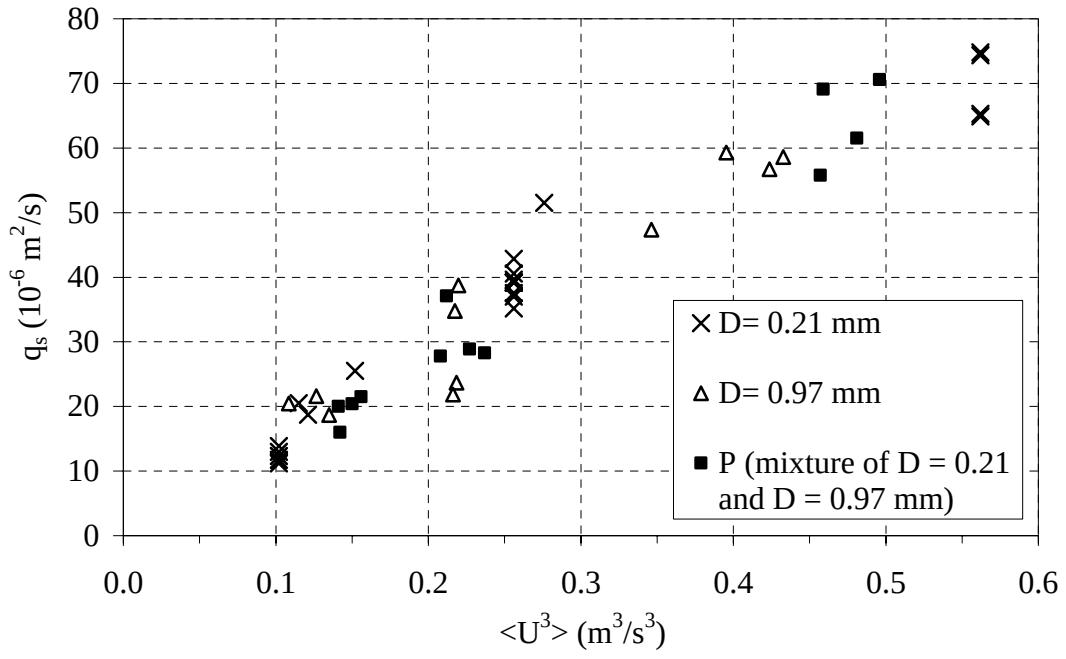

Figure 7.5: Comparison between measured net total transport rates of two uniform sands (0.21 and 0.97 mm) and a mixture of these two sands (series P), as a function of the third power velocity moment $<U^3>$.

Figure 7.6 shows that in the low flow velocity regime ($<U^3> < 0.15$ m^3/s^3) the measured net transport rates of uniform sands and the sand mixture S are quite similar. On the other hand, in the higher velocity regime ($<U^3> > 0.15$ m^3/s^3), the measured transport rates of the mixed sand S are deviating from all uniform sands. Although, the sand mixture S has a median diameter (D_{50} = 0.15 mm) close to that of the uniform fine sand (D_{50} = 0.13 mm), the net transport rates are strongly affected by the presence of coarse grains. For series S the net transport is 'onshore' for the full range of velocities.

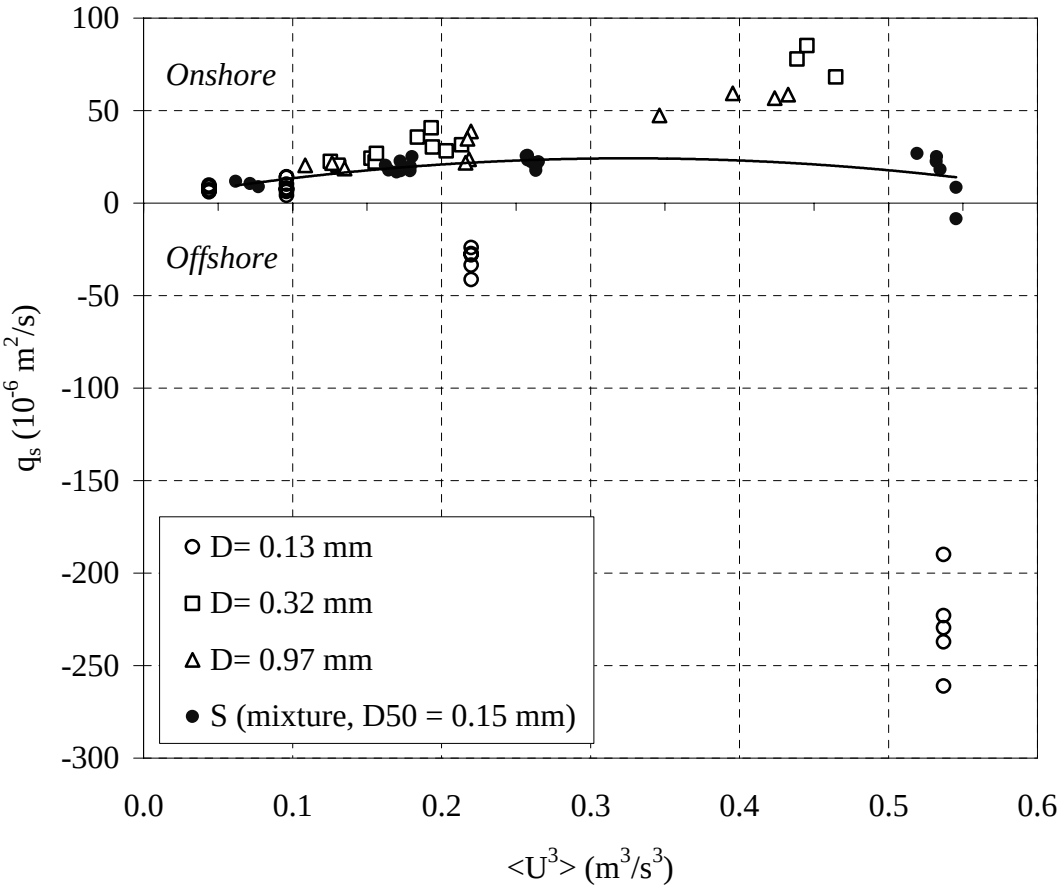

Figure 7.6: Comparison between measured net total transport rates of three uniform sands (0.13, 0.32 and 0.97 mm) and of a mixture of these three sands (series S), as a function of the third power velocity moment $<U^3>$.

This difference in behaviour may be due to the difference in behaviour of the individual sand sizes, as is also shown in figure 7.3. Coarse grains in the mixture have the tendency to be transported in the 'onshore' direction, while fine-grains are transported in the 'offshore' direction. The result is a net total transport rate close to zero. These differences in transport behaviour of different sizes under the same flow

conditions (selective behaviour) make the prediction of the net total transport rates of graded sand a complicated task. Apparently, complication increases when fine grains ($D_{50} \leq 0.13$ mm) are present in a sand mixture.

7.3.3 Net transport rates of size-fractions in a mixture

Net transport rates per size-fraction were calculated using the method described in section 6.4.2, using the PBLT. Only the transport in the lower part of the concentration profile is considered (called the 'bed-load transport layer', $0 < z < 8$ mm). This height corresponds with the internal diameter of the nozzles of the PBLT. In this way the net transport in the suspension layer is left out of consideration. However, earlier tunnel experiments Ribberink & Al-Salem (1995) and Dohmen-Janssen (1999) showed that in sheet-flow conditions 95% - 100% of the net transport takes place in the near bed bed-load layer (also see section 7.6.3).

Figure 7.7 shows measured net total transport rates and the transport rate of each size-fraction of series P (averaged values of different tests) versus the third moment of the flow velocity $<U^3>$. The net transport rates are all positive in the direction of the wave propagation ('onshore' direction) and they are increasing for increasing flow velocities.

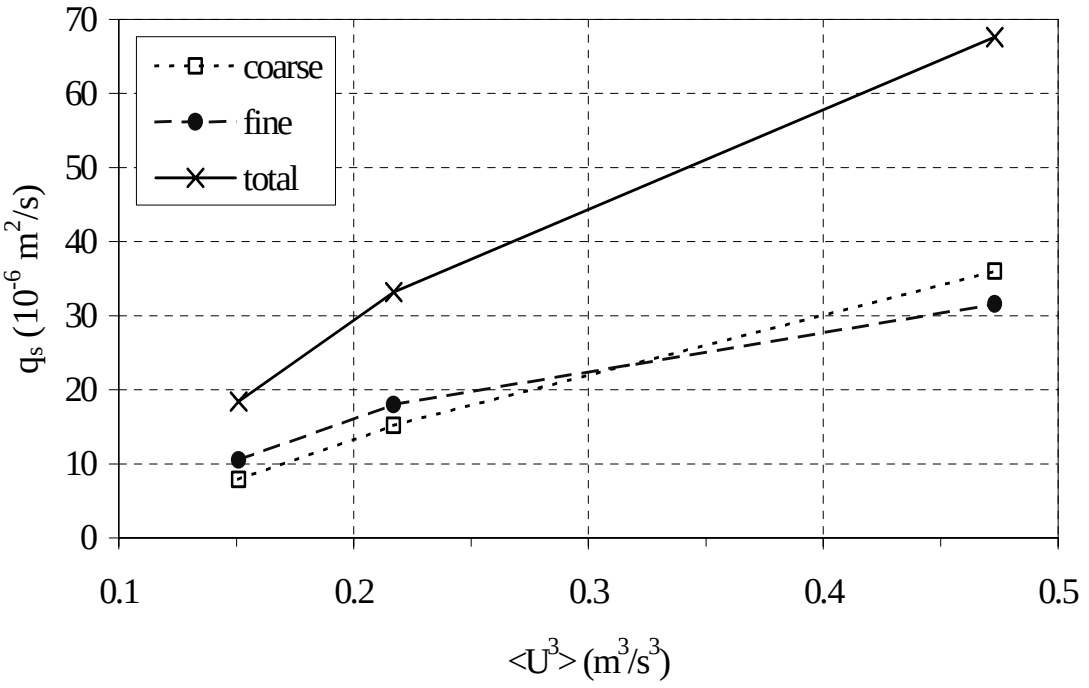

Figure 7.7: Measured net total transport rates and transport rates per size-fractions as a function of $<U^3>$ (series P).

The net transport rate of the coarse fraction appears to be almost equal to the net transport rate of the fine fraction (50/50%). This is remarkable, as the proportion of both size-fractions in the sand bed is 70% fine fraction and 30% coarse fraction. At higher flow velocities the share of the coarse fraction in transport rate seems to increase even more. This so-called selective transport of the size-fractions may be explained by the coarse fraction being more exposed to the flow than the fine fraction.

Similar selective processes were observed during series S experiments. Figure 7.8 shows that again measured net transport rates of the coarse fraction are more or less equal to or slightly lower than the transport rates of the fine fraction. Note that the fine fraction transport concerns the finest size (D_{50} = 0.13 mm) and the medium size (D_{50} = 0.32 mm) together, while the coarse fraction transport refers to the coarse grains only (D_{50} = 0.97 mm). Also note that the original sand bed during series S consists of 20% coarse fraction and 80% fine fraction.

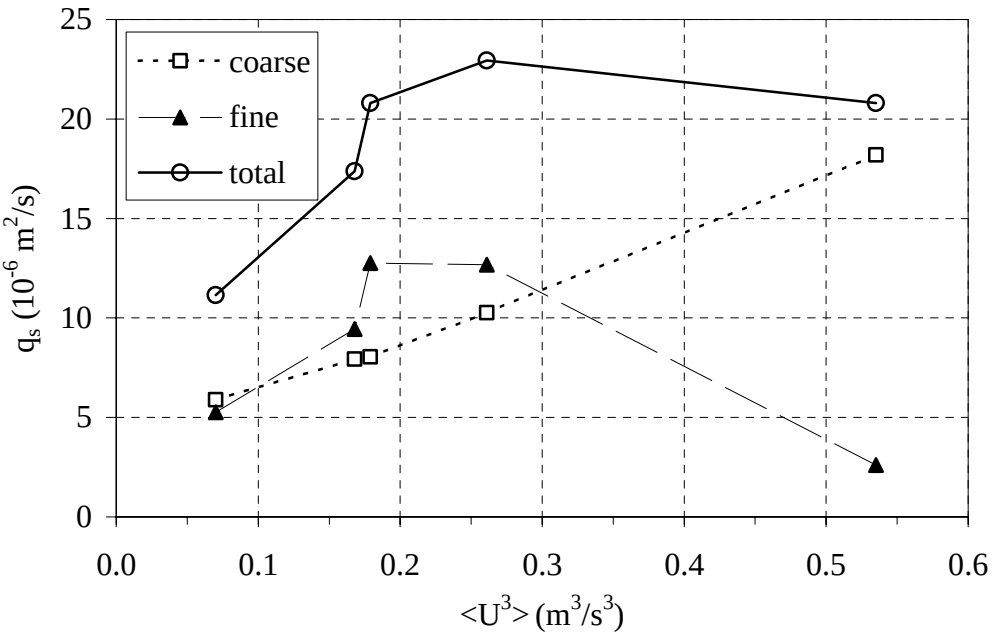

Figure 7.8: Measured net total transport rates and net transport rates per size-fraction as a function of <U^3> (series S).

7.3.4 Grain-size interactions in sand mixtures

Hiding of fine grains

In order to study the interaction between different grain sizes in mixtures, the measured transport rates of individual size-fraction in a mixture are compared with the transport rate of the same fraction in case of uniform sand. First the transport

rates of the fine fraction are studied for comparable hydraulic conditions. Different probabilities of occurrence in the sand bed (P_i) were taken into account by dividing the transport rates by this probability (P_i = 0.7 for series P; P_i = 1.0 for uniform fine sand).

In figure 7.9 it is shown that the fine fraction (D = 0.21 mm) is transported with lower rates in case of being part of a sand mixture (series P) than as in a 'uniform fine material' situation (series C of Al-Salem, 1993). This can be explained by the so-called hiding-effect due to which small sand-grains are sheltered behind coarse particles and are therefore less exposed to the flow. This reduction in transport rates is more pronounced at higher velocities ($<U^3> > 0.25\ m^3/s^3$).

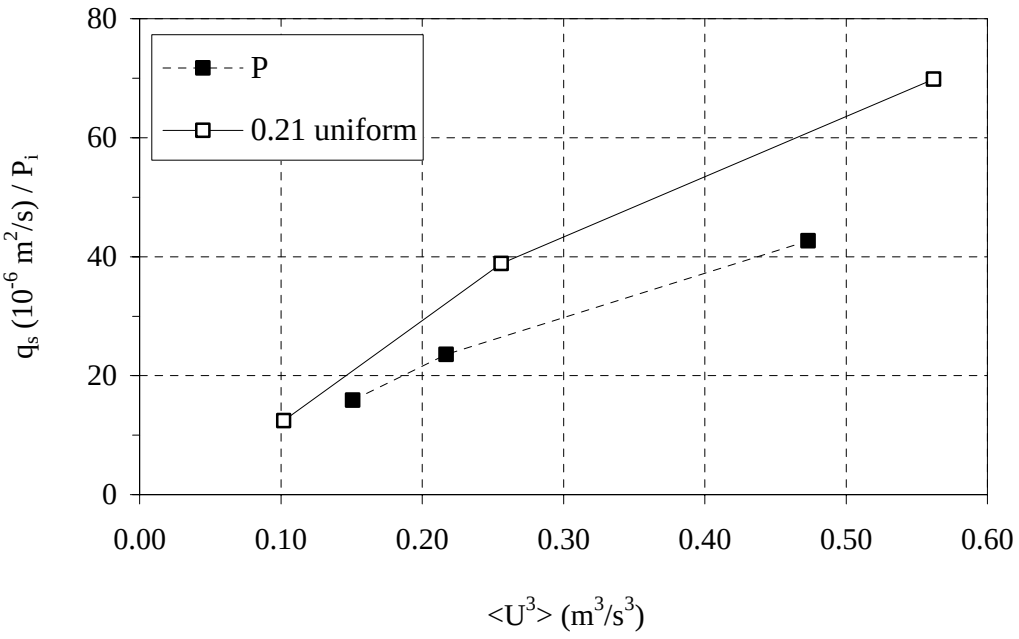

Figure 7.9: Comparison between measured net transport rates of uniform fine sand (0.21 mm) and the same sand as fine fraction in a mixture (series P).

Figure 7.10 shows a similar comparison for the grain-size D = 0.13 mm as part of a mixture and in uniform sand situation. The uniform sand data are from Ribberink and Chen (1993). The data with graded sand are series K (Cloin, 1998) and the present experiments (series S). Series K is a sand mixture consists of (50/50%) of two different sizes with D_{50} = 0.13 and 0.32 mm with similar flow conditions as used in series S.

Figure 7.10 shows also that the presence of coarse grains in sand mixtures (series K and S) has a clear effect on the net transport rate of the fine fraction. This can also be explained by hiding of fine grains between coarse grains. In the high velocity range

($<U^3>$ > 0.3 m^3/s^3), the absolute magnitude of the (negative) transport rates of the fine fraction is strongly reduced. For some cases the direction of net transport rates of the fine fraction changed from 'offshore' to 'onshore' around $<U^3>$ = 0.2 m^3/s^3. Apparently, there is no clear effect on net transport rates in the lower velocity range ($<U^3>$ < 0.2 m^3/s^3).

The results of the comparison in figure 7.10 indicate that the hiding effect of fine grains does not only lead to reduce the absolute transport rate, but it also seems to reduce the unsteady behaviour of the finest size-fraction. The latter can be deduced from the onshore-offshore transition, taking place at higher velocities. It may be attributed to a decreased entrainment height of the fine size-fraction as part of a mixture, due to its reduced mobility through the hiding process.

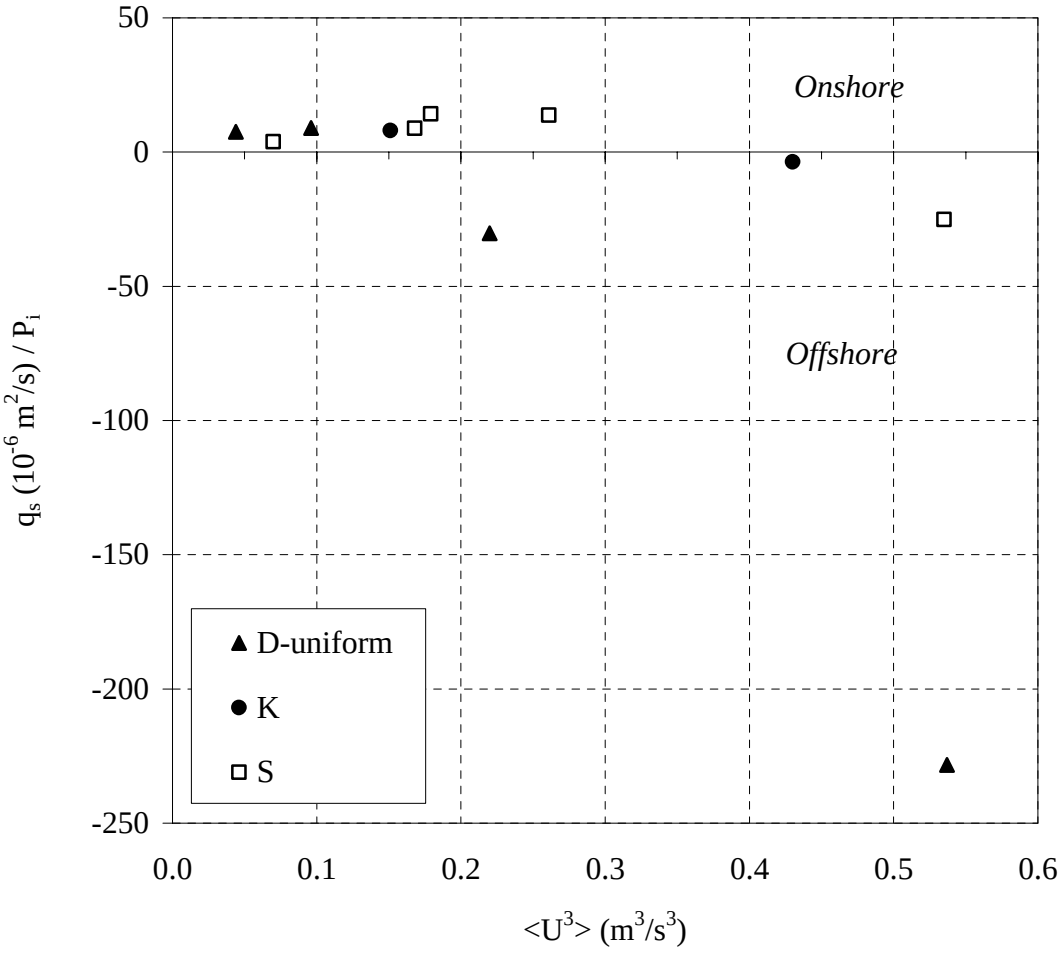

Figure 7.10: Comparison between measured net transport rates of uniform fine sand (0.13 mm) and the same sand as fine fraction in sand mixtures (series K and S).

Exposure of coarse-grains

A similar comparison between measured net transport rates of a 'uniform' coarse fraction (D_{50} = 0.97 mm) with net transport rates of the same coarse fraction in a sand mixture is presented in figure 7.11. The probability of occurrence of the coarse fraction in the sand bed is again taken into account. All data in figure 7.11 are new results as measured during the present study (series Q, P and S).

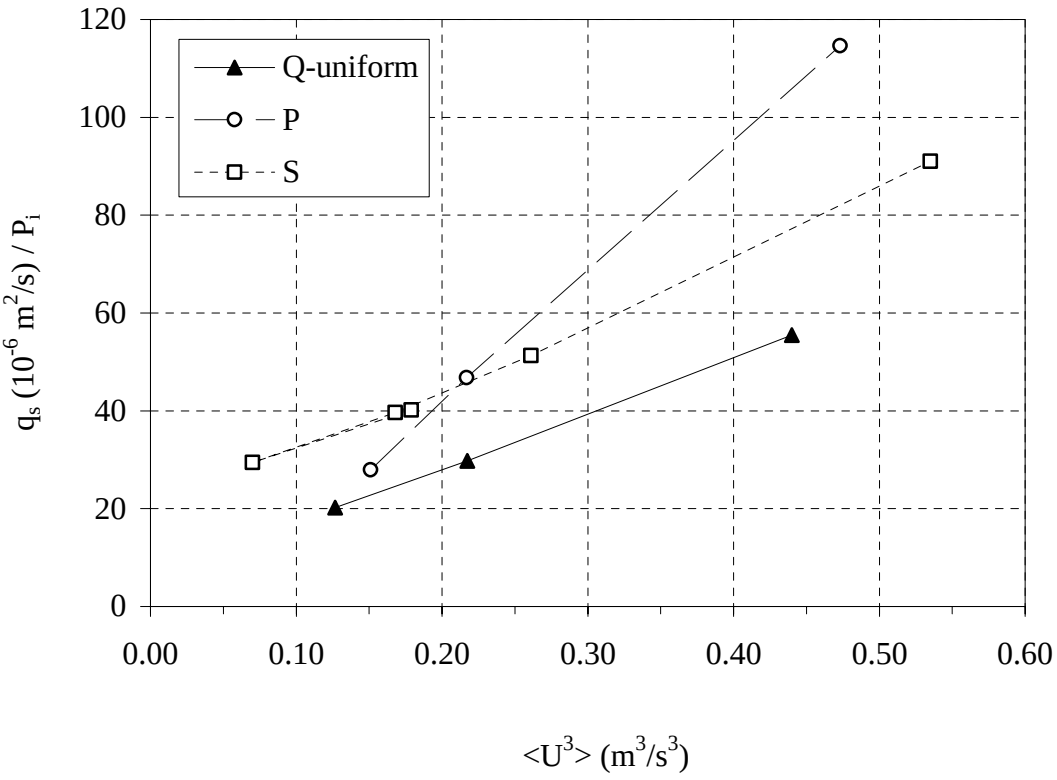

Figure 7.11: Comparison between measured net transport rates of uniform coarse sand (0.97 mm) and the same sand as coarse fraction in sand mixtures (series P and S).

It is clear for all flow conditions that coarse-grains are more transported when they are part of a sand mixture than in a uniform coarse sand situation. This increase in transport rates can be explained by the fact that coarse grains in a mixture are more exposed to the flow than in case of uniform coarse sand. The increased transport of coarse grains in a mixture may also be explained by the presence of fine grains creating a relatively smooth surface under the moving coarse-grains (mobility increase).

7.4 'Onshore' and 'offshore' bed-load transport

7.4.1 'Onshore' and 'offshore' bed-load concentrations

The sand samples extracted by the PBLT ('onshore' and 'offshore') were analysed to determine bed-load sand concentrations. Figure 7.12 shows the ratio between the 'onshore' and 'offshore' bed-load concentration measured during series P (Hassan et al., 1999). Results of individual tests are plotted against root-mean-square values of the flow velocities (U_{rms}). The dashed line in figure 7.12 shows the general trend of the results.

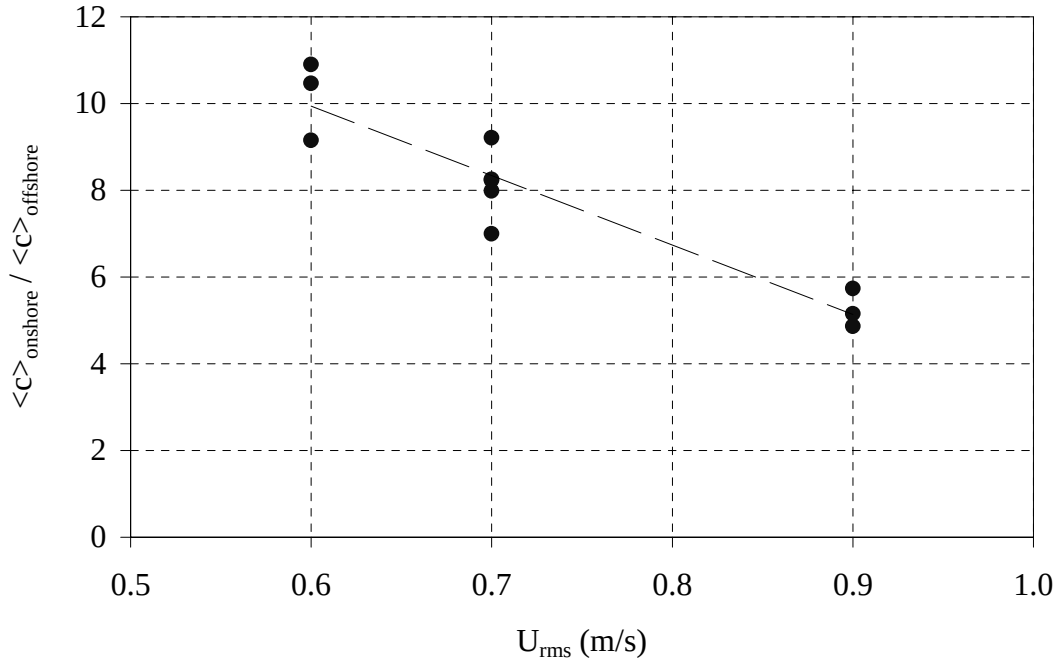

Figure 7.12: The ratio between 'Onshore' and 'offshore' bed-load concentrations, as a function of U_{rms}, measured by PBLT, series P.

Generally, the results show the time-averaged 'onshore' bed-load concentrations is 4 to 8 times higher than the time-averaged 'offshore' bed-load concentration. This difference can be explained by the asymmetry of the wave motion. The ratio between the 'onshore' and 'offshore' bed-load concentration decreases as the flow velocity (U_{rms}) increases. Besides, both the 'onshore' and 'offshore' concentration increase rapidly when the flow velocity increases, see Hassan (1999). Similar results were observed for other flow conditions and during series R and S, see Hassan et al. (2002) and Hassan et al. (1999).

7.4.2 'Onshore' and 'offshore' bed-load composition

Figure 7.13 shows the percentage of the coarse fraction in the bed-load transport during both the 'onshore' and 'offshore' motion as a function of the corresponding peak velocity (u_c = 'onshore' crest velocity, u_t = 'offshore' trough velocity). Since the two experimental series with graded sand (S and P) show the same trend, figure 7.13 shows only the results of series P. More detail can be found in Hassan et al. (2002) and Hassan et al. (1999).

The bed-load compositions show that the 'onshore' bed-load is coarser than the bed-load transported during the 'offshore' wave motion, as an effect of the asymmetric wave motion. During the 'onshore' motion the percentage of coarse fraction is about 45-50% and during the 'offshore' motion about 35-40%. During both wave phases the percentage of coarse material in the transported sand is larger than in the original sand bed (30% coarse). The contribution of the coarse fraction in the transported material increases with increasing velocity amplitude.

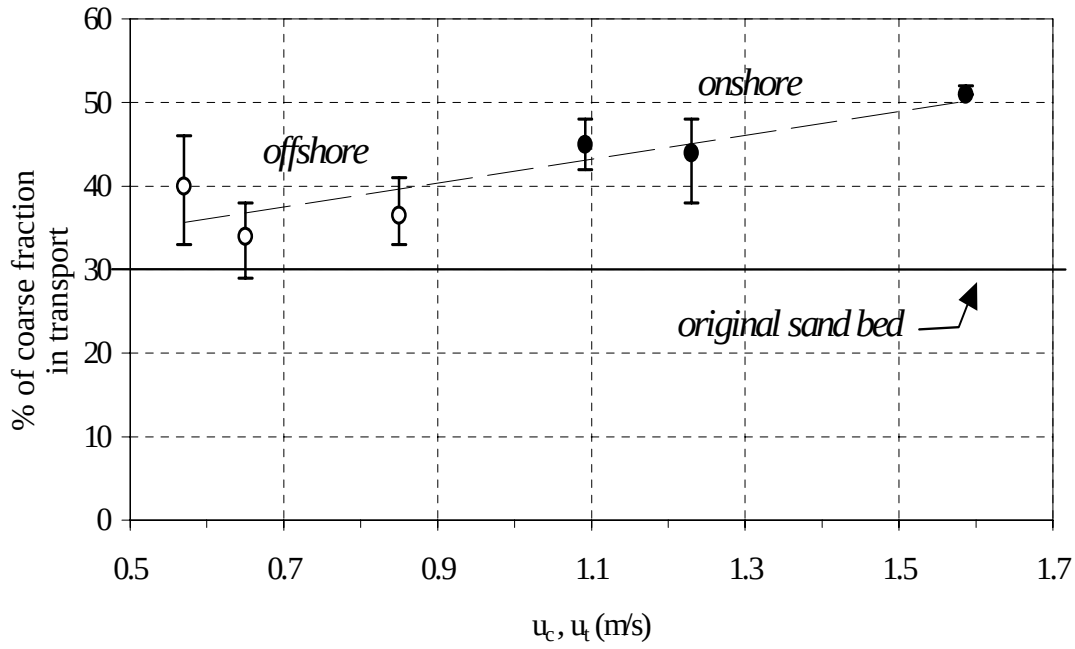

Figure 7.13: 'Onshore' and 'offshore' bed load composition versus peak velocities (u_c,u_t), measured by PBLT ((•) mean values per condition 'onshore', (o) mean value per condition 'offshore'), series P results.

7.5 Time-averaged concentrations

7.5.1 Suspended sand concentrations

A transverse suction system (TSS) was used to measure the time-averaged suspended concentrations during series P and S with graded sand. For each condition at least two tests were performed. The lowest tube of the TSS was positioned about 5 mm above the bed before the start of a test, resulting in a range of elevations from about 260 mm above the bed to about 5 mm above the bed. After a test the distance between the lowest tube and the sand bed was recorded in order to determine the average position of each nozzle above the bed.

Figure 7.14 shows a comparison between measured time-averaged concentration profile of condition S7f (series S, with graded sand) and the time-averaged concentration profile of condition D13 with uniform fine sand (D_{50} = 0.13 mm, data of Ribberink and Chen, 1993). Average values of different tests are presented in figure 7.14. More information on the time-averaged suspended sediment concentrations can be found in Hassan et al. (2002) and Ribberink and Chen (1993).

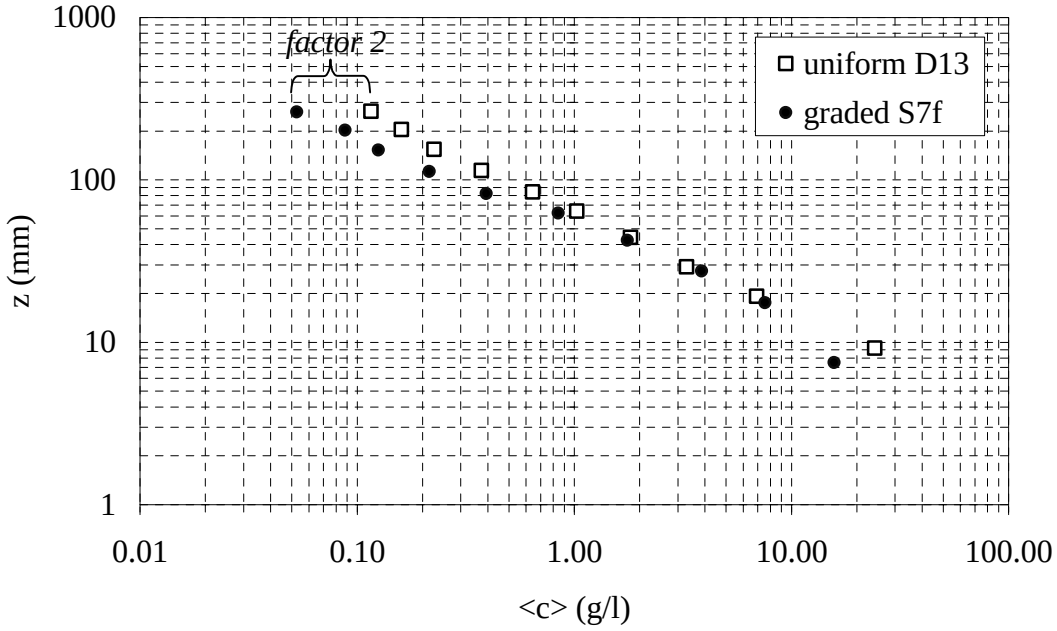

Figure 7.14: Comparison between time-averaged sand concentration profiles of uniform sand (data of Ribberink and Chen 1993, D_{50} = 0.13 mm) and graded sand (series S; 60%: 0.13 mm, 40%: 0.34 and 0.97 mm) for condition S7f (U_{rms} = 0.7 m/s).

The time-averaged suspended sediment concentration decreases rapidly as the height above the bed increases. There seems to be a power-law relation between the suspended sediment concentration and the distance above the sand bed. This was also seen at previous wave tunnel experiments (e.g. Al-Salem, 1993).

The measured time-averaged concentrations with graded sand are slightly lower than the time-averaged concentration with uniform fine sand, in higher levels ($z > 40$ mm) and in the lower levels ($z < 20$ mm). Generally we can conclude that the suspended sediment load of graded sand is slightly lower than of the uniform sand alone, but still within error ranges of the TSS. Apparently, the smaller percentage of finer sizes in the graded sand ($P_i < 1$) reduces the time-averaged concentrations. Note that the size composition analysis showed that only finer grains of the 0.13 mm fraction are present in the suspension layer (see also the following section). Kroekenstoel (1999) found similar results when he compared the time-averaged concentrations of series P (mixed sand) and series C (uniform sand) of Al-Salem (1993).

7.5.2 Composition of suspended sand

The sand samples collected by the TSS were analysed in the Visual Accumulation Tube (VAT) to determine the grain-size distribution and the percentage of coarse and fine fraction. Detailed information of the composition of the suspended sediment samples can be found in Hassan et al. (1999) and Hassan et al. (2002).

The results from the VAT analysis of suspended sediment samples of series P are summarised in figure 7.15. The values of two tests of one condition have been averaged. Note that only in this series the lower 5 or 6 tubes extracted enough suspended sediment to determine the grain-size distribution.

The following can be concluded from the grain size distribution in the suspension layer:

- Only the smaller particles of the fine fraction from the sand mixture go into suspension (D_{50} of original fine fraction = 0.23 mm, while D_{50} of the lowest suspended sand samples < 0.175 mm);
- The suspended sediment contains no coarse fraction at all. Coarse grains are only transported close to the bed;
- The grain size of the suspended sediment becomes smaller as the distance above the bed increases;
- As the flow velocity (U_{rms}) increases, the suspended sediment at a certain elevation becomes coarser (larger D_{50}).

The vertical distribution of D_{50} of suspended sediment during series S showed exactly the same trend as in series P (see Hassan et al., 2002).

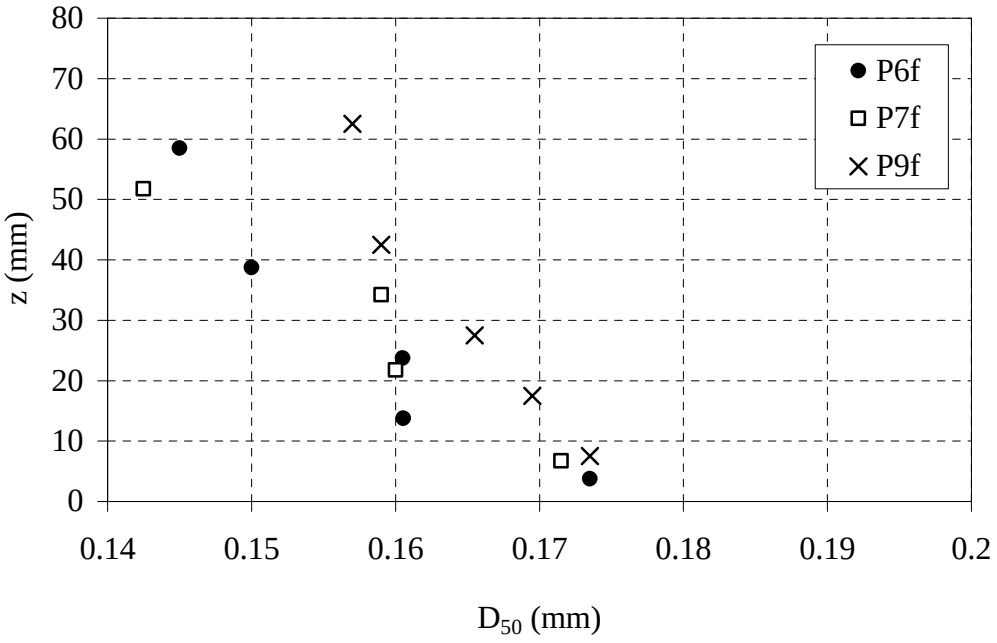

Figure 7.15: Vertical distribution of D_{50} of suspended sediment for three flow conditions, measured by TSS (series P).

Finally, we can conclude that under sheet-flow conditions vertical segregation is taking place in the suspension layer. Coarse grains are transported at low elevations ($z < 6$ mm), while at higher elevations only the finer fractions are found. This is consistent with the idea that especially the transport of the finer grains in a mixture is affected by phase-lag effects (large entrainment height and large settling lags).

7.5.3 Upper sand-bed layer

As mentioned before, after each test with graded sand (series P and S) bed samples were taken at different locations along the tunnel using the Bed Sampler (see section 6.3). Bed samples analyses of series P and S show more or less the same trend in the upper bed layer (the active layer). Since series P and S show similar results, only the results of series P will be discussed here. All information about the bed samples can be found in Hassan et al. (1999) and Hassan et al. (2002).

Before each test, a bed of mechanically mixed sand was brought into the LOWT. Analyses of bed samples taken during the test phase, preliminarily to this experimental series, showed that the coarse sand and the fine sand were very well mixed. It must be emphasised that the upper layer of the sand bed is replaced before every test, in contrast with previous experimental series in the LOWT (e.g. series K of Cloin, 1998). Thus, each test started with the same fully-mixed bed composition for the whole test section.

For two tests of conditions P6f and P9f bed samples were taken at 3 locations inside the tunnel (at x = - 2.5 m, x = + 1.0 m and x = + 3.5 m). A distinction was made between three separate slices or layers of 3 mm (3 slices of 3 mm). For other tests the composition of the sand bed after a test was examined more thoroughly. Samples were taken at 5 different locations (at x = - 2.5 m, x = + 1.0 m, x = + 3.5 m, x = + 4.5 m and x = + 5.5 m). Here separate slices or layers of 3 to 10 mm (3 slices of 3 mm, 4 slices of 5 mm and 2 slices of 10 mm) were distinguished, covering a total depth of 50 mm. The individual bed samples were analysed in the Visual Accumulation Tube (VAT) to study the grain-size distribution and the percentage of coarse fraction and fine fraction (see section 6.4.5).

Figure 7.16 shows the distribution of the percentage of coarse fraction against depth, for two conditions (P6f and P9f). These grain-size distributions have been obtained by taking the average of all locations along the tunnel (concerning all tests of one condition). Note that for the layers from 10 to 50 mm only one test per condition is available (average from five different locations along the tunnel).

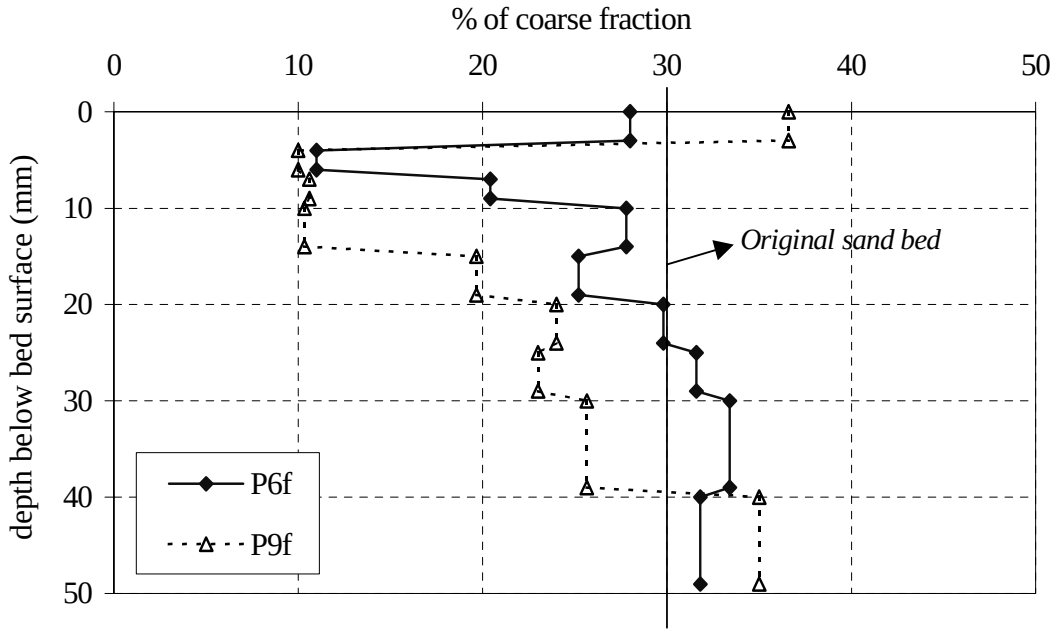

Figure 7.16: Distribution of the percentage of coarse fraction with depth for two different flow conditions (average values per condition), series P.

The following can be concluded from the sand bed samples analysis:

- The bed composition (percentage of coarse fraction and fine fraction) after a tunnel test is no longer uniform with depth. Vertical sorting has occurred, i.e. the upper layers (active layers) of the bed have changed in composition. The top 3

mm of the bed has roughly the same composition as before the test (condition P6f) or is a little coarser (condition P9f). Beneath the top layer there is a layer that mainly contains fine sand (10-20% coarse sand). This layer is about 10 to 20 mm thick. At larger depths the composition of the bed seems not to have changed much;

- The thickness of the active bed layer increases with increasing velocity. For condition P6f the "active layer" is about 10 to 20 mm thick, for condition P9f about 20 to 30 mm;
- On the average, the bed has become less coarse during a test. This occurs for each of the two wave conditions. This is in accordance with the composition of the sand collected in the sand traps (contains more than 30% coarse sand fraction). As the flow velocity (U_{rms}) increases the upper layers of the bed seem to become more and more fine. The coarse fraction is washed out from the upper layers of the bed more than the fine fraction.

7.6 Time-dependent transport processes inside the sheet-flow layer of uniform sand

7.6.1 Time-dependent concentrations

Ensemble-averaged concentrations at different elevations (mm) above and inside the sheet-flow layer and the sand bed of condition Oc4 (0.13 mm sand, sine wave superimposed on a net current, see table 6.2) with uniform sand are presented in figure 7.17 at different phases of the wave-cycle. Time-dependent concentrations were measured by the CCM. The zero level is defined at the initial bed level before starting a test. The upper part shows the flow velocity above the boundary layer (z = 100 mm) measured by the LDA. The general behaviour of time-dependent concentrations inside the sheet-flow layer in figure 7.17 is quite similar to the other conditions (Oc7 and Oc8) and therefore only results of Oc4 are presented. The complete time-dependent results can be found in Hassan (2001) and Trouw et al. (2001).

In general, the measured time-dependent concentrations for the different wave-periods show two different layers inside the sheet-flow layer. The first layer is located between the non-movable sand up to z = 0.0 mm and is called the pick-up layer. The second layer, above the pick-up layer z > 0.0 mm is called the upper sheet-flow layer. These two layers show opposite behaviour during the wave-cycle: the pick-up layer shows that concentrations are decreasing for increasing velocities because sand particles are being picked-up from the bed and brought to higher levels in the bed and into the flow. When the velocity decreases sand particles settle back to the bed and concentrations increase again. Opposite to this, the upper sheet-flow layer shows that concentrations increase for increasing velocity and decrease for decreasing velocity. Concentration peaks are observed at the moments of flow reversal, in the upper sheet-flow layers. These peaks are not present in the pick-up layer.

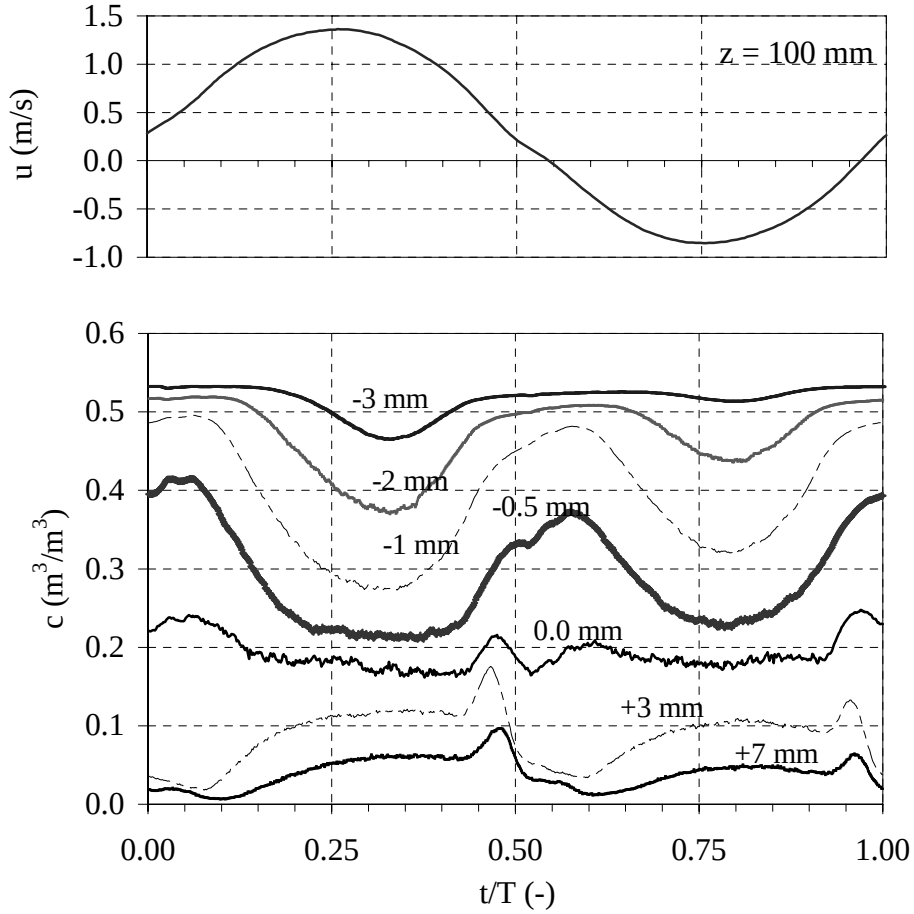

Figure 7.17: Time-dependent sediment concentrations at different levels (mm) inside the sheet-flow layer, condition Oc4 (data of Hassan, 2001).

These flow reversal peaks were observed also during the experiments of Dohmen-Janssen (1999) under sine waves superimposed on a net current. Although these peaks have been observed in different laboratory experiments (e.g. Ribberink and Al-Salem, 1995), a clear physical explanation for their occurrence is not yet available.

Observed phase-lag within sheet-flow layers

Figures 7.18 and 7.19 show ensemble-averaged concentrations (normalised by the wave-averaged mean concentration c_m) as occurring in the upper and in the pick-up sheet-flow layers, respectively. The concentrations were measured during one wave-cycle for the situation of three different wave-periods (T = 4, 7.2 and 12 s). In these two figures concentrations were measured at the same elevation, z = +7 mm in the upper layer and z = -1 mm in the pick-up layer. Note that figure 7.19 shows only two wave-periods (T = 4.0 and 12 s).

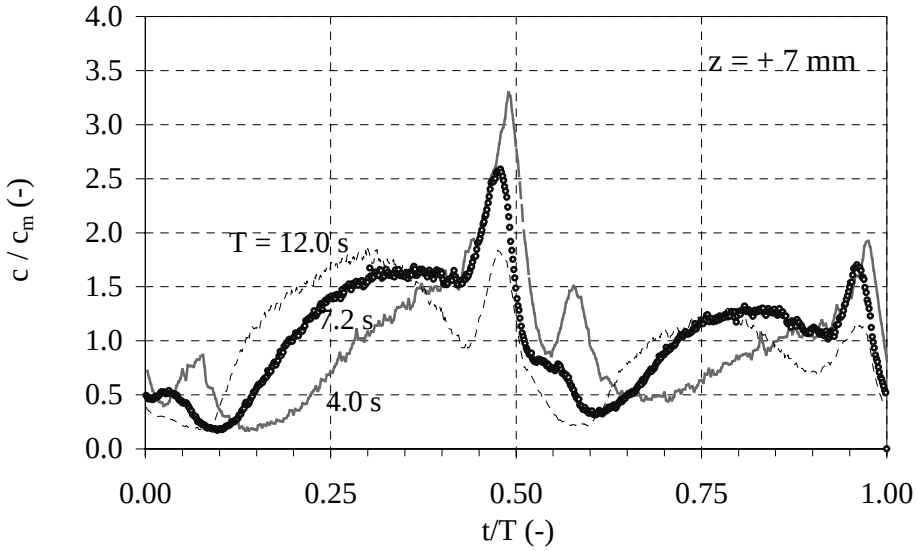

Figure 7.18: Increasing phase-lags of sediment concentrations in the upper sheet-flow layer for decreasing wave-periods (Hassan, 2001).

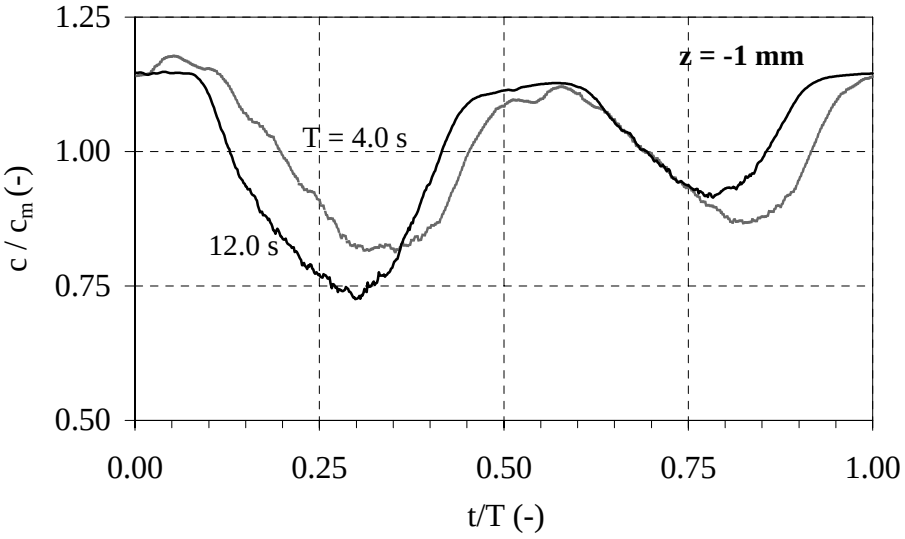

Figure 7.19: Increasing phase-lags of sediment concentrations in the pick-up sheet-flow layer for decreasing wave-periods (data of Hassan, 2001).

The concentration increases and decreases during each of the two half cycles of the periodic water motion. In the long-period case (12 s), the concentration shows a more or less direct response to the time-dependent velocity variations, for the shorter wave-periods, increasing phase-lags can be observed. The sediment entrainment

from the bed as well as the deposition process back to the bed lags behind the wave motion (see also Hassan et al., 2001c). Similar phase-lags are observed with the same flow conditions and different grain-sizes (see Dohmen-Janssen, 1999).

From the measured time-dependent concentrations inside the sheet-flow layers we can conclude the following wave-period effects:

- As the wave-period decreases, the sediment entrainment process, as well as the deposition process, shows an increasing phase-lag inside the pick-up and the upper sheet-flow layers with respect to the instantaneous velocity;
- Time-dependent concentrations inside the upper sheet-flow layer ($z > 0$ mm) are strongly affected by the wave-period. For the long wave-period ($T = 12.0$ s) concentrations reach a maximum value during each half of the wave-cycle, which is then followed by a concentration reduction before the flow reversal. This reduction in concentration is significantly reduced for the case with 7.2 s and not present at all during the short wave-period $T = 4.0$ s. For the shortest wave- period time-dependent concentrations even have a sawtooth shape;
- For long wave-periods ($T = 12.0$ s) sand particles have enough time to follow the flow velocity. For small wave-periods ($T = 4.0$ s) sand particles are not able to follow the flow instantaneously indicating that unsteady processes play a role inside the sheet-flow layer;
- The flow reversal peaks are increasing with decreasing wave-period. For $T = 4.0$ s, they are relatively dominant over the maximum sand concentrations in the upper sheet-flow layer.

7.6.2 Sand particle velocities

Using a cross-correlation technique for the signals of two CCM sensors (described in section 6.4.4), it was possible to measure time-dependent grain velocities inside the sheet-flow layer (McLean et al., 2001). Figure 7.20 shows an example of the measured time-dependent velocities of condition Oc4 against the wave phase. The solid line presents the measured velocities above the wave boundary layer ($z = 100$ mm), measured by LDA. The other symbols represent velocities obtained from the cross-correlation technique at different elevations (mm) above the initial sand bed, inside the sheet-flow layer.

It is clear that the measured velocities are nearly sinusoidal, and that the amplitude decreases with the distance from bed. The measured velocities are less accurate around the moments of flow reversal. This might be caused by the fact that velocities are derived from measured concentrations and at that phase sharp concentration-peaks are generated (vertical sand motion instead of horizontal motion), see figure 7.20. Reducing the distance between the two CCM sensors to 11 mm (instead of 20 mm as used before by McLean et al., 2001) improved the cross-correlation technique. The smaller distance between the two sensors made the technique suitable

for measuring the velocities during the complete wave-cycle including the smaller velocities in the pick-up layer.

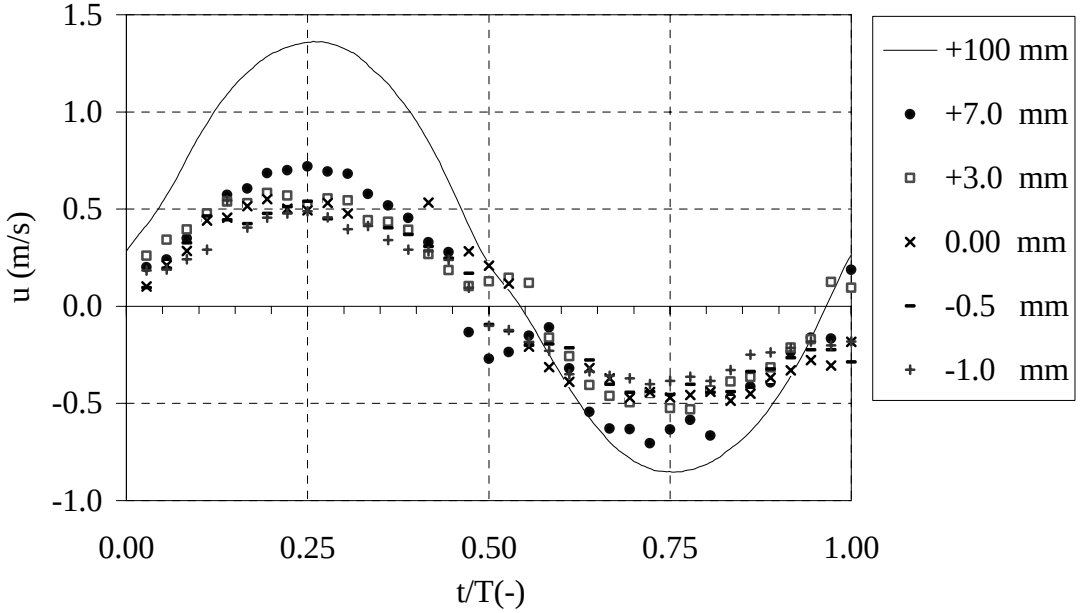

Figure 7.20: Ensemble-averaged particle velocities at different levels inside the sheet-flow layer, determined using a cross-correlation technique between 2 CCM sensors (Hassan, 2001).

7.6.3 Sediment fluxes inside the sheet-flow layer

It is clear from the previous two sections that the two CCM sensors are capable of measuring instantaneously both sand concentrations and particle velocities inside the sheet-flow layer. Multiplying the velocity (u) with the concentration (c) for each wave phase yields estimates of the time-dependent sediment flux.
The time-averaged flux profiles can be obtained by averaging time-dependent fluxes over the wave-period. Figure 7.21 shows time-averaged sediment fluxes at different levels inside the sheet-flow layer for three different conditions (Oc4, Oc7 and Oc12, see table 6.2) with the same velocity and different wave periods.

The upper panel shows the total fluxes, the middle panel shows the wave-related fluxes and the lower panel shows the current-related fluxes. The wave-related flux is the time-averaged value of the product of the oscillatory components of velocity and concentration. Meanwhile, the current-related flux is the product of the net current velocity and the time-averaged concentration. The total flux is the sum of the wave- and current-related components. Although the sediment flux profiles are based on a limited number of measurements and the scatter is rather large, some general trends can be observed.

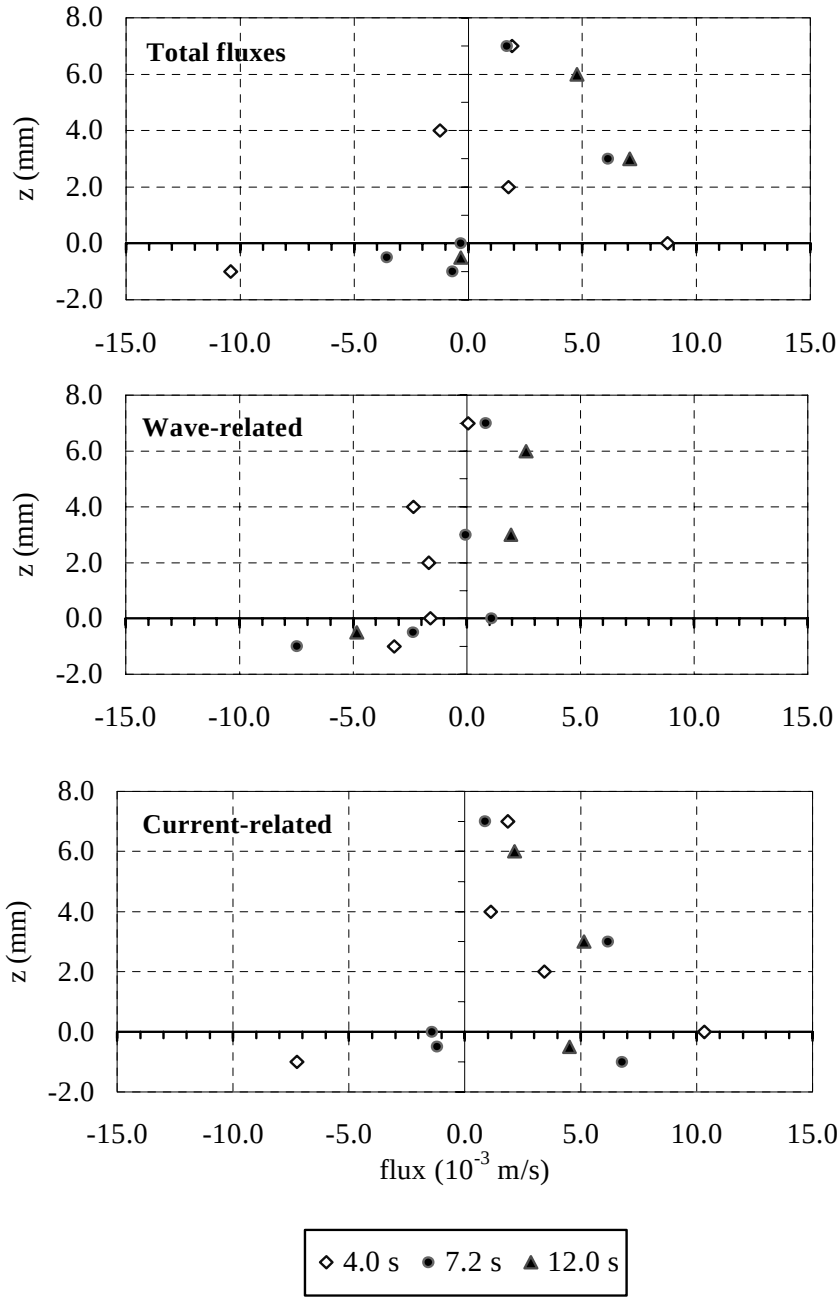

Figure 7.21: Time-averaged fluxes inside the sheet-flow layer with different wave-periods, total, wave-related and current-related flux (data of Hassan, 2001).

In general, we can conclude the following from the measured sediment-fluxes inside the sheet-flow layer:

- Generally we can observe that reducing the wave-period leads to a reduction in sediment fluxes over depth;

- A clear difference can be observed between wave-related fluxes for different wave-periods. Gradual changes in the flux profile are observed from positive sediment fluxes with large wave-period (T = 12.0 s) to negative fluxes with the shortest wave-period (T = 4.0 s). The positive wave-related-flux means that sand is transported in the direction of the crest velocity ('onshore'). The negative flux means that the sediment is transported in the direction of the trough velocity ('offshore'). The change in direction can be explained by the phase-lag effects, which increase as the wave-periods decreases;
- Generally, the current-related flux has positive values for all wave-periods (above the initial sand bed), because it is just the product of the (positive) net current and the time-averaged sand concentration. The shortest wave-period shows slightly smaller values compared to the longer wave-periods. This might be due to smaller sand concentrations with the shortest wave-period;
- The shorter wave-period results in changing the direction of the wave-related fluxes from the 'onshore' to the 'offshore' direction and consequently the total fluxes are reduced as compared to the longer wave-periods (see the upper panel of figure 7.21);
- It is clear that almost all sand is transported inside the sheet-flow layer. The measured time-averaged fluxes have small values above z = 6 - 8 mm;
- Although flow velocities close to the bottom of the sheet-flow layer have small values the wave- and current-related fluxes in the lower levels below the initial sand bed (z < 0.0) still have large values. In fact, these high fluxes can be explained by the very high concentrations at these levels (see figure 7.17);
- The current-related fluxes in the pick-up layer show a strong variation with positive and negative values. This is attributed to relatively large variations of the small mean current in this layer due to measuring inaccuracies.

By integrating the measured total fluxes over the depth it is possible to make a rough estimate of the net transport rates of each condition in the lowest 7 mm. Table 7.5 shows the net transport rates calculated from the integration of flux profiles in the upper panel of figure 7.21 and measured net transport rates, using the MCT from earlier experiments in the tunnel (Dohmen-Janssen, 1999). The earlier experiments were performed with the same sand and flow conditions. Table 7.5 includes also the name of the conditions as used in the present study as well as the names as used during the previous experiments of Dohmen-Janssen in the first column.

It is found that the general trend of the net transport rates is quite similar to earlier results of Dohmen-Janssen (1999). Increasing the wave-period leads to increasing net transport rates. Better results can be obtained using the CCM sensors by measuring more points over depth inside the sheet-flow layer. Moreover, measuring sediment fluxes in the suspension layer might improve the results for the 12 s case.

The differences between the measured transport rates using the two methods are due to the fact that both of the techniques have different sources of errors. For example the MCT technique results are based on measuring transport rates along the tunnel test section and averaged over the cross section of the tunnel. While the CCM

sensors are measuring a limited number of points over the vertical at only a certain location in the middle of the cross section of the tunnel. Moreover, the two methods suffer from inaccuracies associated with measuring a small quantity by subtraction of two large quantities (i.e. onshore and offshore parts of the wave-cycle).

Table 7.5: Comparison between measured net transport rates using the CCM sensors and the MCT.

Condition	**Wave-period (s)**	**q_s (10^{-6} m^2/s)**	
		CCM	MCT (Dohmen-Janssen, 1999)
Oc7/H44	4.0	10	9
Oc4/H4	7.2	28	40
Oc8/H412	12.0	37	97.1

From the CCM results we can conclude that under sheet-flow conditions sand is transported in a very large amounts very close to the bed in a thin layer with thickness < 10 mm. Although this layer is very thin unsteady effects are taking place and have a clear effect on the net transport rates.

7.7 Summary of experimental results and data comparisons

In the present study, five series of laboratory experiments have been conducted in the Large Oscillating Water Tunnel of WL | Delft Hydraulics. The main objective of these series was to study the near bed sediment transport mechanisms under prototype flow and sediment conditions. Uniform and graded sand were used to study selective transport processes, as well as size-gradation effects on net total transport rates and net transport rates per size-fraction. The hydraulic conditions have been chosen in close correspondence with previous experimental series in the wave tunnel, for reasons of comparison. The main results of the present experiments and their comparison with previous results are summarised per topic as follows.

7.7.1 Uniform sand

Grain-size effect on net transport rates

- For sand sizes 0.21 < D < 0.97 mm, the net transport rates are always directed ‘onshore’, i.e. transport rates are in the same direction as the wave crest velocity;

- Grain-size has almost no effect on the measured transport rates when $0.21 < D < 0.97$ mm;
- For $0.21 < D < 0.97$ mm, the measured net transport rates are proportional to the third power velocity moment ($<q_s> \sim <U^3>$); under oscillatory flow conditions quasi-steadiness can be assumed;
- Fine grains ($D = 0.13$ mm) show a strongly deviating net transport behaviour in the high velocity regime $<U^3> > 0.2$ m^3/s^3. The net transport rate changes direction from 'onshore' to 'offshore', due to unsteady effects. Therefore, Al-Salem's (1993) assumption of quasi-steadiness does not hold for the fine sand cases.

Time-dependent transport processes inside the sheet-flow layer

Time-dependent concentrations

- Time-dependent concentrations show two different layers inside the sheet-flow layer. The first layer extends between the undisturbed bed up to $z = 0.0$ mm and is called the pick-up layer. The second layer is located on top of the pick-up layer $z > 0.0$ mm and is called the upper sheet-flow layer. The concentrations in these two layers show opposite behaviour through the wave-cycle;
- For the largest wave-period (12.0 s) sand concentrations show an almost immediate response to the time-dependent velocity variations, for the smaller wave-periods (4.0 and 7.2s) increasing phase-lags are observed. The sediment entrainment from the bed, as well as the deposition process back to the bed, lags behind the wave motion more and more as the wave-period decreases;
- Concentration peaks are observed at flow reversal, but only in the upper sheet-flow layer. These peaks are not found in the pick-up layer. The flow reversal peaks are increasing as the wave-period decreases.

Sand particle velocities

- Using two CCM sensors inside the sheet-flow layer it was possible to measure both instantaneous sand concentrations and instantaneous particle velocities;
- Reducing the distance between the two CCM sensors to 11 mm, instead of the 20 mm used by McLean et al. (2001), improved the particle velocity measurements;
- The measured particle velocities are nearly sinusoidal, similar to the velocities above the wave boundary layer. An increase in velocity amplitude with the distance from the bed is observed. The measured velocities are less accurate around the moments of flow reversal.

Sediment-fluxes

- Reducing the wave-period from 12.0 to 4.0 s leads to increasing phase-lag effects in the wave-related flux profiles. Gradual changes in the wave-related flux profiles were observed from 'onshore' to 'offshore' directed as the wave-period was decreased;
- The measured net transport rates using the CCM sensors ($z < 7.0$ mm) showed a quite similar trend as earlier results of Dohmen-Janssen (1999). Reducing the wave-period leads to a general reduction of the net transport rate.

7.7.2 Graded sand

Transport rates of size-graded sand

Size-gradation effects on net total transport rates

- During the experiments of sand mixtures P and S a flat-bed/sheet-flow situation developed. The net total sand transport rates are increasing for increasing flow velocities and are directed 'onshore' for all conditions of series P. The net transport rates (series P) follow the power law $\langle q_s \rangle \sim \langle U^3 \rangle$;
- For sediment mixtures containing grain sizes $0.2 < D < 0.97$ mm this power-law is very similar to the one found for uniform sediments;
- Net transport rates for graded sand can be quite different from those for uniform sand if fine grains ($D = 0.13$ mm) are present in a mixture (series S). In the low velocity range ($\langle U^3 \rangle < 0.15$ m^3/s^3), the size-gradation has no clear effect on the measured net transport rates. The transport rates are closely proportional to the third power velocity moment $\langle U^3 \rangle$. In the higher velocity regime ($\langle U^3 \rangle > 0.15$ m^3/s^3), the size-gradation has a very clear effect and much lower transport rates are found than according to the power-law description.

Net transport rates of size-fractions and grain-size interactions in a mixture

- Sediment transport of grain-size mixtures under oscillatory sheet-flow conditions generally shows a preferential transport of the coarse fractions of the mixture. Their relative contribution to the transport is generally larger than would be expected on the basis of i) its volume proportion in the original sand mixture and ii) uniform coarse sand behaviour of the same size;
- Comparing the net transport rate per size-fraction in a mixture with the transport rate of uniform sand with the same D_{50} showed that the transport of each size-fraction is strongly influenced by the presence of other fractions. Fine particles in sand mixtures (series P and S) are less transported than in a uniform sand bed (hiding effects), while the opposite occurs for coarse fractions in a mixture (increased exposure);

- The latter indicates that 'uniform sediment' transport models are generally not adequate for the description of transport (rate and size-composition) of sediment mixtures. Interaction processes between size-fractions should be accounted for.

'Onshore' and 'offshore' bed-load transport

Bed-load transport

- The time-averaged 'onshore' bed-load concentrations are a factor 5 to 9 higher than their 'offshore' equivalents. This ratio decreases as the flow velocity increases and is explained by the asymmetry of the wave motion;
- As the flow velocity increases both the time-averaged 'onshore' and the 'offshore' bed-load concentration increase rapidly. There seems to be a linear relationship between the flow velocity and the 'onshore' and 'offshore' bed-load concentrations (see figure 7.12).

Bed-load composition

- Generally, the sand transported as bed-load (series P and S) in the 'onshore' direction is coarser than that in the 'offshore' direction. For both directions, the percentage of coarse material is larger than in the original sand bed. This sorting process was observed for all flow conditions;
- The contribution of the coarse fraction in the transported material increases with increasing flow velocity.

Time-averaged concentrations

Suspended sediment

- The time-averaged suspended sediment concentrations decrease rapidly with the height above the bed. There seems to be a power law relation between the concentration and the distance to the bed. This was also observed in previous wave tunnel experiments with uniform sediment (e.g. Al-Salem, 1993);

Vertical sorting in the suspension layer

- The suspended sediment contains no coarse size fractions at all; only the finer part of the 0.21 or 0.13 mm size fraction is present in the suspension layer. Coarser grains are only transported close to the bed ($z < 6$ mm);
- The grain-size of the suspended sediment becomes finer as the distance to the bed increases;
- As the flow velocity increases the suspended sediment at a certain elevation becomes coarser (larger D_{50}).

Sorting in the upper sand bed layer

- The composition of the sand bed after a test (series P and S) is no longer uniform over depth. The upper 3 mm of the bed after a test has roughly the same composition as before or is even coarser. Beneath the upper layer there is a layer that mainly consists of fine sand. The thickness of this layer is related to the flow velocity. At larger depths below the sand-surface/active-layer the composition of the bed is the same as in the original sand bed mixture;
- As the flow velocity increases the upper active layer of the bed seems to become finer. On the average, the sand bed becomes less coarse during a test. The coarse fraction is washed out from the upper layers of the bed more than the fine fraction.

Finally, we can conclude that under oscillatory sheet-flow conditions vertical sorting processes are taking place from the lowest point in the active sand bed layer through to the highest point of the suspension layer. Consequently, different grain-sizes show different transport behaviour at different levels in the flow.

Chapter 8

VERIFICATION OF SAND TRANSPORT MODELS WITH LABORATORY DATA

8.1 Introduction

A large dataset of oscillatory sediment transport measurements (flat-bed/sheet-flow conditions) is used to verify a series of transport models. The data were collected in the Large Oscillating Water Tunnel of WL | Delft Hydraulics (LOWT) and in the oscillating water tunnel of the University of Tokyo (TUWT), during the last ten years.

During the last ten years many experiments were performed in the LOWT under several flow conditions (sine and 2^{nd}-order Stokes waves) with different wave periods with and without steady currents, using different uniform and size-graded sands. Information about the LOWT experiments can be found in Dohmen-Janssen (1999, 1996), Cloin (1998), Hassan (1996), Ribberink and Al-Salem (1995), Ramadan (1994), Ribberink and Chen (1993) and Al-Salem (1993). Additionally, Dibajnia & Watanabe (1992, 2000), Inui et al., (1995) and Tanaka (2000) performed experiments in TUWT.

Moreover, new sand transport data has been collected during the present study, with uniform and graded sand (Hassan et al., 2002, Hassan et al., 1999). See chapters 6 and 7. These new data in combination with previous laboratory data from the two wave tunnels have been used to verify the transport models as discussed in chapters 4 and 5. The complete dataset (uniform and graded sands) consists of 190 different experiments, with different sand sizes and for a wide range of different flow conditions.

The main goals of the transport model verifications can be briefly described as follows:

- To identify which type of models (quasi-steady, intermediate, unsteady) are able to predict transport rates correctly for a wide range of hydraulic conditions and to determine the limitations of each type of model;
- To investigate the importance of including the phase-lag phenomenon in the sand transport models;
- Testing the validity of using the size-fraction approach, as described in chapter 5, for modelling size-graded sand transport.

Basically, the complete dataset of 190 experiments is divided into two main parts for model verifications. The first part includes all the data with uniform sand (118 experiments with one size-fraction, $\sigma_g < 1.3$), while the second part includes all the data with graded sand (72 experiments).

The graded sand data (72 experiments) are divided into two different parts. The first part is used for verification of graded transport models (using the size-fraction approach) as presented in the present chapter 8. Moreover, it is used for model improvements as described in chapter 9. This first part includes the graded sand data of Inui et al. (1995) and Tanaka (2000). The second part is used for final verification of the improved transport models (chapter 9). This part includes the data of Cloin (1998), Dibajnia et al. (1998) and the new data obtained in the present study, series P and S (see chapter 7).

In the present chapter model verifications with uniform sand data are presented in section 8.2. Moreover, the importance of modelling the phase-lag phenomenon on predicting transport rates is presented in this section. In section 8.3 predicted transport rates using the graded transport models (based on the size-fraction approach) are compared with the measurements. This verification concerns the total net transport rates as well as the transport of each individual size-fraction. Section 8.4 gives a summary of the main results of the sand transport model verifications.

8.2 Model verifications with uniform sand data

8.2.1 Description of uniform sand data

The complete set of uniform sand data (geometric standard deviation σ_g <1.3) in the present study consists of 118 different experiments, 51 from the LOWT and 67 from TUWT. Figure 8.1 shows the two (complementary) datasets in a wave period T, maximum flow velocity U_{max} diagram for different median grain sizes. R is the degree of asymmetry and equal to $U_c/(U_c+U_t)$, in which U_c is the maximum crest velocity and U_t is the maximum trough velocity.

In 1992 Dibajnia & Watanabe performed a set of experiments in TUWT with cnoidal waves with and without steady current, using uniform sand with median diameter D_{50} = 0.20 mm. The oscillating water tunnel of Tokyo University (TUWT) has a loop-shape with a horizontal rectangular test section with glass sidewalls. The test section is of 2.0 m length, 0.22 m height and 0.24 m width. For some cases Dibajnia & Watanabe provided a smaller width (0.12 m) in order to provide larger velocities. The tunnel is provided with a piston to generate oscillatory motion and a pump to superimpose a steady current on the oscillation. Long oscillating periods could not be used in this tunnel, because of the limited length of the test section.

During the last ten years many experiments were performed in the LOWT under several flow conditions (sine and 2nd-order Stokes waves) with different wave periods with and without steady currents, using different uniform sands (D_{50} = 0.13, 0.21 and 0.32 mm). From figure 8.1 it is clear that the complete dataset of LOWT and TUWT with uniform sand covers a wide range of velocities ($0.5 < U_{max} < 2$ m/s) and a wide range of wave periods between 2 and 12 seconds. More information about the data can be found in Dohmen-Janssen (1999), Ribberink and Al-Salem (1995), Ramadan (1994), Ribberink and Chen (1993) and Al-Salem (1993). The LOWT data include also the new measured data as obtained during the present study with uniform sand (D_{50} = 0.32), see chapter 7.

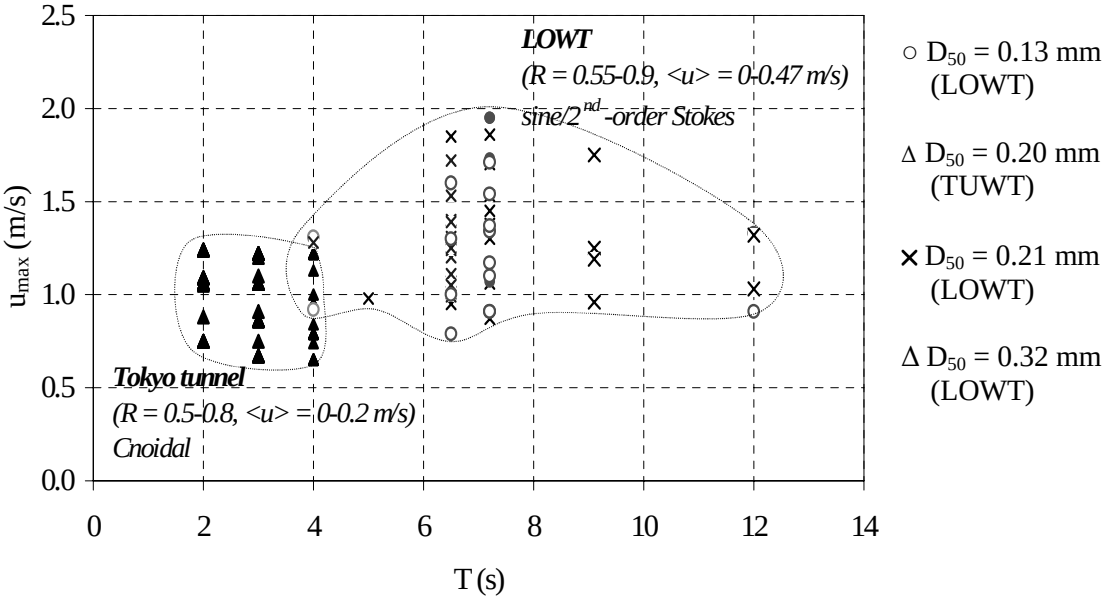

Figure 8.1: U_{max} -T diagram of all uniform sand data used for model verifications (<u> = time-averaged velocity, R = degree of asymmetry).

8.2.2 Quasi-steady models

The measured net transport rates of both datasets are first used for a verification of the quasi-steady sediment transport models of Bailard, Ribberink and D&W-qua. The D&W-qua is a quasi-steady version of D&W, with phase-lag effects switched off ($\Omega'_c = \Omega'_t = 0$ in equation 4.27, see section 4.4). It should be realised that for the development of the model of Ribberink only a small part (18%) of the present LOWT dataset were used (see Ribberink, 1998). The remaining 82 % of the LOWT data and 100% of the TUWT data are new for this model. For the development of the model of D&W (1996) all TUWT data were used, and therefore 100% of the LOWT data are new for this model. All data from the two water tunnels are 100% new for the model of Bailard (1981).

Figures 8.2 through 8.4 show the results of the model verifications of the model of Bailard (1981), Ribberink (1998) and the quasi-steady version of the D&W (1996) model (D&W-qua), respectively, on linear scales. The dotted line shows the line of perfect agreement between the model predictions and the measurements. The two solid-lines show a factor two over- or underprediction of the model. (note that in figure 8.2 the model of Bailard has a different y scale).

It can be observed that the LOWT dataset, obtained in the large velocity regime, generally shows much larger transport rates than the TUWT dataset. For many cases of both datasets a good agreement is found between the computations and the measurements (within ± factor 2), especially for the models of Ribberink and D&W-qua. However, for another considerable part of the data the models generally overpredict the net transport rates with more than a factor 2. Moreover, for some cases all three quasi-steady models are not able to predict the direction of the transport rate correctly (see also Hassan et al., 2001c). For these cases the measured transport rates are < 0, i.e. in ‘offshore’ direction and the predicted transport rates are > 0, i.e. in ‘onshore’ direction. The ‘onshore’ direction means the direction of the flow during the wave crest phase and the ‘offshore’ direction refers to the wave trough phase.

In fact the shortcoming of all quasi-steady models in correctly predicting the transport direction in some cases is not a surprise, because all quasi-steady models assume an instantaneous relation between flow velocity and sediment transport. This assumption always leads to onshore-directed net transport rates for most of the selected experiments, which might not be always the case in reality due to the presence of unsteady effects. Note that for these quasi-steady models some predicted transport rates have a negative sign while also the measured $q_s < 0$. In those cases, the asymmetric waves were superimposed on an opposing current $\langle u \rangle < 0$.

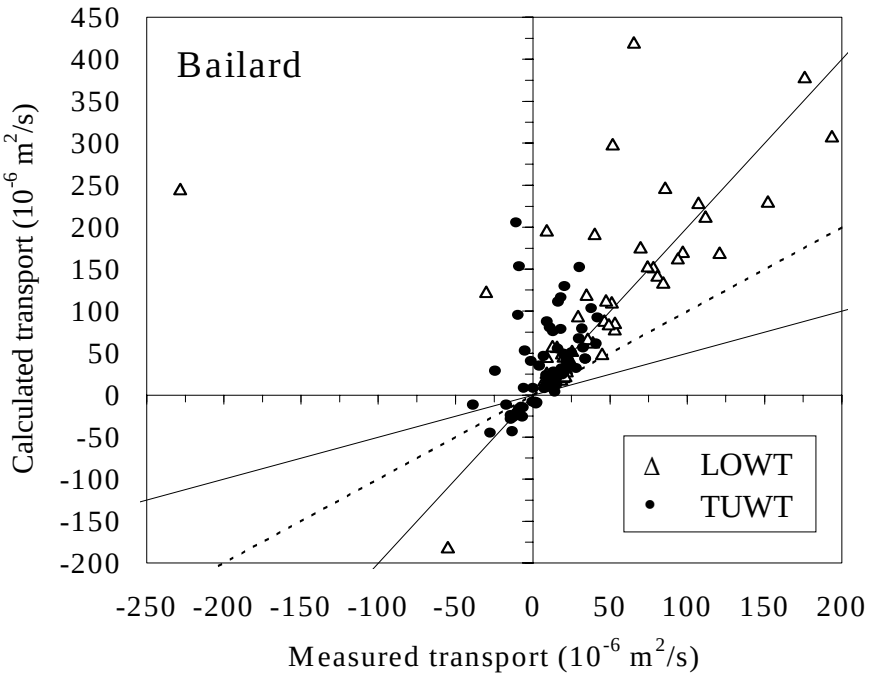

Figure 8.2: Verification of the quasi-steady models of Bailard (1981) with uniform sand data.

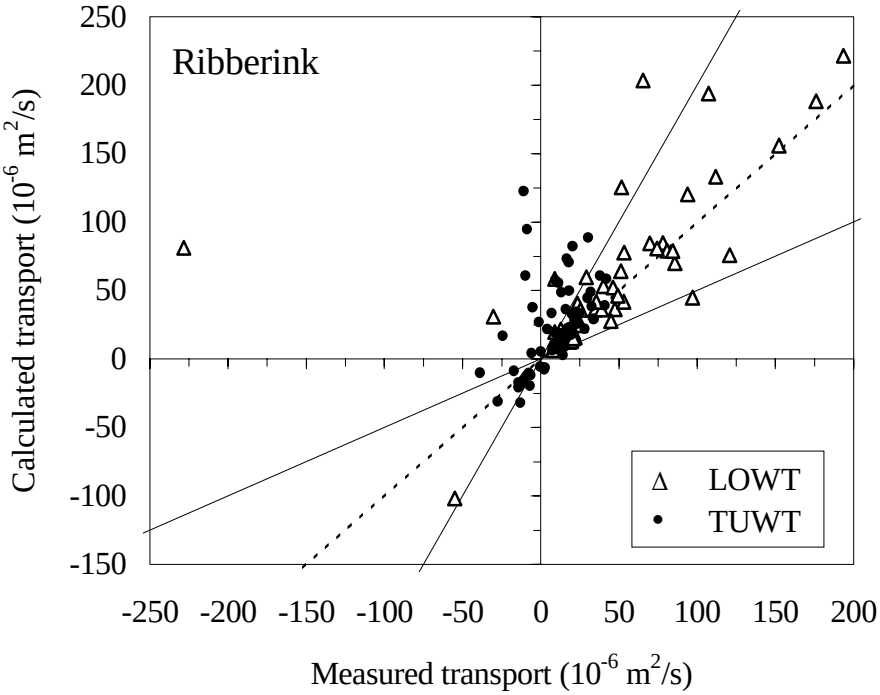

Figure 8.3: Verification of the quasi-steady models of Ribberink (1998) with uniform sand data.

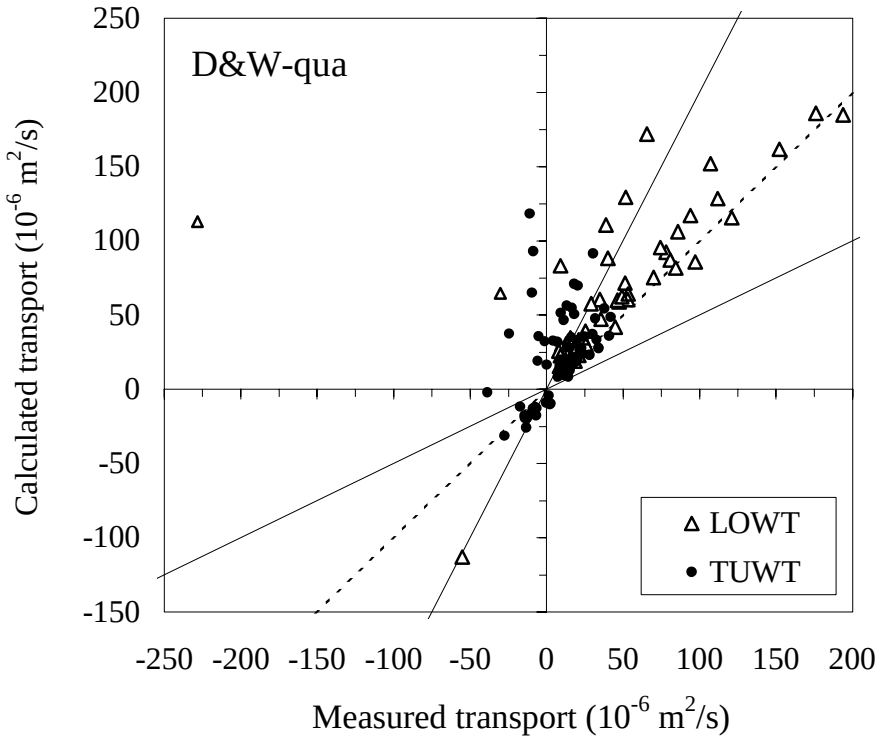

Figure 8.4: Verification of the quasi-steady model of D&W-qua (1996, phase-lag effect switched off) with uniform sand data.

Phase-lag effect

From the verification of quasi-steady models with uniform sand data, it was found that for some cases the models are not able to predict transport directions correctly. This concerned cases with a short wave period and small sand particles, indicating that the ratio between the settling time for sand particles and the wave period plays a role in the transport processes in oscillatory sheet-flow.

In order to investigate whether the observed differences between measurements and model predictions is related to the presence of phase-lag phenomena, the values of the phase-lag parameter p were calculated for all experimental cases. Hereto, Dohmen-Janssen's (1999) definition of p was used (see equation 4.22 in section 4.4).

Figure 8.5 shows the ratio of computed and measured transport rates as a function of the phase-lag parameter p for all uniform sand data. The upper panel shows the results using the model of Bailard (1981), the middle panel shows the results using the model of Ribberink (1998) and the lower panel shows the results of the D&W-qua model. The solid lines show the general trend of the results. The negative values are indicated with the open triangles.

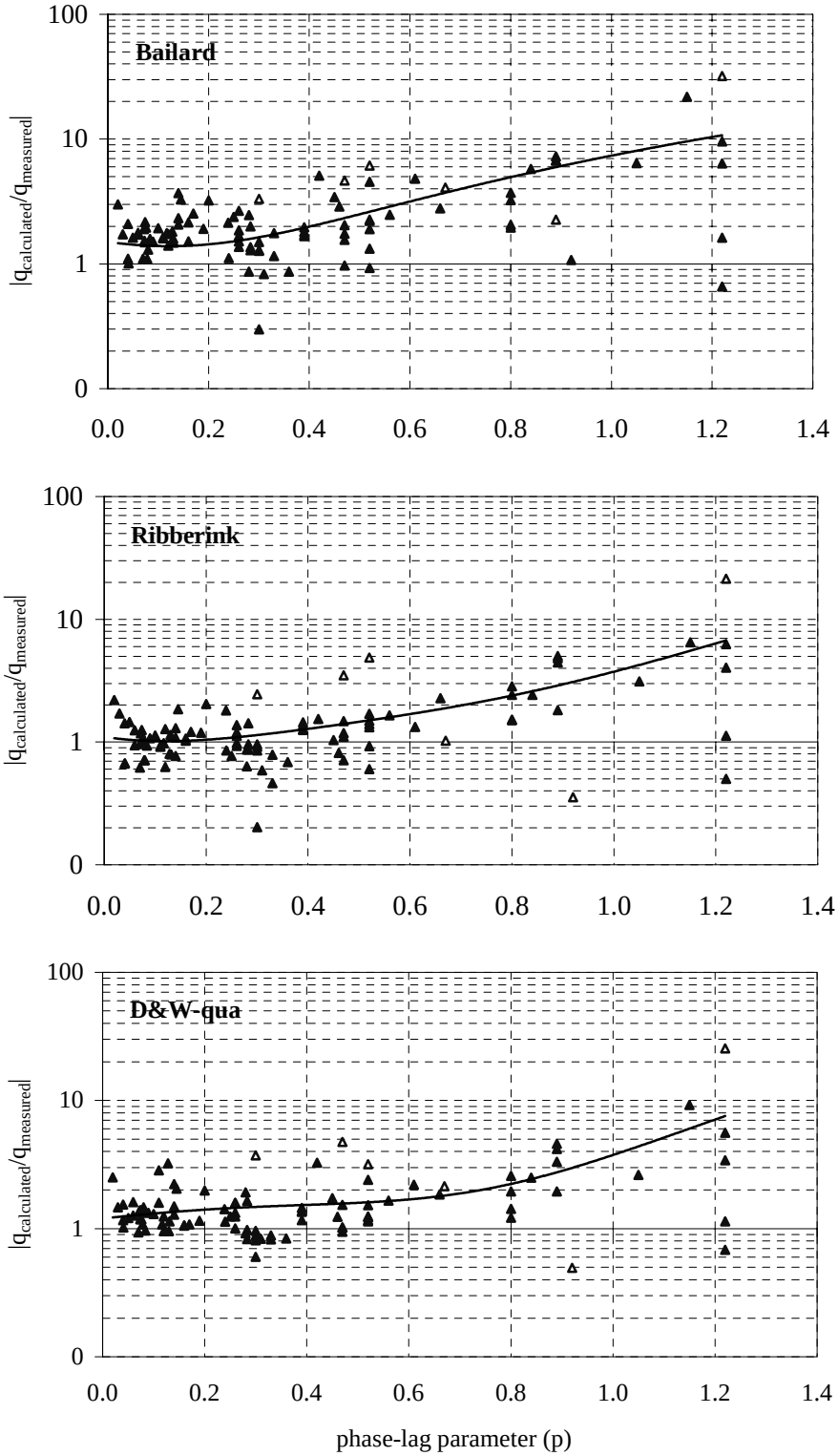

Figure 8.5: Ratio of computed and measured transport rates as a function of phase-lag parameter p (models of Bailard, Ribberink and D&W-qua).

Despite the considerable scatter of the results a consistent increase of this ratio can be observed for large values of p. These results indicate that the assumption of a 'quasi-steady' transport process is only valid for a certain range of p. If p is greater than that range phase-lag effects should be taken into account in transport models. It is also shown in figure 8.5 that the results do not depend strongly on the selected quasi-steady transport model. For all models it is clear that phase-lag effects become important when the value of p exceeds 0.4 - 0.6. These values are similar to the results obtained by Dohmen-Janssen (1999), who concluded on the basis of a limited number of data that phase-lag effects are important if $p > 0.5$, using only the model of Ribberink.

8.2.3 Intermediate models

The results of the verification of the two intermediate models (Dibajnia & Watanabe (1996) and Dohmen-Janssen (1999)), see section 4.4) are shown in figure 8.6. The upper panel shows the results of the model of D&W, while the lower panel shows the results of D-J's model. The dashed lines show the perfect agreement between the model predictions and the data while the solid lines show a factor 2 difference.

For both intermediate model concepts the agreement between measurements and computations has improved considerably in comparison with the quasi-steady model results, see figures 8.3 and 8.4. Apparently, the inclusion of phase-lag influences in the models leads to a strong improvement of the model performance.

Apart from a low number of data around zero and in the negative range, most of the data fall within the limits of ± factor 2 agreements for both models. The D&W-model shows a remarkably good correlation in the large (positive) transport range of the LOWT tunnel data.

The correlation coefficient between the model predictions and the measurements and the % of data predicted within a factor 2 are selected as parameters to evaluate the transport model performance. The first parameter gives an indication about the scatter of the data. While, the second parameter shows the ability of the model to predict absolute magnitudes of the measured transport rates within a certain range (± factor 2) around the line of perfect agreement. Equation 8.1 shows the definition of the correlation coefficient as used in the present study.

$$Corr_{x,y} = \frac{cov(x,y)}{\delta_x \, \delta_y} \qquad (8.1)$$

where: $Corr_{x,y}$ = correlation coefficient of measured (x) and calculated (y) transport rates; cov (x,y) = covariance between x and y; and δ_i = standard deviation (i = x, y).

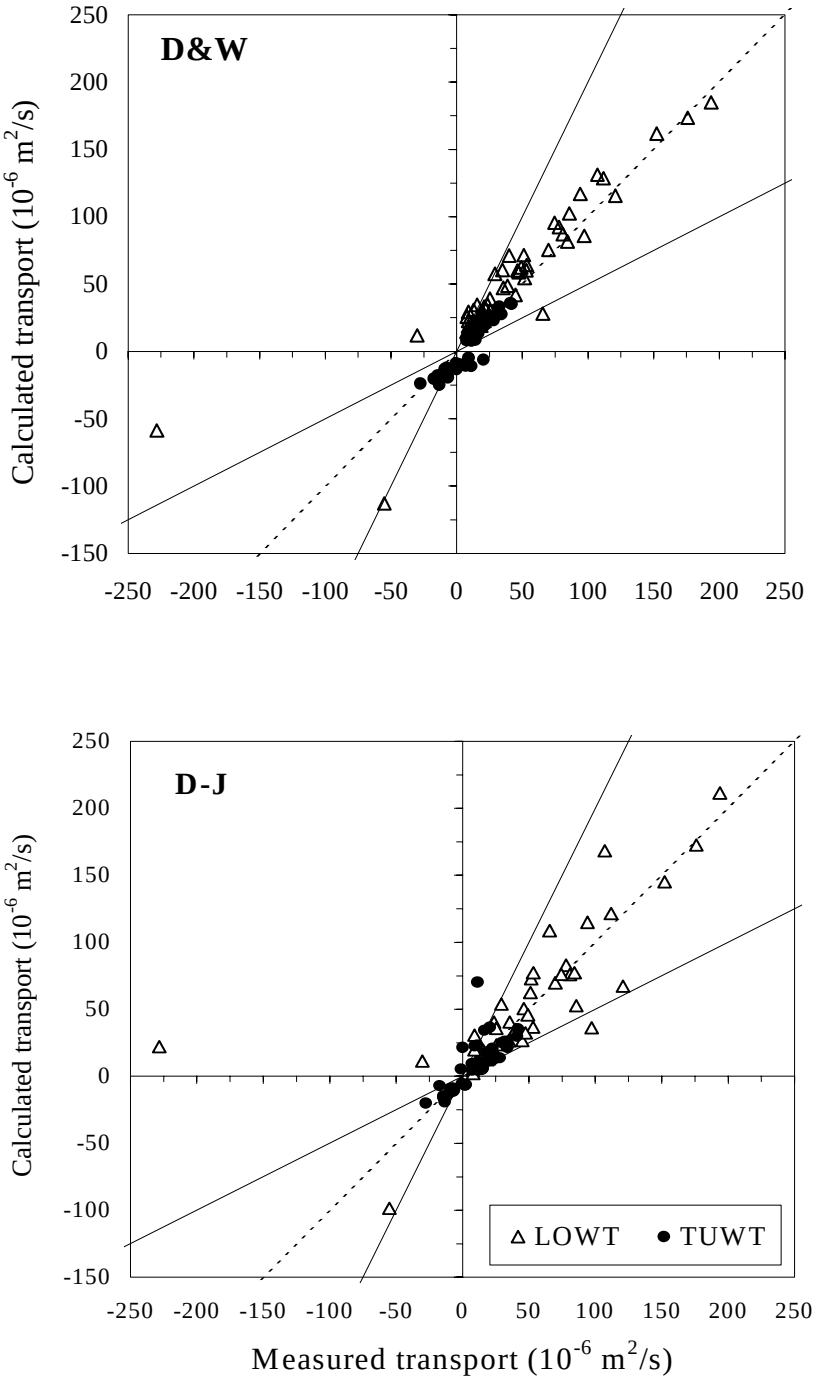

Figure 8.6: Verification of the intermediate models of Dibajnia & Watanabe (D&W) and Dohmen-Janssen (D-J), using uniform sand data.

The correlation coefficient measures the relationship between two datasets that are scaled with the standard deviation to be independent of the unit of the measurement. A positive correlation means that the large values of one dataset are associated with large values of the other. A negative correlation coefficient means that small values of one dataset are associated with large values of the other. When the values of both datasets are unrelated the correlation coefficient gets close to zero.

Figure 8.7 shows the performance of all quasi-steady and intermediate models in terms of the correlation coefficient, in the upper panel and in terms of percentage of data predicted within ± a factor 2, in the lower panel. These two parameters are calculated for the two individual datasets (LOWT and TUWT) and for all data together. It is clear that the two intermediate models show a better performance compared to the quasi-steady models. The D&W-model shows the highest correlation coefficient (ca. 0.9) for all data, while the model of D-J shows the largest percentage of data within ± a factor 2 (80-90%).

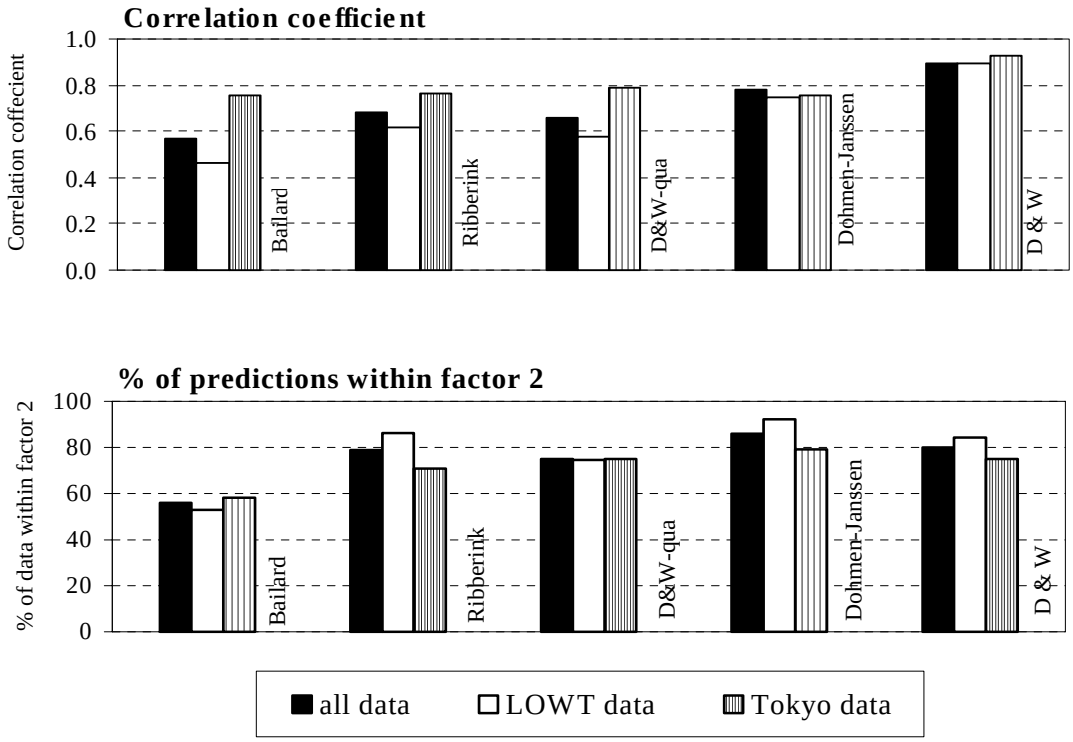

Figure 8.7: Performance of quasi-steady and intermediate models for all uniform sand data, in terms of a correlation coefficient and in terms of % of data within ± a factor 2.

The models of Ribberink (1998) and D-J (1999) were developed using only uniform sand data from the LOWT. Similarly, the model of D&W (1996) was developed using only a data from TUWT. This means that each model was developed and

calibrated in a certain range of flow velocities and wave periods depending on the laboratory facility. Nevertheless, the results show that these models are able to reproduce the data from the two water tunnels rather well. The model of D&W (1996), for instance, shows a correlation coefficient 0.93 and 75 % of the data within a factor 2 for the TUWT data. At the same time, the D&W model shows a correlation coefficient 0.90 and 84 % of the data within a factor 2 for the LOWT data.

8.2.4 The POINT-SAND model

In order to verify the POINT-SAND model, a part of the dataset with uniform sand has been used. The selected data include all the measurements of the LOWT and 14 cases from TUWT. In total 65 cases have been used for model verification covering the full range of flow/sediment conditions of the complete dataset. The reason for reducing the number of cases to verify the PSM model is the long time required for performing computations with the PSM model. The latter is related to the detailed character of the process-based PSM model (see chapter 4). All uniform sand data used in the model verification are totally new for the POINT-SAND model. The PSM model has never been calibrated with laboratory data before.

All computations with the PSM model are based on using the original settings of the input parameters, which means that the original model settings as recommended by Uittenbogaard et al. (2000) have been used. The original settings include the following: Prandtl Schmidt number = 0.7; using the k-ε model for turbulence closure; the boundary condition for the velocity computation at the bed is specified as for $z_0 = 2D_{50}/30$; Zyserman and Fredsøe (1996) boundary condition for sediment concentration.

Introductory computations with the PSM model show that the optimal number of computational layers should be 100, the computational time should be more than 40 waves and the time-step should be less than 0.05 s in order to get stable results.

Figure 8.8 shows the predicted transport rates against measurements. Again the dotted line shows the perfect agreement and the two solid lines show a factor 2 difference.

In general the PSM model shows reasonable results in comparison with the measured data. The PSM model is able to predict the directions and transport rates correctly, so apparently includes a better representation of phase-lag effects than the quasi-steady models. Most of the model predictions are within ± factor 2 of the measurements. However, almost all model predictions are under the line of perfect agreement. In other words: the PSM model gives a systematic underprediction of the measured transport rates. This may be related with the fact that the PSM model is a suspension model with no separate bed-load description.

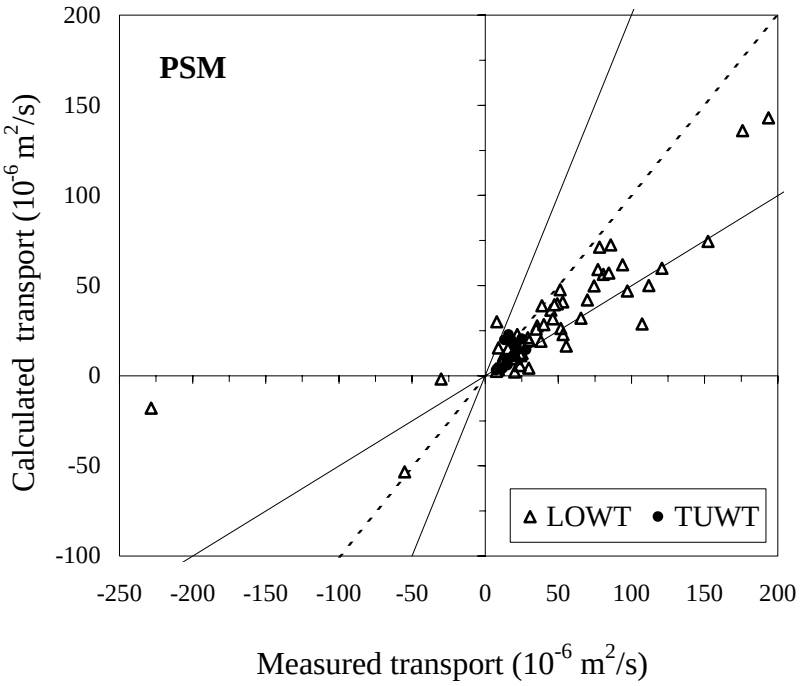

Figure 8.8: Verification of the POINT-SAND model, with uniform sand data.

In order to evaluate the performance of the PSM model in relation to other transport models, the correlation coefficient and the % of model predictions within a factor 2 are presented in figure 8.9 for three different models, viz. the PSM model and the two intermediate models of D-J (1999) and D&W (1996). The two parameters are computed for all models, for the 65 experiments used in the PSM model verification. The intermediate models were chosen for this comparison, because they showed a better performance than the quasi-steady models (see figure 8.7).

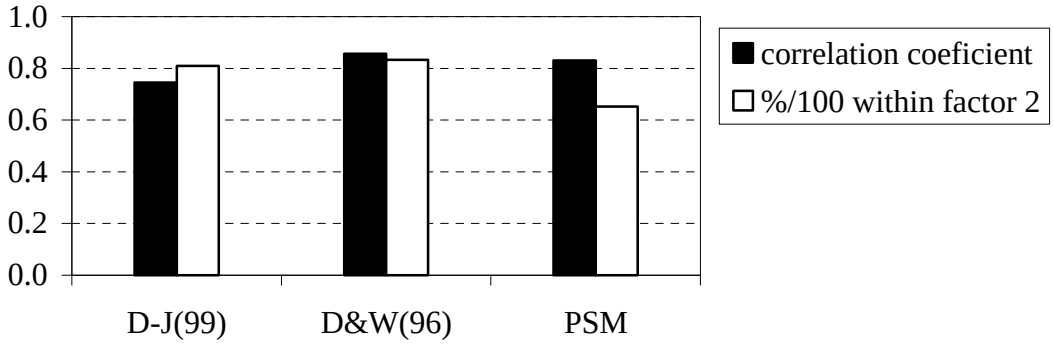

Figure 8.9: Performance of the PSM model in comparison with the two intermediate models, in terms of a correlation coefficient and in terms of % of data within ± factor 2 range.

From figure 8.9 it is clear that the PSM model is generally showing good results compared to the other intermediate models, taking into account that these were developed on the basis of laboratory data and partially developed on the basis of the presently used laboratory dataset. The PSM model shows a correlation coefficient close to the model of D&W and higher than the model of D-J. On the other hand, the PSM model shows the lowest percentage of predictions within ± a factor 2. Using an empirical correction or the inclusion of a separate bed-load model may significantly improve this percentage. Note that the PSM model was never calibrated before with sand transport data.

8.3 Model verifications with graded sand data

8.3.1 Description of graded sand data

Table 8.1 shows a general overview of the laboratory dataset with graded sand that was used for transport model verifications. The transport models are described in chapter 5 in combination with the size-fraction approach. All data are obtained from TUWT under oscillatory sheet-flow conditions. In total 37 experiments with graded sand have been used to verify the transport models. The experiments were performed with mixtures of 2 uniform sands (bi-modal sands) and cnoidal waves with different wave velocities and periods. Inui et al. (1995) used a degree of asymmetry R equal to 0.7, while Tanaka (2000) used a value equal to 0.6.

Table 8.1: Laboratory data with graded sand used for model verifications.

Series		**Sand fractions D_{50} (mm)**	**Wave conditions**		
			Type	**U_c (m/s)**	**Wave period (s)**
TUWT	Inui et al., 1995	0.2/0.87	cnoidal	0.63-1.0	3, 5
	Tanaka, 2000	0.2/0.8	cnoidal	1.1-2.0	3

The measured net transport rates in case of graded sand include both the net total transport rates and the net transport rates of each individual size-fraction. These measured net transport rates of per size-fraction provide the opportunity to study the selective transport processes in sand mixtures.

The following procedure was used for measuring net transport rates in the TUWT, under asymmetric waves. First a vertical thin plate was carefully placed at the middle of the tunnel test section, to separate its two sides (‘onshore’ and ‘offshore’) completely, the sand mixtures were weighed and replaced at either side of the plate,

so as to make a uniform flat bed. Then the plate was removed and the tunnel was set into the required motion. Finally, the thin separation plate was used again in the middle section. The sand from each side was removed again and weighed to give the net transport rates. The percentage of the weight of each size-fraction in the total weight of a sand mixture was used to determine the net transport rate of each individual size-fraction. More detail about the used data can be found in Inui et al. (1995) and Tanaka (2000).

8.3.2 Quasi-steady models

Figures 8.10 through 8.12 show the verification of the three quasi-steady graded transport models, the model of Bailard, the model of Ribberink and the model of D&W-qua, respectively. These models are described in chapter 5. The upper panel in each figure shows the results of the net total transport rates, the middle panel shows the net transport of the fine fraction alone and the lower panel shows the net transport rates of the coarse fraction alone. The dotted lines are the lines of perfect agreement between the model predictions and the measurements. The solid lines show a factor 2 difference. Note that in figures 8.10 through 8.12 the x and y axis may have different scales, for clarity's sake. In all figures the data are sorted by test series, Inui et al. (1995) and Tanaka (2000). See table 8.1 for more detail.

In many cases the model of Bailard (1981) overpredicts the total transport rates, as well as the transport rates of the fine fraction, as shown in the upper and the middle panels in figure 8.10. For part of the data the direction of the net transport is not predicted correctly, especially for the fine fraction, when the phase-lag effects become more pronounced. On the other hand, the transport rates of the coarse fractions are slightly underpredicted. Nevertheless, the model of Bailard yields better results for the coarse fraction than for the total and fine fraction transport rate.

In general, the two models of Ribberink (1998) and D&W-qua (1996) show more or less the same behaviour, see figures 8.11 and 8.12. The two models yield better results than the model of Bailard (1981), especially for the total and coarse fraction transport rates (see the upper and the lower panels in figures 8.10 through 8.12). Like the model of Bailard (1981), however the two models are not able to reproduce the fine fraction data correctly. For a considerable part of the fine fraction data the models generally overpredict the transport rates by more than a factor 2 and even the transport direction is not predicted correctly. The failure of the quasi-steady models in reproducing most of the fine fractions transport rates can be explained by the presence of phase-lag effects, which are not accounted for in these models.

The results of section 8.2 show that phase-lag effects can play an important role in transport processes under oscillatory sheet-flow conditions, also in the case of graded sediments. In general, the three models underpredict the coarse fraction transport rates and overpredict the transport rates of the fine fractions. Including phase-lag effects in the models might improve the fine fraction transport rate predictions, like

in the uniform sand cases (see section 8.2). This will be tested in the following section.

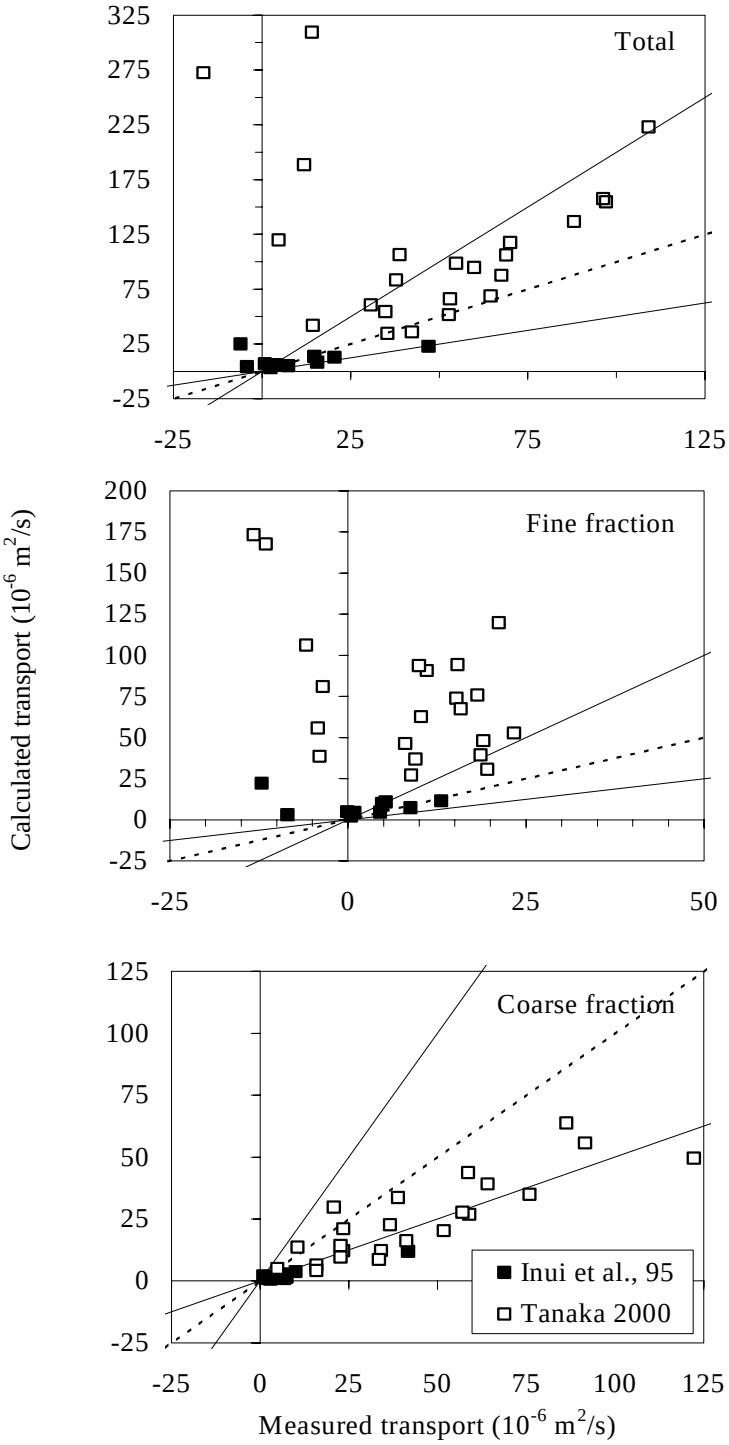

Figure 8.10: Verification of the multi-fraction model of Bailard with graded sand data from TUWT.

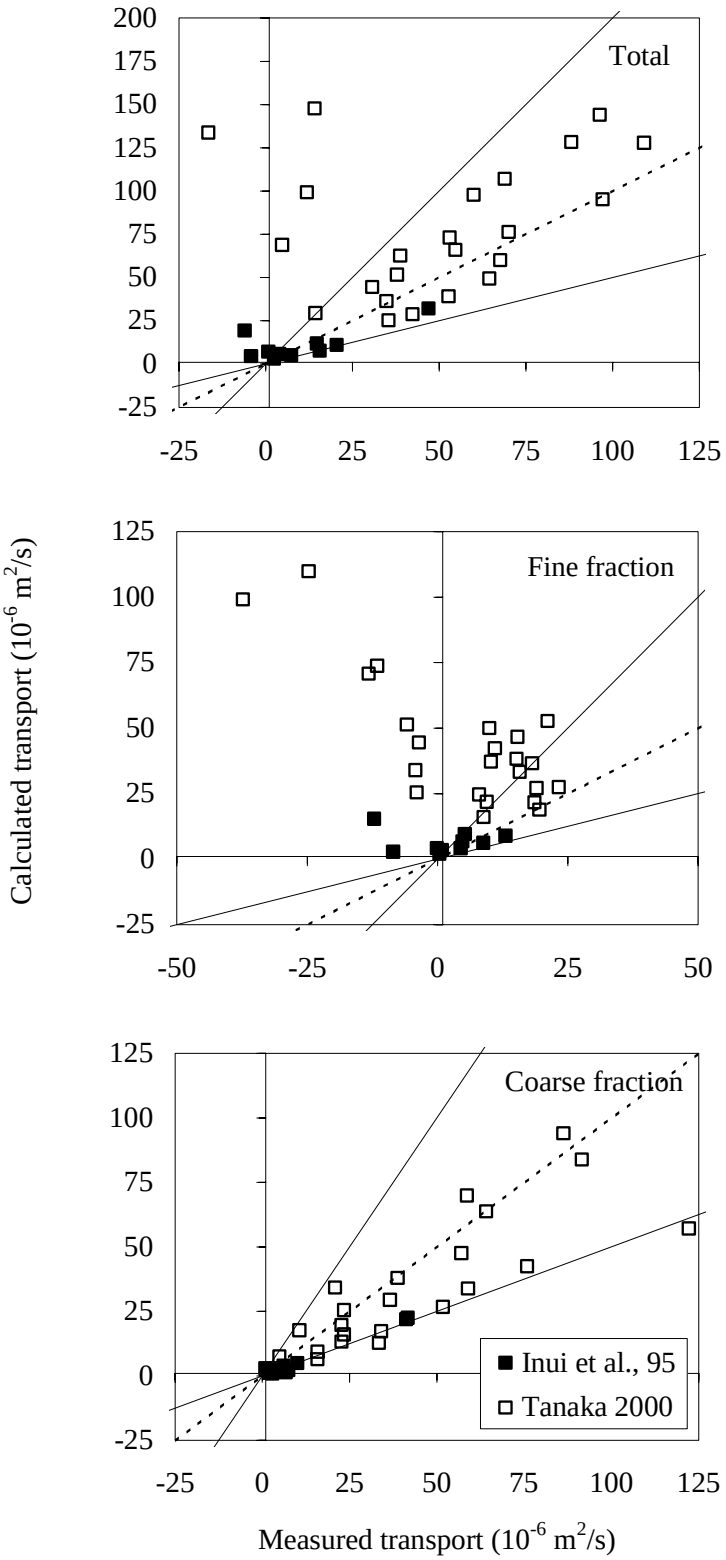

Figure 8.11: Verification of the multi-fraction model of Ribberink with graded sand data from TUWT.

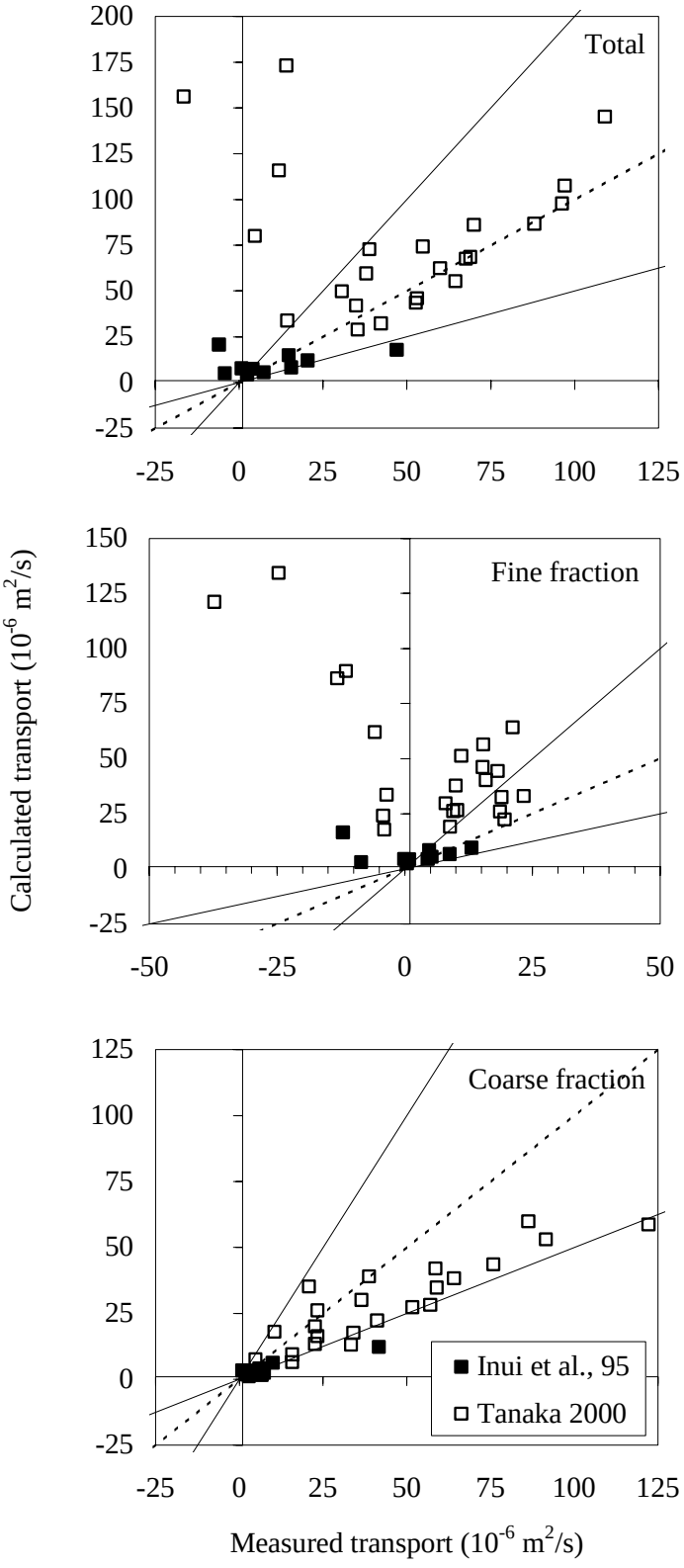

Figure 8.12: Verification of the multi-fraction model of D&W-qua (no phase-lag effects) with graded sand data from TUWT.

8.3.3 Intermediate models

Figures 8.13 and 8.14 show the comparisons between the predictions of the two intermediate models (D-J (1999) and D&W (1996)) and the measured net transport rates. The upper panels in the two figures show the results of the net total transport rates, the middle panels show the net transport of the fine fraction alone and the lowest panels show the net transport rates of the coarse fraction alone.

It is clear from figure 8.13 that modelling phase-lag effects according to the method of D-J (1999) in the model of Ribberink (1998) leads to better predictions of the transport rates of the fine fractions. Compare the middle panels of the figures 8.11 and 8.13. Apparently the model of D-J overestimates the phase-lag effects when the measured transport rates of the fine fraction are > 0, leading to underprediction of the net transport rates. On the other hand the D-J model underestimates the phase-lag effects when the measured transport rates of fine fractions are < 0. In this range the model also fails to reproduce the direction of the net transport rates correctly. The model of D-J leads to a small reduction in predicted transport rates of the coarse fraction compared to the model of Ribberink. In general it can be concluded that using the model of D-J leads to improving the transport rates of the fine fractions. However, this improvement still does not lead to a satisfactory agreement between the model results and the graded sand measurements.

The verification results of the model of D&W in figure 8.14 shows that the model strongly underpredicts the measured net total transport, the transport rates of fine fractions and the transport rates of the coarse fraction. However, the predicted transport rates of the coarse fraction are still within the range of ± factor 2. Most of the data for the fine fractions and the net total transport rates are strongly underpredicted, mostly outside the range of ± factor 2. In fact, this strong underprediction may be due to an overestimation of the phase-lag effects. The model of D&W (1996) was developed and calibrated using uniform sand data only. Due to interactions between grain-sizes, the phase-lag effects might work out differently in the case of graded sands.

In 1996 D&W adjusted their model for cases with graded sand (D&W-adj.), as described in section 5.4. They assumed that a percentage of the total flow energy equal to the percentage of fine sand is consumed to carry the fine sand. Based on that assumption, they added a correction factor to the parameter ω_i (see equation 5.13 in section 5.4). Although not explained by D&W (1996), the correction factor of D&W-adj. also increases the energy for transporting coarse grains in a mixture, as compared to uniform sand cases. This seems contradictory with the conclusion of D&W from their experiments at TUWT that the transport rates of coarse grains were almost unaffected by the presence of fine sand in a mixture.

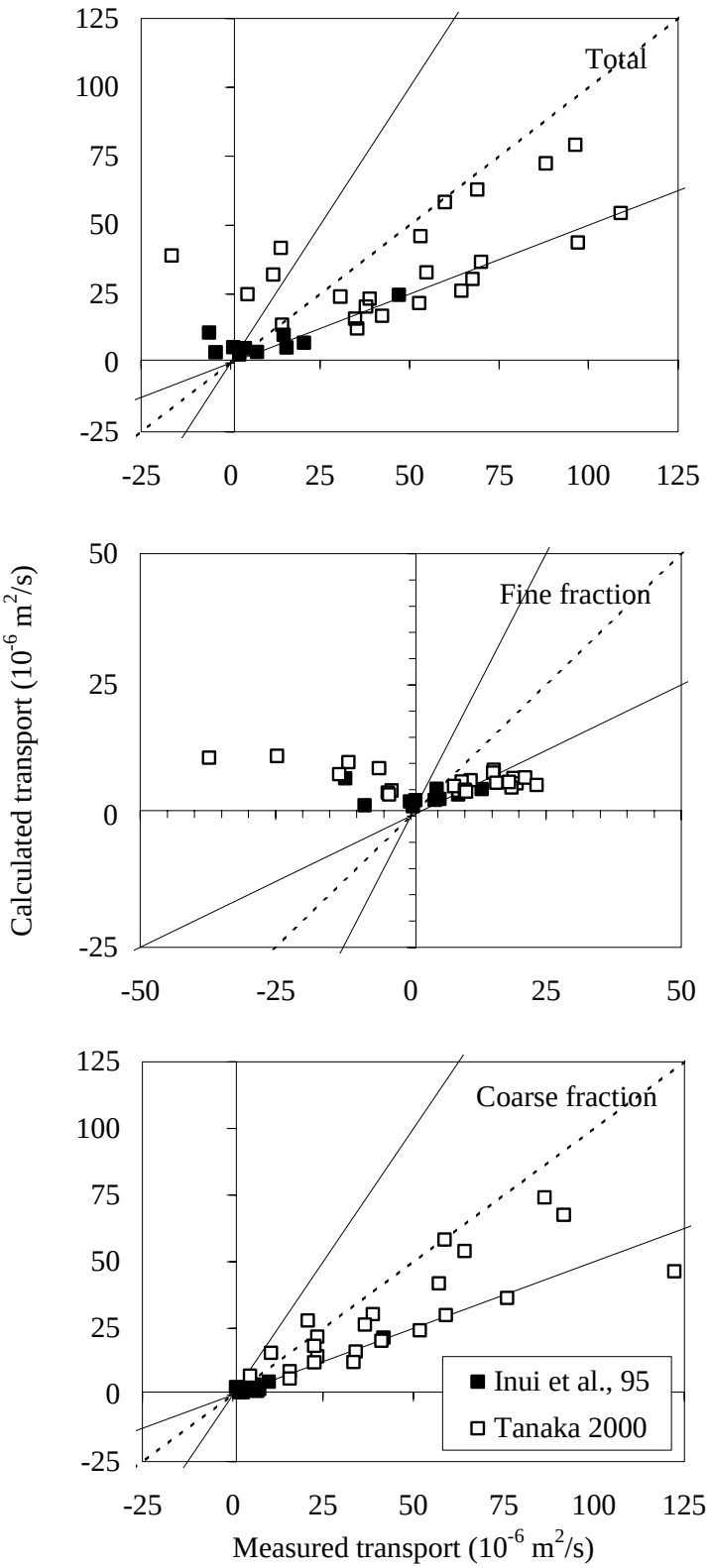

Figure 8.13: Verification of the multi-fraction model of Dohmen-Janssen with graded sand data from TUWT.

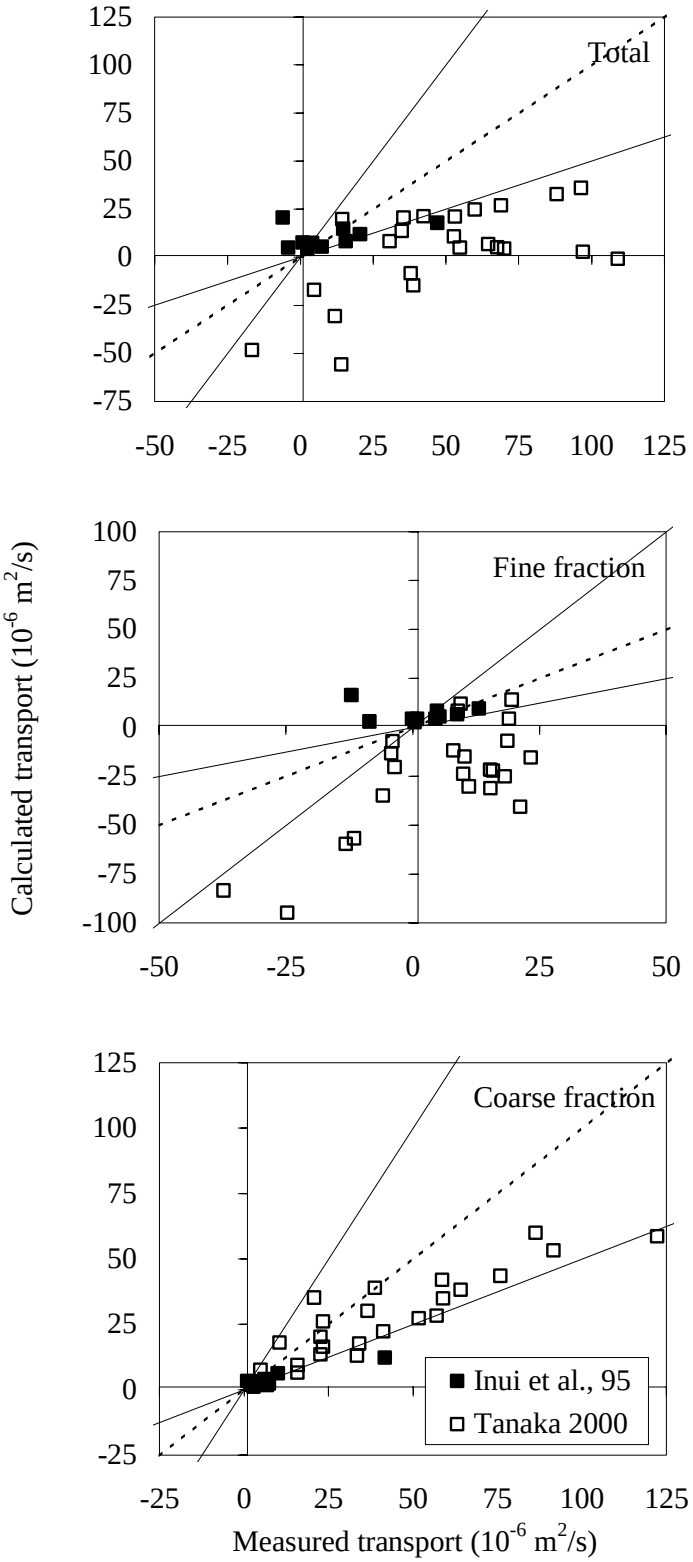

Figure 8.14: Verification of the multi-fraction model of Dibajnia & Watanabe with graded sand data from TUWT.

Using the adjustments of D&W (1996) leads to a better agreement between calculated and measured transport rates. Figure 8.15 shows the predictions of the model of D&W-adj. against the measurements. For many cases a good agreement is found between the computed and the measured total net transport, as well as for the transport rates per size-fraction (within ± factor 2). Note that the D&W-adj. model is developed for a sand mixture with two size-fractions only. Moreover, the model was also calibrated using the Inui et al. (1995) data, which are also used here for verification.

Apparently, reducing the energy for transporting the fine particles and at the same time increasing the energy for transporting coarse particles leads to significant improvement in the D&W's model predictions. This improvement concerns the net total transport rates, as well as the transport rates per size-fraction. In fact, these results can also be interpreted in the sense that hiding/exposure processes are taking place in graded sand cases under oscillatory sheet-flow conditions.

8.3.4 The POINT-SAND model

The three panels of figure 8.16 show the computed and the measured net total transport rates, fine fraction transport rates and coarse fraction transport rates using the POINT-SAND transport model in combination with the multi-fraction approach, as described in chapter 5. Only the experimental data of Tanaka (2000) were used for the model verification, in order to reduce the number of (time-consuming) computations.

It is clear that almost all model predictions are outside the factor 2 range. The PSM model underpredicts all transport rates, total, fine fraction and coarse fraction. The underprection of the fine fraction transport indicates that the PSM model overpredicts the phase-lag effects in case of graded sand. Although the PSM model underpredicts the coarse fraction transport rates, the model still shows a good correlation, indicating that a correction factor might be sufficient to improve the model results for the coarse fraction transport rates. It is important to state that this is the first time to verify the PSM model with sand transport data and the model is not calibrated before.

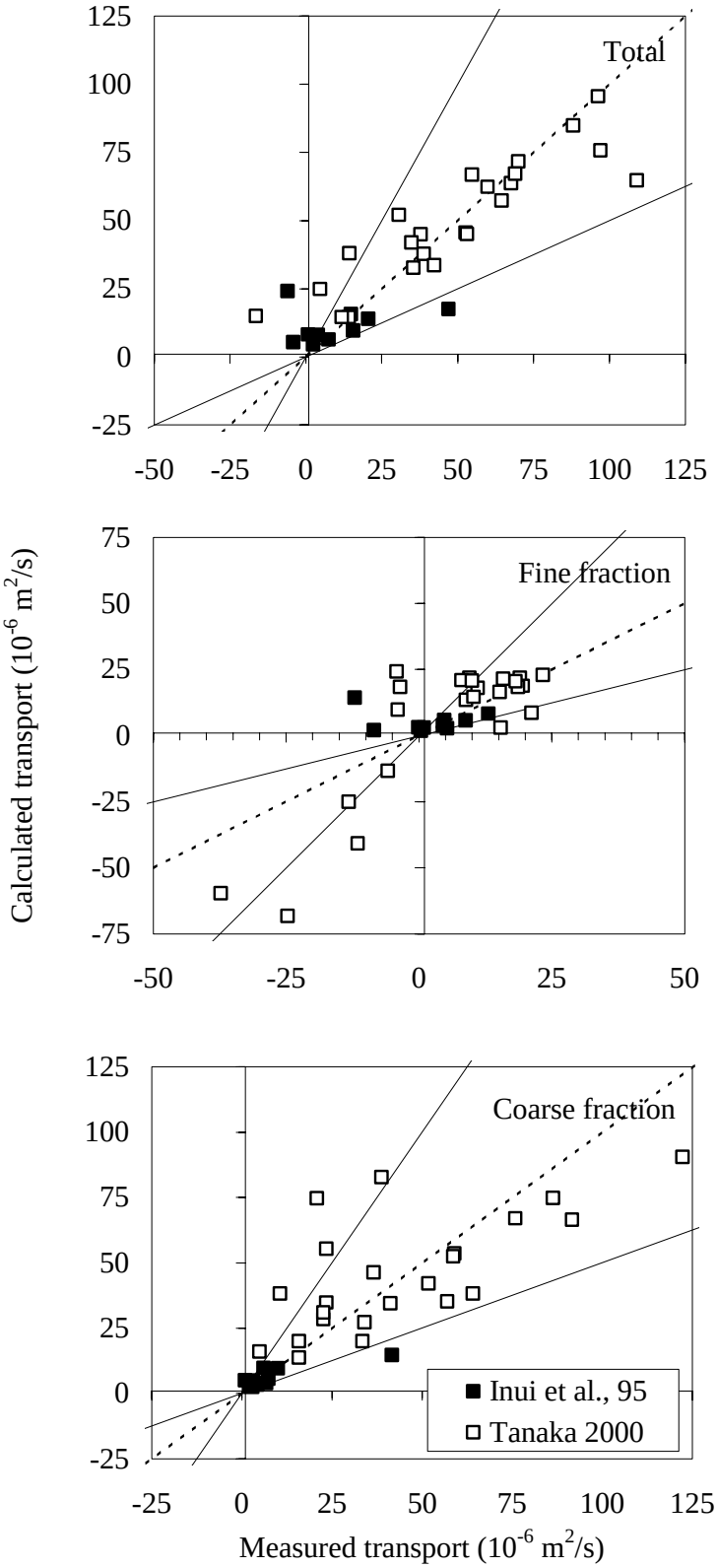

Figure 8.15: Verification of the model of Dibajnia & Watanabe-adjusted (1996) with graded sand data from TUWT.

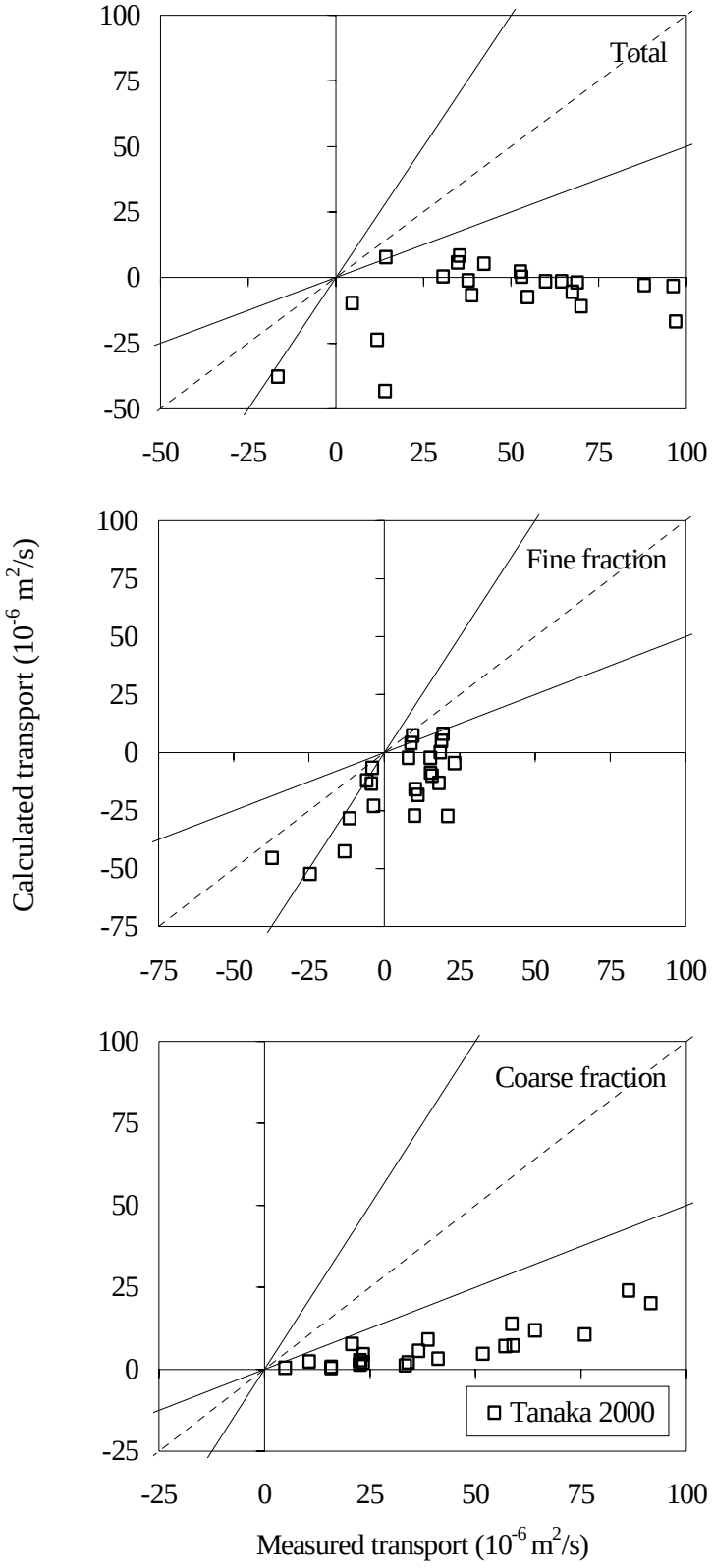

Figure 8.16: Verification of the multi-fraction POINT-SAND model with graded sand data from TUWT.

8.4 Summary of sand transport model verifications

In this chapter a selected large dataset of oscillatory sediment transport measurements (flat-bed/sheet-flow conditions) was used to verify different classes of transport models, as described in the chapters 4 and 5. The data were collected in the LOWT of WL | Delft Hydraulics and in TUWT. The complete dataset consisted of 118 different experiments with uniform sand and 37 experiments with graded sand and included measured net transport rates of different sand sizes under different flow conditions. The main results of the model verifications can be described as follows:

Uniform sand transport models

The main conclusions from the verification of the uniform sand transport models under oscillatory sheet-flow conditions are:

- From the verification of quasi-steady models with uniform sand data, it was found that for some cases the models are not able to predict transport directions correctly. These cases involve cases with short wave periods and small sand particles (small settling velocity), indicating that the assumption of quasi-steadiness is not valid and phase-lag effects play a role in the transport processes. In general terms this situation occurs when the settling time for the sand particles is not small compared to the wave period;
- For all quasi-steady transport models, it became clear that phase-lag effects become important when the value of the phase-lag parameter p (as defined by D-J, 1999) exceeds 0.4 - 0.6. These results confirm the previous results of Dohmen-Janssen (1999), who concluded that phase-lag effects are important for $p > 0.5$;
- For both intermediate model concepts (D-J, 1999 and D&W, 1996) the agreement between measurements and computations has improved considerably in comparison with the quasi-steady model results. Apparently, the inclusion of phase-lag influences in the transport models leads to a strong improvement of the model performance;
- Although it is the first time that the PSM model is verified with laboratory data, the model shows reasonably good results in comparison with the intermediate models, which have all been developed/calibrated using laboratory data (using parts of the present verification dataset);
- In general, the full unsteady PSM model shows reasonable results for the uniform sand data. The PSM model is able to predict the directions and net transport rates correctly, so apparently it inherently gives a good representation of phase-lag effects. Most of the PSM model predictions are within a factor 2 from the measurements. Although the PSM model gives a systematic underprediction of the measured net transport rates, the predictions correlate well. The PSM model may be improved by simple empirical corrections and/or adding a separate bed-load description.

Graded sand transport models

The graded transport models using the size-fraction approach, as described in chapter 5, were also verified with selected laboratory data. These graded sand data were collected at TUWT. Figure 8.17 shows an overall comparison of all graded transport models in terms of the correlation coefficient (between the data and the predictions) and in terms of the percentage of predictions within a factor 2 from the measured data. The upper panel shows the results of total transport data. The middle panel shows the fine fraction data and the lower panel shows the coarse fraction data. For intercomparison purposes for all models the dataset of Tanaka (2000) is used.

The models used in the intercomparison were the quasi-steady models of Bailard, Ribberink and the quasi-steady version of D&W (D&W-qua). Moreover, the three intermediate models of D-J, D&W96 and the adjusted model of D&W (1996) (D&W-adjusted) for graded sand cases are considered. Finally, the PSM (full unsteady sand transport model) was used in this intercomparison. From figure 8.17 we can conclude the following:

- In general, all graded transport models are able to predict coarse fraction transport rates better than the fine fraction and net total transport rates;
- Both the models of Ribberink (1998) and D&W (1996) show the best performance for predicting coarse fraction data. The two models show a correlation coefficient = 0.9 and 80 % of the predictions within a factor 2 from the measurements;
- Although the model of D&W-adjusted was calibrated to predict transport rates of graded sand, the model does not show the best performance to predict coarse fraction data of experiments with mixtures. On the other hand the D&W-adjusted model shows the best performance compared to all other models to predict the fine fraction data and the total transport rates;
- The middle panel of figure 8.17 shows that almost all transport models are not able to predict the transport rates of the fine fractions correctly. The percentage of data within a factor 2 has a maximum value of 45% for the best model (D&W-adjusted). The correlation coefficients fall in the range of – 0.7 to + 0.8. All quasi-steady models and the model of D-J show negative correlation coefficients. Only the models of D&W (1996), D&W-adjusted and the PSM model show positive but low correlation coefficients;
- The PSM model does not show a good performance for all graded sand data including the total transport rates and transport rates per size-fraction. Most of the data are outside the factor 2 differences. Note that the PSM model was not calibrated with experimental data before;
- It is clear from these model verifications and comparisons that, using the size-fraction approach only is not sufficient for modelling graded sand transport. Adjustments as made by D&W 1996 to account for interactions between grain sizes in a mixture seem to be necessary. In the next chapter, further model improvements will be discussed for the different transport model types for graded sediment.

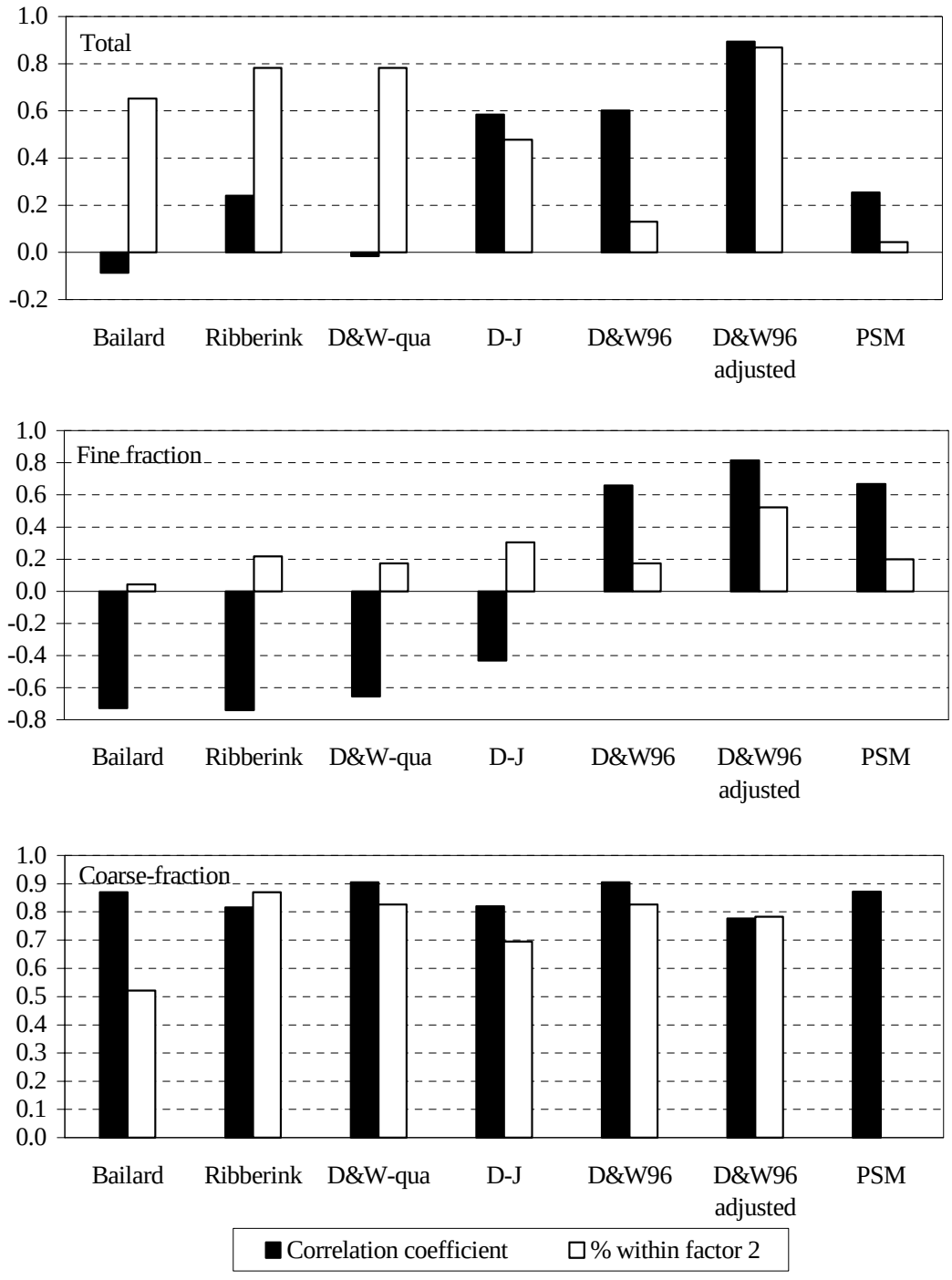

Figure 8.17: Overall intercomparison of all graded transport models in terms of the correlation coefficient and in terms of the percentage of predictions within a factor 2 (% / 100).

Chapter 9

IMPROVEMENTS OF GRADED SAND TRANSPORT MODELS

9.1 Introduction

The results of the model verifications in chapter 8 show that using the size-fraction approach alone and assuming that there are no interactions between grain-sizes in a sand mixture are not sufficient to predict transport rates correctly. The transport models show generally that transport rates of coarse fractions are underpredicted and the transport rates of the fine fractions are overpredicted. Therefore, in the present chapter attention is focused on including grain-size interaction effects in graded transport models in order to improve the performance of these models.

The model improvements are based on the same graded sand dataset as used in chapter 8 for model verifications (see table 8.1). Section 9.2 shows improvements of the model of Ribberink (1998) using hiding/exposure correction methods as commonly used in river flows. In section 9.3, an improved Dibajnia and Watanabe (1996) model is presented. Improvements of the PSM model for uniform sand as well as for graded sand are presented in section 9.4. Section 9.5 presents a verification of all improved graded transport models using a new dataset, i.e. the new graded sand dataset as collected during the laboratory experiments of the present study and in previous experiments. Finally, section 9.6 gives a summary of the results obtained.

9.2 Improving the model of Ribberink

9.2.1 Hiding/exposure correction factors

Splitting up a sediment mixture into different size-fractions alone does not include any interaction between the different fractions. In the case of a sediment mixture of different grain-sizes, the motion of individual sizes will be affected by the presence of other sand sizes. The small grains can be sheltered or hidden by the large grains, while larger grains can be more exposed to the flow than in case of a uniform sand bed. Generally, the interaction of the size fractions can be represented in sand transport models by increasing the critical shear stress of the finer particles and decreasing the critical shear stress of the coarser particles. Most of the methods that account for hiding/exposure effects have been developed for river flows (e.g. Egiazaroff, 1965, Day, 1980 and Komar & Wang, 1984). In literature, the hiding/exposure correction is applied in two different ways:

1. Correction of the effective Shields parameter, θ_{eff}. This implies reducing its value for the finer fractions and increasing it for the coarser fractions;

2. Correction of the critical Shields parameter, θ_{cr}. This implies increasing its value for the finer fractions and reducing its value for the coarser fractions.

However, most river flow formulations have been developed for the lower Shields regime rather than for oscillating sheet-flow in the higher Shields regime. Under sheet-flow conditions, when a small top layer of the bed is set in motion, the effective Shields parameter (θ_{eff}) is generally much larger than the critical Shields parameter (θ_{cr}). Therefore, a correction of θ_{cr} may not have much impact on the total transport rate.

In the sand transport formulas described in chapter 4 only the model of Ribberink (1998) uses the two parameters θ_{eff} and θ_{cr}. In the model of Ribberink the transport rate is proportional to (θ_{eff} - θ_{cr}). All hiding/exposure correction methods lead to a reduced transport rate for the finer fractions and a larger transport rate for the coarser fractions.

Hiding/Exposure formulations of Egiazaroff (1965), Ashida & Michiue (1973), Day (1980) and Komar & Wang (1984) were implemented in the model of Ribberink. The first three formulations were originally formulated for river flow and not for oscillatory flow. Komar & Wang's (1984) formula was especially developed for wave conditions. These four methods can be described briefly as follows:

Egiazaroff (1965)

Egiazaroff derived an expression for the critical bed shear stress for each fraction using a balance of forces on individual grains in a mixture on a flat bed with uniform flow. This expression reads the following:

$$\xi_{cr,i} = \frac{\theta_{cr,corrected}}{\theta_{cr,Shields}} = \left| \frac{\log 19}{\log\left| 19\frac{D_i}{D_m} \right|} \right|^2 \qquad (9.1)$$

where: $\xi_{cr,i}$ = correction factor for critical shear stress for size-fraction i; D_m = mean diameter of the bed material and D_i = median diameter of fraction i.

Egiazaroff verified his formula indirectly using experimental transport data from other researchers and found good results.

Ashida & Michiue (1973)

Ashida & Michiue corrected empirically the formula of Egiazaroff, using new experimental data with uniform flow. They came with the following correction in the range of $D_i/D_m < 0.4$:

$$\xi_{cr,i} = 0.85\frac{D_m}{D_i} \qquad (9.2)$$

The difference between the formulas of Egiazaroff and Ashida & Michiue for the parameter ξ_{cr} is shown in figure 9.1.

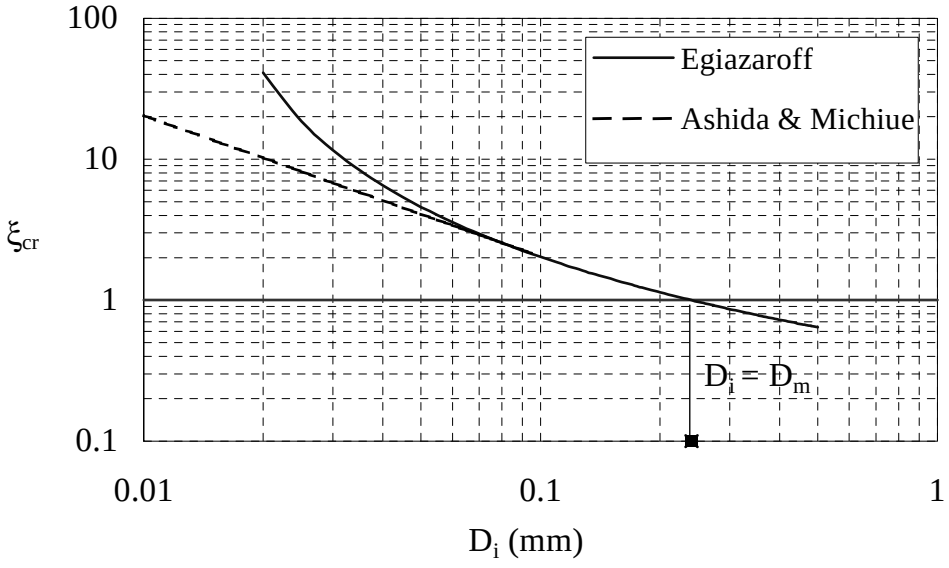

Figure 9.1: Values of the correction factor for critical shear stress ξ_{cr} according to Egiazaroff (1965) and Ashida & Michiue (1973).

Day (1980)

A correction factor for the effective Shields parameter is given by Day (1980). On the basis of an extensive series of laboratory experiments with sediment mixtures, Day corrected the mobility number, which is a kind of dimensionless bed-shear stress.

$$\xi_{eff,i} = \left| \frac{0.4}{\left| D_i / D_A \right|^{0.5}} + 0.6 \right| \tag{9.3}$$

where: $\xi_{eff,i}$ = correction factor for effective shear stress for size-fraction i (corrected shear stress = shear stress/ξ_i) and D_A = grain-size in the mixture that needs no correction.

D_A is not equal to D_{50} or D_m, but depends on the gradation of the sand mixture, as follows:

$$\frac{D_A}{D_{50}} = 1.6 \left| \frac{D_{84}}{D_{16}} \right|^{-0.28} \tag{9.4}$$

Komar & Wang (1984)

Komar & Wang developed a new expression for the critical Shear stress under wave conditions based on a consideration of the horizontal forces working on a spherical grain and empirical fitting of experimental data:

$$\xi_{b,cr} = 0.00071 (\xi_s - \xi)\, g\, D_i^{0.57} \tan\xi \tag{9.5}$$

where: α = angle of repose for a single grain in degrees.

The above formula is valid for grains smaller than 1 mm. The shear stress is normalised as follows:

$$\theta_{cr\ (k\&w)} = \frac{\xi_{b,cr}}{(\xi_s - \xi) g D_i} = 0.00071 D_i^{-0.43} \tan\xi \tag{9.6}$$

Miller and Byrne (1966) gave the following empirical relation for the angle of repose:

$$\xi = a\left|\frac{D_i}{K}\right|^b \tag{9.7}$$

where: K = size of the surrounding grains, generally taken as the median grain-size of the complete sediment mixture, $D_{50,}$ a = empirical coefficient related to the shape of the sand particles = 61.5 degrees for intermediate sphericity and roundness, and b = - 0.3 empirical sorting parameter.

The dimensionless shear stress according to Komar & Wang can also be expressed as a correction factor ξ_{cr}. The correction factor can be found now by dividing the Shields parameter, as found by Komar & Wang by the critical Shields parameter (also following Komar & Wang):

$$\xi_{cr,i} = \frac{\theta_{cr,i}}{\theta_{cr,m}} \tag{9.8}$$

where: $\xi_{cr,i}$ = correction coefficient of the critical Shields parameter of grain-size i; $\theta_{cr,i}$ = dimensional critical shear stress for size fraction i in a mixture according to Komar and Wang ($D = D_i$) and $\theta_{cr,m}$ = dimensionless critical shear stress for uniform sediments according to Komar and Wang ($D = D_m$).

$$\theta_{cr,i} = 0.00071\frac{\tan\xi_i}{D_i^{0.43}} \qquad \text{and} \qquad \theta_{cr,m} = 0.00071\frac{\tan\xi_m}{D_m^{0.43}} \tag{9.9}$$

$$\xi_{cr,i} = \frac{\theta_{cr,i}}{\theta_{cr,m}} = \frac{\tan\xi_i}{\tan\xi_m}\left|\frac{D_m}{D_i}\right|^{0.43} = \frac{\tan\left|61.5\left|\frac{D_i}{D_m}\right|^{-0.3}\right|}{\tan(61.5)}\left|\frac{D_m}{D_i}\right|^{0.43} \tag{9.10}$$

$$\xi_{cr,i} = \frac{\tan\left|61.5\left|\frac{D_m}{D_i}\right|^{0.3}\right|}{\tan(61.5)}\left|\frac{D_m}{D_i}\right|^{0.43} \tag{9.11}$$

The expression of Komar & Wang gives a correction smaller than unity for the coarser grains implicating that these grains are set in motion at a lower shear stress than in uniform sediment. Smaller grains require a higher shear stress to be set in motion, as they are hidden between large grains.

9.2.2 Comparison between hiding/exposure correction factors

In section 9.2.1, different expressions for hiding/exposure corrections were presented. It appeared that the hiding/exposure correction can be applied in two different ways: correction of the effective Shields parameter or correction of the critical Shields parameter. In order to study the effect of the different correction factors on the transport rates under oscillatory sheet-flow conditions, a series of transport rate calculations were made with Ribberink's (1998) model using the size-fraction approach. In the calculations a sand mixture consisting of 70% fine sand (D_{50} = 0.21 mm) and 30% coarse sand (D_{50} = 0.97 mm) was used with an asymmetric (2^{nd}-order Stokes) oscillatory flow in the sheet-flow regime (U_{rms} = 0.7 m/s and T = 6.5 s). The sediment is split into two fractions (N = 2) and the critical Shields parameter is related to the median diameter of each fraction. This implies that for each fraction a different critical Shields parameter is found.

Under the selected conditions the expression of Ashida & Michiue gives the same results as the expression of Egiazaroff ($D_i/D_m > 0.4$). Therefore, the correction factor of Ashida & Michiue is not analysed separately in this study.

Figure 9.2 presents the calculated transport rates for the different correction factors. The predicted transport rates (total and per fraction) if no correction factor is applied are presented in the left side. More to the right the predicted transport rates are shown if both fractions are corrected with one of the following expressions: Egiazaroff, Komar & Wang and Day.

The correction factors of Egiazaroff and Komar & Wang seem to have hardly any effect on the predicted transport rates, the correction factor of Day has more influence. The expression of Day reduces the predicted transport rate of the fine fraction a little and increases the predicted transport rate of the coarse fraction strongly. Moreover, the total transport rate significantly increased compared to the other cases. The fact that the correction factors of Egiazaroff and Komar & Wang do not have much influence on the predicted transport rates can be explained by the fact that Egiazaroff and Komar & Wang only correct the critical Shields parameter.

Apparently, the effective shear stress is much larger than the critical shear stress under sheet-flow conditions. Day corrects the value of the effective Shields parameter, which has a clear effect on the results under oscillatory sheet-flow conditions. It is important to state that these different correction factors are all depending only on the grain-size distribution of the sand bed and totally ignore the flow conditions.

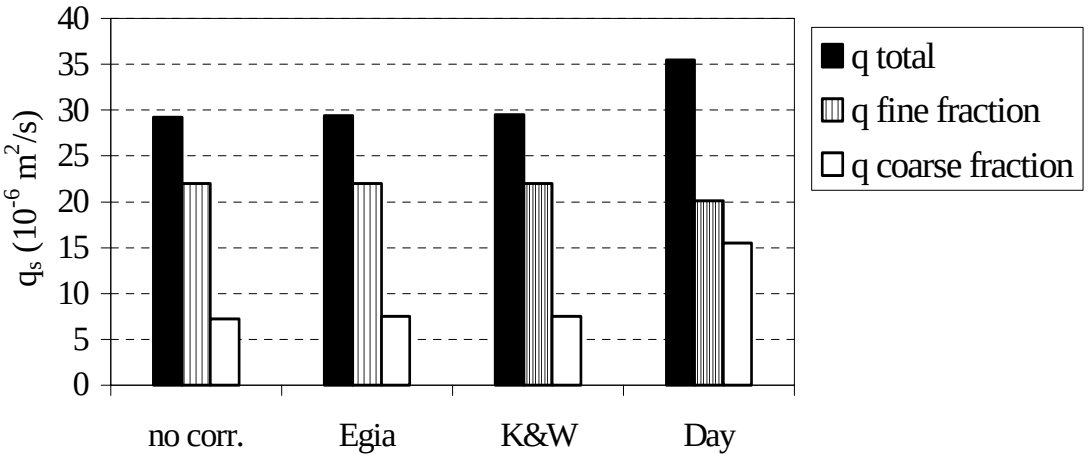

Figure 9.2: Comparison between predicted transport rates using the transport model of Ribberink (1998) with different hiding/exposure correction factors in the case of a bi-modal sediment mixture in oscillatory sheet-flow conditions.

9.2.3 Verification of the adjusted Ribberink/D-J model

It is clear from the comparison between different hiding/exposure correction factors that only the correction factor of Day has a clear effect on the predicted transport rates in Ribberink's model under sheet-flow conditions. Therefore, it was decided to study the performance of the model of Ribberink (1998) in case of graded sand transport, using the hiding/exposure correction factor of Day (1980). Moreover, the phase-lag correction factor of D-J (1999) was added to the model. The new model predictions are compared with the same set of non-uniform sediment data as used for the model verification before (chapter 8, see table 8.1). The new model can be called the modified Ribberink/D-J's model for graded sand as it includes the phase-lag correction factor of D-J (1999).

Figure 9.3 shows the comparison between the new model predictions and the measured net transport rates. The upper panel shows the results of the net total transport rates, the middle panel shows the net transport of the fine fraction alone and the lowest panel shows the net transport rates of the coarse fraction alone.

The results show that including the hiding/exposure correction factor in the model of Ribberink/D-J leads to a significant improvement in the model performance. Most of the predicted net total transport rates and coarse fraction transport rates are within the limit of a factor 2 difference. Compare the results of figure 9.3 with the results of figure 8.11, where the results of the original model of D-J are presented. The lower panels in the two figures show that including Day's (1980) hiding/exposure correction factor in the model leads to a very good description of the coarse fraction

data. In fact, these results indicate that coarse grains are more exposed to the flow in sand mixtures under sheet-flow conditions.

However, adding the correction factor of Day (1980) hardly affects the predictions of the fine fractions. The fine fraction predictions seem to be dominated mainly by a wrong phase-lag correction. Previous results of the model of D-J with uniform sand show that the model is able to predict transport rates rather good for different grain-sizes (see figure 8.4). Nevertheless, the model is not able to show the same good performance when phase-lag effects are important for fine grains in a sand mixture. In fact, this indicates that the phase-lag process and its effects on transport processes are different in sand mixtures compared to uniform sand.

Figure 9.4 shows a comparison between the results of the model of D-J (1999) and the new D-J/Day model as used in the present study. The comparison includes the net total transport rates and the transport rates per size-fraction in terms of the correlation coefficient and the percentage of data within a factor 2 difference. It is clear that including the hiding/exposure correction factor of Day (1980) leads to a better model performance. The percentage of data within a factor 2 is improved significantly, for the total transport rates as well as for the coarse fraction. On the other hand, the transport rates of the fine fractions are hardly affected.

For sand mixtures the phase-lag correction of D-J (1999) leads to a general reduction in transport rates of fine grains, however it gives too much reduction for $<q_s>_{measured} > 0$ and too little reduction for $<q_s>_{measured} < 0$. An improved phase-lag correction model is required for graded sand cases in order to make the transport model perform better.

9.3 Improving the model of Dibajnia & Watanabe

Although the original model of D&W (1992) is based on an energy concept, it can also be expressed in terms of shear stress or mobility number through the parameter Ψ.

$$\Psi = 2\,\omega_i\,\frac{w_s\,T_i}{D_{50}} = \frac{1}{2}\frac{u_i^2}{\Delta g w_s T_i}\,2\,\frac{w_s T_i}{D_{50}} = \frac{u_i^2}{\Delta g D_{50}} = \text{mobility number} \qquad (9.12)$$

The definition of all parameters in equation 9.12 can be found in section 4.4.2. It is clear from equation 9.12 that the correction of hiding/exposure in case of graded sand can be included in the model of D&W (1996) through the parameter Ω. Actually this means that the correction will also affect the phase-lag parameter ω_i, which represents the ratio of the time required of a suspended sand particle to reach the bed to the period of each half-wave-cycle (T_f/T_i). In other words, ω_i may be increased if more flow energy is conveyed to entrain sediment particles into the flow (increased exposure) and it may be reduced if less energy is conveyed to entrain

sediment particles into the flow (decreased exposure or hiding). Basically, the increased exposure is expected for the coarse grains and hiding is expected for the fine grains in a mixture.

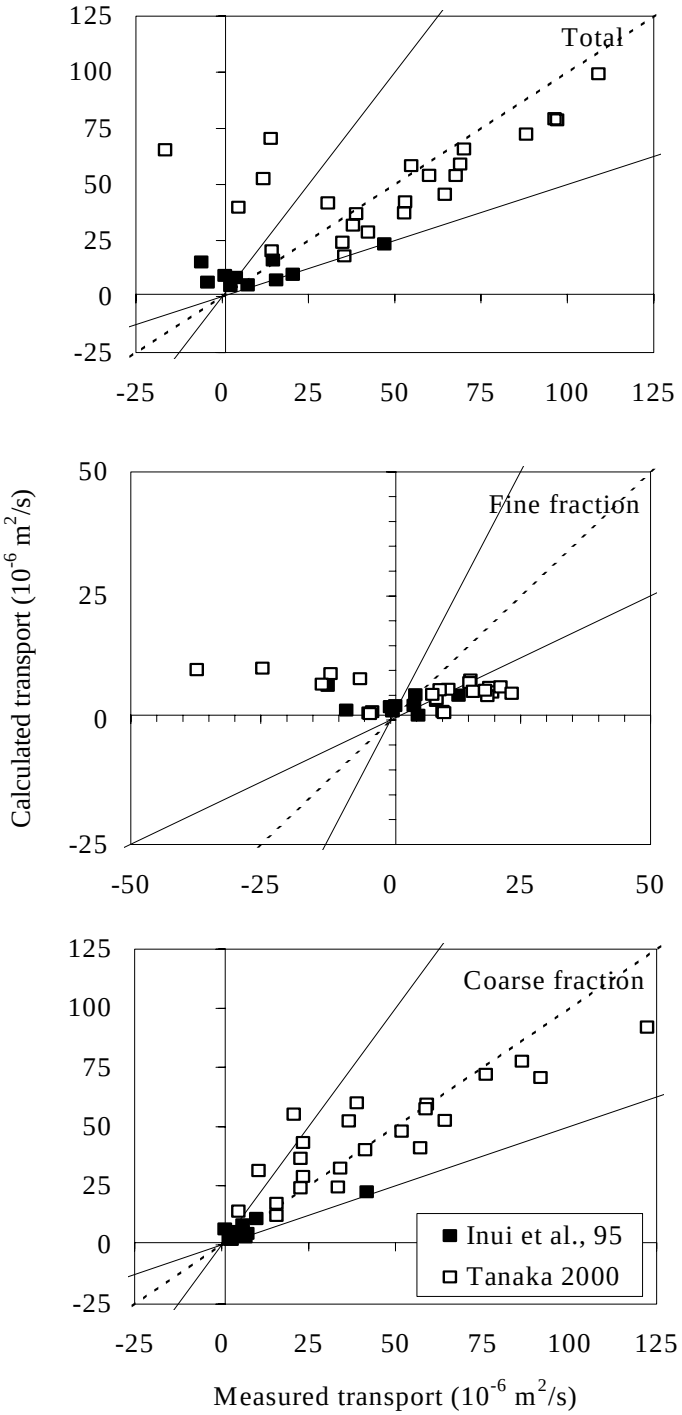

Figure 9.3: Verification of the multi-fraction model of Ribberink/Dohmen-Janssen in combination with the hiding/exposure correction factor of Day (1980).

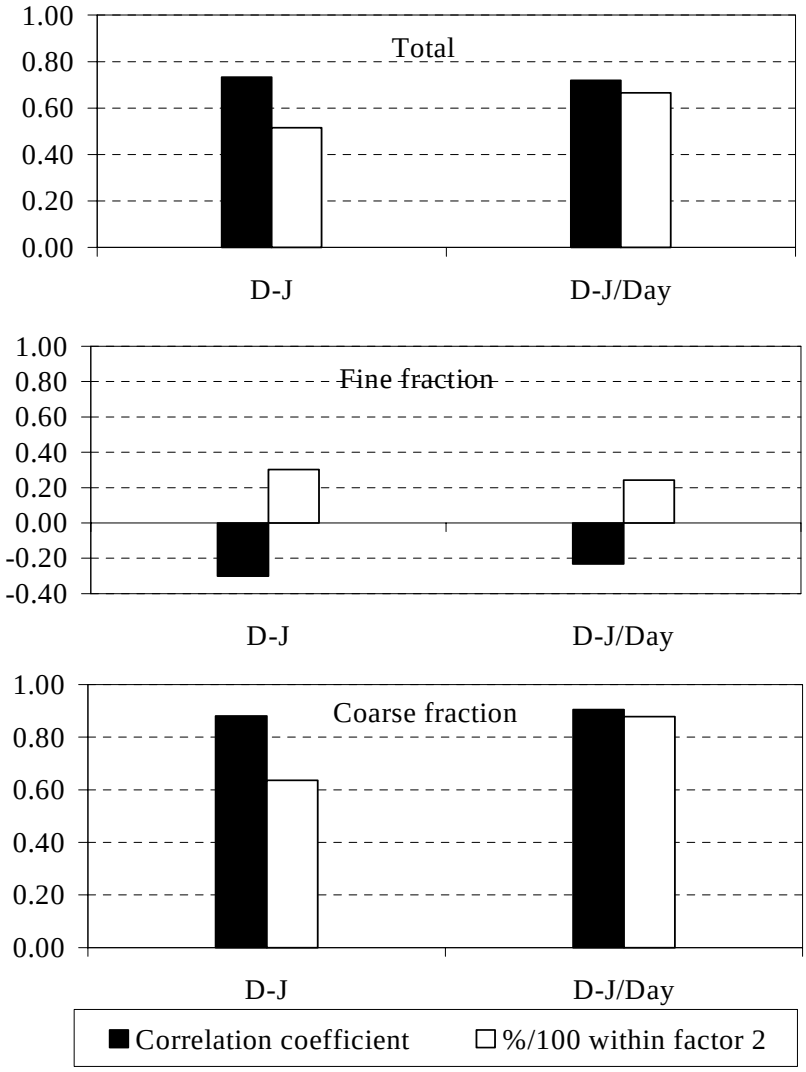

Figure 9.4: Comparison between the model of Ribberink/D-J and the model of Ribberink/D-J in combination with the hiding/exposure correction factor of Day (1980).

In fact, this consideration matches with assumptions made by D&W (1996) for improving their model for graded sand (see section 5.4). Although the adjusted model of D&W (1996) for graded sand is able to give a better prediction of transport rates, the background of the correction factors α of each size-fraction was not made clear (see equation 5.13). Moreover, the method is limited to situations of only two size-fractions with two specific grain-sizes. They adjusted the model using one dataset, in which only one sand mixture with D_{50} = 0.2 and 0.87 mm sand was used. Different factors α are probably required for other sand mixtures. Therefore, in the following a more general correction factor for graded sand is proposed, which can be applied to any number of size-fractions and any sediment mixture.

The model of Dibajnia & Watanabe (1996) is improved by adjusting the size-fraction approach as proposed in the present study (see equation 5.11 in chapter 5), using the following exposure correction factor for the parameter ω_j (see also equation 5.12).

$$\omega_{j,corr} = \omega_j \ \alpha \left| \frac{D_i}{D_m} \right|^{\beta} \qquad (9.13)$$

where: $\omega_{j,corr}$ = the corrected phase-lag parameter for size-fraction i; ω_j = the calculated phase-lag parameter using the model of D&W (1996) for each size-fraction, D_i = median diameter of the size-fraction, D_m = mean diameter of the sand mixture and α and β are constants.

Using the experimental data of Inui et al. (1995) and Tanaka (2000) with graded sand, it was found that β should be 0.4 for all size-fractions, and α 1.2 if $D_i/D_m > 1$ (coarse grains) and 0.7 if $D_i/D_m < 1$ (fine grains). Figure 9.5 shows the comparison between the new modified D&W model predictions and the laboratory measurements. The upper panel shows the results of the net total transport rates, the middle panel shows the net transport of the fine fraction alone and the lower panel shows the net transport rates of the coarse fraction alone. For all these results the calculated net total transport rates correspond quite well with the measured transport rates, total and per size-fraction. Most of the data are within the factor 2 range. Moreover, the new modified D&W model gives better predictions than the model of D&W-adjusted (1996) for graded sand (compare figure 9.5 with figure 8.14).

Figure 9.6 shows comparisons between the original D&W model (1996) using the size-fraction approach (described in chapter 5), the D&W-adjusted (1996) model for graded sand and the new D&W model as modified in the present study. The three model results are compared in terms of correlation coefficient and the percentage of model predictions within the factor 2 range. It is clear that the new D&W model shows the best performance compared to the other two models. The new model shows better predictions of the total transport rates, as well as of the transport rates per size-fraction.

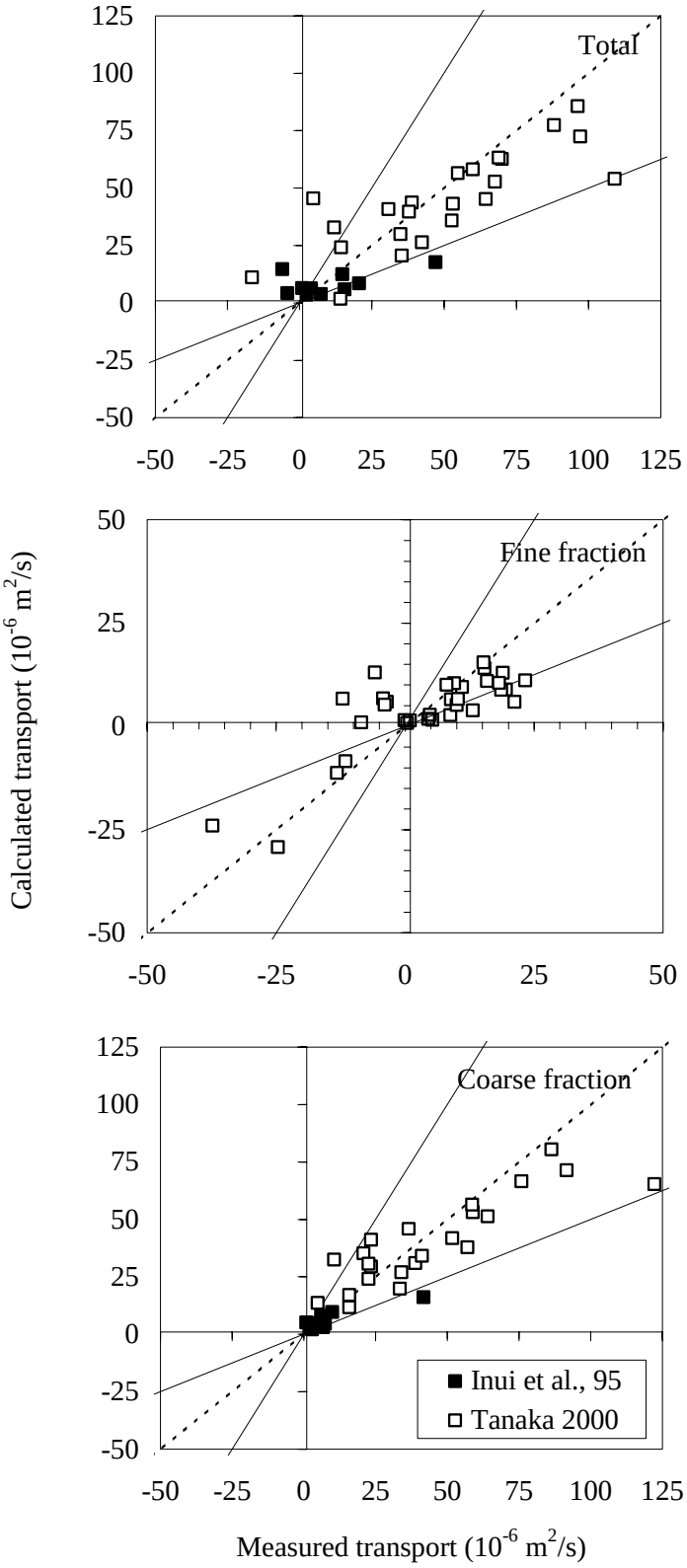

Figure 9.5: Verification of the multi-fraction model of D&W with graded sand data from TUWT.

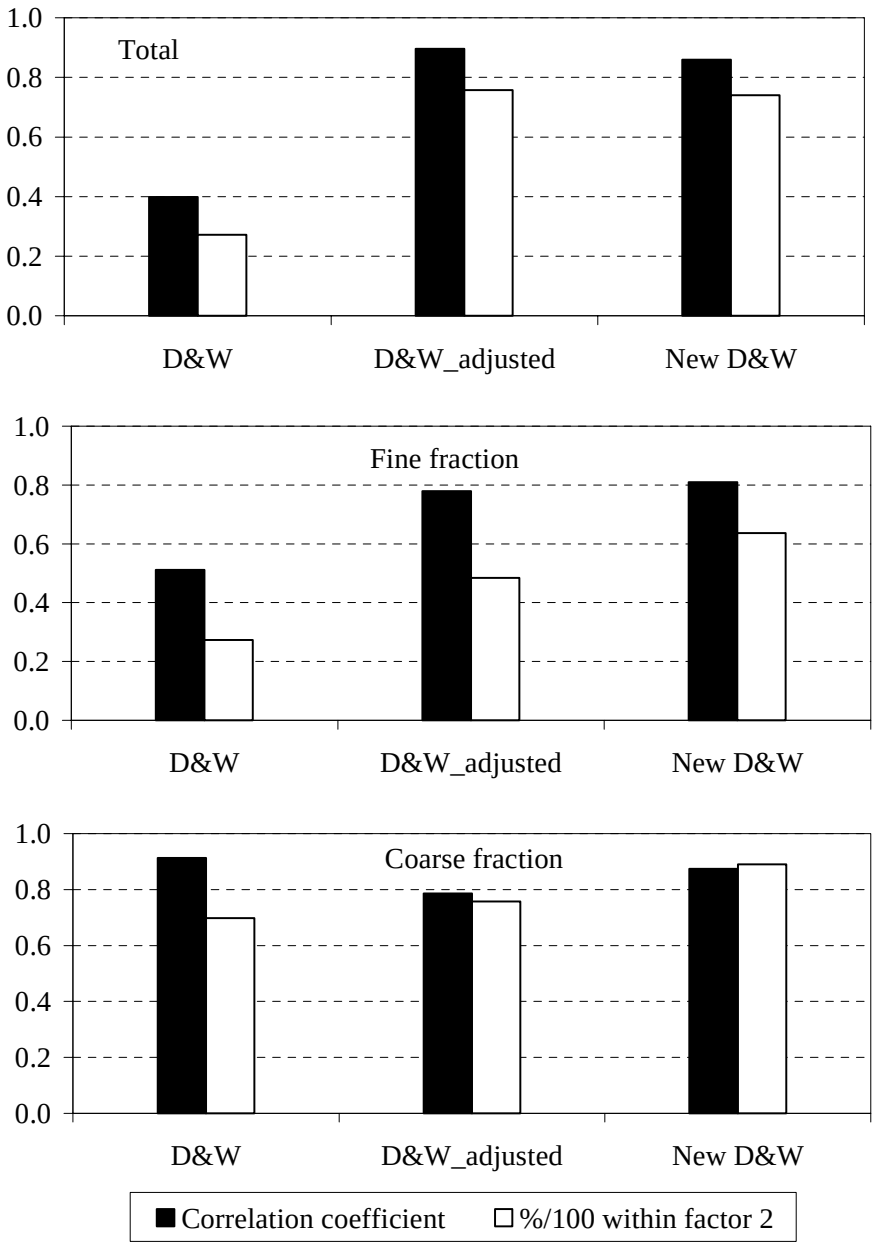

Figure 9.6: Comparison between the new multi-fraction model of D&W and the original model of D&W (1996) and the adjusted D&W (1996) model.

Recently, Ahmed (2002) found experimentally in the Tokyo University water tunnel that the moving layer thickness of fine sand is reduced in a sand mixture compared to the uniform fine sand case. Figure 9.7 shows the temporal variation of the ratio of the moving layer thickness in a sand mixture to the thickness with uniform fine sand (D_{50} = 0.2 mm). The probability of occurrence of the fine sand in the mixture is equal

to 0.7. The moving layer thickness was measured using a PIV (Particle Image Velocimetry) technique. It is clear that the moving layer thickness of fine sediment in a mixture is lower than in case of uniform fine sand and seems to scale with the lower probability of occurrence of the fine sand. This reduction in moving layer thickness might be due to a dynamic armouring process (mutual interaction between grain sizes in motion). The presence of coarse grains prevents further erosion of the sheet-flow layer into the bed and reduces the entrainment height of fine grains. In fact these results confirm the idea of correcting ω_i in graded sand cases, as used in the present study.

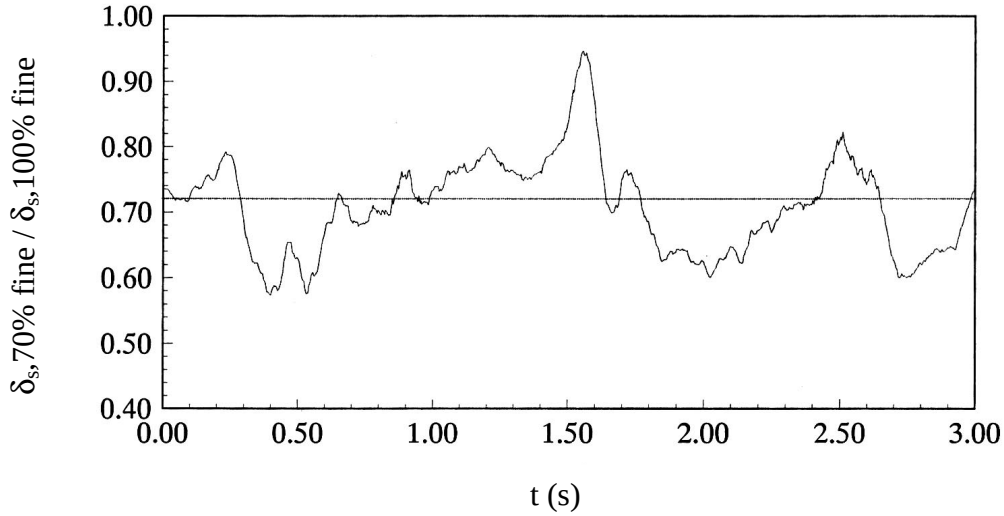

Figure 9.7: Temporal variation of relative moving layer thickness of fine sand in a mixture and uniform fine sand alone (Ahmed, 2002).

9.4 Improving the POINT-SAND model

9.4.1 Uniform Sand

In section 8.2.4, the PSM model verification showed that the model gives reasonably good results in comparison with uniform sand measurements. However, the PSM model slightly but systematically underpredicts the data (see figure 8.6). In order to improve the PSM model results it is proposed here to add a bed-load transport component to the (basically suspended sediment) model. The bed-load formula of Engelund & Fredsøe (1976) was selected to be included in the PSM model, which brings the model in line with the distinction between bed-load and suspended-load as used by Fredsøe et al. (1985).

Bed-load formula
The bed-load formula of Engelund & Fredsøe (1976) has been implemented in the POINT-SAND model. This formula is based on the Shields parameter and reads:

$$\varphi_b = \frac{q_b}{\left[(s-1)\,g\,D^3\right]^{0.5}} = 5p\left(\sqrt{\theta'} - 0.7\sqrt{\theta_{cr}}\right) \qquad (9.14)$$

Where: φ_b = dimensionless bed load transport; θ' = dimensionless bed shear stress; θ_{cr} = critical Shields parameter for initiation of motion (see Van Rijn, 1993). p = probability that all the particles in a single layer will be in motion and is defined as:

$$p = \left| 1 + \left| \frac{\frac{\pi}{6}\mu_d}{\left(\theta' - \theta_{cr}\right)} \right|^4 \right|^{-0.25} \qquad (9.15)$$

where μ_d = dynamic friction coefficient.

Figure 9.8 shows the predictions of the modified PSM model, after including the bed-load formula of Engelund & Fredsøe (1976) (total-load PSM), against the measurements. The total-load PSM model shows a slightly better performance than the original PSM model (compare the figures 9.8 and 8.8).

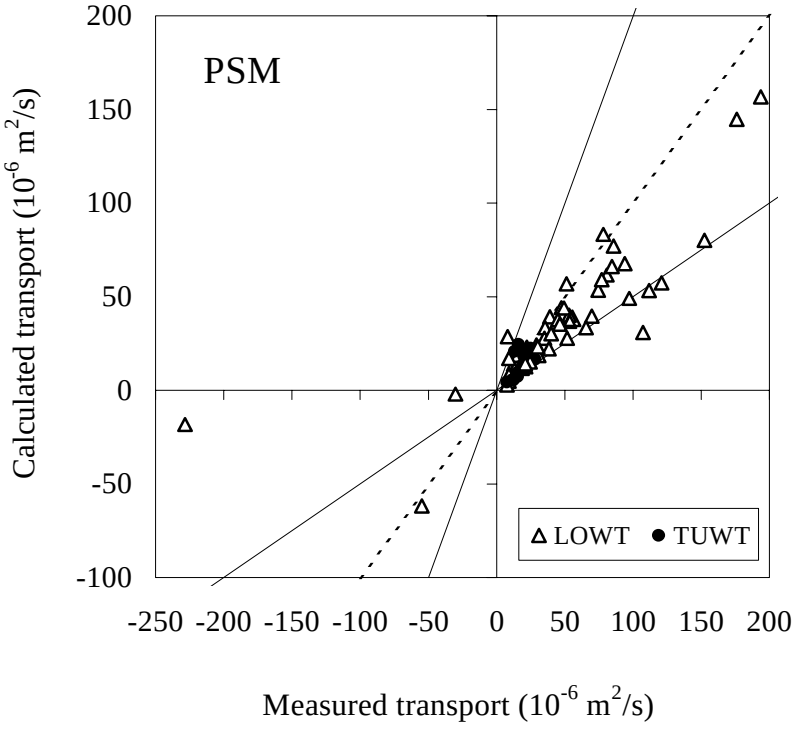

Figure 9.8: Comparison between measurements and the modified PSM model predictions, after including the bed-load formula of Engelund & Fredsøe (1976).

Figure 9.9 shows comparisons between the modified PSM model results and the original PSM model in terms of the correlation coefficient and the percentage of predictions within the range of a factor 2. Moreover, figure 9.9 includes the results of the two intermediate models of D-J (1999) and D&W (1996). It is clear that adding the bed-load formula of Engelund & Fredsøe (1976) to the PSM model does not clearly improve the correlation coefficient. Nevertheless, the predicted net transport rates within the factor 2 range are significantly better than those from the original PSM model. Moreover, the modified PSM model (total-load model) shows slightly better results than the two intermediate transport models of D-J and D&W.

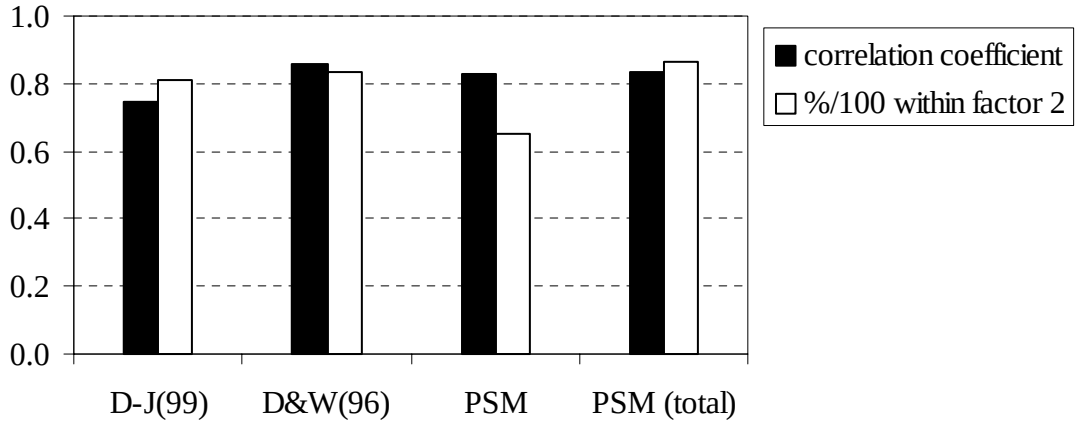

Figure 9.9: Comparison between the performance of the modified PSM model, the original PSM model and the two intermediate models (D-J and D&W), in terms of a correlation coefficient and in terms of percentage of predictions within ± factor 2 range, using uniform sand data.

9.4.2 Graded sand

After extending the PSM model for uniform sand cases with the bed-load formula of Engelund & Fredsøe (1976), it was decided to apply the size-fraction approach in the total-load PSM model for modelling graded sand cases. The comparison between the total-load PSM model predictions and the measurements can be found in figure 9.10. The three panels in this figure show the total, fine fraction and coarse fraction transport rates, respectively.

It can be concluded that adding a bed-load component does not significantly improve the performance of the PSM model for graded sand. Compare the results of figure 9.10 with those of figure 8.16. Although the transport rate of the coarse fraction and the total transport rates are slightly better predicted, almost all predicted total and size-fraction transport rates are still outside the factor 2 range.

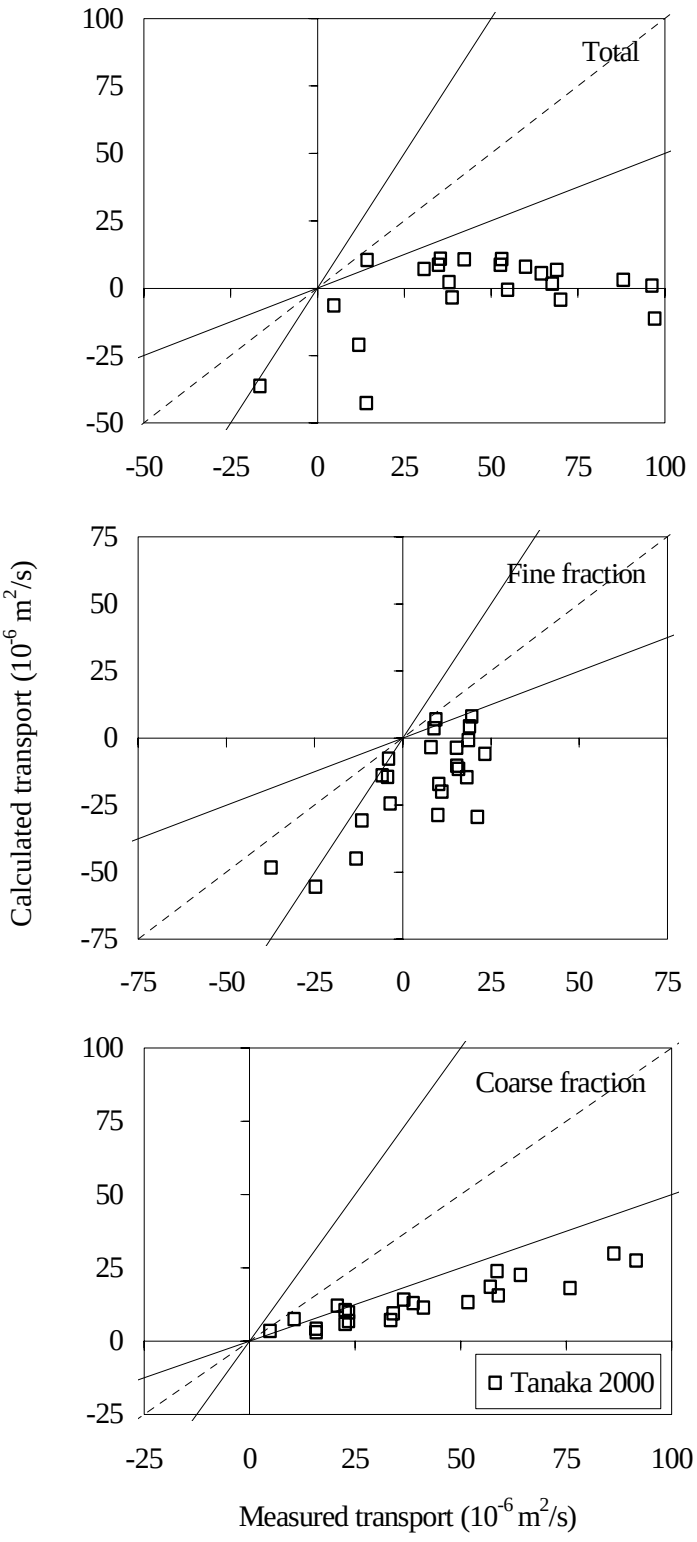

Figure 9.10: Verification of the multi-fraction PSM model, after including the bed-load formula of Engelund & Fredsøe (1976) with graded sand data from TUWT.

Zyserman and Fredsøe (1996) size-fraction approach

Zyserman & Fredsøe (1996) suggested a different size-fraction approach to calculate the suspended-load in case of graded bed material. In their approach they assumed that only part of the grain sizes can be brought into suspension by the flow, using the following criterion:

$$w_s \leq 0.80 \; U'_{f\,max} \tag{9.16}$$

where: $U'_{f\,max}$ = maximum value attained by the instantaneous skin friction velocity over the wave period. The criterion states that only the particles having a fall velocity w_s less than the threshold value given in equation (9.16) will be entrained into the water column. The critical diameter for suspension is indicated as D_{crit}.

The suspended part of the sediment mixture is divided into N fractions, each with the same probability of occurrence. The diffusion equation for suspended sediment is then solved for each of the N fractions, with the settling velocity of each size-fraction w_i, and the bed concentration $c_{b,i}$ calculated on the basis of D_i. Two conditions are applied to the values of concentration calculated this way:

1) The composition of the sediment in suspension is assumed to be equal to the composition of the original bed material (i.e. for that part finer than D_{crit}). The suspended part of the original bed material is divided in probability intervals (fractions). If ϕ_i is a proportionality factor for the time-averaged amount of sediment in suspension for each fraction i, this results in the following requirement for each of the N fractions in suspension:

$$\phi_1 \, M_1 = \phi_2 \, M_2 = \phi_3 \, M_3 = ... = \phi_N \, M_N \tag{9.17}$$

Where: ϕ_i = a correction factor to make the suspended loads of all fractions i the same and M_i = computed time-averaged total load of sediment in suspension for each fraction i, defined as:

$$M_i = \int_{2D_{50}}^{h} \overline{c}_i \; dz \tag{9.18}$$

Where: h = the local water depth, c = sand concentration, z = the vertical coordinate measured upwards from the bed, and the overbar indicates time averaging.

By making $\phi_N = 1$, the remaining ϕ_i can be readily calculated.

2) At z = a, the total bed concentration must be equal to the one determined on the basis of D_{50}. Taking into account the gradation of the sediment, i.e.:

$$K\left|\prod_{i=1}^{N} \bar{c}_{b,i}\ \phi_i\right| = \bar{c}_b(D_{50}) \qquad (9.19)$$

In equation (9.19) K is another correction factor for the reference bed concentrations $c_{b,i}$. Finally, all concentrations c_i are corrected with the factor $K\phi_i$.

Z&F (1996) considered that condition (1) is a reasonable assumption under equilibrium situations, because the dispersive stresses associated with the coarse suspended fractions, which are kept in suspension closer to the bed than the finer ones, limit the capacity of the flow to pick-up amounts of fine sediment from the bed.

Figure 9.11 shows the comparisons between the total-load PSM model predictions, using the Z&F (1996) size-fraction approach, and the measurements. The upper panel shows the total transport rates, the middle panel the fine fraction transport rates and the lower panel the coarse fraction transport rates. It is clear that the model is not able to predict the total transport rates correctly, due to the fact that the transport rates of coarse fractions are systematically underpredicted by almost a factor 4 (see the lower panel in figure 9.11), which is worse than the original size-fraction approach (see figure 9.8). On the other hand, the model is able to predict the transport rates of the fine fractions rather well and better than the results in figure 9.10. In general most of the fine fraction data are predicted within the range of a factor 2 difference, and the transport directions are predicted quite well.

It is concluded that using the Z&F (1996) size-fraction approach gives acceptable results for the fine fraction transport rates and an underestimation of the transport rates of the coarse fraction. The worse representation of the coarse fraction transport rates in the considered experiments is mainly due to the fact that the coarse fraction is not entrained into suspension since criterion of equation 9.16 is not fullfilled.

Improving the total-load PSM model for graded sand transport

The PSM model does not include an exposure correction factor for the coarse grains. The results of the total-load PSM model can be improved, using the size-fraction approach of Z&F (1996) and applying a correction factor for the coarse fraction transport rates, in order to account for exposure effects. Improved model results can be obtained by using the following exposure correction factor to correct the computed net transport rates of the coarse fraction, which is obtained through data fitting:

$$R = 2.5\,(D_i/D_m) \qquad \text{for} \qquad D_i/D_m > 1.0 \qquad (9.20)$$

where: D_i = median diameter of the coarse fraction and D_m = mean diameter of the sand mixture.

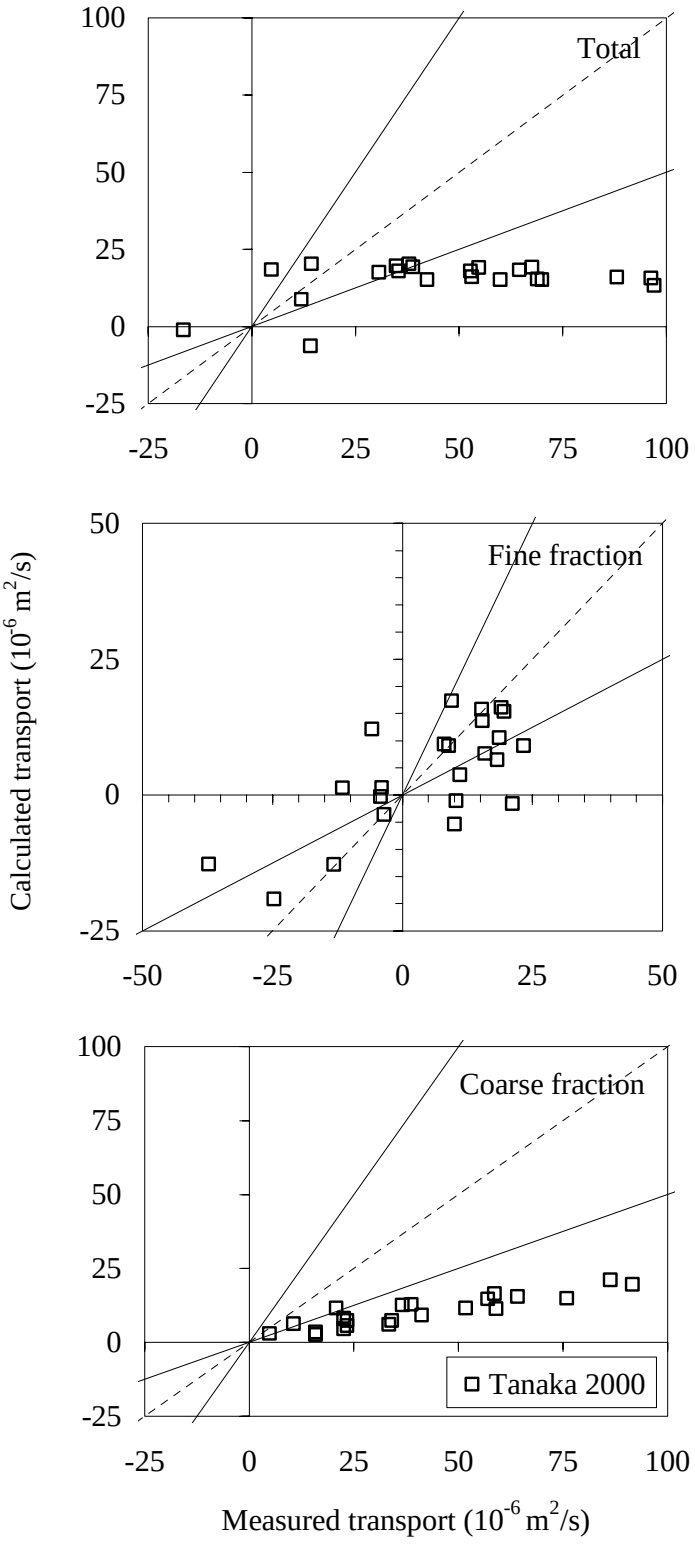

Figure 9.11: Verification of the multi-fraction total-load PSM model, using Z&F (1996) size-fraction approach with graded sand data from TUWT.

Figure 9.12 shows the comparisons between this modified total-load PSM model and the measurements. Significant improvements are obtained for the coarse fraction transport rates and consequently for the net total transport rates. Almost all model predictions are within the factor 2 range.

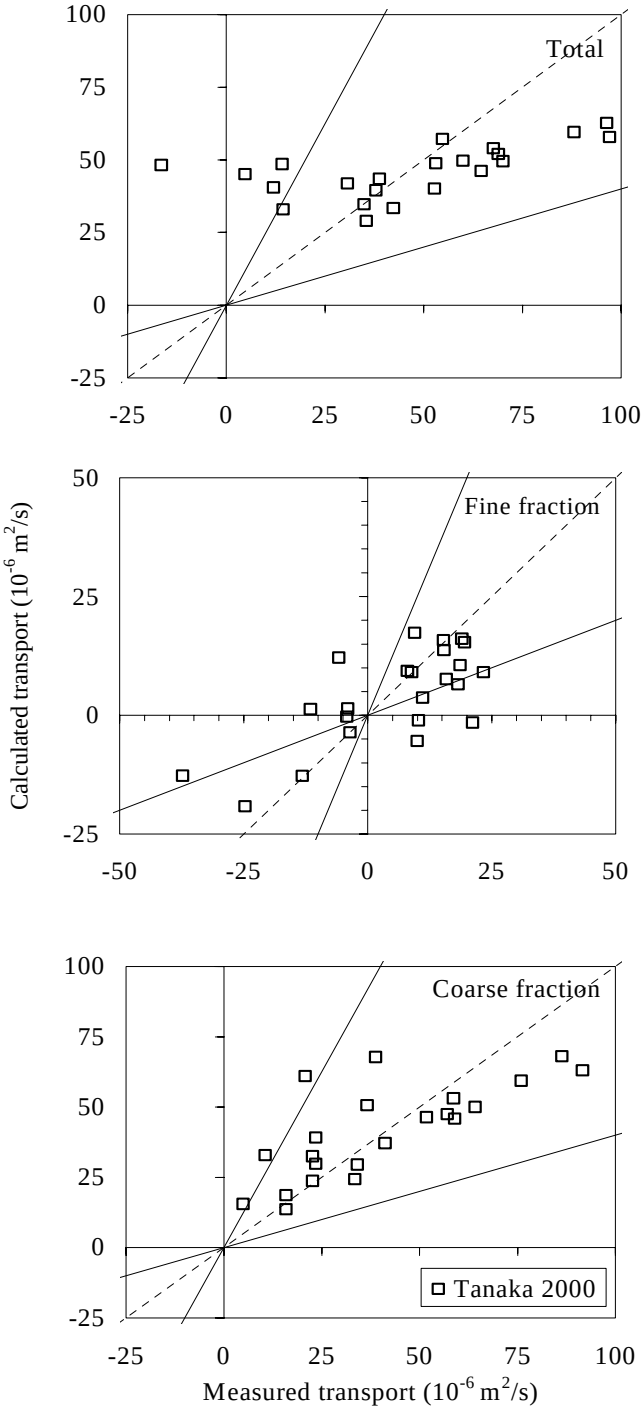

Figure 9.12: Verification of the multi-fraction total-load PSM model, using Z&F (1996) size-fraction approach with graded sand data from TUWT.

Figure 9.13 shows the comparison between three different versions of the total-load PSM model in terms of the percentage of data within a factor 2 difference and the correlation coefficient between the measurements and the model predictions. The first version shows the results of the total-load PSM model, using the simple size-fraction approach. The second version shows the results of the total-load model using Z&F (1996) size-fraction approach. The third model includes the size-fraction approach of Z&F and the exposure correction factor for the coarse grains (equation 9.20). It is clear that using the size-fraction approach of Z&F (1996) leads to better predictions of the fine fraction transport rates and a negligible effect on the predicted total transport rates. Adding an exposure correction factor to the PSM model leads to a much better model performance. The predicted net transport rates of the coarse fractions are significantly improved and so are the total transport rates.

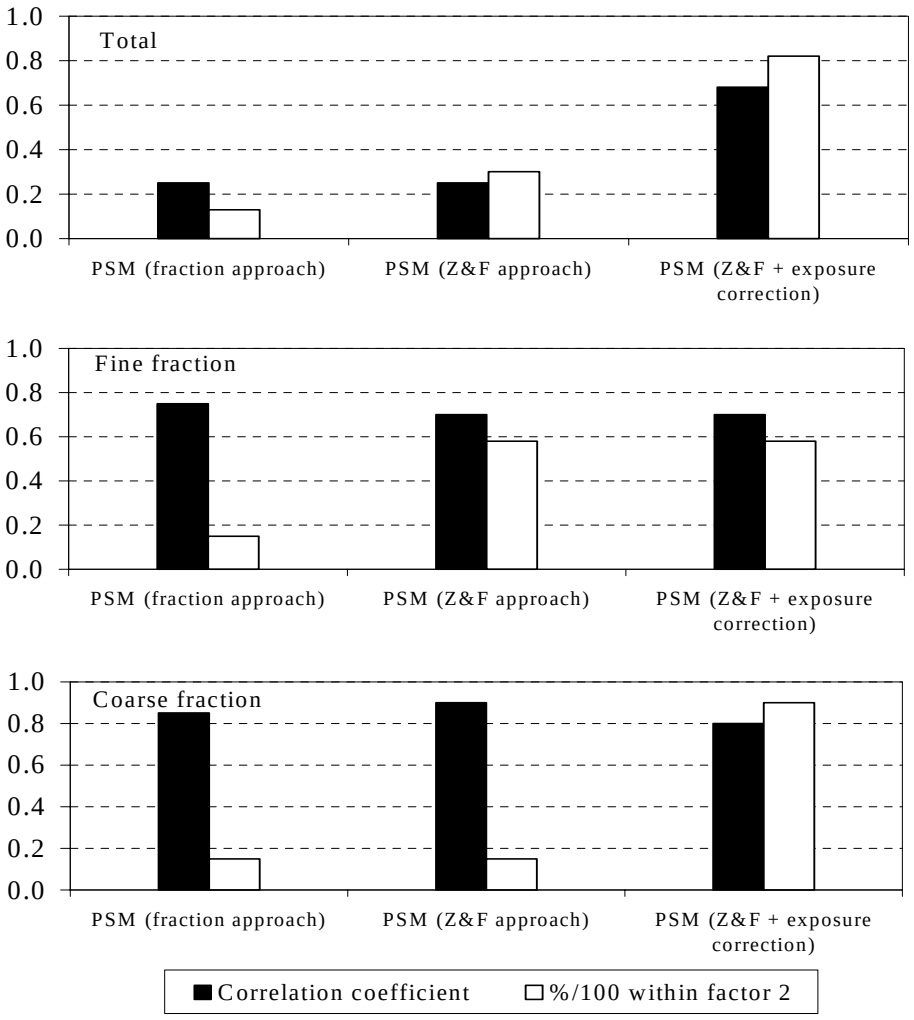

Figure 9.13: Performance of three different versions of the total-load PSM model in terms of the percentage of data within a factor 2 difference and the correlation coefficient between the measurements and the model predictions.

9.5 Verification of the improved graded transport models

9.5.1 Graded sand data used for new model verifications

Table 9.1 shows a general overview of the new laboratory dataset with graded sand used for the new model verifications. The data were obtained from the LOWT of WL | Delft Hydraulics and TUWT under oscillatory sheet-flow conditions. In total 28 experiments with graded sand have been used to verify the new graded transport models. The TUWT experiments were performed using bi-modal sands and cnoidal waves with different wave velocities and the same wave period (3 s). Dibajnia & Watanabe (2000) used a degree of asymmetry R equal to 0.6. Note that the TUWT graded sand data used for new model verifications are different from the dataset used earlier in chapter 8, table 8.1 for model verifications and used in previous sections in chapter 9 for model improvements.

Table 9.1: Laboratory data with graded sand used for new model verification.

Series		**Sand fractions D_{50} (mm)**	**Flow conditions**		
			Type	**U_{crest} (m/s)**	**Wave period (s)**
LOWT	K	0.13 (50%) /0.32 (50%)	2nd order Stokes, sine + current	1.1-1.72	6.5, 7.2
	P *(new data)*	0.21 (70%) /0.97 (30%)	2nd order Stokes	1.1-1.6	6.5
	S *(new data)*	0.13 (60%) /0.32 (20%) /0.97 (20%)	2nd order Stokes	0.87-1.65	6.5, 12
TUWT	D&W, 2000	0.2/0.8, 0.2/0.55	cnoidal	1.1-1.62	3

Most of the experiments in the LOWT were performed with 2nd-order Stokes waves with different velocities and different wave periods, using a nonlinearity index equal to 0.65. Only the series K experiments include two conditions with sine waves superimposed on different currents. The two series of P and S are new data, which have been performed during the present study (see chapters 6 and 7). Note that only series S includes a sand mixture consisting of 3 different size-fractions. For the present model computations the sand mixture was treated as two fractions only, the coarse fraction D_{50} = 0.97 mm (20%) and the fine fraction D_{50} = 0.18 mm (80%).

All the measured net transport rates in case of graded sand include both the measured net total transport rates and the net transport rates of each individual size-fraction.

These net transport rates of each size-fraction give the opportunity to study in detail the selective transport processes of graded models. More detail about the used laboratory data is given in table 9.1 and can be found in Dibajnia et al. (1998), Dibajnia & Watanabe (2000), Cloin (1998), Hassan et al. (1999) and Hassan et al. (2002).

9.5.2 Verification of new graded sand transport models

In the previous sections in chapter 9 different graded sand transport models were improved. In order to test the performance of these new graded transport models, it was decided to verify these models with the new graded sand dataset as described in table 9.1. The results of the model verifications are described hereafter.

The improved model of Ribberink/D-J
The model predictions of the improved Ribberink/D-J model, using the hiding/exposure correction factor of Day (1980) are plotted against the measurements in figure 9.14. The upper panel shows the total transport rates. The middle and the lower panels show the results of the fine fraction and the coarse fractions, respectively.

It is clear that the new model is able to reproduce the total transport rates and the transport rates of the coarse fractions reasonably well. Almost all model predictions are within the factor 2 range. The model is also able to predict correctly a considerable part of the fine fraction transport rates. Part of the points is outside the range of a factor 2 (see the middle panel in figure 9.14). It was found that these cases are associated with very strong phase-lag effects, with fine particles or very short wave periods (3 s). This again indicates that phase-lag effects in case of graded sediment work out differently than for uniform sand. The model of Ribberink/D-J needs further development on this aspect.

The improved model of D&W
Figure 9.15 shows the comparison between the new D&W model predictions and the measurements. The predicted total and coarse fractions transport rates show very good results, almost all model predictions are within the factor 2 range and the transport directions are predicted correctly. Although, the model predicts most of the fine fractions transport rates correctly, a small part of the data is outside the range of a factor 2 difference and even the direction of the transport rate is not always predicted correctly. Again these data are cases with strong phase-lag effects.

The improved PSM model
Figure 9.16 shows the new model predictions against the measurements. The PSM model was verified using the LOWT data only, in order to reduce the time of computations. The PSM model shows very good results for the total transport rates as well as for the transport rates per size-fraction. The model somewhat over predicts the coarse fraction data.

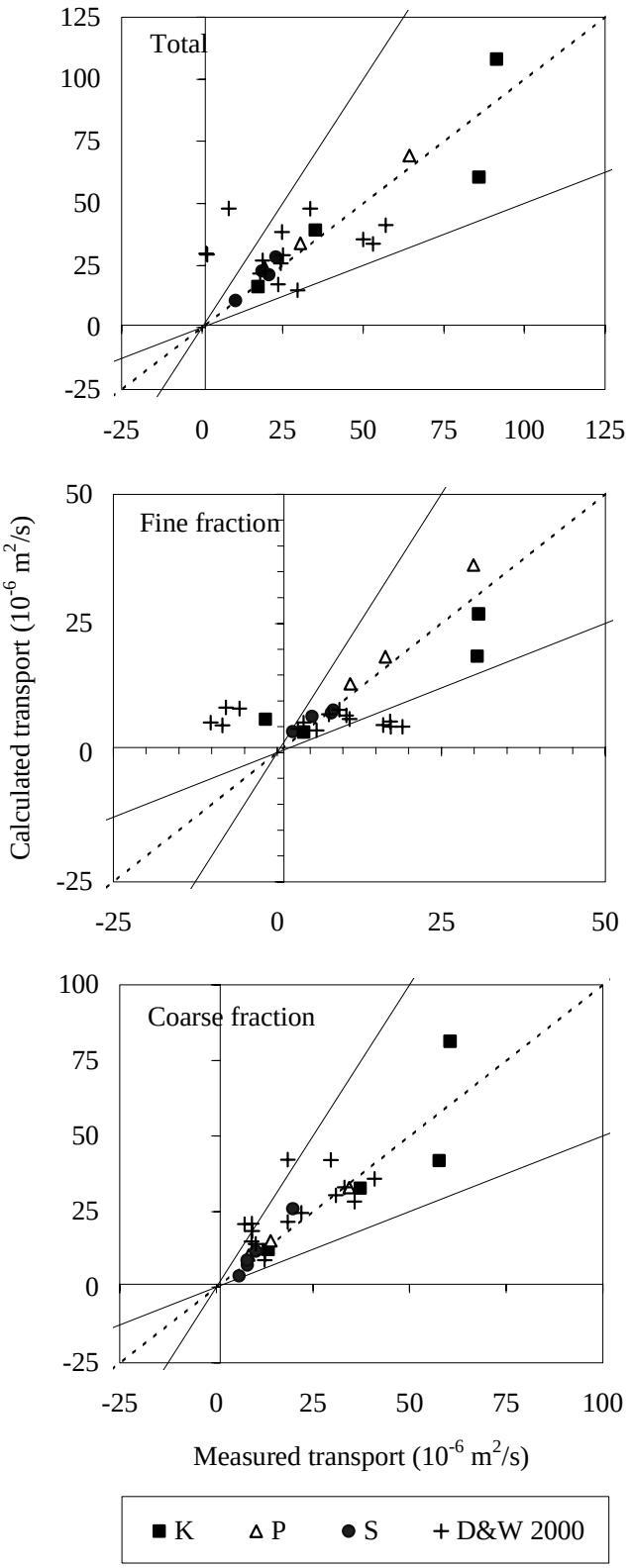

Figure 9.14: Verification of the improved graded Ribberink/D-J model with graded sand data from the LOWT.

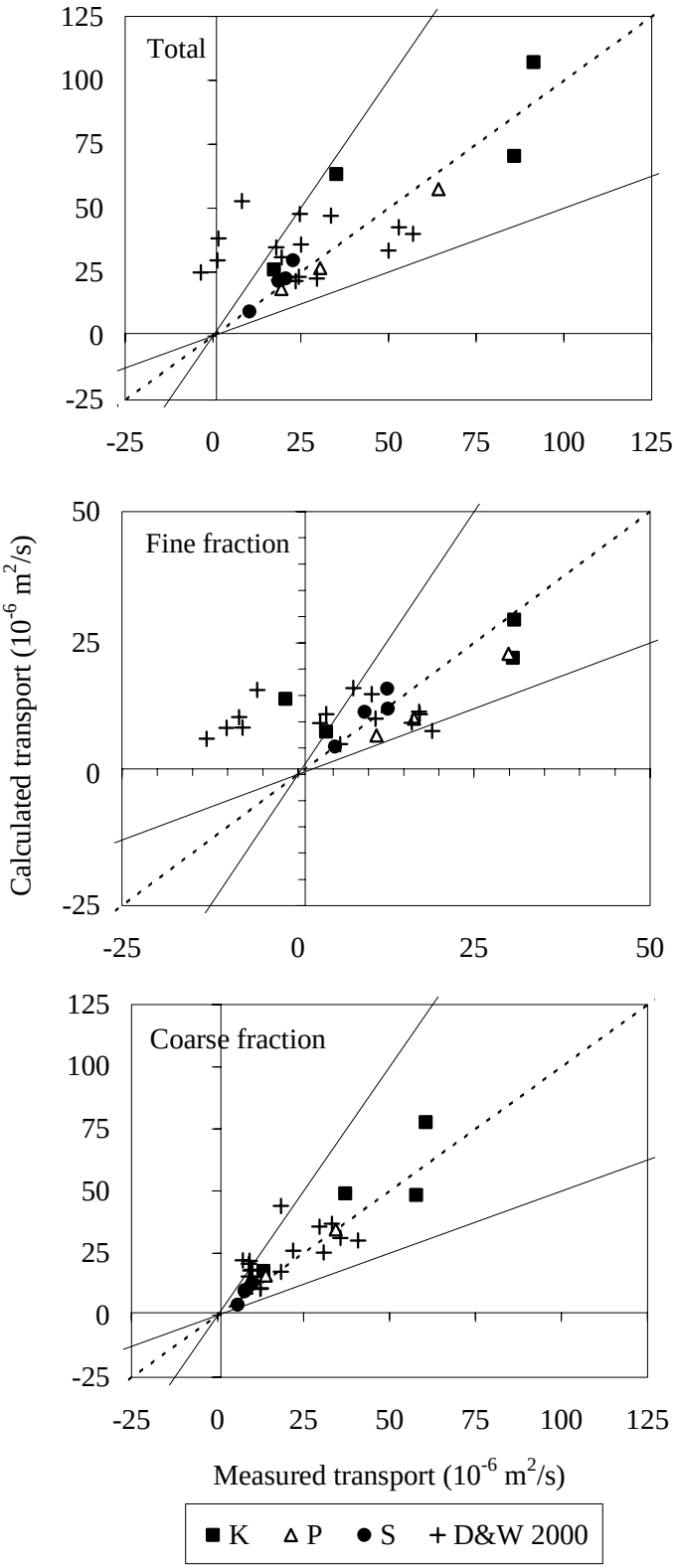

Figure 9.15: Verification of the improved graded D&W model with graded sand data from the LOWT.

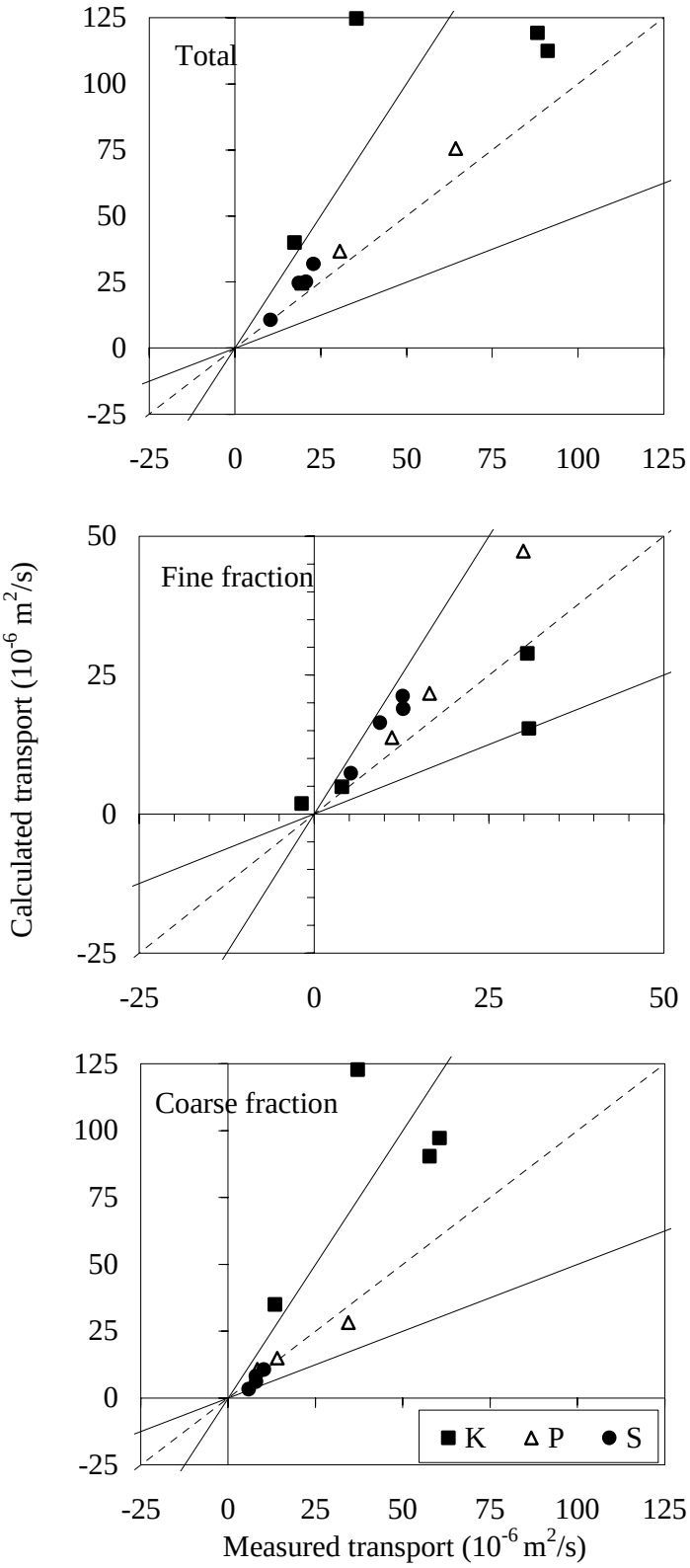

Figure 9.16: Verification of the improved graded PSM model with graded sand data from the LOWT.

9.6 Summary of graded model improvements

In chapter 9 different types of transport models were adjusted in order to improve their performance of predicting transport rates of graded sand under oscillatory sheet-flow conditions. The model improvements were aimed at better predictions of the total net transport rates, as well as the transport rates per size-fraction. In other words: each transport model should be able to predict the total net transport rates but should also reproduce the composition of the transported sand correctly in order to be able to deal with the grain-size sorting process. The main conclusions from the model improvements in this chapter can be summarised as follows:

- Hiding/exposure effects play an important role in graded sand transport mechanisms under oscillatory sheet-flow conditions. Including these effects is essential to predict the size composition of the transported sediment correctly;
- Correcting the critical Shields parameter in the model of Ribberink (1998) does not show much influence on the predicted transport rates. On the other hand correcting the effective shear stress has a clear effect on the transport rates per size-fraction. Apparently, the effective shear stress is much larger than the critical shear stress under sheet-flow conditions;
- The model of Ribberink showed the best results by combining it with the D-J (1999) phase-lag correction and using the hiding/exposure correction of Day (1980). The correction factor of Day (developed for river flow) increases the effective shear stress of the coarse grains and at the same time reduces the effective shear stress of the fine grains;
- The correction factor of Day (1980) hardly improved the predictions of the fine fraction transport rates. The fine fraction transport seems to be dominated by phase-lag effects. The results indicate that phase-lag processes in sand mixtures work out differently than in uniform sand. Dynamic armouring, as observed by D&W (1996), probably plays a dominant role in mixed sand transport;
- It was possible to improve the performance of the model of D&W (1996) for graded sand by including a hiding/exposure correction in the model. Reducing the entrainment height of fine grains in the flow and increasing the entrainment height of coarse grains leads to this model improvement. The implemented correction factor in the model of D&W (1996) is a function of D_i/D_m (see equation 9.13) which can be applied for all grain-sizes and for any number of size-fractions in a mixture under oscillatory sheet-flow conditions;
- The new intermediate graded models of D-J and D&W predicted the measured transport rates much better for the large-scale LOWT data than the small-scale TUWT data. In fact the LOWT data are more representative of field conditions;
- Adding the bed-load formula of Engelund & Fredsøe (1976) to the PSM model improved the model performance for uniform sand cases;
- Using the Zyserman and Fredsøe (1996) size-fraction approach in the total-load PSM model led to better model predictions of fine fraction transport rates

than the simple size-fraction approach, which is only based on applying the size-fraction approach to the bed reference concentration;

- The total-load PSM model results could be improved significantly by using the size-fraction approach of Z&F (1996) and applying an exposure correction factor for the coarse grains;

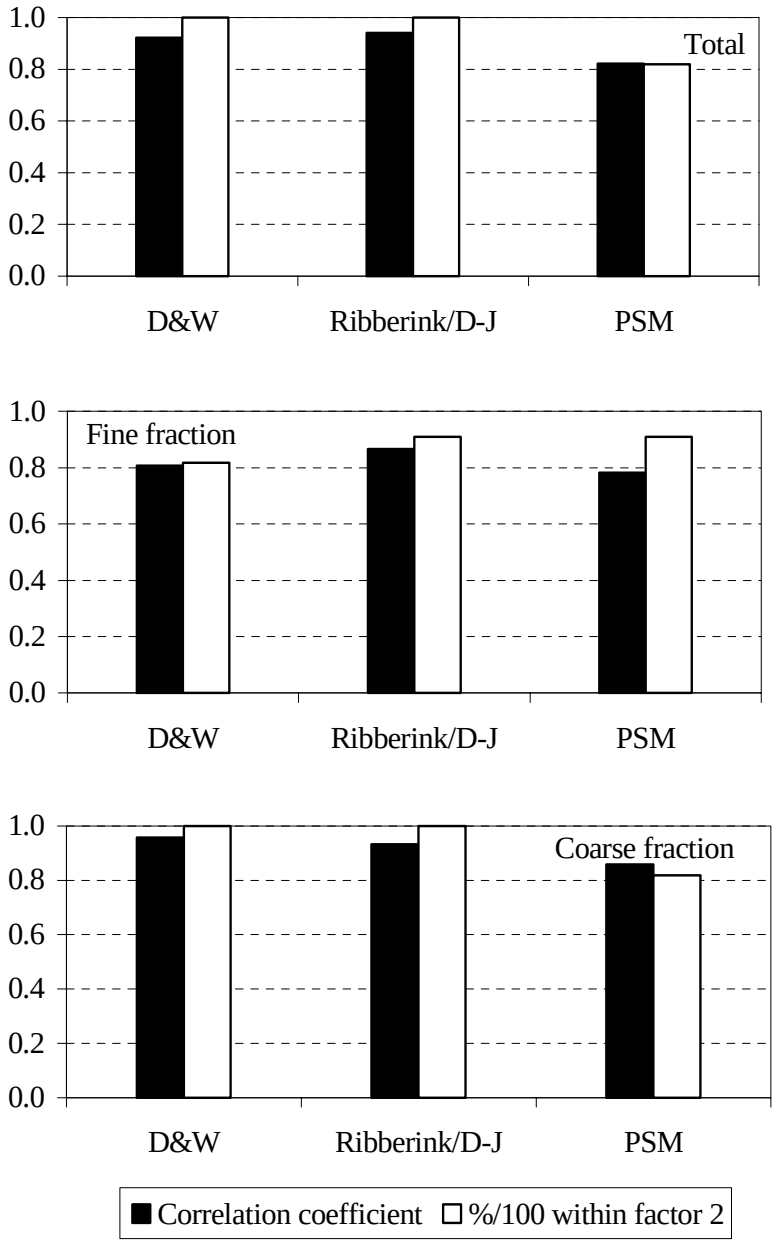

Figure 9.17: Comparison between the results of the three modified multi-fraction models of D&W, Ribberink/D-J and the PSM with graded sand.

- Finally, the new modified graded transport models were verified with a new dataset with different grain-sizes, compositions and flow conditions. These new data were collected in the LOWT. All new graded transport models show a reasonably good performance for predicting total transport rates as well as transport rates per size-fraction;
- Figure 9.17 shows a comparison between the three modified models of D&W, Ribberink and the PSM for graded sand. The comparison is based on the graded sand data of the full-scale conditions of the LOWT only (11 conditions). Generally the models are showing a good performance in predicting the total transport rates as well as the transport rates per size-fraction. The modified model of Ribberink/D-J is showing slightly better results than the other two models.

Although, the fully unsteady PSM model is more sophisticated and includes a description of many transport processes (including phase-lag effects), it was not possible to achieve clearly better model performance than the other more parameterized models. In fact, this is due to the existing lack in our knowledge about the size-size gradation effects on the near-bed transport processes (e.g. hindered settling, flow stratification, grain-grain-flow interactions).

Chapter 10

CONCLUSIONS AND RECOMMENDATIONS

10.1 General

The overall objectives of this study were to gain a better understanding of size-selective sediment transport processes and to develop well-founded predictive models for wave-induced transport of size-graded as well as uniform sands under oscillatory plane-bed/sheet-flow conditions. At present it is not possible to perform field measurements under storm/sheet-flow conditions, therefore new experiments were carried out under controlled (full-scale) conditions with oscillatory sheet-flows in the Large Oscillating Water Tunnel (LOWT) of WL | Delft Hydraulics.

The new data with uniform and size-graded sand were analyzed in detail in combination with previously collected data from the LOWT and from the Tokyo University Water Tunnel (TUWT) for improving our understanding of oscillatory sand transport processes (e.g. grain-size effect and selective transport). It is important to state that the data from both water tunnels are useful for the present study since they cover different ranges of asymmetric flow velocities and wave-periods. The working range of each tunnel can be considered as an extension of the other one.

The complete dataset from the two tunnels was used to verify and improve various sediment transport model types (quasi-steady-, intermediate- and unsteady-models) for uniform as well as size-graded sand conditions. The uniform sand data were used to study the performance of the various transport model types and to identify controlling underlying processes (e.g. phase-lag effects) which should be accounted for in order to improve modelling of sand transport in oscillatory sheet-flows. For modelling graded sand transport and to predict net total transport rates as well as the size-composition of the transported sand, a size-fraction (or multi-fraction) approach was proposed and implemented in the various transport models. The multi-fraction

transport models were verified with tunnel data and the data were used for transport model modifications and improvements.

Section 10.2 presents the main conclusions from the experimental studies (10.2.1) and from the transport modelling study (10.2.2). Finally, section 10.3 presents a series of recommendations for future research.

10.2 Conclusions

10.2.1 Experimental results and data analysis

The main objective of the experimental study was to answer the following research questions:

i) How does size-gradation of bed sediments affect the magnitude, direction and size-composition of wave-induced sediment transport in the sheet-flow regime?
ii) How do individual size-fractions of a mixture of sizes interact with each other and how do these interactions affect the transport processes?
iii) What are the effects of grain-size and wave-period on the sediment transport processes and on net transport rates in oscillatory sheet-flows?

The answers to these research questions are summarised below.

Uniform sand transport in oscillatory sheet-flows

Three different series of experiments were performed in the LOWT of WL | Delft Hydraulics with different hydraulic conditions and relatively uniform sand sizes. The first two series aimed at measuring net transport rates under 2nd-order Stokes waves using two different sand sizes (D = 0.97 and 0.34 mm). The experiments with coarse sand (D = 0.97 mm) were carried out with half-wave-cycle motion in order to obtain flat-bed/sheet-flow conditions and avoid the generation of large dunes (see also Hassan et al., 1999). The third series of uniform sand experiments (D = 0.13 mm) aimed at measuring (and improving a measuring technique) of the time-dependent transport processes inside the sheet-flow layer, i.e. time-dependent concentrations, velocities and sediment-flux profiles. The main conclusions can be summarised as follows:

Grain-size and the importance of unsteady effects
(research question iii)

- Grain-size has almost no effect on the measured net transport rates under 2nd-order Stokes waves. The measured transport rates are proportional to the third power velocity moment ($q_s \sim \langle U^3 \rangle$) for sand sizes between $0.21 < D < 0.97$ mm. In this range of grain-sizes the assumption of quasi-steadiness can be

used and in the case of 2nd-order Stokes waves net transport rates are always directed 'onshore', i.e. in the direction of the wave-crest velocity;

- Finer grains (D = 0.13 mm) show a different behaviour in the high velocity range, i.e. for $<U^3> > 0.2$ m^3/s^3. In this regime net sand transport rates change from the 'onshore' direction into the 'offshore' direction due to the presence of unsteady effects. The assumption of quasi-steadiness of Al-Salem (1993) does no longer hold;
- For waves with a long wave-period (T = 12.0 s) time-dependent concentrations inside the sheet-flow layer are approximately in phase with the time-dependent flow velocity variations. Meanwhile, for shorter wave-periods (7.2 and 4.0 s) increasing phase-lags are observed. As the wave-period decreases, the sediment entrainment from the bed as well as the deposition process back to the bed lags behind the wave motion more and more;
- Concentration peaks are observed at the moments of flow reversal, only in the upper sheet-flow layers. These peaks are not present in the deeper pick-up layers. The strength of the flow reversal peaks increases with decreasing wave-period.

Sand particle velocities and sediment-fluxes
(research question iii)

- Using two conductivity concentration meter (CCM) sensors inside the sheet-flow layer made it possible to measure instantaneously both the sand concentrations and the particle velocities using a cross-correlation technique. By reducing the distance between the two CCM sensors to 11 mm, instead of 20 mm as used by McLean et al. (2001), particle velocities could now be measured during the complete wave-cycle, which considerably improves the performance of the new measuring technique;
- By using two CCM sensors it was possible to measure the influence of the wave-period on the time-dependent sediment fluxes during the wave-cycle. Reducing the wave-period from 12.0 to 4.0 s leads to gradual changes in the net wave-related fluxes from the 'onshore' to the 'offshore' direction. These results showed the correctness of the earlier conclusion that unsteady/phase-lag effects are responsible for the general reduction in net transport rates for fine sand (see Dohmen-Janssen, 1999).

Graded-sand transport in oscillatory sheet-flows

Size-gradation effects on net total transport rates
(research question i)

- For size-graded sediments, net total sand transport rates (i.e. net transport of all size-fractions) are increasing for increasing flow velocity and they are

directed 'onshore' as long as D_{10} of the mixture exceeds 0.16 mm. In this case the net transport rates follow the power law formulation ($q_s \sim \langle U^3 \rangle$), similar as for uniform sands;

- Size-gradation has almost no effect on the net total transport rates, provided that the grain sizes of the sand mixture are in the range of $0.21 < D < 0.97$ mm;
- If very fine grains ($D = 0.13$ mm) are present in the mixture net transport rates of graded sand may be different from those of uniform sand (with the same D_{50}). In the low velocity range ($\langle U^3 \rangle < 0.15$ m^3/s^3), size-gradation has no clear effect and the transport rates in this range are still related to the third power velocity moment $\langle U^3 \rangle$. However, in the higher velocity regime ($\langle U^3 \rangle > 0.15$ m^3/s^3) size-gradation has a strong effect on both the magnitude (general reduction) and the direction of net total transport rate.

Size-gradation effects on net transport rates of each size-fraction
(research question ii)

- Sediment transport of grain-size mixtures under oscillatory sheet-flow conditions generally shows a preferential transport of the coarse fractions of the mixture. Their relative contribution to the transport is generally larger than would be expected on the basis of i) their volume proportion in the original sand mixture and ii) uniform coarse sand behaviour of the same size;
- Comparing the net transport rate per size-fraction in a mixture with the transport rate of uniform sand with the same D_{50} shows that the transport of each size-fraction is strongly influenced by the presence of other fractions. Fine particles in sand mixtures are less transported than in a uniform sand bed (hiding effects), while the opposite occurs for coarse fractions in a mixture (increased exposure);
- The latter indicates that 'uniform sediment' transport models are generally not adequate for the description of transport (rate and size-composition) of sediment mixtures. Interaction processes between size-fractions should be accounted for.

'Onshore' and 'offshore' bed-load transport and sorting
(research question ii)

- The time-averaged 'onshore' bed-load concentrations are a factor 5 to 9 higher than their 'offshore' equivalents. This ratio decreases as the flow velocity increases and is explained by the asymmetry of the wave motion. As the flow velocity increases both the time-averaged 'onshore' and the 'offshore' bed-load concentration increase rapidly. There seems to be a linear relationship between the flow velocity and the 'onshore' and 'offshore' bed-load concentrations;
- Generally, the sand transported as bed-load in the 'onshore' direction is coarser than that in the 'offshore' direction. For both directions, the percentage of coarse material is larger than in the original sand bed mixture.

This sorting process was observed for all flow conditions. The contribution of the coarse fraction in the transported material increases with increasing flow velocity.

Suspended sand and vertical grain-size sorting
(research question ii)

- In oscillatory sheet-flow conditions time-averaged suspended sediment concentrations decrease rapidly with the elevation above the bed. Also for graded sediments a power law relation exists between the concentration of suspended sediment and the distance above the bed (see Al-Salem, 1993 for uniform sands);
- Grain-size sorting over depth is taking place in the sheet-flow and suspension layers. During the new LOWT experiments only the smaller grains of the finest fraction were present in the suspension layer. The grain-size of the suspended sediment becomes finer as the distance above the bed increases. Meanwhile, coarse grains are mainly transported very close to the bed inside the sheet-flow layer;
- As the flow velocity increases the suspended sediment increases in concentration and becomes coarser (larger D_{50}) at all elevations above the sand bed;
- Grain-size sorting is also taking place in the upper active bed-layers, which are disturbed by the wave action. The upper layer of the bed (thickness of a few millimeters, depending on the flow condition) has roughly the same composition as the original sand bed or is even coarser. Beneath this upper layer there is a layer that mainly consists of fine sand. At larger depths below the sand-surface, the size-composition of the bed is again similar to that of the original sand bed mixture;
- During the experiments the upper active layer of the sand bed seems to become finer, due to selective removal of especially coarse sizes from the test section. This is a consequence of the relatively large net transport of coarse sizes and the relatively small net transport of the fine sizes.

We can conclude that in oscillatory sheet-flow conditions vertical sorting processes are taking place throughout the water column, starting at the lowest point in the active sand bed-layer until the highest point of the suspension layer. Different grain-sizes are transported at different levels in the flow and may have different transport directions at different elevations above the bed.

10.2.2 Sand transport modelling

Five different sediment transport models (quasi-steady, intermediate and fully unsteady models) were investigated in the present study, in combination with a large dataset of oscillatory sediment transport measurements (flat-bed/sheet-flow conditions) collected in the LOWT and in the TUWT. The complete dataset consists

of 118 different experiments with uniform sand and 37 experiments with size-graded sand. The sand transport modelling focused mainly on:

- ◊ Studying different types of transport models for oscillatory sheet-flow conditions and different ways of modelling phase-lag effects in case of relatively uniform sands;
- ◊ Providing the existing single size-fraction transport models with a multi-fraction approach for modelling graded sand transport;
- ◊ Improving these multi-fraction techniques for predicting the net total transport rate and the size-composition of the transported sand.

The sand transport modelling study aimed at answering the following questions:

iv) Can size-fraction techniques as commonly used in river applications (uni-directional steady flow) also be used in the marine coastal environment (unsteady oscillatory flows)?
v) What are the effects of using a size-fraction transport modelling technique on the prediction of the net total transport rate with different model types?
vi) What is the performance of these multi-fraction models as far as the prediction of the size-distribution of the transported sand is concerned?
vii) What is the performance of the different transport models, varying from quasi-steady, intermediate, to fully unsteady boundary layer models, in the description of the transport rate of graded and uniform sediments, respectively?
viii) How can we improve these transport models for predicting both net transport rates and size-composition of the transported sand?

The main conclusions from the sand transport modelling are summarised below:

Uniform sand transport modelling
(research question vii, uniform sediments)

- Quasi-steady models are not always able to predict transport rates and directions correctly. This occurs especially for short wave-periods and small sand particles, indicating that the assumption of quasi-steadiness does not hold and phase-lag effects play a role in the transport process;
- For the used quasi-steady transport models it was found that phase-lag effects become important when the phase-lag parameter p (as defined by Dohmen-Janssen, 1999) exceeds a value of 0.4-0.6;
- The inclusion of phase-lag effects in the transport models leads to a strong improvement of the models performance. For both intermediate model concepts (Dohmen-Janssen, 1999 and Dibajnia & Watanabe, 1996) the agreement between measurements and computations is considerably better than for the quasi-steady models;
- Taking into consideration that no oscillatory flow and transport data were used for its development, the fully unsteady PSM model shows reasonably

good results as compared with the more empirical intermediate transport models;
- For the uniform sand data the PSM model is able to give good predictions of transport directions and net transport rates, so apparently it inherently gives a good representation of phase-lag effects;
- Adding the bed-load formula of Engelund & Fredsøe (1976) to the PSM model, which was basically developed for suspended sediment, improves the model performance for uniform sand cases.

Graded sand transport modelling: model verifications
(research questions iv, v, vi)

The verification of multi-fraction transport models with graded sand data leads to the following conclusions:

- Using a multi-fraction approach and assuming that there is no interaction between grain sizes is generally not sufficient for predicting the net transport rates and the size-composition of graded sand transport;
- In general the three transport models (Ribberink/D-J, D&W, PSM) are not able to predict transport rates of the fine and the coarse fractions in the mixture correctly;
- Although the adjusted model of D&W (1996) was especially developed for graded sands, the model does not give good predictions for coarse fraction transport rates. On the other hand, the model shows the best performance for the fine fraction transport rates;
- The multi-fraction total-load PSM model (multi-fraction approach for the reference concentration as well as the bed-load) does not show a good performance for graded sand transport rates (total and per size-fraction).

Graded sand transport modelling: model improvements
(research questions vii, viii)

It is clear from the model verifications that, using the size-fraction approach only is not sufficient for modelling graded sand transport. Adjustments as made in the model of D&W (1996) to account for interactions between grain-sizes in a mixture are necessary for correct transport predictions.

Three different graded transport models (Ribberink/D-J, 1999, Dibajnia & Watanabe, 1996 and the PSM model, Uittenbogaard et al., 2000) were selected and provided with correction methods to include the interaction between grain-sizes in a mixture using the TUWT data with graded sediments. The main conclusions from the multi-fraction model improvements are summarised as follows:

- Exposure correction applied to the critical Shields parameter in the model of Ribberink (1998) does not show much influence on the predicted net transport rates. On the other hand, correcting the effective shear stress (Day, 1980) has a clear improving effect on the transport rates per size-fraction. This is to be attributed to the fact that the effective shear stress under oscillatory sheet flows is much larger than the critical shear stress;
- The intermediate model of Ribberink/D-J (1999) shows an improved performance using the exposure correction method of Day (1980). The correction factor of Day, originally developed for steady (river) flow situations, increases the effective shear stress on the coarse grains and at the same time reduces the effective shear stress on the fine grains;
- Adding the correction factor of Day (1980) to the model of Ribberink/D-J (1999) improves the transport predictions of the coarse fractions but hardly improves the predictions of the fine fraction transport rates. The fine fraction transport seems to be dominated by phase-lag effects, which, due to dynamic armouring processes, appear to work out differently for sand mixtures than for uniform sand;
- The performance of the model of D&W (1996, the uniform sand model) for predicting graded sand transport is improved considerably by including an exposure correction in the model. This can be achieved by reducing the entrainment height of fine grains and increasing the entrainment height of coarse grains. The correction factor implemented in the model of D&W (1996) is modelled as a general function of D_i/D_m (see equation 9.13) and can be applied for any number of size-fractions;
- Using the Zyserman and Fredsøe (1996) size-fraction approach in the total-load PSM model leads to improved model predictions of the fine fraction transport rates. Meanwhile, the total transport rates are only slightly improved since the Z&F approach (for suspended sands) does not affect the prediction of coarse bed-load fractions;
- The total-load PSM model results is improved significantly by using the size-fraction approach of Z&F (1996) in combination with an exposure correction for the coarse grains;

As a final step, the modified graded transport models (D&W, Ribberink/D-J and the PSM model) were verified with a separated dataset consisting of all experiments of the LOWT with graded sediments. All models show a reasonably good performance for predicting net total transport rates as well as transport rates per size-fraction. The modified model of Ribberink/D-J perform slightly better than the other two models. The modified multi-fraction models of Ribberink/D-J and D&W predict the measured transport rates much better for the large-scale LOWT data than for the small-scale TUWT data. The LOWT data are more relevant for field conditions.

10.3 Recommendations

Measuring the particle velocities inside the sheet-flow layer, using a cross-correlation technique between two small conductivity probes (CCM), seems to be a promising technique. This technique needs further improvements with extra tests in the LOWT, large wave flumes and in the field. It is recommended also to develop a more sensitive instrument with a smaller measuring volume and higher resolution.

Laboratory experiments of the present study were carried out in the LOWT for asymmetric waves without a net current. It is therefore recommended to extend the graded sand experiments with waves superimposed on steady currents with different wave-periods. Moreover, it is recommended to extend the graded sand data with more sand mixtures with different sizes and more natural sand (with various D_{50} and σ_g) under sheet-flow as well as rippled bed conditions.
In general, further improvement of the intermediate and the unsteady models for graded sand cases can be achieved by additional verification and calibration of these models with extended large-scale datasets of transport measurements with graded sand.

The present study has shown that the sheet-flow layer thickness (or entrainment height of the sand grains) is a crucial parameter for the occurrence of unsteady effects and for adequate prediction of transport rates of uniform and size-graded sand. Therefore, it is recommended to systematically study the behaviour of the sheet-flow layer thickness in case of uniform and size-graded sediments (see e.g. Wright, 2002). A better insight into the entrainment height of uniform sands and size-fractions of a mixture (dynamic armouring process) increase our understanding of phase-lag effects on the transport rates of size-graded sand. This better understanding will lead to further improvements of sand transport modelling techniques (e.g. the phase-lag correction factor of Dohmen-Janssen et al., 2002 and 1999).

New experiments with graded sand are required in a big wave flume under propagating surface waves, in order to investigate the transport processes due to wave-induced currents, e.g. streaming in the wave boundary layer. These experiments are quite important for improving the existing transport models for real wave situations as in the field.

The PSM model has a good potential for further improvements as the model includes most of the available knowledge about hydrodynamic and transport processes, such as wave-current interaction processes and phase-lag effects.

Developing multi-fraction models for predicting reference concentrations per size-fraction at a fixed reference level or on the interface of bed-load (sheet-flow) and suspension are quite important for improving the PSM model and any other unsteady transport models (see also Malarkey et al., 2001).

It is recommended to study in detail the time-dependent behaviour of the PSM model (time-dependent velocities and concentrations) and to verify the results with time-dependent measurements from the laboratory as well as from the field. The PSM model should also be verified with real surface wave data, since the complete water column is modelled including all wave-current interaction effects. Special attention should be paid to modelling hindered settling and flow stratification for uniform as well as graded sand under sheet-flow conditions.

References

Ahmed, S.M.A. (2002): Sheet flow transport mechanism of heterogeneous sediments under nonlinear oscillatory flows. *Ph.D. Thesis, Dep. of Civil Eng., Univ. of Tokyo, Japan.*

Al-Salem, A.A. (1993): Sediment transport in oscillatory boundary layers under sheet flow conditions. *Ph.D. Thesis, Delft Univ. of Technology, The Netherlands.*

Allen, J.R.L. (1982): Sedimentary structures, Their Character and Physical Basis. *Elseviers Science Publishers, Amsterdam, The Netherlands.*

Armanini, A. and P. Ruol (1988): Non-uniform suspended sediments under waves. *Proc. 21st Int. Conf. on Coast. Eng., Malaga, pp. 1129-1139.*

Ashida, K. and M. Michiue (1973): Study on hydraulic resistance and bed-load transport rate in alluvial streams. *JSCE, Vol. 4, pp. 122-123.*

Bagnold, R.A. (1963): Mechanics of marine sedimentation. *In: The Sea, Vol. 3, ed. M.N. Hill, Interscience, NewYork.*

Bailard, J.A. (1981): An energetics total load sediment transport model for a plane sloping beach. *J. Geoph. Research, Vol. 86, No. C11, pp. 10938-10954.*

Bailard, J.A. (1982): Modeling on-offshore sediment transport in the surf zone. *Proc. 18th Int. Conf. on Coast. Eng., Cape Town, pp. 1419-1438.*

Bailard, J.A. and D.L. Inman (1981): An energetics bedload model for a plane sloping beach: Local transport. *J. Geoph. Research, Vol. 86, No. C3, pp. 2035-2043.*

Bijker, E.W. (1971): Lonshore transport computations. *J. Waterways, Harbors and Coast. Eng. Div., ASCE, WW4.*

Blom, A., J.S. Ribberink and H.J. de Vriend (2003): Vertical sorting in dunes - flume experiments with a natural and a tri-modal sediment mixture. *J. Water resources research, Vol. 39 No. 2, 10.1029/2001WR001088.*

Blom, A. (2003): A vertical sorting model for rivers with non-uniform sediment and dunes *Ph.D. Thesis, Univ. of Twente, The Netherlands. ISBN 90-9016663-7.*

Bonnefille, R. (1963): Essais de synthese des lois de debut d'entrainment des sediments sous l'action d'un courant en regime uniforme bull. *du CREC, No. 5, Chatou.*

Bosman, J.J., E.T.J.M. van der Velden and C.H. Hulsbergen (1987): Sediment concentration measurement by transverse suction. *Coast. Eng. Vol. 11.*

Bosboom, J. and G. Klopman (2000): Intra-wave sediment transport modelling. *Proc. of the 27th Int. Conf. On Coast. Eng., Sydney, Australia, pp. 2453-2466.*

Chatelus, Y., I. Katopodi, C.M. Dohmen-janssen, J.S. Ribberink, P. Samothrakis, B. Cloin, J.C. Savioli, J. Bosboom, B.A. O'Connor and R. Hein (1998): Size gradation effects in sediment transport, *Proc. Of the 26th Int. Conf. on Coast. Eng., Copenhagen.*

Cloin, B. (1998): Gradation effects on sediment transport in oscillatory sheet-flow. *Report H2305, March 1998, WL ⁄Delft Hydraulics, The Netherlands.*

Davies, A.G., J.S. Ribberink, A. Temperville and J.A. Zyserman (1997): Comparisons between sediment transport models and observations made in wave and current flows above plane beds. *Coast. Eng., Vol. 31, pp. 163-198.*

Dally, W.R. and R.G. Dean (1984): Suspended sediment transport and beach profile evolution, *J. Waterways, Port Coast. and Ocean Eng., Vol. 110, No.1, pp. 15-33.*

Day, T.J. (1980): A study of the transport of graded sediments. *HRS Wallingford Report No. IT 190, UK.*

Dean, R.G. (1991): Equilibrium beach profiles. *J. Coast. Research, V 7,1, pp. 53-84.*

De Meijer R.J., J. Bosboom, B. Cloin, I. Katopodi, N. Kitou, R.L. Koomans and F. Manso (2002): Gradation effects in sediment transport. *J. Coast. Eng., Vol. 47, pp. 179-210.*

De Vriend, H.J. and W.Th. Bakker (1993): Sedimentary processes and morphological behaviour models for mixed-energy tidal inlets. *Report H1887, WL ⁄Delft Hydraulics, The Netherlands.*

Dibajnia, M. and A. Watanabe (1992): Sheet flow under nonlinear waves and currents. *Proc. of the 23rd Int. Conf. on Coast. Eng., Venice, pp. 2015-2028.*

Dibajnia, M. and A. Watanabe (1996): A transport rate formula for mixed-size sands. *Proc. of the 25th Int. Conf. on Coast. Eng., Orlando, pp. 3791-3803.*

Dibajnia, M. et al. (1998): Experimental Study on Moving Layer Thickness and Transport Rate of Mixed-Size Sand. *Proc. Coast. Eng., JSCE, Vol. 45, pp. 481-485. (in Japanese).*

Dibajnia, M. and A. Watanabe (2000): Moving layer thickness and transport rate of graded sediment. *Proc. of the 27th ICCE, ASCE, pp. 2752-2765.*

Dohmen-Janssen (1999): Grain size influence on sediment transport in oscillatory sheet flow, phase lags and mobile-bed effects. *Ph.D. Thesis, Delft Univ. of Technology, The Netherlands.*

Dohmen-Janssen, C.M., W.N.M. Hassan and J.S. Ribberink (2001): Mobile-bed effects in oscillatory sheet flow. *J. Geophysical research, Vol. 106(C11), pp. 27103-27115.*

Dohmen-Janssen, C.M., D.F. Kroekenstoel, W.N.M. Hassan, and J.S. Ribberink (2002): Phase lags in oscillatory sheet flow: experiments and bed load modelling. *J. Coast. Eng., Vol. 46, pp. 61-87.*

Dong, P. and K. Zhang (1999): Two-phase flow modelling of sediment motions in oscillatory sheet flow. *Coast. Eng., Vol. 36, pp. 87-107.*

Egiazaroff, J.V. (1965): Calculation of non-uniform sediment concentrations. *Proc. ASCE, J. Hydr. Div, 91, HY4, July.*

Engelund, F. and J. Fredsøe (1976): A sediment transport model for straight alluvial channels. *Nordic Hydrol., 7, pp. 293-306.*

Fenton , J.D. and J.E. Abbott (1977): Initial movement of grains on a stream bed: the effect of relative protrusion. *Proc R. Soc. London, A. 352, p. 523-537.*

Fredsøe, J. and Deigaard (1992): Mechanics of coastal sediment transport, *world scientific, Singapore, 369 p.*

Fredsøe, J., O.H. Andersen and S. Silberg (1985): Distribution of suspended sediment in large waves. *J. Waterway, Port, Coastal and Ocean Eng., ASCE, Vol. 111, No. 6, pp. 1041-1059.*

Grant, W.D. and O.S. Madsen, (1982): Movable bed roughness in unsteady oscillatory flow. *J. Geoph. Research, Vol. 87, No. C1, pp. 469-481.*

Guillen, J. (1995): Sediment response in a littoral system, Island of Terschelling, The Netherlands. *Report 95-20, Dep. Of Phys. Geography, Univ. of Utrecht, The Netherlands.*

Hassan, W.N.M., D.F. Kroekenstoel, J.S. Ribberink and L.C. van Rijn (1999): Gradation effects on sand transport under oscillatory sheet-flow conditions. *Research. report, WL/Delft Hydraulics and Univ. of Twente, The Netherlands, 165 pp.*

Hassan, W.N.M. and J.S. Ribberink (2000): Modelling of graded sand transport mechanisms in oscillatory flows. *Literature study, Civil Engineering & Management Research report 2000W-005/MICS-014, Univ. of Twente, Enschede, The Netherlands.*

Hassan, W.N.M. (2001): Sand transport processes in oscillatory sheet flows with different wave periods – CCM measurements in the Large Oscillating Water Tunnel. *MICS report 2001W-002, Civil Eng. and Management, Univ. of Twente, The Netherlands.*

Hassan, W.N.M., D.F. Kroekenstoel and J.S. Ribberink (2001a): Size-gradation effect on sand transport rates under oscillatory sheet-flows *Proc. Coast. Dynamics '01, ASCE, Lund, Sweden, pp. 928-937.*

Hassan, W.N.M., J.S. Ribberink and L.C. van Rijn (2001b): Wave-related transport of graded sediment in the sheet-flow regime based on wave tunnel experiments *SEDMOC Sediment Transport Modelling in Marine Coastal Environments, End Document EC MAST Project No. MAS3-CT97-0115, Paper BA.*

Hassan, W.N.M., D.F. Kroekenstoel and J.S. Ribberink (2001c): Modelling of sand transport in oscillatory sheet-flows *Proc. 2nd IAHR symposium on River Coastal and Estuarine Morphodynamics (RCEM 2001), Obihiro, Japan.*

Hassan, W.N.M., D.F. Kroekenstoel and J.S. Ribberink (2001d): Sand transport modelling of graded sediments in oscillatory flows above plane beds. *SEDMOC Sediment Transport Modelling in Marine Coastal Environments, End Document EC MAST Project No. MAS3-CT97-0115, Paper CF.*

Hassan, W.N.M., P. van der Scheer and J.S. Ribberink (2002): Oscillatory flow experiments over flat sandy beds using coarse sand, medium sand and a sand mixture of coarse, medium and fine sand. *Research report, WL/Delft Hydraulics and Univ. of Twente, The Netherlands.*

Hamm, L., I. Katopodi, C.M. Dohmen-Janssen, J.S. Ribberink, P. Samothrakis, B. Cloin, J.C. Savioli, Y. Chatelus, J. Bosboom and R. Hein (1998): Grain size and gradation effects on sediment transport processes in oscillatory flow conditions, *part1: Gradation effects (series K). Data report Z2153, WL/Delft Hydraulics.*

Hinze, J.O. (1975): Turbulence. *McGraw-Hill, Classic Textbook Reissue series.*

Houman, K.T. and P. Hoekstra (1994): Shoreface sediment dynamics. *Report part 2, field measurements near Egmond aan Zee, Imau, R94-2, Univ. of Utrecht, The Netherlands.*

Hout, G. van der (1997): Grain-size and gradation effects on sediment transport under sheet-flow conditions. *Part 2: Data-analysis and modelling. Report Z2137, WL /Delft Hydraulics, The Netherlands.*

Huynh Thanh, S., T. Thran Thu and A. Temperville (1994): A numerical model for suspended sediment in combined currents and waves. *Euromech 310, Le Havre, Sept. 1993, Sediment Transport Mechanisms in Coastal Environments and Rivers, ed. M. Belorgey, R.D. Rajaona and J.F.A. Sleath, World Scientific, Singapore, pp. 122-130.*

Inui, T., M. Dibajnia, M. Isobe and A. Watanabe (1995): A transport rate formula for mixed-size sands and its application, *Proc. 42nd Japanese Annual Conf. On Coast. Eng., JSCE, pp. 356-360 (in Japanese).*

Jackson, P.S. (1981): On the displacement height in the logarithmic velocity profile. *J. Fluid Mech., Vol. 111, pp. 15-25.*

Janssen, C.M., W.N.M. Hassan, R. v.d. Wal and J.S. Ribberink (1996): Net sand transport rates and transport mechanisms of fine sand in combined wave-current sheet flow conditions. *Data report H2462, Part IV, WL /Delft Hydraulics, The Netherlands.*

Janssen, C.M. and G. van der Hout (1997): Sediment transport for two sands with different grain diameters under combined wave-current sheet flow conditions. *Data Report Z2137, Part I, April 1997, WL /Delft Hydraulics, The Netherlands.*

Jonsson, I.G. (1966): Wave boundary layers and friction factors. *Proc. 10th Int. Conf. on Coast. Eng., pp. 127-148.*

Katoh, K. and S. Yanagishima (1995): Changes of sand grain distribution in surf zone, *Coast. Dynamics, Gdansk, Poland, pp. 639-649.*

Katopodi, I., J.S. Ribberink, P. Ruol, H. Koelewijn, C. Lodahl, S. Longo, A. Crosato and H. Wallace (1994a): Intra-wave sediment transport in an oscillatory flow superimposed on a mean current. *Data Report H1684, Part III, August 1994, WL /Delft Hydraulics, The Netherlands.*

Katopodi, I., J.S. Ribberink, L. Hamm, N. Kitou, P. Smothrakis, C.M. Dohmen-janssen and J.C. Savioli (1999): Composition of concentration measurements with well-sorted and bimodal sand, *Proc. Coast. Dyn., Long Island, New York.*

King, D.B. (1991): Studies in oscillatory flow bedload sediment transport. *Ph.D. Thesis, Univ. of California, San Diego.*

Kleinhans, M.G. (2002): Sorting out sand and gravel: sediment transport and deposition in sand-gravel bed rivers *Ph.D. Thesis, Utrecht Univ., The Netherlands.*

Klopman, G. (1994): Vertical structure of the flow due to waves and currents. *Report H840.30, Part II, WL /Delft Hydraulics, The Netherlands.*

Koelewijn, H. (1994): Sediment transport under sheet-flow conditions. *M.Sc. Thesis, Delft Univ. of Technology, October 1994.*

Komar, P.D. and C. Wang (1984): Processes of selective grain transport and the formation of placers on beaches. *J. Geology, Vol. 92, pp. 637-655.*

Koomans, R.L. (2000): Sand in motion: Effects of density and grain size, *Ph.D. Thesis, Univ. of Groningen, The Netherlands. ISBN. 90-367-1338-2.*

Kroekenstoel D.F. (1999): Transport of non-uniform sediments under oscillatory sheet-flow conditions, experimental research and modelling. *M.Sc. Thesis, Univ. of Twente, The Netherlands.*

Kroekenstoel, D.F., W.N.M. Hassan and J.S. Ribberink (2000): Sediment transport program: *A reference guide. Civil Engineering & Management Research report 2000W-012 / MICS-018. Univ. of Twente, Enschede, The Netherlands.*

Li, Z. and A.G. Davies (1995): Towards predicting sediment transport in combined wave-current flow. *J. Waterway, Port, Coast. and Ocean Eng., ASCE, Vol. 122, No. 4, pp. 157-164.*

Liu, J.T. and G.A. Zarillo (1987): Partitioning of shoreface sediment grain-sizes. *Coast. Sediments, New Orleans, USA, pp. 1533-1548.*

Longuet-Higgins, M.S. (1953): Mass transport in water waves. *Phil. Trans. Roy. Soc. London, Vol. 245 A, pp. 535-581.*

McLean, S.R., J.S. Ribberink, C.M. Dohmen-Janssen and W.N.M. Hassan (2001): Sediment transport measurements within the sheet flow layer under waves and currents. *J. Waterway, Port, Coast. and Ocean Eng., ISSN 0733-950X.*

Madsen, O.S. and W.D. Grant (1976): Quantitative description of sediment transport by waves. *Proc. 12th Int. Conf. on Coast. Eng., pp. 1093-1112.*

Madsen, O.S. and W.D. Grant (1976): Sediment transport in the coastal environment. *Rep. 209, Ralph M. Parsons Lab. for Water Resources and Hydrodynamics, Massachusetts Inst. of Tech., Cambridge, Massachusetts.*

Malarkey, J., A.G. Davies and Z. Li (2001): A one-phase sheet flow model of sediment transport. *SEDMOC Sediment Transport Modelling in Marine Coastal Environments, End Document EC MAST Project No. MAS3-CT97-0115, Paper BG.*

McFetridge, W. F. and P. Nielsen (1985): Sediment suspension by non-breaking waves over rippled beds. *Tech Rep UFL/COEL-85/008, Coast. & Oceanographical Eng. Dept., Univ. of Florida, Gainesville.*

Meyer-Peter, E. and R. Muller (1948): Formulas for bed-load transport. *In Sec. Int. IAHR congress, Stockholm, Sweden.*

Miller, R.L. and R. L. Byrne (1966): The angle of response for a single grain on a fixed rough bed. *Sedimentology, Vol. 6, pp. 303-314.*

Nielsen, P. (1979): Some basic concepts of wave sediment transport. *Inst. of Hydrodyn. and Hydr. Eng., Tech. Univ. of Denmark, series Paper no. 20.*

Nielsen, P. (1983): Analytical determination of near shore wave height variation due to refraction, shoaling and friction, *Coast. Eng., Vol. 7, pp. 233-251.*

Nielsen, P. (1992): Coastal bottom boundary layers and sediment transport, *World Scientific, Singapore, 324 p.*

Petit, F. (1994): Dimensionless critical shear stress evaluation from flume experiments using different gravel beds. *Earth Surface Processes and Landforms, Vol. 19, pp. 565-576.*

Pruszak, Z. (1993): The analysis of beach profile changes using Dean's method and empirical orthogonal functions. *Coast. Eng., Vol. 19, pp. 245-261.*

Ramadan, K.A.H. (1994): Time-averaged sediment transport phenomena in combined wave-current flows. *Report H1889.11, Part I, WL/Delft Hydraulics, The Netherlands.*

Ribberink, J.S. (1987): Mathematical modelling of one-dimensional morphological changes in rivers with non-uniform sediment. *Ph.D. Thesis, Univ. of Technology Delf, The Netherlands.*

Ribberink, J.S. (1989): The large oscillating water tunnel. *Technical specifications and performances. WL/Delft Hydraulics, Rep. H840, Part I, The Netherlands.*

Ribberink, J.S. and A.A. Al-Salem (1991): Near bed sediment transport and suspended sediment concentrations under waves. *Int. Symp. On: "the transport of suspended sediments and its mathematical modelling", IAHR Florence, Italy.*

Ribberink, J.S. and A.A. Al-Salem (1992): Time-dependent sediment transport phenomena in oscillatory boundary layers under sheet-flow conditions. *Data Report H840.20, Part VI, December 1992 WL/Delft Hydraulics, The Netherlands.*

Ribberink, J.S. and Z. Chen (1993): Sediment transport of fine sand under asymmetric oscillatory flow. *Report H840, Part VII, January 1993, WL/Delft Hydraulics.*

Ribberink, J.S. and A.A. Al-Salem (1994): Sediment transport in oscillatory boundary layers in cases of rippled beds and sheet flow. *J. Geophysical Research, Vol. 99, No. C6, pp. 12,707-12,727.*

Ribberink, J.S. and A.A. Al-Salem (1995): Sheet flow and suspension in oscillatory boundary layers. *Coast. Eng., Vol. 25, pp. 205-225.*

Ribberink, J.S. (1998): Bed-load transport for steady flows and unsteady oscillatory flows. *Coast. Eng., Vol. 34, pp. 59-82.*

Ribberink J.S., W.N.M. Hassan and D.F. Kroekenstoel (2001): Sand transport modelling for oscillatory flows above plane beds. *Sediment Transport Modelling in Marine Coastal Environments, End Document EC MAST Project No. MAS3-CT97-0115, paper CI.*

Richardson, Y.F. and W.N. Zaki (1954): Sedimentation and Fluidization. *Part I, Trans. Inst. Chem. Eng., Vol. 32, pp. 35-53.*

Roelvink, J.A. (1993): Surf beat and its effect on cross-shore profiles. *Ph.D. Thesis, Dep. of Civil Eng., Delft Univ. of Technology, Delft, The Netherlands.*

Roelvink, J.A. and I. Brøker Hedegaard (1993): Cross-shore profile models. *Coast. Eng., Vol. 21, pp. 163-191.*

Sato, S. and K. Horikawa (1986): Laboratory studies on sand transport over ripples due to asymmetric oscillatory flows. *20th ICCE, Taipeh, Taiwan.*

Sawamoto, M. and T. Yamashita (1986): Sediment transport rate due to wave action. *J. Hydrosc. and Hydr. Eng., Vol. 4, No. 1, pp. 1-15.*

Shields, A. (1936): Anwendung der Aehnlichkeitsmechanik und Turbulenzforchung auf die Geschiebebewegung. *Mitt. Preuss Versuchsanstalt fur Wasserbau und Schiffbau, No. 26, Berlin.*

Shlingerland, R. (1984): Role of hydraulic sorting in the origin of fluvial placers. *J. sedimentary Petrology, Vol. 54(1), pp. 137-150.*

Short, A.D. and T. Aagaard (1991): Beach morphodynamic systems of the central Netherlands coast, Den Helder to Hoek van Holland. *Report Geopro 1991.01 Dep. of Physical Geography, Univ. of Utrecht, The Netherlands.*

Sistermans, P.G.J. (2002): Graded sediment transport by non-breaking waves and a current. *Ph.D. Thesis, Delft Univ. of Technology.*

Sleath, J.F.A. (1978): Measurements of bed load in oscillatory flow. *J. Waterway, Port, Coast. and Ocean Eng., ASCE, Vol. 104, No. WW4, pp. 291-307.*

Smith, J.D. (1977): Modelling of sediment transport on continental shelves. *In: The Sea, Vol. 6, Wiley-Interscience, New York, pp. 539-577.*

Stive, M.J.F. (1986): A model for cross-shore sediment transport. *20th ICCE, ASCE, Taipei, Taiwan.*

Stolk, A. and P. Seeger (2000): Anticipating the challenges, the management of marine sand extraction in the Netherlands. *Quarry Management March 2000, pp. 27-32.*

Suzuki, K., A. Watanabe, M. Isobe and M. Dibajnia (1994): Experimental study on transport of sediment with mixed-grain size due to oscillatory flow, *Proc. 41st Japanese annual Conf. On Coastal Eng., JSCE, pp. 356-360 (in Japanese).*

Swart, D.H. (1974): Offshore sediment transport and equilibrium beach profiles. *Delft Hydr. Publ., No. 131, WL /Delft Hydraulics, The Netherlands.*

Takeshi, I., M. Dibajnia, M. Isobe and A. Watanabe (1995): Transport rate formula for mixed-size sands and its Application. *Proc. of Coast. Eng., JSCE, Vol. 42, pp. 521-525. (in Japanese).*

Tanaka, M. (2000): Study on sand transport rate and beach deformation for mixed-grain size beds. Ph.D. *Thesis, 136 p. Tokyo Univ., Japan.*

Takasawa, S., M. Dibajnia, and A. Watanabe (1996): A generalized sheet flow transport formula, *Proc. 51st Annual Civil Eng. Conf., JSCE, Vol. B2, pp. 124-125 (in Japanese).*

Terwindt, J.H.J. (1962): Study of grain size variations at the coast of Katwijk (in Dutch), The Netherlands, *Note K-324, Rijkswaterstaat, The Hague, The Netherlands.*

Trouw, K., B. Cloin, A. Arnott, W.N.M. Hassan, P. Dong, J. van de Graaff, C. Rose, J. S. Ribberink and P. Sistermans (2001). Vertical sediment entrainment characteristics in oscillatory sheet-flow conditions, *Data report Z2454, WL /Delft Hydraulics, The Netherlands.*

Uittenbogaard, R.E. (2000): 1DV Simulation of Wave Current Interaction. *In Proc. 27th Int. Conf. On Coast. Eng., Sydney, Australia, pp. 255-268.*

Uittenbogaard, R.E., J. Bosboom and T. van Kessel (2000): Numerical simulation of wave-current driven sand transport. *Theoretical background of the beta-release of the POINT-SAND model. Revised edition, report Z2899.10, WL /Delft Hydraulics, The Netherlands.*

Van der Wal, R.J., (1996): Grain-size influence on sediment transport in sheet flow conditions for combined wave-current flow. *M.Sc. Thesis, Delft Univ. of Technology, The Netherlands, 104 p.*

Van Rijn, L.C. (1989): Handbook of sediment transport by currents and waves. *Report H461, WL /Delft Hydraulics, The Netherlands.*

Van Rijn, L.C. (1990): Principles of fluid flow and surface waves in rivers, estuaries and oceans. *Aqua Publications, Amsterdam, The Netherlands.*

Van Rijn, L.C. (1993): Principles of sediment transport in rivers, estuaries and coastal seas. *Aqua Publications, Amsterdam, The Netherlands.*

Van Rijn, L.C., A. Reiniers, T. Zitman and J.S. Ribberink (1995): Yearly-averaged sand transport at the – 20 m and – 8 m NAP depth contours of the Jarkus-profiles 14, 20, 76 and 103. *Report H1887, Kustgenese project, WL ⏜Delft Hydraulics, The Netherlands.*

Van Rijn, L.C. (1997a): Cross-shore modelling of graded sediments. *WL ⏜Delft Hydraulics, Report Z2181, The Netherlands.*

Van Rijn, L.C. (1997b): Sand transport and bed composition along cross-shore profile. *Coast Dynamics, Plymouth, England.*

Van Rijn, L.C. (1997c): Calibration of mechanical bed load transport sampler. Note, *WL ⏜Delft Hydraulics, The Netherlands.*

Van Rijn, L.C. (1998a): The effect of sediment composition on cross-shore profile. *Int. Conf. on Coast. Eng., 3 (Ed. By B.L. Edge. ASCE, Copenhagen), pp. 2495-1509.*

Van Rijn, L.C. (1998b): Principles of coastal morphology. *Aqua Publications, Amsterdam, The Netherlands.*

Watanabe, A., Y. Riho and K. Horikawa (1980): Beach profiles and on-offshore sediment transport. *Proc. 17th Int. Conf. on Coast. Eng., pp. 1106-1121.*

Wilcock, P.R. (1993): Critical shear stress of natural sediments. *J. of Hyd. Eng., Vol. 119, No 4, pp. 491-505.*

Wilcock, P.R. et al. (1988): Experimental study of incipient motion in mixed-size sediment. *Water Resources Research, Vol. 24, No 7, pp. 1137-1151.*

Wilson, K.C. (1987): Analysis of bed-load motion at high shear stress. *J. Hydr. Eng., ASCE, Vol. 113, No. 1, pp. 97-103.*

Wright, S. (2002): Well-sorted and graded sands in oscillatory sheet-flow. *Ph.D. thesis, Univ. of Aberdeen, Scotland.*

Xu, J. (1993): Suspended sediment concentration profiles in the bottom boundary layer. *Ph.D. Thesis, The College of William and Mary, Virginia, 131 p.*

Yalin, M.S. (1972): Mechanics of Sediments Transport. *Pergamon Press.*

Zyserman, J.A. and J. Fredsøe (1994a): Data analysis of bed concentration of suspended sediment. *J. Hydr. Eng., ASCE, Vol. 120, No. 9, pp. 1021-1042.*

Zyserman, J.A. and J. Fredsøe (1994b): Bed concentration of suspended sediment and total load transport in asymmetric oscillatory flow. *Book of Abstracts Overall Workshop MAST, September 1994, Gregynog, Wales.*

Zyserman, J.A. and J. Fredsøe (1996): Validation of a deterministic sediment transport model for sheet-flow conditions. *Prog. Rep. 76 Technical Univ. of Denmark.*

Appendix A

The phase-lag correction of Dohmen-Janssen

In section 4.4.1 the basic formulae for the model of Dohmen-Janssen was described for the situation with sine waves superimposed on net current (described with $u(t) = u_0+u_1\sin(\omega t)$). In this appendix the basic formulae for the more general case with 2nd-order Stokes waves and an imposed net current (described with $u(t) = u_0+ u_1\cos(\omega t) + u_2\cos(2\omega t)$) are described as follows (see also figure 4.1):

$$< q_s > = r < q_s >_{\text{Ribberink}} \tag{A.1}$$

$$r = \frac{< q_{s,r} >}{< q_{s,eq} >} = \frac{u_0^3 + \frac{1}{2}u_0u_1^2 + \frac{1}{2}u_0u_2^2 + u_0u_1^2G_1 + \frac{1}{2}u_2u_1^2G_1 + u_0u_2^2G_2 + \frac{1}{4}u_1^2u_2G_2}{u_0^3 + 1\frac{1}{2}u_0u_1^2 + 1\frac{1}{2}u_0u_2^2 + \frac{3}{4}u_2u_1^2} \tag{A.2}$$

$$G_1(p) = \frac{P_1\cos\varphi_1 + Q_1\sin\varphi_1}{\left(P_1^2 + Q_1^2\right)^{3/2}} \tag{A.3}$$

$$G_2(p) = \frac{P_2\cos\varphi_2 + Q_2\sin\varphi_2}{\left(P_2^2 + Q_2^2\right)^{3/2}} \tag{A.4}$$

$$\varphi_1 = \arctan\left[-\frac{Q_1}{P_1}\right] \tag{A.5}$$

$$\varphi_2 = \arctan\left[-\frac{Q_2}{P_2}\right] \tag{A.6}$$

$$P_1 = \frac{1}{2} + \left[\frac{1}{16} + p^2\right]^{\frac{1}{4}} \cos\left(\tfrac{1}{2}\alpha_1\right) \tag{A.7}$$

$$P_2 = \frac{1}{2} + \left[\frac{1}{16} + (2p)^2\right]^{\frac{1}{4}} \cos\left(\tfrac{1}{2}\alpha_2\right) \tag{A.8}$$

$$Q_1 = \left[\frac{1}{16} + p^2\right]^{\frac{1}{4}} \sin\left(\tfrac{1}{2}\alpha_1\right) \tag{A.9}$$

$$Q_2 = \left[\frac{1}{16} + (2p)^2\right]^{\frac{1}{4}} \sin\left(\tfrac{1}{2}\alpha_2\right) \tag{A.10}$$

$$\alpha_1 = \arctan(4p) \tag{A.11}$$

$$\alpha_2 = \arctan(8p) \tag{A.12}$$

$$p = \frac{\mu f_w u_a^2 \omega}{2\Delta g w_s} \qquad (\text{“}\textit{phase-lag parameter p}\text{”}) \tag{A.13}$$

The wave friction factor f_w is again calculated from Swart’s formula (1974) (see, equation 4.14).

Appendix B

Measuring instruments

Laser Doppler Velocity Meter (LDA)

A forward-scatter Laser Doppler Anemometer (LDA), developed by WL | Delft Hydraulics (see Klopman, 1994), was used for two-dimensional flow-velocity measurement in a vertical plane along the centre of the tunnel test section. The LDA has a relatively small measuring volume, with a height and width of approximately 0.22 mm. The length of the measuring volume in direction perpendicular to the flow is approximately 6.47 mm. The standard range of bi-directional velocities, which can be measured with this system is 0.001 – 2.0 m/s. Figure B.1 shows the configuration of the LDA-beam in the test section of the water tunnel.

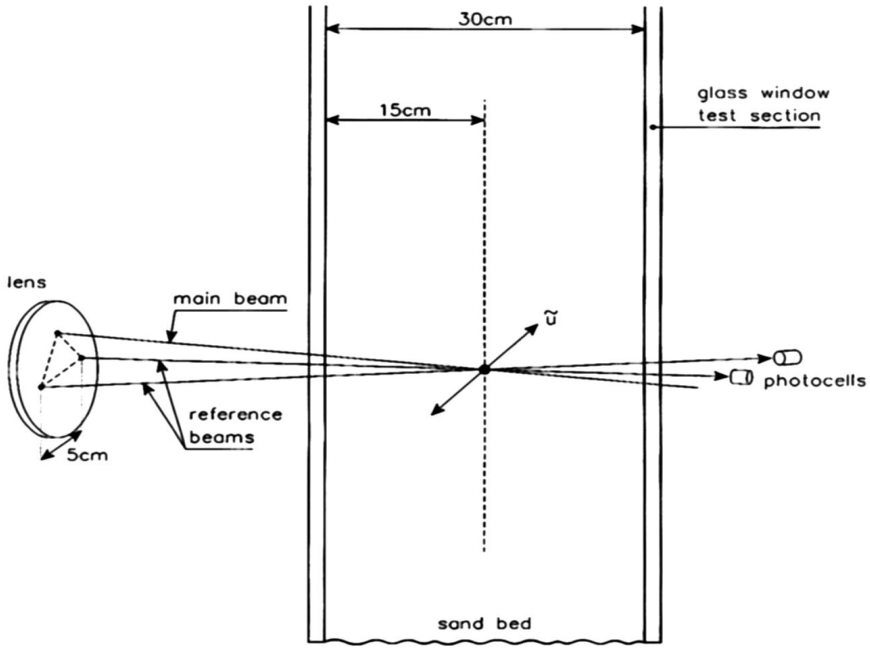

Figure B.1: Laser-beam configuration in the water tunnel (vertical section).

The LDA was positioned on a rigid carriage that stands over the tunnel, rather than on top of it, in order to eliminate the effect of tunnel vibrations. The LDA measures two velocity components, at about 45^{o} to the x-axis, in order to increase the measured velocity range. The two velocity components are transferred to horizontal and vertical directions afterwards.

Bed level profiling system (PROVO)

The bed level profiling system was used to measure the bed level before and after a test (for net transport measurements, see section 6.4.1). The system consists of three profilers on a carriage, which can be moved along the test section, a positioning counter (which determines the exact location of the three profilers along the test section) and measuring and processing software installed on a computer. Each profile measures the vertical position of the bed surface. The carriage is installed on rails inside the wave tunnel and can be moved along the whole test section by a cable system from outside the test section. The three profilers on the carriage are installed normal to the direction of motion, so that the bed level can be measured at three locations across the width of the tunnel (at the centre, 0.10 m to the left and 0.10 m to the right, that is 0.05 m from the side walls).

The bed level in the tunnel is then determined by averaging the bed level measurements of the three locations across the width of the tunnel. In figures B.2 and B.3 the configuration of the PROVO-system is shown.

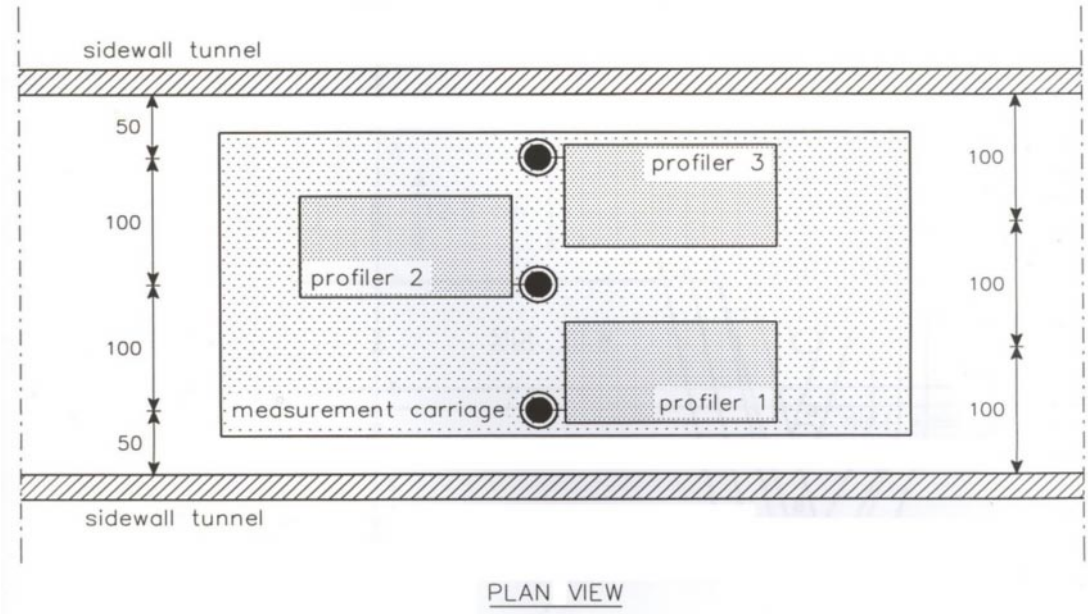

Figure B.2: Configuration of Bed Level Profiling System (PROVO), measurement carriage (plan view).

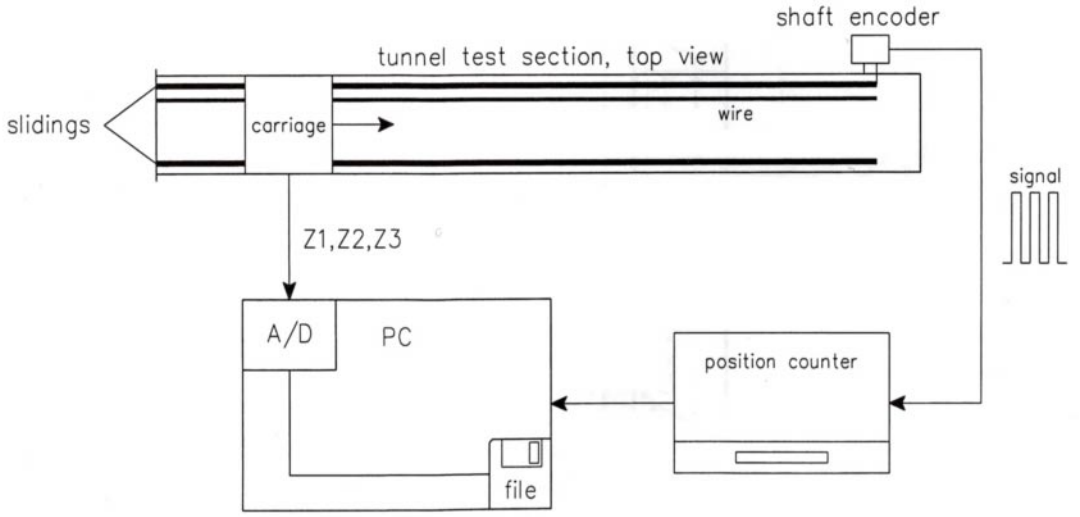

Figure B.3: Configuration of Bed Level Profiling System (PROVO) in the tunnel, general layout (top view).

The measuring principle of the profiler is based on conductivity or electro-resistance of water-sand mixtures. While moving along the tunnel, the conductivity in the sampling volume at the end of each profiler (probe tip) is held constant by keeping a constant distance of the probe tip to the bed (order: 1 mm). A potentiometer measures the vertical position of the probe, which is directly related to the bed level in the tunnel. At every centimetre along the tunnel, the measuring signal of the three profilers is stored on a computer, giving a detailed description of the sand bed height along the test section.

A shaft encoder connected to the cable pulling the carriage measures the horizontal position of the profiler (see figure B.3).

Transverse Suction System (TSS)

A Transverse Suction System developed by Bosman et al. (1987) was used for measuring the time-averaged concentration profiles of the suspended sediment. Water-sediment samples are extracted in a direction normal to the flow direction. The system consists of 10 separate intake nozzles with an inner diameter of 3 mm placed above each other at an increasing distance. Figure B.4 gives the general outline of the TSS. The numbers in the right part of this figure present the distance (cm) between the nozzles.

Ten peristaltic pumps drive the suction system, each connected to one of the intake nozzles. The water samples containing the suspended sediment are collected in 10 buckets. The sand volumes of the collected samples are measured using calibrated

glass tubes and converted into sand weights using the sand density and the porosity of loosely packed sand. The TSS system was calibrated using trapping efficiency factors (see Bosman, 1987). The main parameters, which determine the trapping efficiency are the nozzle dimensions, their orientation to the ambient flow, the ratio of the intake velocity over the ambient flow velocity, the sediment particle characteristics and the relative sediment density. For the present tests a constant trapping efficiency of 0.78 could be used.

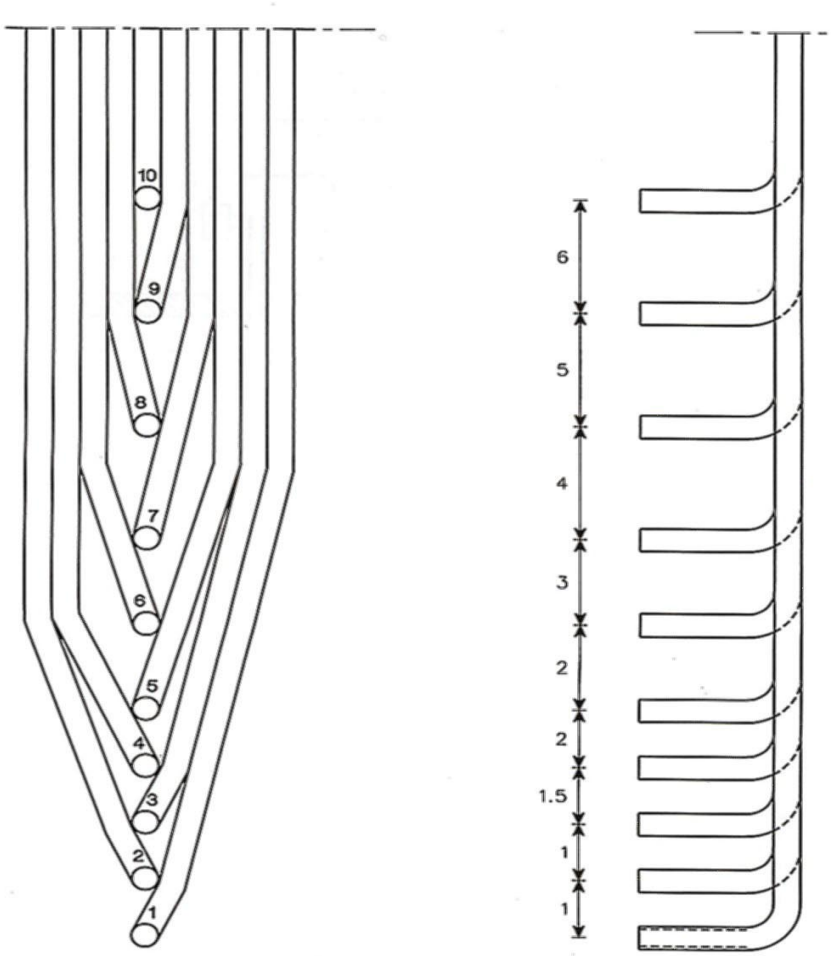

Figure B.4: General outline of Transverse Suction System (TSS); dimensions in (cm).

The position of the lowest nozzle of the TSS was approximately 5 mm above the initial sand bed for all tests. The height of the TSS above the bed was measured before and after each test in order to determine the average height above the bed. The sand samples collected with TSS have also been used to determine the grain-size distribution of the suspended sediment, using a settling tube (Visual Accumulation Tube, VAT).

Pump Bed-Load Trap sampler (PBLT)

The PBLT developed by Van Rijn (1997) was used to measure the 'onshore' and 'offshore' time-averaged bed-load concentrations. The PBLT consists of two tube-type intake nozzles placed in opposite direction on a metal footplate (length of about 0.1 m, width of about 0.05 m) as shown in figure B.5.

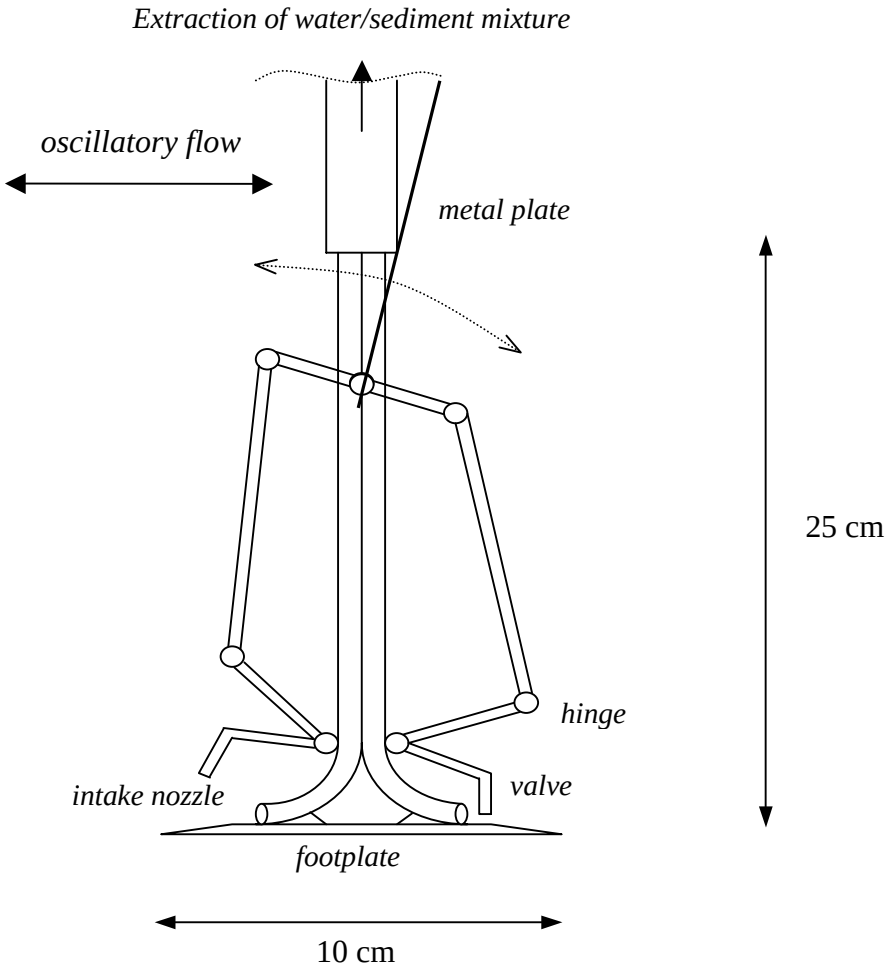

Figure B.5: General outline of the Pump Bed-load Trap sampler (PBLT).

Each nozzle (internal diameter of 8 mm) is connected to a plastic hose for pumping of water and sediment. The nozzles are opened and closed alternatively by circular metal valves (with rubber cover) through the action of oscillatory fluid drag on a metal pivoting plate connected by thin steel rods to the valves. The valve of the nozzle facing the forward (onshore) fluid motion will be opened during the forward stroke of the wave and closed during the backward stroke. The intake nozzle facing the forward motion will be termed the 'onshore' nozzle and that facing the backward motion will be termed the 'offshore' nozzle.

The scour around the instrument was found to be minimum during previous tests with orbital velocities up to 1.7 m/s (see Van Rijn, 1997). The maximum scour depth behind the offshore nozzle was about 5 mm. The scour length was about 50 mm. More details about the PBLT can be found in section 6.4 and Van Rijn (1997).

Calibration of the PBLT

Van Rijn (1997) calibrated the PBLT in the LOWT using uniform sand (D = 0.21 mm) and the net transport rates of Al-Salem (1993), series B with comparable hydraulic conditions. Van Rijn found that the measured mean sand concentrations varied between 1 and 100 kg/m^3. Using the data of Van Rijn (1997) and equation 6.7, it was found that the calibration factor α varies between 0.4 and 0.8.

For the present wave tunnel experiments the calibration factor α (equation 6.7) was found to be a function of the time-averaged bed-load concentration as shown in figure B.6 for all data with uniform and graded sands. The calibration points of Van Rijn match well with the new data of the present tests. The following power relation can be used as a general form for determining the calibration factor α under sheet-flow/flat-bed conditions:

$$\alpha = \frac{5.37}{< c >^{0.8}} \qquad \text{(B.1)}$$

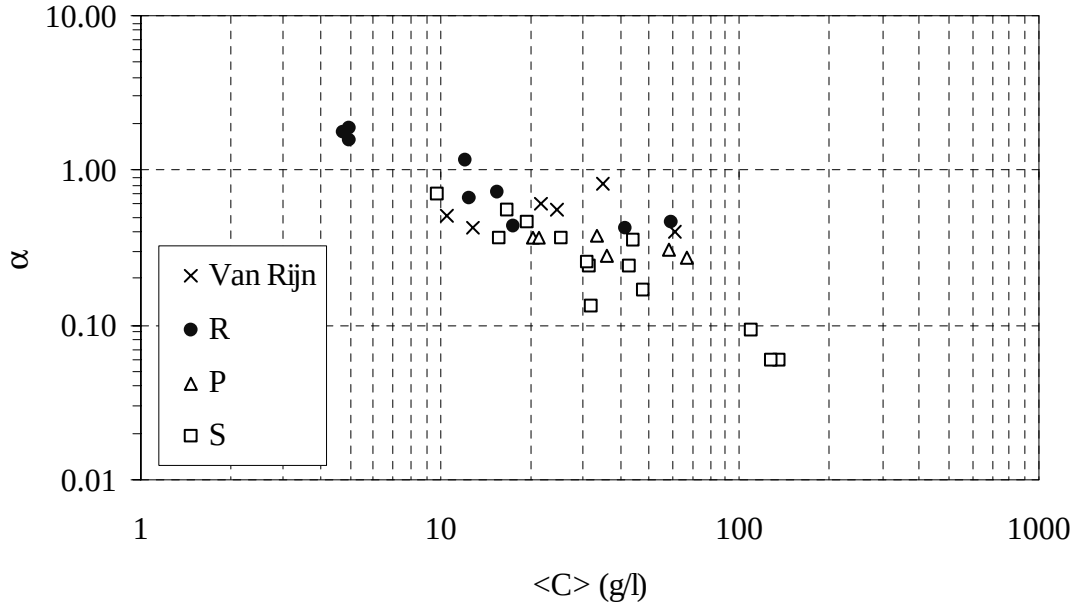

Figure B.6: Calibration factor α of the PBLT as a function of the time-averaged bed-load concentrations, with different uniform sand size-graded sands.

In equation B.1 it is clear that the calibration factor α is inversely proportional to the time-averaged concentrations, i.e. high concentrations are associated with small values of α and vice versa. Small α values were found in cases with small net transport rates and large time-averaged sand concentrations in the flow. In fact, large time-averaged concentrations do not always lead to large net transport rates like in uni-directional flow. Unsteady effects in oscillatory flows may determine the magnitude and the direction of the net transport rates. In equation 6.7 different values of α can be obtained, if net transport rates stay more or less the same for the same flow condition and different grain-sizes (see figure 7.3, $0.2 < D < 0.97$ mm), while sediment concentrations are dependent on the grain-size, increasing concentrations are expected for finer sands (see Dohmen-Janssen, 1999).

Conductivity Concentration Meter (CCM)

Two CCM probes (spaced 11 mm) are brought into the middle of the test section from below through the tunnel bottom and the sand bed in order to minimise the flow disturbance. Figure B.7 shows the configuration of the CCM in the tunnel and the CCM probe. The sensors were mounted on a positioning gage that measured the vertical position within a precision of 0.01 mm.

The CCM uses an electro-resistance measuring technique, developed by WL | Delft Hydraulics for measuring sediment concentrations in sediment-water mixtures. The CCM was used for measuring the time-dependent sediment concentrations in the sheet-flow layer and inside the sand bed. The CCM measures large concentrations (5 – 50 % volumes, 100 – 1600 g/l) with a four-point electro-resistance probe.

The CCM measuring principle is based on the conductivity change of a sand-water mixture due to the variation of the quantity of (non-conductive) sand particles present in the measuring volume. A constant electrical current is generated between two outer electrodes and the voltage between the inner electrodes is measured. The measured voltage is proportional to the electro-resistance of the sand-water mixture in a small measuring volume directly above the electrodes. The height and the length of the volume are 1 and 2 mm, respectively (Koelewijn, 1994).
The absolute change in electrical current strength in the case of a sand-water mixture in comparison with clear water is determined by the change in conductivity. The water conductivity can vary considerably, therefore a relative conductivity Gr is used, defined as:

$$Gr = (1 - (V_0 / V_m)) * 100\ \% \qquad (B.2)$$

$$C\ (\text{volume}\ \%) = K * Gr \qquad (\%) \qquad (B.3)$$

where: V_0 = output voltage of the probe for clear water; V_m = output voltage of the probe for the sand-water mixture and K = calibration factor (see figure, B.8).

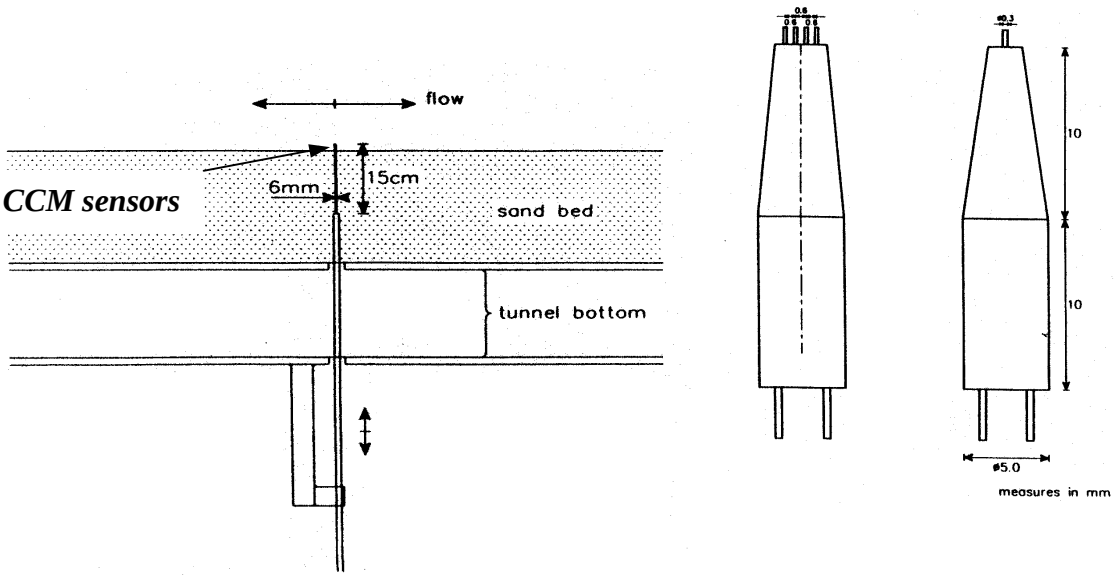

Figure B.7: CCM configuration in the water tunnel and CCM probe outline (measured in mm).

CCM probe tests in various sand-water mixtures with different sand grain sizes show a constant linear calibration (K = 1.0-1.2), with an error band of ± 10 % (see Koelewijn, 1994, and Van der Wal, 1996).

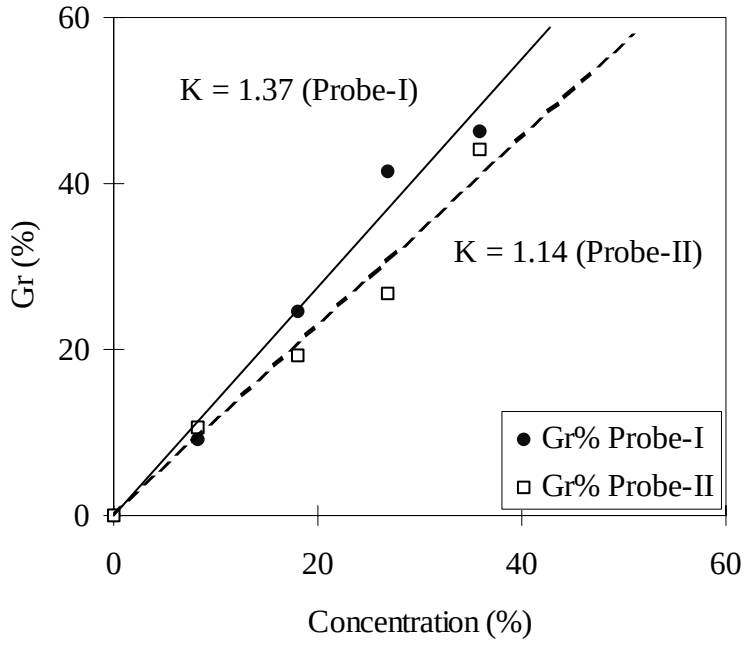

Figure B.8: Calibration factors of the two CCM probe.

Bed Sampler (BS)

A Bed Sampler was used to take small core samples out of the sand bed at different positions along the tunnel after a tunnel run, in order to measure vertical profiles of grain-size composition in the upper layer of the sand bed (vertical sorting). The BS consists of a perspex cylinder with inner diameter 25 mm and a height of about 100 mm, which was pushed into the sand bed.

For each test, bed samples were taken at 3 to 5 positions along the tunnel before and after tunnel runs. Generally, the upper 9 mm of the samples were divided into different subsamples with a thickness of about 3 mm each. The remaining part of the bed sample was not further analysed. The grain-size distribution and the size-fractions of each sample were determined by using the Visual Accumulation Tube (VAT).

During some tests bed samples were taken at more positions and in some other tests the samples were divided into more subsamples with an increasing thickness of the layers with depth (depth up to 50 mm).

List of figures

List of tables

List of symbols

Operators

$\langle X \rangle$	averaging parameter X over the wave period
$\overline{X}$	averaging parameter X over the turbulence time-scale
$\tilde{X}$	oscillatory component of parameter X
$\hat{X}$	amplitude of parameter X

Roman symbols

a	empirical coefficient related to the shape of the particles = 61.5 degrees for intermediate sphericity and roundness
â	amplitude of horizontal excursion of water particles near the bed
$\hat{A}_b$	semi-excursion length of the water particles, $\hat{A}_b = \hat{u}_b T / 2\pi$
b	empirical sorting parameter = -0.3
B_k	buoyancy flux ($= \nu_t/(\sigma_\rho N^2)$)
c	sediment concentration (kg/m^3 or m^3/m^3 or vol %); solids without pores
c_a	reference concentration at the reference level z_a (m^3/m^3)
$c_{a(Di)}$	reference concentration of size-fraction i, based on uniform bed material, with median diameter $D_i = D_{50}$ of each size-fraction (kg/m^3 or m^3/m^3 or vol %)
c_b	bed concentration c_b (m^3/m^3)
c_m	time-averaged sediment concentration (kg/m^3 or m^3/m^3 or vol %);
c_t	time-dependent sediment concentration (kg/m^3 or m^3/m^3 or vol %);
C	volume fraction of the all suspended sediment (kg/m^3 or m^3/m^3 or vol %)
C_{off}	time-averaged 'offshore' bed-load concentration (kg/m^3 or m^3/m^3 or vol %)
C_{on}	time-averaged 'onshore' bed-load concentration (kg/m^3 or m^3/m^3 or vol %)

C_m	maximum concentration = 0.48 (kg/m^3 or m^3/m^3 or vol %)
C_s	a maximum volume fraction of solids in a non-cohesive porous bed = 0.65 (kg/m^3 or m^3/m^3 or vol %)
$Corr_{x,y}$	correlation coefficient of measured (x) and calculated (y) transport rates; cov (x,y) = covariance between x and y
D_{crit}	critical diameter for suspended sediment (m); used in Zyserman & Fredsoe (1996)
D	grain diameter of the sediment (m)
D	internal diameter of intake nozzle (= 0.008 m)
D_{50}	median grain size (m)
D_A	grain-size in the mixture that needs no correction (-)
D_i	median diameter of fraction i (m)
D_i	grain diameter for which i% of the sediment, by weight is smaller (m)
D_m	mean diameter of the bed material (m)
D_s	diameter of the suspended sediment (m)
D_T	mean diameter of the transported material (m)
D_*	dimensionless particle diameter (-)
E_k	kinetic energy of a sand particle
f_c	current friction factor (-)
f_c	empirical coefficient based on data for turbulent flow
f_{crit}	probability of the critical grain diameter
f_{cw}	friction factor for combined wave current flow (-)
f_w	wave friction factor (-)
g	gravity acceleration (m/s^2)
G	$G_l + G_r$ = total (dry) weight of the sand collected in both traps
G_l	total (dry) weight of the sand collected in the left trap (underneath the piston)
G_r	total (dry) weight of the sand collected in the right traps (underneath the open cylindrical riser)
Gr	relative conductivity used in the calibration of the CCM (-)
h	water depth (m)
H	wave height (m)
k_s	bed roughness height (m)
$k_{s,c}$	current roughness height (m); in model of Ribberink (1998)
$k_{s,w}$	wave roughness height (m); in model of Ribberink (1988)
K	size of the surrounding grains, generally taken as the median grain-size of the complete sediment mixture

K	calibration factor
K	correction factor for the reference bed concentrations c_{bi}
l_m	mixing-length (m)
m	coefficient (-) =11; in bed-load transport model of Ribberink (1998)
M_i	time-averaged total load of sediment in suspension for each fraction i
n	exponent (-) = 1.65; in bed-load transport model of Ribberink (1998)
N	number of size fractions in a mixture
N^2	buoyancy frequency
p	pressure (N/m^2)
p	phase-lag parameter (-) = $\varepsilon_s\omega/w_s^2$
p	protrusion of a sediment particle above others
p	probability that all the particles in a single layer will be in motion
$p^/$	phase-lag parameter (-); based on the expressions for sheet-flow thickness derived from the present measurements
P	parameter (-); in the intermediate model of Dohmen-Janssen
P_i	volume ratio of fraction i in the mixture (-)
P_k	turbulence production
$P_{T,i}$	contribution of fraction i to the net total transport rate
q_s	net transport rate without pores per unit width and time (m^2/s)
q_s	sand transport rate in volume of solids without pores per unit width (m^2/s)
q_s	net total transport rate during the full wave-cycle (m^2/s)
q_{sc}	net transport rate during the crest period (T_c) of the wave-cycle (m^2/s)
q_{st}	net transport rate during the trough period (T_t) of the wave-cycle (m^2/s)
q_i	net transport rate for fraction i (m^2/s)
$q_{u,i}$	transport rate for fraction i as if the sand bed was composed of a single sand size D_i alone (m^2/s)
$q_{s,r}$	real sand transport rate per unit width, i.e. including phase-lag effects (m^2/s)
$q_{s,eq}$	equilibrium sand transport rate per unit width, i.e. without phase-lag effects (m^2/s)
$q_{s,b}$	bed-load transport (m^2/s)
$q_{s,s}$	suspended-load transport (m^2/s)
Q	parameter (-) in the intermediate model of Dohmen-Janssen
r	phase-lag correction factor (-)

R	degree of asymmetry (-)
R	exposure correction factor (-)
R_e	grain Reynolds number (-) ($R_e = u_* D/\nu$)
t	time (s)
t_{settle}	settling time of a sediment particle (s); $t_{settle} = \delta/w_s$
T	wave period (s) = $T_{crest} + T_{trough}$
T_{crest}	period of the wave crest (s)
T_{trough}	period of the wave trough (s)
u	horizontal flow velocity (m/s)
u	sediment particle velocity (m/s)
u_0	time-averaged component of horizontal velocity (m/s)
u_1	first harmonic component of horizontal velocity (m/s)
u_2	second harmonic component of horizontal velocity (m/s)
u_b	amplitude of the horizontal near-bed orbital velocity (m/s)
$u_{b,on}$	onshore drift very close to the seabed (m/s)
u_c	equivalent sinusoidal velocity amplitude of positive half wave cycle (m/s); applied in model of Dibajnia and Watanabe (1996)
$u_{m,off}$	undertow velocity (m/s)
$u_{s,on}$	onshore flux of water above the trough level of the waves
u_t	equivalent sinusoidal velocity amplitude of negative half wave cycle (m/s); applied in model of Dibajnia and Watanabe (1996)
u_*	horizontal shear velocity (m/s)
$\bar{u}$	the depth-averaged velocity (m/s)
u_∞	horizontal free-stream velocity, i.e. outside the wave boundary layer (m/s)
U_{max}	maximum horizontal velocity (m/s)
U_{rms}	root-mean-square value of flow velocity (m/s)
$\hat{U}$	velocity amplitude of the oscillatory flow (m/s)
U_{crest}	onshore wave velocity (m/s)
$U'_{f\,max}$	maximum value attained by the instantaneous skin friction velocity over the wave period
U_{trough}	offshore wave velocity (m/s)
$\hat{U}_{\delta,crb}$	critical velocity amplitude (m/s)
U_{laser}	horizontal flow velocity measured by LDA (m/s)
V	sand volume (m^3)
V_0	output voltage of the CCM-probe for clear water (Volt)

V_m	output voltage of the CCM-probe for a sand-water mixture (Volt)
$w_{s,0}$	settling velocity of a single particle in infinite fluid without wall effects (m/s)
w_s	settling velocity of the sediment particle (m/s)
W	width of the tunnel test section (m)
x	horizontal co-ordinate in flow direction (m)
y	horizontal co-ordinate perpendicular to flow direction (m)
z	vertical co-ordinate, i.e. level above the bed (m)
z_a	reference level for the sediment concentration (m)
z_0	level where velocity is assumed to be zero (m); $z_0 = k_s/30$
z_∞	level just outside the wave boundary layer where $u = u_\infty$ (m)

Greek symbols

α	calibration factor (-)
α	constant (-)
α_i	empirical coefficient, depending on the ratio of the mean diameter of each size-fraction to that of the other size-fraction (-)
α	parameter in the unsteady model of Dohmen-Janssen (-)
α	trapping efficiency of Transverse Suction System (-)
α	angle of repose for a single grain in degrees
β	constant (-)
Γ	transport parameter (-); in model of Dibajnia and Watanabe (1996)
δ	height to which a particle is entrained into the flow (m)
δ_s	sheet flow layer thickness (m)
Δ	relative density = $(\rho_s - \rho)/\rho$
Δt	test duration (s)
ΔV_{ip}	total volume change, including pores in the tunnel test section (m^3)
$\Delta V_{l,ip}$	volume change of the sand bed, including pores in the left-hand side of the LOWT test section (m^3)
$\Delta V_{r,ip}$	volume change of the sand bed, including pores in the right-hand side of the LOWT test section (m^3)
Δx	length interval (m)
ε	dissipation rate
ε_0	porosity (-)
ε_b	efficiency factor for bed-load transport (-) = 0.1; in model of Bailard (1981)

ε_s	efficiency factor for suspended-load transport (-) = 0.02; in model of Bailard (1981)
ε_s	sediment diffusivity ; sediment mixing coefficient (-)
θ	Shields parameter (-); non-dimensional bed shear stress (-)
θ_{cr}	critical Shields parameter for initiation of motion (-)
θ_{eff}	effective Shields parameter (-)
θ_{cm}	dimensionless critical shear stress for uniform sediments according to Komar and Wang
θ'	dimensionless effective bed shear stress (-)
κ	Von Karman constant; $\kappa = 0.4$
μ_d	dynamic friction coefficient; in the bed-load formula of Engelund & Fredsoe (1976)
μ	constant (-)
ν	kinematic viscosity (m^2/s)
ν_t	eddy viscosity in flow direction (m^2/s)
$\xi_{c,i}$	correction factor for critical shear stress for size-fraction i (-)
$\xi_{eff,i}$	correction factor for effective shear stress for size-fraction i (-)
ρ	fluid/water density (kg/m^3)
ρ_m	density of sand-water mixture (kg/m^3)
ρ_s	density of sediment (kg/m^3)
ρ_w	density of water (kg/m^3)
σ_g	geometric standard deviation of the grain size distribution (-)
σ_ρ	Prandtl/Schmidt number
σ	standard deviation of the mean value (-)
τ_b	bed shear stress (N/m^2)
$\hat{\tau}$	peak bed shear stress (N/m^2)
φ	parameter (-); in the intermediate model of Dohmen-Janssen (1999)
φ	non-dimensional sediment transport rate parameter (-)
φ	sediment flux (m/s)
ϕ_i	a correction factor to make the suspended loads of all fractions i the same; Zyserman & Fredsoe (1996) size-fraction approach
ϕ	angle of repose (°); angle of internal friction of the sediment
ϕ_b	dimensionless bed-load transport (-)
ω	angular frequency of the wave (s^{-1}); $\omega = 2\pi/T$
$\omega_{i,corr}$	corrected ratio of the time required of suspended sand particle to reach the bed to the period of each half-wave-cycle of size-fraction i

ω_c	ratio of fall time of a particle to the period of the positive half wave cycle (-); used in the model of Dibajnia and Watanabe (1996)
ω_t	ratio of fall time of a particle to the period of the negative half wave cycle (-); used in the model of Dibajnia and Watanabe (1996)
Ω_c	parameter representing the amount of sand entrained and transported during the positive half wave cycle (-); used in model of Dibajnia and Watanabe (1996)
$\Omega_c^{/}$	parameter representing the amount of sand entrained during the preceding positive half wave cycle that has not settled back to the bed and is therefore transported in negative direction (-); used in model of Dibajnia and Watanabe (1996)
Ω_t	parameter representing the amount of sand entrained and transported during the negative half wave cycle (-); used in model of Dibajnia and Watanabe (1996)
$\Omega_t^{/}$	parameter representing the amount of sand entrained during the preceding negative half wave cycle that has not settled back to the bed and is therefore transported in positive direction (-); used in model of Dibajnia and Watanabe (1996)

Abbreviations

BS	Bed Sampler
CCM	Conductivity Concentration Meter
D-J	Dohmen-Janssen
D&W	Dibajnia & Watanabe
LOWT	Large Oscillating Water Tunnel
LDA	Laser Doppler Velocity Meter
MCT	Mass Conservation Technique
PBLT	Pump Bed-Load Trap sampler
PROVO	Bed level profiling system
TKE	turbulent kinetic energy
TSS	Transverse Suction System
TUWT	Tokyo University Water Tunnel
VAT	Visual Accumulation Tube
Z&F	Zyserman & Fredsoe

Acknowledgements

Many people have provided me with help, guidance and support during the time it has taken me to complete this PhD. The greatest and most enduring presence was that of my supervisors, prof. *Huib de Vriend* and dr. *Jan Ribberink*. Their relentless pursuit of excellence and constant quest for knowledge is unlimited. Without their support this PhD would not have been possible.

I am also grateful to prof. *McLean* for his comments and suggestions and his wonderful hospitality during the period I spent at the University of California, Santa Barbara.

Particular mention must be made of prof. *Leo Van Rijn* who provided much advice and guidance during the SEDMOC project.

I am very thankful to dr. *Rob Uittenbogaard* and *René Buijsrogge*. Both of them contributed much to the software development related to the sand transport models in this thesis. I wish to acknowledge also the contributions of Ir. *David Kroekenstoel* and Ir. *Peter van der Scheer* to this study.

There are many other people that I will not list, with whom I have had useful and inspiring conversations about my work and related topics. They have made my stay in the Netherlands very worthwhile. I am grateful to all my colleagues at the Faculty of Engineering, University of Twente, for their support and cooperation.

I also would like to express my appreciation for the help provided by the staff members of WL | Delft Hydraulics during all the experiments I carried out at WL | Delft Hydraulics.

I want to thank Dr. *Dibajnia* for providing me with the uniform sand data from Tokyo University and the great help of *Ahmed Sayed* who helped to collect the graded sand data of Tokyo University.

Special thanks goes to all my Jordanian and Indonesian friends at the UT for the good times we have together during the weekends.

I am most indebted to all my family for their love, support and encouragement. In particular, I would like to thank my wife *Abeer* who has provided me with the emotional support that kept me going to the end of my research. I am extremely obliged to my *mother* and my *father* who suffered a lot for being a long time away from home. I dedicate this thesis to my mother, father and my wife for standing by me in good and bad times during all my life. Finally, all my love to my two kids *Mohaned* and *Mo'men*.

Thank you all!

About the author

Wael Neiazy Mohamed Hassan was born in Shein El-Kom, Egypt, on 10 January 1967. In 1990 he gained his B.Sc. degree in Civil Engineering at El-Menofia University, Egypt. In the same year he started his professional career at the Ministry of Public Works and Water Resources in Egypt as a research assistant in the field of water drainage. During this period he joined different projects in the Nile delta and in the northern part of Sinai, Egypt.

In 1992 he joined the Hydraulics Research Institute (HRI) in Cairo as research assistant in the river engineering department. In September 1994 he started his study towards the M.Sc. degree in hydraulic engineering in IHE, Delft, the Netherlands, which was obtained in June 1996. After that he worked for one year as assistant researcher in HRI, Cairo.

In September 1997 he became a guest researcher at University of Twente, the Netherlands. From August 1998 he started his PhD research at the University of Twente, Department of Civil Engineering in the field of cross-shore sediment transport modelling. During this period he was engaged in many European research projects with leading European institutes and universities in the field of hydraulics research. During his professional and research assignments he gained thorough experience in the field of sediment transport modelling, through using large-scale laboratory facilities (at WL | Delft Hydraulics and HRI) as well as various sediment transport models.